Monte Carlo Simulations of Lipid Bilayers containing Cholesterol

by

Yvonne Nga Fong Yuan

B.Sc., University of Waterloo, 1999

A thesis submitted in partial fulfilment of
the requirements for the degree of

MASTER OF SCIENCE

in the

Department of Physics

SIMON FRASER UNIVERSITY

July 2004

APPROVAL

Name: **Yvonne Nga Fong Yuan**

Degree: **Master of Science**

Title of Thesis: **Monte Carlo Simulations of Lipid Bilayers Containing Cholesterol**

Examining Committee:

Chair: **Dr. Mike Hayden**
Associate Professor, Department of Physics

Dr. Jenifer Thewalt
Senior Supervisor
Associate Professor, Department of Physics

Dr. Martin Zuckermann
Co-Supervisor
Adjunct Professor, Department of Physics

Dr. David Boal
Supervisor
Professor, Department of Physics

Dr. Michael Wortis
Internal Examiner
Professor Emeritus, Department of Physics

Date Approved: **2 July, 2004**

SIMON FRASER UNIVERSITY

Partial Copyright Licence

ABSTRACT

The effects of cholesterol on the phase behaviour of lipid bilayers composed of Dilauroyl phosphatidylcholine (DLPC) and Dipalmitoyl phosphatidylcholine (DPPC) are investigated. Metropolis Monte Carlo simulations are performed on a 2-dimensional multi-state lattice model, which is a direct extension of the Pink model originally proposed to describe the main phase transition of single-component lipid bilayers. The binary mixture containing DLPC and DPPC was chosen because it is assumed to mimic lipid systems used in experimental investigations of the properties of rafts. Our calculations proceed as follows: (i) Simulations were first performed on single-component phosphatidylcholine (PC) bilayers with chain length ranging from 12 to 22. Our results were found to be in excellent agreement with previous simulations performed by different groups with the same parameter sets. (ii) Simulations on DLPC/cholesterol and DPPC/cholesterol bilayers were then performed, which were found to agree with experimental data from differential scanning calorimetry (DSC) and deuterium nuclear magnetic resonance (^{2}H-NMR). A liquid-ordered (**lo**) phase which displays characteristics that are consistent with experimental observations is obtained from our model. Moreover, we found that formation of domains of different sizes can be induced by varying the interaction between the kink state and cholesterol in our model. (iii) Simulations on the binary DLPC/DPPC bilayers in the absence of cholesterol were next performed and reasonable agreement of our theoretical phase diagram with experimentally determined phase diagram from DSC and Fourier Transform Infrared

(FTIR) experiments was found. (iv) Finally, simulations of DLPC/DPPC/cholesterol bilayers were performed, in conjunction with an exploration of the parameter space of the interaction between cholesterol and different lipid conformational states. We found that different parameter sets result in formation of domains of different size and component concentration. Two sets of parameters were chosen for which the system contains **lo** domains at physiological temperature, and at the same time exhibits a molecular order parameter profile that best resembles those from experimental FTIR data.

DEDICATION

To my parents

Alice laughed. "There is no use trying," she said: "one can't believe impossible things."

"I daresay you haven't had much practice," said the Queen. "When I was your age, I always did it for half-an-hour a day. Why, sometimes I've believed as many as six impossible things before breakfast."

Lewis Carroll

Through The Looking Glass, 1872

ACKNOWLEDGEMENTS

I would like to thank first and foremost my research supervisors Martin Zuckermann and Jenifer Thewalt for providing me with the wonderful opportunity of working with them. I could not have asked for a better combination of expertise in theoretical and experimental biophysics as well as the synergy in their styles of supervision. It has been my pleasure to work with both Jenifer and Martin for the past two years. The two of you really make a dream team!

I would like to thank Martin for his friendly style which always made me feel welcomed, his incredible patience and encouragement in guidance, and for giving me a critical push at times I needed it badly. I have enjoyed our conversations, whether they were about physics, ethnic food adventures, or even complaining about junk emails. I am grateful to him for teaching me the Monte Carlo simulation techniques, his immense help in proofreading the countless drafts of this thesis, and his generous financial support of this work.

Thanks to Jenifer for her warm smile, listening ears and words of encouragement filled with enthusiasm. The help she has given me in understanding biochemistry and on various experimental studies was indispensable. Her insightful comments and suggestions also led to distinct improvements of this thesis. Thanks for taking us to the numerous group lunches, which I enjoyed and am going to miss tremendously.

I would also like to express my gratitude to my supervisory committee. Thanks to David Boal who first introduce me to the world of biophysics and computer simulations.

I am also grateful for his favour in introducing me to Jenifer and Martin, as well his continual interest in my work. His ideas in the simulation algorithm of this work have proved invaluable. I am indebted to Mike Wortis for his invaluable inputs to my work. He played a crucial role in the last stage of this work which saved me from many errors. I am grateful for his 'tough love' approach to research and his friendliness and patience in teaching.

I would like to extend my thanks to Ole Mouritsen (Technical University of Denmark) for the friendly discussions and his useful input to my work. I owe a lot to Howard Trottier, graduate chair of the Physics Department, whose helpfulness and flexibility has made my graduation as smooth as it can be.

My fellow graduate students have made my graduate life much more pleasant. Thanks to all of your friendship and your help, and the interesting conversations that we had. The Physics Department probably houses some of the best staff around. Thanks to Candida, Susan, Dagni and Helen for giving the Physics Department a 'soft touch'. Your friendliness and helpfulness mean a lot to me; also thanks for the many enjoyable conversations that range from cooking to hair treatments. I would also like to thank Sada and Mehrdad for their excellent assistance and their friendly humour.

A special word of gratitude goes to my best friend Amy, who has always stood by me through thick and thin. Without your love and support, I would not have been able to overcome many hurdles in the last few years. Thanks for sharing your life with me, and for continuously inspiring me to be a better person. You earned your way to becoming my honorary financial advisor, so hereby I wish you a happy and prosperous future! Best friends always!

Many thanks go to my dear friends who have made my stay in Vancouver infinitely more enjoyable, for they are like family to me. Thanks to Rev. Stephen Leung and Anna for believing in me and creating opportunities for me to grow; to my landlady Karina, my landlord Henry for their care during the most hectic days of my graduate life; to my buddies Clemmie, Winnie (a.k.a. McWinwin), Ikki, Cecilia—who deserves special credit for her help in editing the thesis, Gillian, Serena, Vivian, Christine, Selina, Ah Dup, Tommy, Ka Yan, Samuel, Jason, Ken, Chung, Sunita and Philip Patty for their friendship and fellowship. I am grateful for your constant care and support, and am indebted to many of you who provided numerous rides that made my life easier.

Finally, I would like to thank my parents for giving me the freedom to choose what I want; and for supporting me and allowing me a carefree stay here.

TABLE OF CONTENTS

LIST OF TABLES

LIST OF FIGURES

LIST OF ACRONYMS

DLPC	Dilauroyl phosphatidylcholine
DMPC	Dimyristoyl phosphatidylcholine
DPPC	Dipalmitoyl phosphatidylcholine
DSPC	Distearoyl phosphatidylcholine
DAPC	Diarachidoyl phosphatidylcholine
DBPC	Dibehenoyl phosphatidylcholine
PC	Phosphatidylcholine
DSC	Differential Scanning Calorimetry
FTIR	Fourier Transform Infrared
MC	Monte Carlo
MD	Molecular Dynamics

1 Introduction

Sterols have long been recognized as important molecular components of the plasma membranes of eukaryotic cells. They are ubiquitous both as structural components of the membrane as well as initiators and modulators of biological processes. Different animals and plants are found to require different sterols for proper cell functions and growth. Examples are cholesterol in mammalian cells, ergosterol in fungi, yeast and protozoans, and sitosterol and stigmasterol in plants.

Cholesterol is the dominant sterol component of the plasma membranes of mammalian cells. It is also the most abundant lipid species in the membrane, comprising a fraction of 30 to 50% of the membrane. It has been surmised that nature has, through an unimaginably long and laborious process, selected cholesterol for its ability to optimise important functions of the membranes [1, 2]. In fact, the synthesis of cholesterol in a mammalian cell follows a long, complicated, and energetically expensive biosynthetic pathway. It requires about 30 enzymatically catalysed steps, an extensive use of reducing equivalents, a number of enzymes and cofactors (all of which must be synthesized by the cell), and molecular oxygen [3]. Moreover, along the biosynthetic pathway of cholesterol, 19 different sterols are synthesized as intermediates, with lanosterol being the first cyclic precursor of cholesterol. It has been argued by Bloch [1, 2] that the evolutionary pathway of cholesterol has been preserved in its biosynthetic pathway. His argument is that lanosterol, which he regards as the molecular fossil of cholesterol, went through the

process of being streamlined by nature in the removal of its three methyl groups on the α-face to become a cholesterol molecule. It turns out that this streamlining which creates the ultra-smooth α-face in cholesterol is especially important regarding the effects of cholesterol on membrane fluidity. For instance, both theoretical and experimental studies on model membranes have shown that the effect of cholesterol at high concentrations in phospholipid bilayers is the elimination of the phase transition and the concomitant appearance of the so-called liquid-ordered (**lo**) phase. This **lo** phase contains highly conformationally ordered acyl chains while at the same time possessing a fluidity comparable to the liquid phase, which both are desirable for membrane functions. Experiments [4] have also shown that cholesterol—with a smoother hydrophobic face than lanosterol—is more effective than lanosterol in inducing the formation of the **lo** phase and stabilizing it under the same condition, which supports Bloch's hypothesis. Although the **lo** phase was successfully characterized in model membrane systems more than ten years ago, its implications to biological membranes continue to gain tremendous interest to this day. When Monte Carlo simulations were carried out for this thesis, special attention was given to the presence of the **lo** phase and its properties. To this effect, a detailed description of the **lo** phase will be presented later in this thesis.

Cholesterol, besides its functions in membranes, also plays many important roles in other aspects of cellular function. For example, one study [5] has shown that cholesterol is a key factor in synaptogenesis in the central nervous system. Furthermore, cholesterol is known to be the precursor of vitamin D, steroid hormones and bile acids. It also participates in cellular signalling and as a regulator of enzymes.

The influence of cholesterol on membrane fluidity serves as a means for the cell to manipulate the behaviour and functions of membrane proteins [6]. The reason is that a variety of integral membrane proteins, including ion channels, membrane receptors and enzymes, are sensitive to physical changes in the surrounding lipid bilayer. Moreover, studies over the last decade have shown that the plasma membrane is not a random sea of lipids as portrayed in the fluid mosaic model (Fig. 1.1). Rather, it is hypothesized that there are localized regions within the membrane called "rafts" which are liquid-ordered domains enriched in cholesterol and sphingolipids. The formation of these domains is made possible by the presence of cholesterol and lipids with highly saturated acyl chains. As a result, these regions are more tightly packed and therefore exhibit less fluidity than the surrounding plasma membrane (Fig. 1.2). In common usage, the term "rafts" encompasses both "planar rafts" and caveolae. Caveolae are small plasma-membrane invaginations. Like "planar rafts", caveolae have a high content of cholesterol and sphingolipids, but in addition, they also contain the cholesterol-binding protein caveolin-1, which appears to be responsible for stabilizing the invaginated structure of caveolae [7].

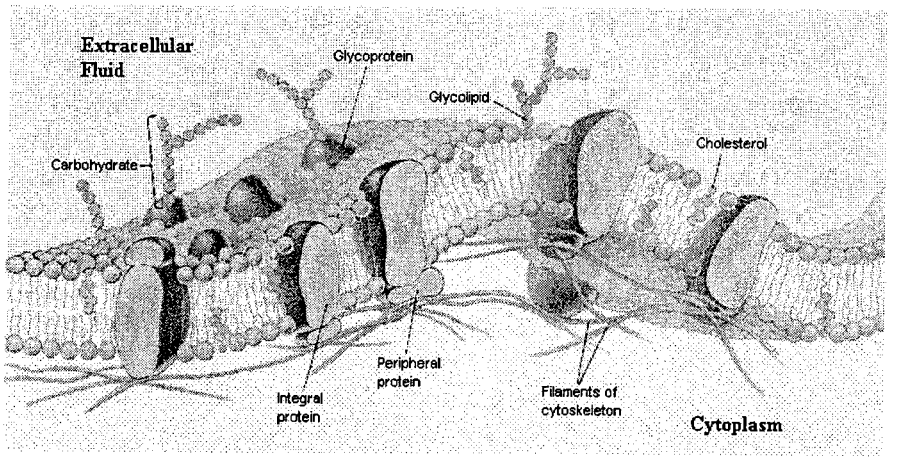

Figure 1.1 **The fluid mosaic model of lipid membrane bilayers. Reproduced from reference [103] with permission of the publisher.**

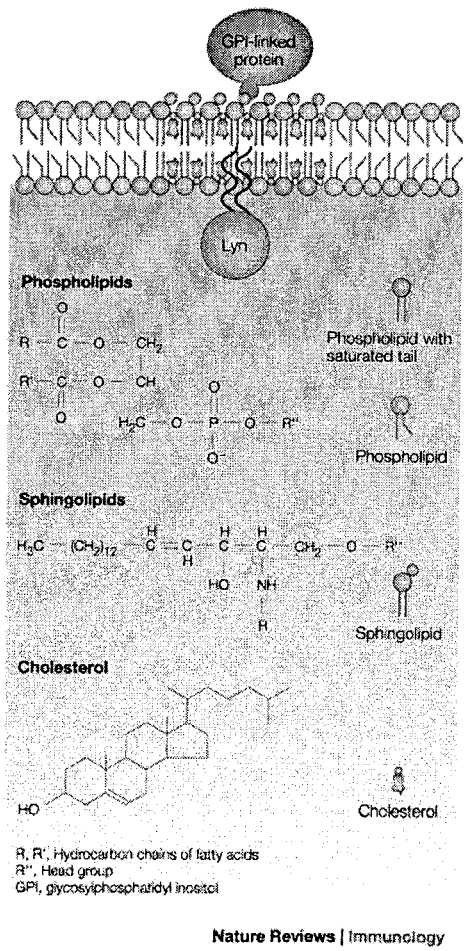

Figure 1.2 **"Rafts": liquid-ordered domains enriched in cholesterol and sphingolipids.**
Note that in reality, cholesterol also exists in the non-'raft' part of the membrane bilayer.
Reproduced from reference [96] with permission of the publisher.

Despite extensive work and tremendous interest among the scientific community since the concept "raft" was first hypothesized about fifteen years ago, the nature of "rafts" remains elusive. Experimental studies in the past decade have created the following two operational definitions of "rafts": 1) It was found that when biomembranes are treated with cold non-ionic detergents like Triton X-100, there is a separable and insoluble fraction that is rich in cholesterol, sphingolipids and GPI-anchored proteins which literally "floats" like a raft to the top of the density gradient. 2) It was also found that the acute or chronic depletion of cholesterol from cells results in perturbations of cell functions. However, despite the convenience of the detergent extraction method and its continuous usage, there have been concerns about the contamination or loss of components during extraction and the nonstandardized extraction procedure [8]. Others even question the practical value of the method fundamentally and object to its usage. Similarly, it was argued that cholesterol depletion in cell membranes can affect a series of important cell functions and in general makes the cell 'sick' [87]. Therefore the correlation between cholesterol depletion and the loss of a particular cellular function cannot necessarily be taken to show that lipid "rafts" are directly involved in that cellular function [8]. Although the definitions of lipid "rafts" are not without problems, they nevertheless have opened the way for vigorous pursuit of this subject in the scientific community.

Lipid "rafts" are regarded as functional microdomains. They were first conceived as part of a mechanism for lipid and protein sorting. In polarized epithelial cells, the apical side of the cell is found to be enriched in sphingolipids and glycophosphoinositol (GPI)-anchored proteins, which were believed to aggregate into a distinct domain in the

Golgi and sort apically as a unit-membrane patch [9]. Furthermore, it was recently proposed that properties of different lipid domains such as thickness and the relative sizes of the head and tail groups allow them to sort integral membrane proteins as well as direct membrane curvature [10]. Besides lipid and protein sorting, "rafts" are also believed to be involved in the regulation of signal transduction. A variety of proteins, especially those involved in cell signalling, have been shown to partition into lipid "rafts". Experimental evidence suggests that there are several possible mechanisms by which rafts control cell signalling, ranging from direct acquisition of required molecules into the raft to complete the signalling pathways to limiting the signalling activities by physically sequestering signalling components to block interactions [7].

The purpose of this thesis is the theoretical simulation of ternary lipid bilayers containing phospholipids and cholesterol, which are regarded as in-vitro models for raft formation. Here we begin by introducing the basics of lipid bilayers as well as reviewing the experimental and theoretical studies that have been done on these systems.

1.1 Lipids in Biomembranes

Mammalian cell membranes contain a vast variety of different lipid species which play diverse roles in membrane functions. Phospholipid is by far the most abundant class of membrane lipids in eukaryotic cells. Within this class, phosphatidylcholine (PC) and sphingomyelin (SM) together constitute more than 50% of membrane phospholipids. Lipids are amphiphilic molecules which contain a hydrophilic ("water-loving", or polar) head and two hydrophobic ("water-hating", or nonpolar) tails that are normally 12 to 24

carbon atoms long. PC molecules have a glycerol backbone, to which two fatty acid chains and a polar head group are attached. SM molecules, on the other hand, contain no glycerol, but a long-chain amino alcohol sphingosine as a backbone, which is attached to one fatty acid chain and a polar head group. Fig. 1.3 shows the structure of a SM molecule and an unsaturated PC molecule (i.e., contains a double bond). In biomembranes, naturally occurring PCs are typically found to be much less saturated than SMs. However, saturated PCs resemble SMs in their general properties and three-dimensional structure and in having no net charge on their head groups. Therefore, this allows us to use saturated PCs instead of SMs in the modelling of lipid bilayers in this thesis.

Besides phospholipids, sterols are also present in high amounts in many biomembranes. Sterols are compounds made up of a polar head group, a rigid system of four fused hydrocarbon rings and a nonpolar hydrocarbon tail. The structure of a cholesterol molecule is shown in Fig. 1.4.

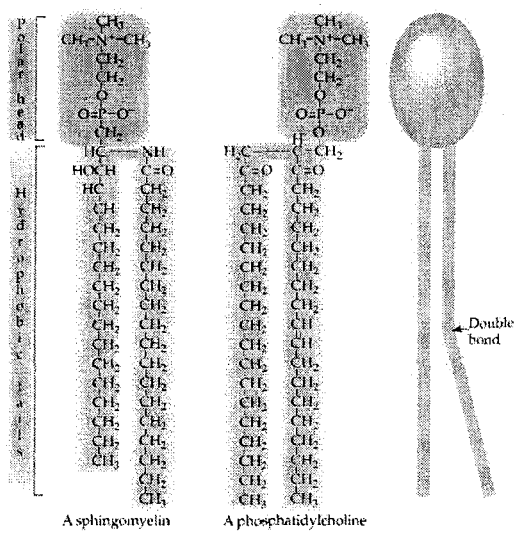

Figure 1.3 Sphingomyelin and phosphatidylcholine.

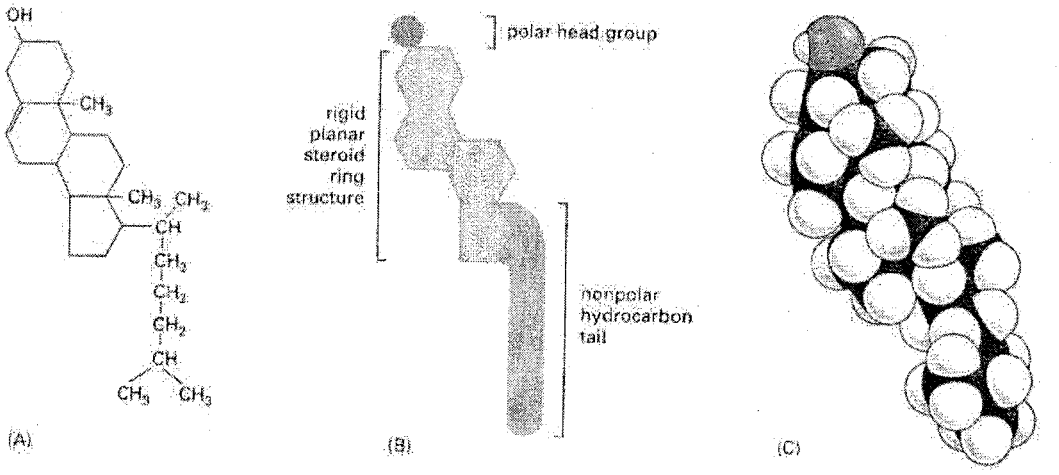

Figure 1.4 **Cholesterol molecule represented by (A) formula, (b) schematic drawing and (C) space-filling model.**
Reproduced from reference [92] with permission of the publisher.

In hydrated lipid systems, the hydrophilic attractions between the lipid polar head and water and the hydrophobic repulsions of the hydrocarbon tails with water result in self-assembly into different lipid structures. Depending on their lateral surface area, molecular volume and the acyl chain length, different lipid species favour different packing geometries, such as spherical micelles, globular or rod-like aggregates and bilayers. The lipid bilayer is the key structural motif of biomembranes. Nature's use of biomembranes makes the diversification of life possible. Membranes act as barriers between living entities and the hostile environment. They enable the cell to organize space into different compartments, and they serve as sites for essential biochemical functions.

1.2 Experimental Studies

Biomembranes are complex systems containing a large number of different lipid and protein molecules. In order to gain insight into the functionalities of such a complex system, a good starting point is to study simple model lipid bilayers containing a few components. A large number of experimental studies using different techniques have been performed on these model systems, among them differential scanning calorimetry (DSC), nuclear magnetic resonance (NMR), fluorescence depolarisation, fluorescence resonance energy transfer (FRET), X-ray diffraction, neutron-scattering, freeze-fracture, infrared and Raman spectroscopy and micromechanics. The results of some of these studies are summarized below.

1.2.1 Single-component Lipid Bilayers

In a saturated lipid chain, free rotations are permitted about each C-C bond. The rotational energy spectrum of a C-C bond (Fig. 1.5) exhibits three energy minima. The ground state that corresponds to the lowest energy of the spectrum is the *trans* configuration. The other two minima are degenerate and are known as *gauche* configurations. The conformational order of an acyl chain is measured by the number of *trans* bonds in the chain. A chain in the all-*trans* configuration contains only *trans* bonds and has the highest conformational order. On the other hand, every addition of a *gauche* bond renders the chain more disordered.

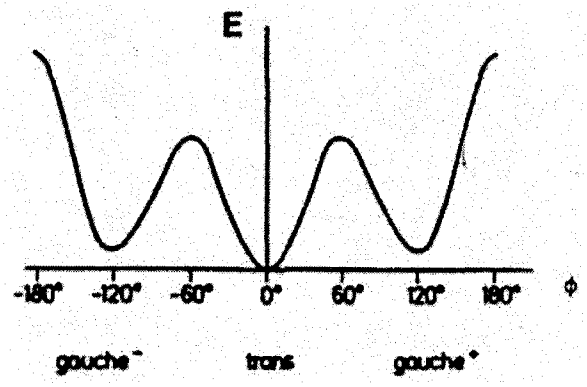

Figure 1.5 **Rotational energy spectrum of a C-C bond in an acyl chain. The angle ø is the rotation angle from the *trans* configurations.**
Reproduced from reference [62] with permission of the author.

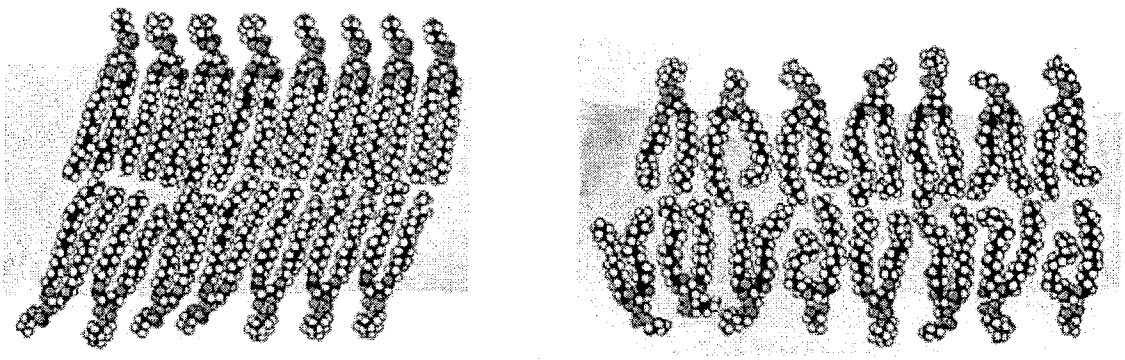

Figure 1.6 **The main transition of lipid bilayers which takes the bilayer from the lamellar gel phase (left) to the liquid-crystalline phase (right).**
Reproduced from reference [95] with permission of the publisher.

The most striking phase property of single-component phospholipid bilayer systems is what is known as the main transition, which occurs at a temperature T_m. The main transition takes the bilayer from a lamellar gel phase to the liquid-crystalline phase (Fig. 1.6). The lamellar gel phase exists below T_m and is characterized by conformationally ordered chains and a lateral quasi-crystalline structure. At temperatures above T_m, the lamellar liquid crystalline phase contains conformationally disordered acyl chains and is characterized by high lateral diffusion of molecules in the plane of the bilayer. In other words, the main transition involves what is known as *chain melting* (i.e.,

the chains become conformationally disordered) as well as the melting of the lateral crystalline structure. This results in a reduction in thickness and an increase in the cross-sectional area of the bilayers.

Despite extensive studies, the nature of the main transition remains elusive. The main transition is characterized experimentally by a latent heat and a narrow specific-heat peak. However, no experimental observation demonstrates the discontinuities in any thermodynamic or thermomechanic property. Instead, all such properties, like membrane area, acyl chain order parameters and membrane thickness, vary in a continuous, although dramatic, fashion through the transition. This has led to the proposal that the main transition is pseudo-critical [54, 55, 78, 79], i.e., in principle of first order but very close to a critical point and consequently strongly dominated by thermal fluctuations. For detailed analysis and discussions on the nature of the main transition please see [11, 54, 55, 78, 79, 105].

The top left hand corner of Fig. 1.8 (0 mol% cholesterol) shows the differential scanning calorimetry (DSC) scans of single-component DPPC-d_{62} bilayers [12]. The main transition is signified by a peak at 37.75°C (which is 4°C lower than the T_m of DPPC bilayers due to the deuteration). As the figure shows, single-component lipid bilayers also exhibit other transitions besides the main phase transition, such as the subtransition near 14°C and the pretransition near 30°C. However, they have relatively insignificant transition enthalpy as compared to the main transition. In this thesis, we shall only concentrate on the main phase transition.

The dominant lipid-lipid interaction affecting the main transition is the van der Waals interaction between the acyl chains. Therefore, the main transition temperature T_m

and the latent heat of transition are strongly dependent on the acyl chain length of the particular lipid species. Longer chain lengths result in higher T_m and larger latent heat of transition. Nevertheless, a variety of other factors also affect the main transition temperature of single-component lipid bilayers, such as the level of saturation of the acyl chains, the conformation of double bonds (i.e., *trans* or *cis*) in the chain, and the polarity and size of the headgroups.

1.2.2 Binary Lipid/sterol Bilayers

The next level of complexity beyond the single-component lipid bilayer is the binary lipid mixture. In phospholipid/cholesterol bilayers, cholesterol is intercalated in the membrane parallel to the phospholipid hydrocarbon chains (Fig. 1.7). The effective length of cholesterol has been estimated to correspond to a 17-carbon all-*trans* hydrocarbon chain [93]. The sterol tetracyclic ring structure is estimated to lie in close proximity to the phospholipid carbons in positions 2 to10. This has a tendency to hinder the formation of *gauche* bonds especially in the upper part of the hydrocarbon chains, which imposes ordering along the entire phospholipid chain.

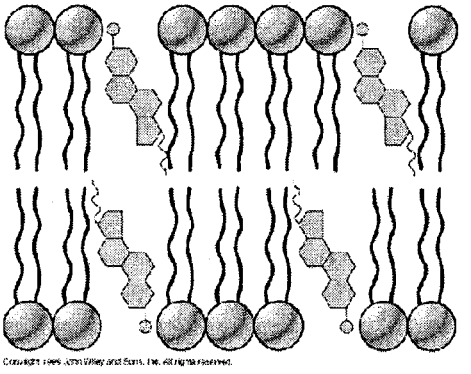

Figure 1.7 Cholesterol in a lipid bilayer.
Reproduced from reference [104] with permission of the publisher.

As discussed above, cholesterol is one of the most important components of vertebrate biomembranes. It is therefore not surprising that binary systems containing cholesterol are studied extensively. In light of the formation of cholesterol-rich domains with possible connection to "rafts", the miscibility of cholesterol with other lipids is currently of special interest. A general consensus among these studies is that, in the liquid-crystalline phase, the addition of cholesterol leads to a dramatic increase in the conformational order of the acyl chains of the phospholipids and an increase in the mechanical strength of the bilayer, while having little effect on their molecular translational and rotational motions [12, 94].

Fig. 1.8 shows the DSC data from Vist and Davis [12] of chain-perdeuterated dipalmitoyl phosphatidylcholine (DPPC-d_{62}) bilayers with cholesterol concentrations from 0 to 22.5 mol%. It is observed that cholesterol at low concentrations broadens the main phase transition and slightly decreases the T_m. Similar DSC studies by Chapman *et al.* [13] show that at, 50 mol%, cholesterol eliminates the main phase transition and stabilizes the overall liquid phase of the bilayer. Furthermore, ^{2}H-NMR studies from Vist and Davis [12] show that the addition of cholesterol increases the average degree of orientational order of the fluid phase of the bilayer. In fact, the simultaneous occurrence of a liquid-crystalline phase and high acyl-chain order signifies the presence of a new phase—the **lo** (liquid-ordered) phase, which was postulated to exist in membrane "rafts", as previously discussed. The notation that is often used to describe the phase properties of lipid-cholesterol bilayers has the first letter referring to the lateral organization (**s** for solid and **l** for liquid) and the second letter referring to the acyl chain conformational order (**o** for order and **d** for disorder). The solid-ordered (**so**) phase is equivalent to the

gel phase and the liquid-disordered (**ld**) phase is equivalent to the liquid crystalline phase of single-component lipid bilayers.

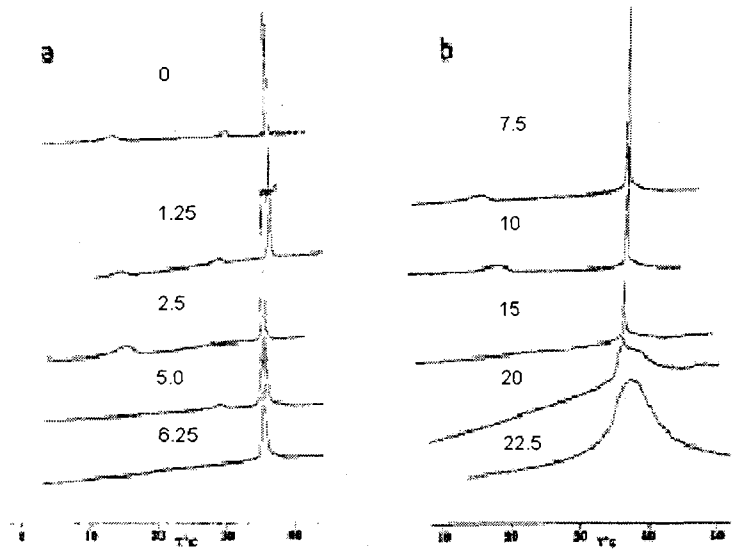

Figure 1.8 **Differential scanning calorimetry traces for DPPC-d_{62} bilayer containing different concentrations of cholesterol [12].**
The respective concentrations of cholesterol in mol% are, from top to bottom (a) 0, 1.25, 2.5, 5.0, 6.25, (b) 7.5, 10, 15, 20, 22.5. (Note that the T_m of the main phase transition of the 0 mol% cholesterol of chain-perdeuterated DPPC-d_{62} is about 3.5°C lower than the T_m of DPPC bilayers) Reproduced from reference [12] with permission of the publisher.

Ergosterol is the counterpart of cholesterol in fungi, yeast and protozoans and has a very similar effect in ordering the lipid bilayers. Fig. 1.9 shows the ^{2}H-NMR spectrum of DPPC/ergosterol bilayers at 42°C as a function of ergosterol concentration by Thewalt *et al.* [14]. The spectra of the bilayers with up to 5 mol% ergosterol exhibit pure **ld** phase. With increasing ergosterol concentration the average spectral width increases and the individual peaks broaden. At 27.5 mol% ergosterol, the individual peaks become sharper and remain sharp at higher ergosterol concentration. These spectra correspond to pure **lo** phase in the bilayers. The high conformational order of the lipid chains in the **lo** phase is evidenced by the spectral width of the Pake doublets (e.g., 107000 s^{-1} for 27.5 mol% erg)

nearly double that of the **ld** phase (e.g., 56000 s^{-1} for pure DPPC). Moreover, for ergosterol concentrations between 10 mol% and 25 mol%, the broadening of the individual doublets in the spectrum suggests an **ld+lo** phase coexistence. The DPPC/ergosterol phase diagram derived from these data is nearly identical to the DPPC/cholesterol phase diagram discussed below.

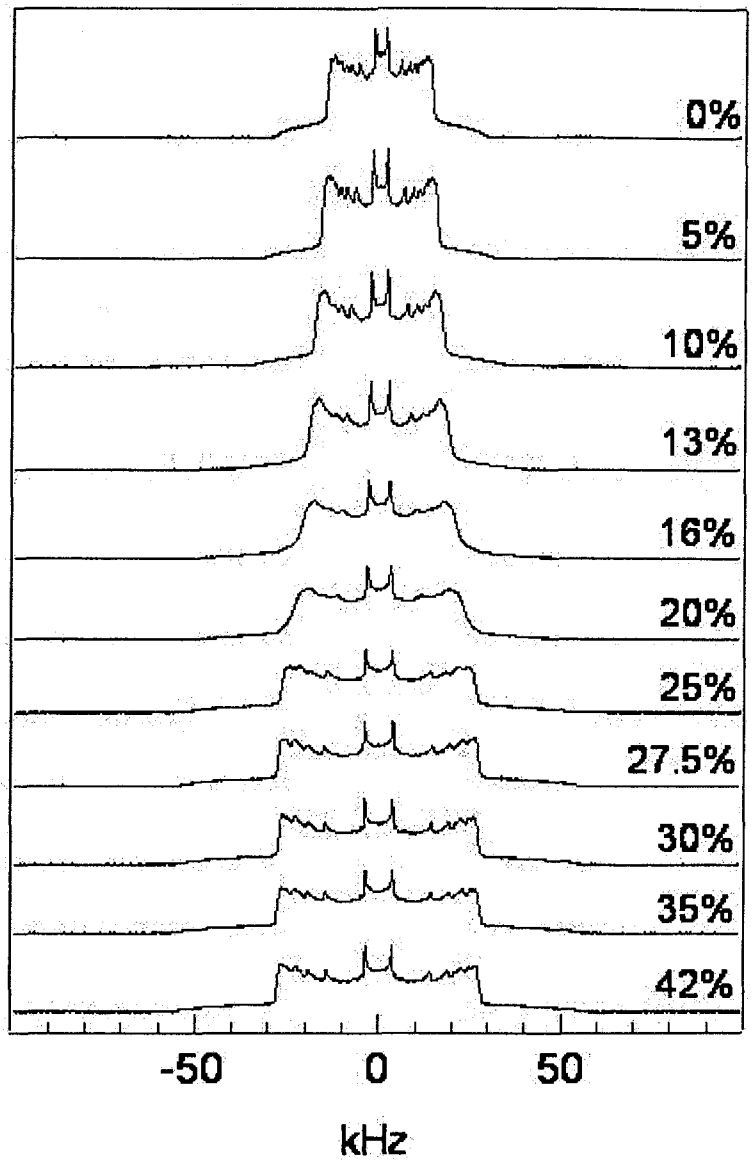

Figure 1.9 **^{2}H-NMR spectra of DPPC-d_{31} and ergosterol bilayers at 42°C as a function of ergosterol concentration [14].**

The experimental phase diagram of DPPC/cholesterol bilayers is shown in Fig. 1.10 [15]. The principle features of the phase diagram include three separate two-phase regions (**ld-so**, **ld-lo** and **so-lo**) and a three-phase line between the **so-lo** and **ld-lo** coexistence regions. In summary, the effects of cholesterol in phospholipid bilayers are the elimination of the phase transition at higher concentrations and the concomitant appearance of the **lo** phase. This results in an increased thickness and mechanical strength of the bilayer while maintaining the "fluid" environment conducive to high lateral mobility that is essential to physiological functions.

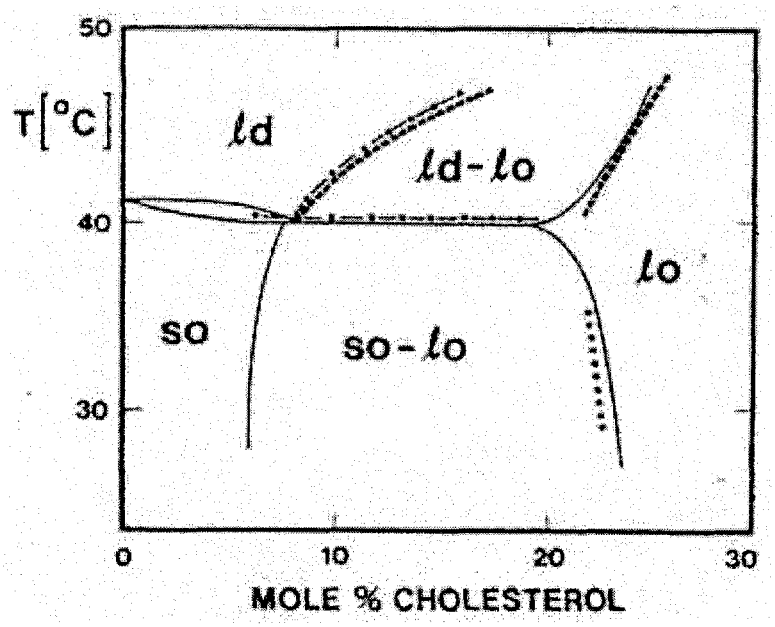

Figure 1.10 **Phase diagram for DPPC/cholesterol bilayers fitted from various experimental data by Ipsen *et al.* [43].**
The phases are denoted by so (solid-ordered), ld (liquid-disordered) and lo (liquid-ordered). Reproduced from reference [43] with permission of the publisher.

1.2.3 Binary Lipid/lipid Bilayers

Thermodynamic studies have clearly demonstrated that saturated phospholipids with the same head group but different hydrophobic chain lengths do not mix ideally.

Different interactions between like species and unlike species result in a preferential arrangement of nearest neighbours in the bilayers. Therefore, in binary systems containing two different phospholipids, lateral phase separations and non-ideal behaviour are observed. Fig. 1.11 shows the phase diagram of DLPC/DPPC bilayers from infrared-spectroscopic studies by Silvius *et al.* [16]. S_1 and S_2 represent the existence of the **so** phase of DLPC and DPPC respectively, where L represents the presence of an **ld** phase. One interesting feature to note is the essentially flat solidus line which indicates the occurrence of solid-solid phase separation up to roughly 60 mol% DPPC.

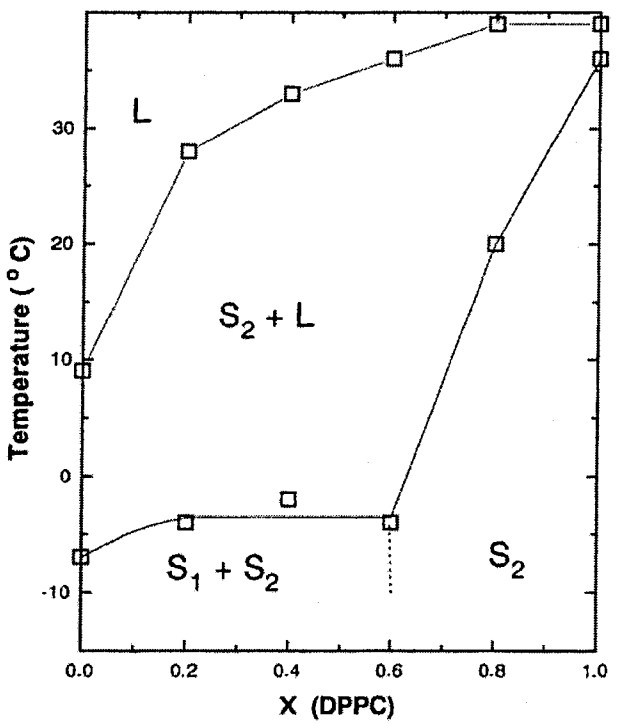

Figure 1.11 IR-derived phase diagram of binary DLPC/DPPC bilayers. S_1 and S_2 represent the existence of two distinct so phases, and L refers to the existence of an ld phase. Reproduced from reference [16] with permission of the publisher.

1.2.4 Ternary Lipid/lipid/sterol Bilayers

From the results of the treatment of biomembranes with detergent like Triton X-100, it is hypothesized that the detergent-resistant 'raft' fraction is probably in an ordered phase (**lo** or **so**), while the soluble fraction is in the **ld** phase. Therefore, in order to model lipid rafts in as simple a system as possible, experiments are usually designed for a ternary mixture which includes three lipid components: a low T_m lipid (usually a PC), a high T_m lipid (a saturated PC or sphingolipid), and cholesterol. In these experiments, it is found that cholesterol at concentrations between 10 to 50 mol% promotes **lo-ld** phase separation. The **lo** phase is enriched in the high T_m lipid and cholesterol, while the **ld** phase is enriched in the low T_m lipid. On the other hand, high concentrations of cholesterol (50 mol%) are found to promote homogeneous intermixing of the lipid components and hence the formation of a unique **lo** phase.

Recent fluorescence microscopic studies using giant unilamellar vessels (~30μm radius) on a variety of ternary mixtures containing high T_m lipid, low T_m lipid and cholesterol were performed by Veatch *et al.* [17]. Their results show that most of these mixtures exhibits micron-scale lipid domains segregation. For instance, with the DPPC/DOPC/Cholesterol system, they observed two coexisting phases over a wide range of lipid composition and temperature, with one phase rich in the unsaturated lipid and the other rich in the saturated lipid and cholesterol. However, the micron-scale inhomogeneities are found to vanish when levels of cholesterol comparable to those found in mammalian cell plasma membranes are incorporated and when the system approaches physiological temperature ($\geq 30^{\circ}C$).

Fourier-transform infrared-spectroscopic (FTIR) studies on ternary systems containing protonated DLPC, chain-perdeuterated DPPC and cholesterol (Fig. 1.12) were performed by Silvius *et al.* [16]. The details of this experiment will be presented in Chapter 7 and compared to our simulation results. In summary, the experiment reveals that cholesterol at lower concentrations in the bilayer modifies the resolved thermal melting profiles for both PC components and, at higher concentrations, produces a convergence of the thermal transitions for the two PC species. Furthermore, fluorescence-quenching measurements, which probe inhomogeneity on a distance scale of the order of nearest-neighbour separations (~1 nm), have been performed by the same group on similar ternary systems containing physiological concentrations of cholesterol. Interestingly, the results show that the system exhibits inhomogeneous lateral organizations of lipids even at physiological temperatures, where the large (micron-sized) domains are observed to vanish in the fluorescence microscopic studies by Veatch *et al.* [17], as discussed above.

A recent study employing Fluorescence Resonance Energy Transfer (FRET) by Silvius [18] was able to detect inhomogeneities in the lateral organization of lipids on an intermediate scale of distances (tens of nanometers or greater) as compared to the above two experiments. His results indicate that at 37°C, for bilayers combining saturated phospho- or sphingolipids with unsaturated phospholipids and physiological proportions of cholesterol, the FRET assay gives strong indications of an inhomogeneous lateral organization on a spatial scale of tens of nanometers or greater. Combined with the results from the two experiments discussed above, this work suggests that the lipid domains detected with FRET may have a dimension of at least tens of nanometers but

considerably less than one micron. This result is significant because it shows that model lipid bilayers whose compositions approximate that of the outer leaflet of mammalian cell plasma membranes can exhibit domain organization on a spatial scale similar to the inferred dimensions of lipid rafts (at least tens of nanometers but less than one micron in size) in biological membranes at physiological temperatures.

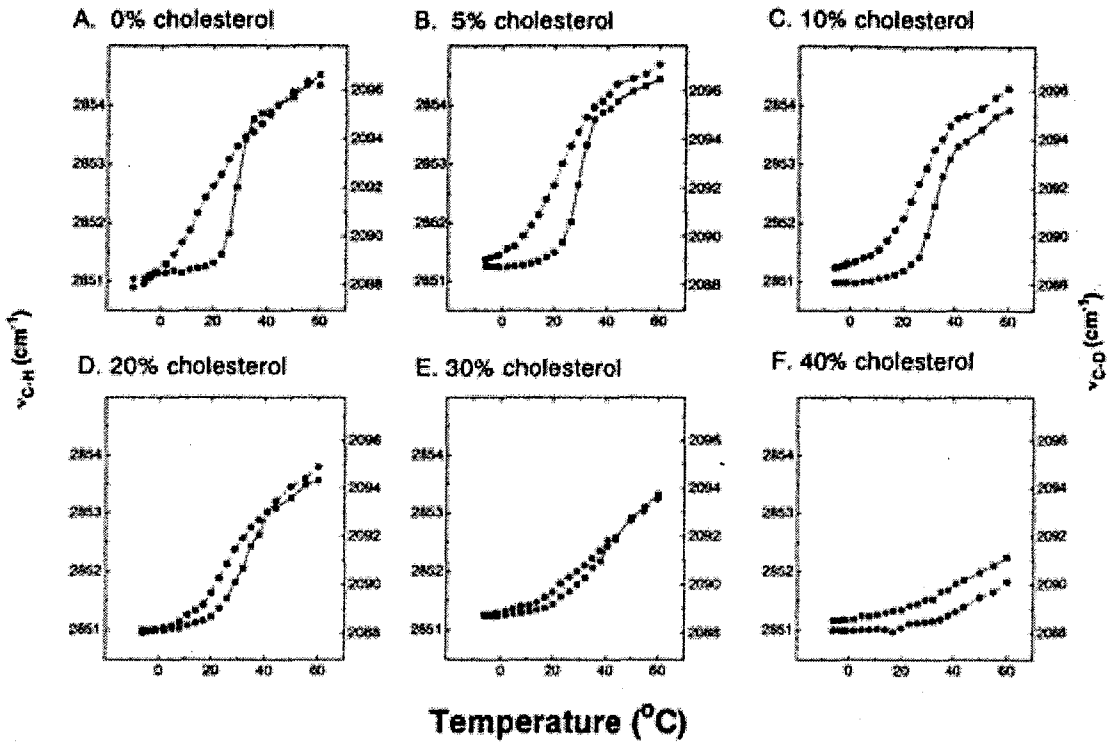

Figure 1.12 **Frequency shift of the methylene symmetric stretching mode with temperature, for DLPC/DPPC-d_{62} mixtures (40:60 molar ratio) containing increasing molar percentages of cholesterol.**
(•) C-H stretch; (■) C-D stretch. Reproduced from reference [16] with permission of the publisher.

1.3 Theoretical Studies

In the last few decades, a large number of theoretical studies on bi- and monolayers of biologically interesting lipids have appeared in the literature. In particular, there has been considerable progress in the development and application of computer

simulations to the study of model membranes. Atomic simulation techniques have developed to the point that it is possible accurately to model phospholipid membranes, demonstrating their potential in supplying the missing details of the molecular picture of lipid bilayers. In the following, we briefly describe some of the recent development of the theoretical models of lipid membranes, especially focusing on computer simulation studies. Different theoretical studies are categorized under the following headings: phase behaviour of lipid systems, structure of the **ld** phase, and lipid/sterol bilayers. Details of the models that are used in this thesis are also given in Chapter 2.

1.3.1 Phase Behaviour of Lipid Systems

Some of the early phenomenological models for lipid systems developed in the 70s include the nematic molecular field theory of Marčelja [19], the lattice-gas model of Nagle [20, 21] and the two-state lattice model of chain melting of Doniach [22,23]. Marčelja [19] developed the nematic model based on his previous work on liquid crystals. The dominant interaction was taken to be the anisotropic part of the attractive van der Waals interaction between the hydrocarbon chains. The molecular-field approximation was applied in order to solve the resulting statistical problem. His calculations of the pressure-area relationship of PC monolayers at constant temperature were in good agreement with measurements by Phillips and Chapman [24]. In his lattice gas model, Nagle [20, 21] approximates a monolayer of hydrocarbon molecules of finite length by a single planar sheet of chains of infinite length. His model yields exactly solvable solutions and the results demonstrate that a first order phase transition is possible in a simple order-disorder model. Doniach's [22, 23] two-state lattice model is a

model that includes the essential features (the excluded volume effect, the attractive van der Waals interaction between molecules and rotational isomerism) of chain melting in lipid mono- and bilayers. He assumes that the molecules are in one of two conformational states, one of which corresponds to an ordered state and the other to a combination of all disordered configurational states. The use of his model in the mean-field approximation allows calculation of the chain-melting transition temperature and the heat of transition and is useful for estimating trends in the thermodynamic and fluctuation properties of the bilayer in the phase transition region.

In addition to applying different analytical approximations in the process of model making, such as those described in the examples above, a second level of analysis is usually invoked in order to derive the properties of a given model. Some of these analyses come in the form of computer simulation techniques such as the Monte Carlo method and the molecular dynamics method.

The Metropolis Monte Carlo simulation method is one of the principle methods for providing information about the equilibrium lateral distribution of the lipid molecules in a given system. Using a limited set of parameters derived from experimental data, the Monte Carlo method can be used to simulate physical properties, the response functions, as well as to obtain the microconfigurations of the system. Below is a brief description of the Monte Carlo simulation studies performed by several groups on lipid mono- and bilayer systems.

Mouritsen *et al.* [25] adapted the 10-state model of Pink [26] for the description of the main phase transition of diacyl phosphatidylcholine (DPPC) bilayers in terms of the acyl-chain conformational degrees of freedom. Calculations were performed with

Monte Carlo simulations which gave system properties such as the specific heat, the lateral compressibility, the lipid-domain size distribution as well as the snapshots of the system. Jørgensen *et al.* [50] modified the 10-state Pink model such that it could be applied to bilayers containing two different PC lipids. The details of the Pink model and the model by Jørgensen *et al.* are presented in Chapter 2.

Sugár *et al.* [29] employed the Doniach two-state lattice model in the canonical ensemble to study single-component as well as binary phospholipid bilayers. Their studies reveal that the **so-ld** transition is a continuous transition for DMPC, DSPC, and all DMPC/DSPC mixtures. Moreover, detailed cluster analysis on the DMPC/DSPC system allows them to make correlations between the cluster size, the population of the clusters, the temperature and the system size [30]. They found that, depending on the temperature and mole fraction, the population of the cluster size is either homogeneous or inhomogeneous. In the inhomogeneous population the size of the largest cluster scales with the size of the system, while the rest of the clusters remain small with increasing system size. In a homogeneous population, however, every cluster remains small with increasing system size. Their results agree with those of small-angle neutron scattering measurements, indicating the non-random lateral distribution of the components exists not only in the gel-fluid mixed phase region, but also in the pure gel and pure fluid regions. Heimburg's group also used the two-state Doniach model in their MC simulations of lipid mono- and bilayers [31]. The Ferrenberg and Swendsen histogram method was applied to their numerical data in order to generate quasi-analytical fits for experimentally obtained heat capacity profiles of DPPC vesicles. Their analysis showed

that a fixed mean bilayer curvature results in a broadening of the bilayer melting profiles. Furthermore, the same method was also used to obtain the chain melting behaviour of simple lipid-peptide mixtures.

Other than MC simulations, the properties of the **ld** phase and the main transition of phospholipid bilayers are also investigated by Whitmore *et al.* [32] using a lattice-based self-consistent field (SCF) theory. Their theory is based on a microscopic picture of the system, with the formalism built on an expression for the partition function for the lipid/solvent mixture which takes into account the hard core repulsion between submolecular units, the long range interaction between them, and the energy due to the sequence of *trans* and *gauche* isomers in each chain. The anisotropic effective field that arises from the above interactions is essential to the modelling of the main transition. In the computational aspect of their theories, the fields, the particle and bond density distributions, free energy and other equilibrium quantities are all calculated self-consistently. Their model exhibits a first order phase transition, and yields quantities such as the equilibrium thickness of the bilayer, the average orientational order parameter in the **ld** phase, and the change in density and entropy in passing through the main transition, which are in reasonable agreement with the experimental data of DPPE. Moreover, microscopic theories such as the SCF theory can also provide a detailed microscopic picture of the system that is not directly available from experiments.

1.3.2 Structure of the ld phase

Cantor *et al.* [33] developed a lattice statistical thermodynamic model of chain packing for lipid monolayers. Their model is based on the model by Scheutjens and Fleer

[34], which incorporates both translational and configurational degrees of freedom of the chains, and the energies of interaction among chain segments, water and solvent. In addition, Cantor's group attempts to account for the effects of orientational anisotropy on the placement of chain segments by including, among other effects, intramolecular correlations among nearest-neighbour segment positions due either to covalent bonds or to intramolecular nonbonded contacts. Their model leads to a set of nonlinear equations, which, when computed numerically, yield predictions of structural properties such as the segment and bond distributions as a function of surface density.

A number of molecular dynamics (MD) simulations have been performed by different groups on fully hydrated DPPC bilayers in the **ld** phase. In general, simulations are performed on systems containing of the order of a hundred lipid molecules and a few thousand water molecules, on a time scale that ranges from a few hundred picoseconds to a few nanoseconds. Different thermodynamic ensemble and different interaction models can be used to extract different results. For instance, Tieleman and Berendsen [37] performed a comparative study on DPPC bilayers under constant pressure, constant volume, and constant surface tension boundary conditions respectively, along with different force fields and different water models. They were able to determine the influence of these variables on a number of properties of bilayers such as the equilibrium box sizes of the simulation, density profiles across the interface, electrostatics, hydration of the lipid head groups, diffusion behaviour, and order parameters.

On the other hand, Pastor *et al.* [35] used the constant normal pressure and fixed surface area (NPAT) ensemble in their MD simulations for DPPC bilayers. This was in order to determine the values of surface area per molecule, A_o, which produced quantities

such as the deuterium order parameter and the electron density profiles that best fit those obtained from NMR and X-ray scattering experiments. Their results indicated that A_o=62.9Å is their best choice.

Using the structure of lipid bilayers from x-ray studies as the initial configurations of their MD simulations, Scott *et al.* [40] found that, upon heating, the **ld** phase of the system emerges. Even though the parameters, initial conditions and boundary conditions used do not require the bilayers to assume the characteristics of the fluid phase. Information such as the surface area per phospholipid molecule and the origin of the measured dipole potential were obtained. Their results also confirm the concept that, for appropriately matched temperature and surface pressure, a monolayer is a close approximation to one-half of a bilayer.

Recently, Klein *et al.* [38; 39] developed a coarse grain (CG) model to be used in his MD simulations of lipid bilayers. In his CG model, instead of accounting for every single interaction among different atoms, simplified representations for water, alkanes and phospholipid molecules were used, which interact in an effective way. The CG model was shown to be about four orders of magnitude less demanding of CPU time and to yield results which compare reasonably well with an all-atom model. The density profile of the DMPC bilayer in the **ld** phase has been produced semi-quantitatively, and simulations of its self-assembly from a homogeneous initial state has been performed.

In addition to being useful in the investigations of the structural properties of lipid bilayers, MD simulations can also be used to examine the dynamical properties of these systems. A MD simulation of a DPPC bilayer for a relatively long time scale of 10-ns was performed by Berkowitz *et al.* [41]. They found that the large contribution of the

dipole potential due to the slow movement of the headgroup is compensated by the fast movement of the water molecules which leads to an almost constant total dipole potential. Moreover, the lateral diffusion coefficient and rotational diffusion coefficient calculated from their simulations were found to be in good agreement with experiments such as neutron scattering.

1.3.3 Lipid/Sterol Bilayers

In order to formulate a model for lipid/cholesterol bilayers, Ipsen *et al.* [42, 43] pointed out that the phase behaviour of DPPC-cholesterol mixtures can be rationalized using some basic assumptions: (i) Cholesterol interacts favourably with DPPC chains in an extended conformation, (ii) the main transition of single-component lipid bilayers is related to changes in translational variables as well as acyl-chain conformational variables, and (iii) cholesterol disturbs the translational order in the **so** state. The theoretical consequences for the thermodynamics of the mixture were derived using a phenomenological thermodynamic model as well as a multi-state Pink model in the mean field approximation, which is extended to account for crystallinity using Potts variables. The authors show that a minimal model of this type is able to explain the experimental thermodynamic data such as specific heat, the hydrophobic thickness of the bilayers, as well as the phase diagram.

A simpler version of this model is used by Cruzeiro-Hansson *et al.* [28] to study the effects of cholesterol on lipid-domain interfacial area for low concentrations of cholesterol (<10 mol%). Their model is based on the 10-state Pink model but extended to account for the interactions between lipids and cholesterol. Their calculations show that

cholesterol at low concentrations increases the interfacial area and tends to accumulate in the interfaces of the **so** and **ld** domains.

However, one shortcoming of this type of model is its lattice description. Experiments and previous approximate theories suggest that cholesterol incorporated into lipid bilayers has different microscopic effects on lipid-chain packing and conformations, and thereby leads to the decoupling of the two ordering processes. The two state off-lattice model developed by Nielsen *et al.* [44] is a microscopic model that takes into consideration this decoupling behaviour. It is based on a two-dimensional random triangulation algorithm, in which lipid and cholesterol molecules are represented by hard-core particles with internal (spin-type) degrees of freedom with nearest-neighbour interactions. Phase properties of the system calculated using MC simulations give a consistent interpretation of the various phases of phospholipid/cholesterol binary mixtures and a phase diagram consistent with experimental observations. Both Ipsen's and Nielsen's models can be adapted to binary systems containing different sterols, such as lanosterol, by simply changing the lipid-sterol interaction parameters.

Using MC simulations to calculate the order parameter profiles of lipid chains interacting with cholesterol, Scott *et al.* [45] found that cholesterol acts to significantly decrease the ability of neighbouring chains to undergo *trans-gauche* isomeric rotations. These results are then used as a guide to develop a theoretical model for lipid/cholesterol mixtures, which allows them to predict the phase properties of the mixture and to investigate the molecular mechanism behind the observed phase behaviours. Furthermore, the same group [46, 47] has recently developed a new hybrid equilibration and sampling procedure for the atomic level simulation of the DPPC/cholesterol bilayer.

Long MD runs were interspersed with configurational bias MC runs to ensure equilibrium and enhance sampling. Bilayers containing different lipid to cholesterol ratios were studied, which enable the authors to determine physical quantities such as the cross-sectional area of cholesterol and that of DPPC molecules in the **lo** phase. Moreover, analysis of the lateral distribution of cholesterol molecules suggests tendencies for small subunits of one lipid plus one cholesterol, hydrogen-bonded together, to act as one composite particle, and perhaps to aggregate with other composites. Their results were shown to be consistent with experiments, which include the condensation effect of cholesterol and the tendency of cholesterol-rich domains to form in lipid/cholesterol bilayers.

MD simulations of cholesterol effects in DPPC bilayers were studied by Klein *et al.* [48]. A 1.4-ns constant temperature and pressure MD simulation of DPPC bilayer containing 12.5% cholesterol at 50°C were performed and compared with previous simulations of single-component DPPC bilayer under the same conditions. They found that the addition of cholesterol to the bilayers leads to an increase in the lamellar spacing and a decrease in the bilayer area. Furthermore, cholesterol was also found to affect the structure and electrical properties of the membrane/water interface, the subnanosecond time scale motions of whole lipid molecules, and the dynamics of conformational rearrangements in the bilayer interior.

MD simulation studies of DPPC/cholesterol bilayers were also by performed Berkowitz *et al.* [49]. Two different ratios of DPPC: cholesterol (8:1 and 1:1) were studied. Their results show that addition of cholesterol to membranes results in a condensing effect: the average area of membrane becomes smaller, hydrocarbon chains

of DPPC have higher order, and the probability of *gauche* defects in DPPC tails is lower. In the simulations of the DPPC: cholesterol (1:1) bilayers, two different initial arrangements of cholesterol were tested. In structure A, cholesterol molecules alternate with DPPC molecules, so that nearest-neighbour interactions occur between DPPC and cholesterol molecules. In structure B, strips of cholesterol molecules are placed between strips of DPPC molecules, so that interactions between like molecules (DPPC: DPPC or cholesterol: cholesterol) are predominant. In structure A the membrane area continued to drift slowly even during the last 1 ns of simulation rather than converging to a constant value, as in structure B. This indicated that structure A is in a metastable state. Furthermore, it is found that structure B attained higher order than structure A. This and several other properties investigated suggest that structures with cholesterol-rich domains are more favourable at high cholesterol concentrations, while membranes with a uniform cholesterol distribution are in a metastable state. However, the author also indicated that the simulation time of 2-ns is not sufficiently long to test this hypothesis directly.

It should be stated at this point that the MD simulations discussed above for lipid bilayers cannot as yet be applied to the phase behaviour of these systems because of computer time and therefore system size constraints. However, these calculations provide invaluable information as to the short-range interaction effects between bilayer components. For example, the work of Berkowitz *et al.* [49] suggests that cholesterol does indeed order neighbouring lipid chains. This is the rationale for using model systems in conjunction with the Metropolis Monte Carlo method in this thesis. This method is guaranteed to approach equilibrium as detailed balance is incorporated in the algorithm.

1.3.4 An Overview of the Theoretical Studies

Single-component Lipid Bilayers

The early lattice models for these systems were examined in molecular field theory (with the exception of Nagle's model) and were used to estimate trends in thermodynamic properties. For example, Doniach [22, 23], in analysing his two-state lattice model in the mean field approximation, was able to conclude that the main phase transition at T_m was a first order phase transition close to a critical temperature, T_c. However, the parameters need to be changed in value when thermal fluctuations are included. In this case, the value of T_m is known exactly but the value of T_c changes considerably as is well known. Heimburg [31] simulated Doniach's model using the Metropolis Monte Carlo technique with only one unknown parameter, this being the interaction between the "gel" and the "fluid" states. He obtained values of this parameter by fitting to experimental specific heat data for DPPC-bilayer systems and thereby predicted that DPPC multibilayers exhibit a well-defined first order phase transition at T_m, whereas there is no phase transition in the case of small unilamellar vesicles of DPPC. In the case of the 10-state Pink model, the unknown parameters were found by fitting mean field results to thermodynamic data for DPPC. The model was easily extended to experimental data for all saturated PCs with chain length from m=12 to m=22 where m is the number of carbon atoms per acyl chain. The mean field equations give a first order phase transition for all these values of m and the thermodynamic properties agree quite well with experimental data. However, Metropolis Monte Carlo simulations of the Pink model with the same data predicts that there is no main phase transition for m<20, whereas a well defined phase transition exists for m≥20. However, for m<20, the

MC simulation data exhibit a "bump" in the response function and the change in specific heat is in good agreement with experimental data for all values of $m<20$. Hence, there is no consensus from the theory as to the nature of the phase transition for m less than or equal to 20.

Binary Lipid/Lipid Bilayers

Sugár *et al.* [29] use the MC technique and a lattice model similar to that of Heimburg to obtain the analogous parameters for binary lipid bilayers. From this data they predict the cluster distribution in the phase-separated region which, as stated above, give good agreement with neutron scattering data. No prediction is made as to the nature of the phase behaviour even though one would expect the fitted parameters to give well-defined phase separation. Mondat [115] used the Pink model for binary mixtures in the molecular field approximation to predict the phase diagrams and specific heat of DMPC/DPPC bilayers and DMPC/DSPC bilayers. The only unknown parameter was the constant for the van der Waal's interaction between unlike lipid chains and the ansatz described in Ch. 6 was used. The agreement with experiment was certainly good qualitatively, but not perfect quantitatively. Jørgensen *et al.*[50] and later Risbo *et al.* [68] used the extension of the same model in MC simulation and found excellent agreement with experimental results. The only additional term was a mismatch interaction between unlike lipid chains whose interaction constant was independent of chain lengths, as required. There are no approximate calculations available for this model.

Binary Lipid/sterol Bilayers

As stated above, Ipsen *et al.* [43] used a modified Pink model in conjunction with a Potts model in the molecular field approximation to examine the phase behaviour and specific heat data of DPPC-cholesterol bilayers. Values for the parameters of the model were obtained by fitting to experimental data for low cholesterol concentrations and resulted in a good fit to specific heat data. Furthermore, a phase diagram which agreed reasonably with experimental results from ^{2}H-NMR and calorimetry was also generated. No exact solutions were derived for this model and it was pointed out that the model did not give a good description of the **lo** phase. A restricted version of this model was examined by Mouritsen and Cruzeiro-Hansson [28], both in mean field and via MC simulations. This model was valid only at low cholesterol concentrations and the extension of this model to higher concentrations is one of the aims of this thesis. This is described in detail in Ch. 5. As noted above, the **lo** and **ld** phases are both fluid phases whereas the **so** phase is usually regarded as a solid phase. The lattice models of Ipsen *et al.* and Mouritsen and Cruzeiro-Hansson cannot be used to describe this situation. Nielsen *et al.* [44], therefore, used the MC method to simulate an off-lattice version of the Doniach model in order to examine the phase behaviours of lipid-cholesterol and lipid-ergosterol bilayers. By fitting to ^{2}H-NMR data, Nielsen *et al.* were able to obtain values for various interaction parameters. This model afforded a theoretical understanding of the phase behaviours with predictions for the nature of the **lo** phase. No approximate calculations exist for this model. Also no multi-state model of this type exists at present. However, we hope that the results of this thesis will act as a guide to the creation of such a model.

The structure of the **ld** phase in single component lipid bilayers has been the subject of several molecular dynamics (MD) simulations and agreement with experimental data for calculated physical properties is continually improving. Recently MD simulations by Jensen *et al.* [116] have confirmed the presence of a pressure profile in lipid bilayers perpendicular to the bilayer plane. This profile was previously predicted by the self-consistent field calculations of Cantor [33] using a packing model of the Scheutjens-Fleer [34] type. MD simulations of Klein *et al.* [48] confirm the "rigidifying" effect of cholesterol on lipid acyl chains and the MD simulations of Berkowitz *et al.* [49] predicted that DPPC/sterol mixtures have the same value for the ^{2}H-NMR order parameter at 11 mol % sterol for cholesterol, ergosterol and lanosterol, as recently found experimentally in a similar system [116].

1.4 An Overview of This Thesis

The primary interest of this thesis is to investigate the effects of sterols on the physical properties and phase behaviour of binary and ternary lipid/sterol bilayers. The model that we used for the lipid/sterol interactions is a modified version of the 2d minimal lattice model of Cruzeiro-Hansson and Mouritsen [28]. This model was originally applied to the case of lipid/sterol bilayers at low sterol concentrations (<10 mol%) [27, 28]. In this thesis, we modified the model by increasing the interactions between sterol molecules and lipid chains in conformations which we proposed to be predominant in the liquid-ordered (**lo**) phase in reality. This change leads to the

emergence of **lo**-like phases in our modified model which gives a much improved description of bilayers with high sterol concentrations in contrast to the original model. Monte Carlo simulation methods were then used to calculate the physical properties, the response functions, and to obtain snapshots of microconfigurations of the system. In this chapter, we described the importance of sterols in lipid biomembranes, and gave an overview of a selection of previous experimental and theoretical studies on biomembranes and model lipid systems. Chapter 2 contains a description of major developments in the modelling of the phase behaviour of lipid mono- and bilayers. In particular, detailed descriptions of the models which are used in this thesis are given in the following order: the 10-state Pink model for single-component lipid bilayers, the Cruzeiro-Hansson and Mouritsen model for lipid/sterol bilayers and our modified version for such systems with high cholesterol concentrations, the model for binary lipid bilayers by Jørgensen *et al.*, and the model for ternary mixtures containing two lipids and one sterol based on the above models. The details of the Monte Carlo simulation methods and procedures for each of these systems are then given in Chapter 3. From Chapter 4 onwards, we present our simulation results on different systems. We begin in Chapter 4 by dealing with single-component lipid bilayers as described by the 10-state Pink model. In particular, bilayers containing lipid chains ranging from 12 carbon units (DLPC) to 22 carbon (DBPC) units were studied. The results in this chapter were used as a comparison to previous simulations in order to verify our simulation algorithm. Simulations of binary DLPC/sterol and DPPC/sterol bilayers using the original and modified version of the Cruzeiro-Hansson and Mouritsen model are presented in Chapter 5. Here we compare the molecular order parameters of our modified model of DPPC/sterol bilayers to ^{2}H-NMR

data, which demonstrates the improvement of the modified model in comparison to the original model in the description of DPPC/sterol systems with high sterol concentrations. Chapter 6 contains the simulation results of DLPC/DPPC binary lipid bilayers using the model by Jørgensen *et al.* [50]. The phase diagram determined from our simulations is in good agreement with FTIR and DSC data. Chapter 7 contains the result of the simulations of ternary DLPC/DPPC(40:60)/cholesterol bilayers, based on a combination of the model for binary lipid bilayers by Jørgensen *et al.* and the modified model of lipid/cholesterol interactions originally due to Cruzeiro-Hansson and Mouritsen. The main feature of this chapter is that we thoroughly explored the parameter space of the lipid/sterol interaction parameter I_C, by manipulating the interactions between lipid chains and sterol. This strategy enables us to determine the set of parameters for which the system manifests the characteristics of the experimental FTIR data by Silvius *et al.* [16]. Finally, Chapter 8 concludes the thesis with a summary and discussions of all the results.

2 Theoretical Models for Lipid Bilayers

In this section, we first present in detail the ten-state Pink Model, which was used to study single-component lipid bilayers. Next, we describe the Cruzeiro-Hansson model for binary lipid/cholesterol bilayers and our corresponding modifications of it for high cholesterol concentrations. Then we present a model for binary lipid/lipid bilayers by Jørgensen *et al.* [50]. Finally, a combined model based on the above two models, which is applicable for ternary lipid/cholesterol bilayers, is presented.

2.1 The Pink Model for Single-Component Lipid Bilayers

The Pink model [26, 59] was originally constructed to describe the main phase transition of saturated phospholipid bilayers and is based on the following assumptions. First, it was assumed that the two monolayers of a lipid bilayer interact weakly with each other and, therefore, in practice only one monolayer needs to be considered. Secondly, the model treated the two acyl chains of a lipid molecule independently, disregarding the fact that the two chains are bound to a single polar head. A two-dimensional triangular lattice with each site occupied by a single saturated lipid chain is used, based on evidence from X-ray studies of multi-lamellar phospholipid bilayers [60, 61].

For the individual chain conformations of the Pink model, the angle between C-C bonds is taken to be 120° instead of 109.5°, in order to conveniently map the chain

conformations into a triangular lattice (note that this is different from the triangular lattice of the membrane). Out of the large number of possible conformational states that a lipid chain can access, ten representative states were chosen based on the Rotational Isomeric Model to characterize the dynamics of the chain. While in reality each saturated carbon-carbon bond has a continuous rotational spectrum, this is replaced in the model by three discrete conformational states corresponding to the three energy minima, i.e., one *trans* bond (ϕ=0°) and two *gauche* bonds (ϕ=-120° and ϕ=120°) respectively. This gives a maximum of 3^{m-1} possible configurations for a free lipid chain, where m is the number of carbons in the chain. However, not all of these configurations are available to a lipid chain in bilayers where steric hindrances of its neighbouring chains are present. In this regard, a set of rules was constructed to govern the selection of the allowed conformational states of each lipid chain on the basis of steric compatibility in the monolayer, which is listed in Appendix A. Each *gauche* bond costs the lipid chain an extra unit of energy $\boldsymbol{E_g}$ and shortens the lipid chain by one unit from a *trans* conformation. Therefore the internal energy of each lipid chain is directly proportional to its number of *gauche* bonds. All lipid chain conformations with the same energy and the same length are considered to be in the same conformational state. Fig. 2.1 shows the mapping of all 10 states. The ground state (α=1) has all C-C bonds in the *trans* conformation; hence it is the dominant state of the gel phase. The eight intermediate energy states (α={2,...,9}) are low energy excitations of the all-*trans* conformation, chosen according to the selection rules stated in Appendix A. The tenth state (α=10) is a high energy 'melted' state representing the fluid phase which is taken to be the average of the rest of the available conformational states.

Each state in the Pink model is characterized by its internal energy, cross-sectional area, and degeneracy (See Table 2.1). Since these parameters were obtained by examining the rotational isomerism of lipid chains in three dimensions, it is in essence a quasi two-dimensional model which provides information relating to the third dimension.

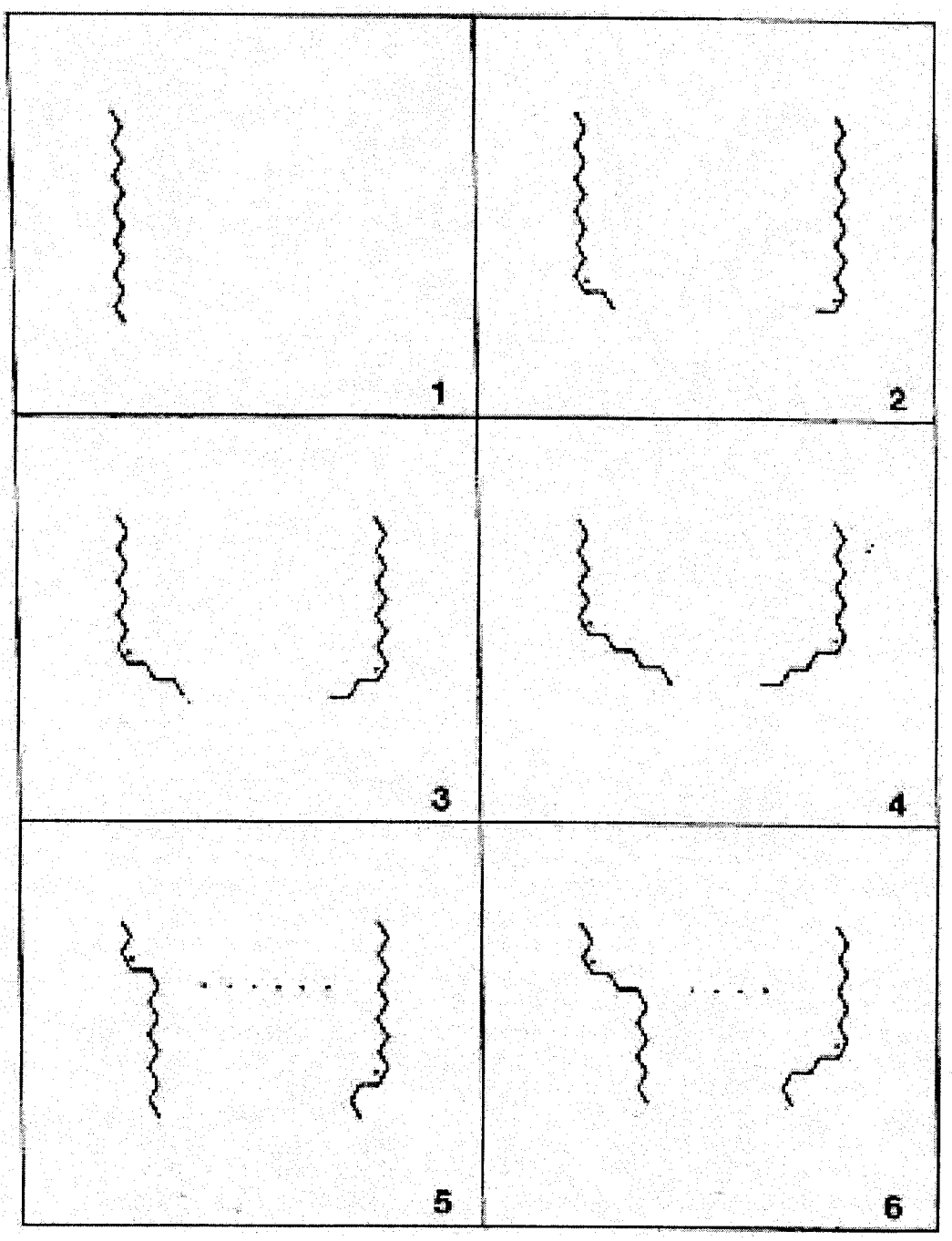
1
2
3
4
5
6

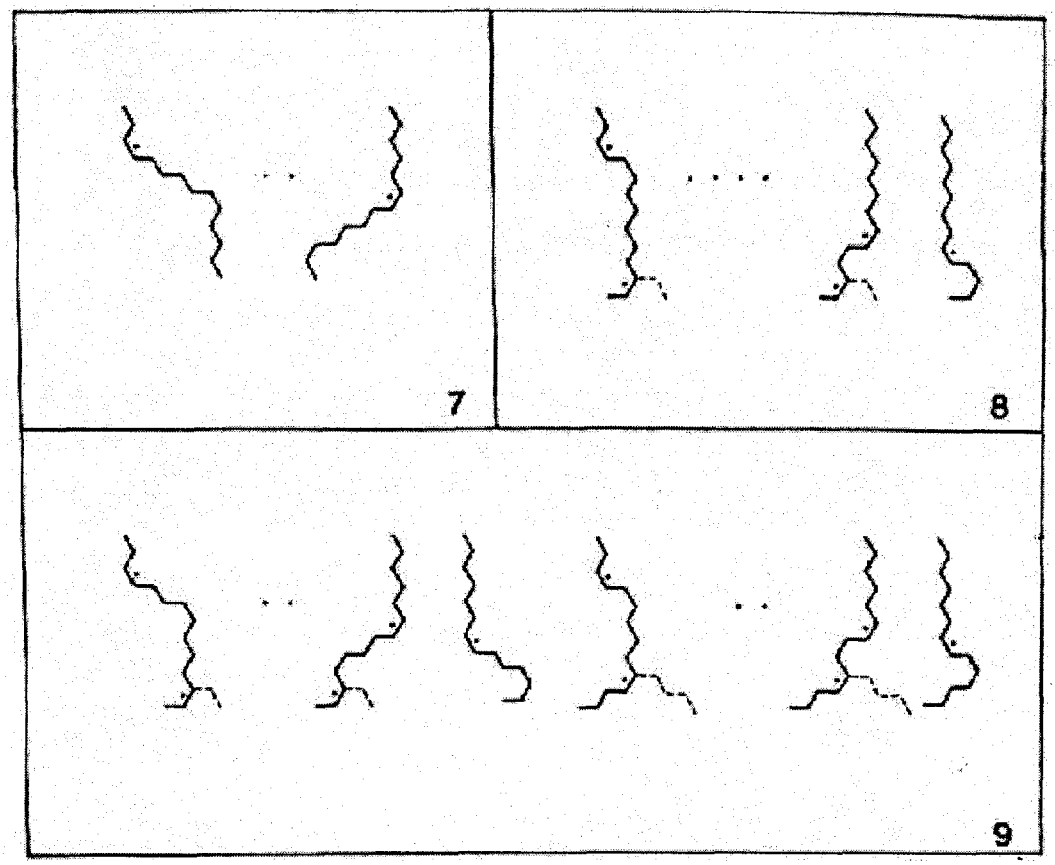

Figure 2.1 **Ground and intermediate energy states (States 1 to 9) of the acyl chain in Pink model. All-*trans* state for a chain with m=14 carbon atoms. 2-9: Intermediate states for a chain with m=14 carbon atoms. All the possible configurations are drawn for states 2,3 and 4. The dot beside a *gauche* bond indicates that the bond has a degeneracy D=2. Therefore the degeneracy of states 2, 3 and 4 is D=4. For states 5,6 and 7 not all the possible configurations are drawn, but there is a systematic way of drawing all of them. Consider for example state 5. For the configuration drawn at the left there is a sequence *gauche-trans-gauche* (g-t-g) in the chain segments 3,4,5 (counting from the top). For the configuration drawn at the right the g-t-g sequence is in the chain segments m-4, m-3, m-2. The rest of the configurations can be obtained starting from the configuration at the left and moving down the g-t-g sequence until the configuration at the right is obtained. IN this case we have m-6 different configurations, each with a degenerate *gauche* bond. Therefore the degeneracy of state 5 is D = 2(m-6). The degeneracy of state 6 is obtained moving down the g-t-t-t-g sequence and its degeneracy is D = 2(m-8). The degeneracy of state 7 is obtained moving down the g-t-t-t-t-t-g sequence and its degeneracy is D = 2(m-10). For states 8 and 9 the dashed line indicates another possible configuration which is identical to the solid line configuration except for the orientation of the last segments. Note that in the case of the dashed line configuration the last degenerate *gauche* bond is one segment above than in the solid line configuration. The configurations for the state 8 are obtained moving down the sequence g-t-g and its degeneracy is D = 8(m-8). The configurations for the state 9 are obtained moving down the sequence g-t-t-t-g when there is a *gauche* bond in the segment m-2 (m-3 in the case of the dashed sequence) and moving down the sequence g-t-g when there is a *gauche* bond in the segment m-4 (m-5 in the case of the dashed sequence). Therefore the degeneracy of state 9 is D = 16(m-10). The number of dots between configurations is the number of configurations not drawn for a chain with m=14. Reproduced from reference [62] with permission of the author.**

The non-degenerate all-*trans* state is taken to be a reference state with zero internal energy and a cross-sectional area of A=20.4 Å^2 determined from experiment [60]. For the intermediate states, the cost of forming each additional *gauche* bond is taken to be E_g =0.45x10^{-13} *erg* [26]. The cross-sectional areas are calculated based on the assumption that the bilayer density, and, hence, the volume, does not change significantly with temperature. In fact, it has been shown by Nagle [63] that the change in density is only ~4% at the main phase transition. Therefore, we have $A_\alpha = A_1 \frac{L_1}{L_\alpha}$, where L_1=m-1 is the chain length (in units of projected chain segments onto the normal of the bilayer) of the all-*trans* configuration, and m is the number of carbon atoms from the carbonyl group to the terminal methyl group of the lipid chain. L_α is the length of a lipid chain in the α^{th} state. The degeneracy D_α is obtained by counting the number of possible configurations with the same energy and same chain length. For the 10th state which is a combination of many disordered conformations, its cross-sectional area is taken to be A_{10}=34Å^2, independent of the chain length. Its degeneracy is given by D_{10}= 6 x 3^{m-6}, where the 'm-6' in the exponential arises from the assumption that the first six chain segments are kept fixed in a *trans* configuration due to polar head effects, and the factor '6' is the number of nearest neighbours per chain. Finally, its energy is assumed to be linear in chain length, and is given by E_{10}=(0.42m-3.94) x 10^{-13} erg.

Table 2.1 **Energies, lengths and degeneracies of the ground and the intermediate states of acyl chains in the Pink model.**

State 1 $E = 0$ $L = m$-1 D =1	State 2 $E = E_g$ $L = m$-2 D = 4	State 3 $E = E_g$ $L = m$-3 D =4
State 4 $E = E_g$ $L = m$-4 D = 4	State 5 $E = 2E_g$ $L = m$-2 $D = 2(m$-6)	State 6 $E = 2E_g$ $L = m$-3 $D = 2(m$-8)
State 7 $E = 2E_g$ $L = m$-4 $D = 2(m$-10)	State 8 $E = 3E_g$ $L = m$-3 $D = 8(m$-8)	State 9 $E = 3E_g$ $L = m$-4 $D = 16(m$-10)

In the Pink model, interactions are restricted to nearest neighbours with the following two contributions:

i. van der Waals interactions between lipid chains

ii. Repulsive forces due to electrostatic interactions between polar head-groups and steric interactions from both the polar head groups and the lipid chains.

The van der Waals interaction is taken to be the product of the isotropic interaction between two long parallel chains and an orientational interaction between individual C-C bonds [19, 58]. This term is written as,

$$E_{int} = -J_o V_{\alpha\beta} S_\alpha S_\beta, \tag{2.1}$$

where J_o is the coupling constant which is different for lipid species with different chain lengths. α and β are indices for the 10 conformational states. Together, $J_o V_{\alpha\beta}$ represents the isotropic van der Waals interaction of two long parallel chains, where $V_{\alpha\beta}$ is derived as follows. The van der Waals interaction of a basic unit of a chain with its neighbouring

unit is $\omega \propto \frac{1}{d^6}$, where d is the distance between them. Using this, Salem [64] showed the interactions between long parallel linear chains to be $W \propto \frac{1}{D^5}$, where D is the distance between two neighbouring chains. In a close-packed configuration, $D \approx r_\alpha + r_\beta$ where r_α is the effective radius of the lipid cylinder in state α. $V_{\alpha\beta}$ is a dimensionless quantity given by:

$$V_{\alpha\beta} = \frac{(2r_1)^5}{(r_\alpha + r_\beta)^5}. \tag{2.2}$$

The coefficient in the expression for W is included in J_o. After writing $r_\alpha = r_\beta + \delta_{\alpha\beta}$ with the consideration that $\delta_{\alpha\beta}$ is generally small for dense chain packing, the following approximation can be made:

$$V_{\alpha\beta} \simeq \frac{r_1^5}{r_\alpha^{\frac{5}{2}}\, r_\beta^{\frac{5}{2}}}. \tag{2.3}$$

Note that the maximum errors for the above approximation, which occur in the case of α=1 and β=9, are estimated to be around 5% for DLPC and 3% for DPPC. The above expression can be rewritten in terms of the cross-sectional areas, assuming that the projections of the lipid chain onto the membrane plane are circular:

$$V_{\alpha\beta} = V_\alpha V_\beta = (\frac{A_1}{A_\alpha})^{\frac{5}{4}}\ (\frac{A_1}{A_\beta})^{\frac{5}{4}}. \tag{2.4}$$

However, this form of interaction is not valid for the 10th state for which the lipid chains are far from being parallel to each other. Therefore, a weakening factor was introduced

such that $V_{10} = \omega(\frac{A_1}{A_{10}})^{\frac{5}{4}}$ where ω was determined to be 0.4 by fitting mean-field results to experimental data for the transition temperature and the transition enthalpy [25]. S_α and S_β are nematic acyl chain order parameters that depend on the angle $\theta_{\alpha n}$ between the nth chain segment and the bilayer normal, which can be calculated using the method of Seelig [65, 66]. The angle $\theta_{\alpha n}$ is 30° for a *trans* bond and 90° for a *gauche* bond. Therefore a normalization factor of $\frac{8}{5}$ is included in order that S_α has the value of 1 for the all-*trans* state (where $\theta_{\alpha n}$=30° for all segments):

$$S_\alpha = \frac{8}{5}\frac{1}{(m-1)}\sum_{n=1}^{m-1}\frac{(3\cos^2\theta_{\alpha n}-1)}{2} \qquad (2.5)$$

Let $n_{30}{}^o$ be the number of *trans* bonds and $n_{90}{}^o$ be the number of *gauche* bonds in the chain. Then $n_{30}{}^o + n_{90}{}^o = m-1$ and $L = L_1 - n_{90}{}^o$, where L is the length of the chain and L_1 is its maximum chain length in the all-*trans* state. Then, by using Eq. (2.5), S_α becomes:

$$S_\alpha = \frac{9}{5}\frac{A_1}{A_\alpha} - \frac{4}{5}. \qquad (2.6)$$

According to Marčelja [19, 59], the steric repulsion among hard cores of each atom, as described in ii, gives rise to a lateral pressure on each chain. The energy associated with the lateral pressure on a chain is proportional to the value of the pressure and the average cross sectional area of the chain. Therefore, it can be taken into account by the coupling of an effective lateral pressure Π to the cross-sectional area A:

$$E_{steric} = \Pi A_\alpha. \qquad (2.7)$$

From the contributions to the energy described above and Eq.(2.1), (2.4) and (2.6), the Pink Hamiltonian can be written as the sum of the self-energy $\mathcal{H}_o^L$ and the lipid-lipid interaction energy $\mathcal{H}_{LL}$:

$$\mathcal{H} = \mathcal{H}_o^L + \mathcal{H}_{LL}, \tag{2.8}$$

where

$$\mathcal{H}_o^L = \sum_i \sum_{\alpha=1}^{10} (E_\alpha + \Pi A_\alpha)\, \mathcal{L}_{i,\alpha} \tag{2.9}$$

and

$$\mathcal{H}_{LL} = -J_o \sum_{<i,j>} \sum_{\alpha,\beta=1}^{10} I_\alpha I_\beta \mathcal{L}_{i,\alpha} \mathcal{L}_{j,\beta}\,. \tag{2.10}$$

In this expression, $E_\alpha = n_\alpha E_g$ where n_α is the number of *gauche* bonds E_g is the energy needed to form one *gauche* bond. The indices α and β refer to conformational states and the indices i and j refer to lattice sites. <i,j> indicates that it is restricted to nearest neighbour interactions. $\mathcal{L}_{i,\alpha}$ is an occupational variable defined as:

$$\mathcal{L}_{i,\alpha} = \begin{cases} 1 \text{ if the state of the lipid at site i is } \alpha \\ 0 \text{ otherwise} \end{cases}, \tag{2.11}$$

so that $\sum_\alpha \mathcal{L}_{i,\alpha} = 1$. I_α is defined as:

$$I_\alpha = \omega_\alpha V_\alpha S_\alpha = \omega_\alpha \left(\frac{9}{5}\frac{A_1}{A_\alpha} - \frac{4}{5}\right)\left(\frac{A_1}{A_\alpha}\right)^{\frac{5}{4}}, \tag{2.12}$$

where $\omega_\alpha = 1$ for $\alpha = [1,\ldots,9]$ and $\omega_{10} = 0.4$.

The values of J_o and Π were also determined from a mean field solution of the model given by Eqs. (2.8) to (2.10). The requirement was that the calculated main phase

transition temperatures and transition enthalpies agree with the experimental values of pure DPPC bilayers. The value of Π was found to be 30 *dyn*/cm [59] for a given saturated lipid bilayer with PC polar heads, and was assumed to be independent of chain length. The values of J_o for the other saturated phospholipids (m=12,14,18,20,22) were derived by simple scaling from the value of DPPC. The experimental transition temperatures and the values of the coupling constant for different saturated phospholipids are shown in Table 2.2.

Table 2.2 **Experimental main phase transition temperatures and theoretical interaction constants for phospholipids with different chain lengths.**

Lipid	T_m (K)	$J_o \times 10^{-13}$ erg
DLPC	271.4	0.5232
DMPC	296.8	0.618
DPPC	314.5	0.7098
DSPC	327.5	0.815
DAPC	339.1	0.930
DBPC	348.1	1.028

2.2 Lipid/Cholesterol Bilayers

Sterols are important both as structural components of the plasma membranes of eukaryotic cells and as initiators and modulators of biological processes. Cholesterol is the dominant sterol component of mammalian cell membranes, often comprising a lipid fraction of at least 30 mol%. Cholesterol molecules orient themselves in a bilayer with their hydroxyl groups close to the polar head groups of the phospholipid bilayer at the level of the ester linkages (see Fig. 1.8). The steroid ring structure partially immobilizes

the region of the hydrocarbon chain of a neighbouring lipid molecule near the head group.

The effect of cholesterol on the physical properties of phospholipid bilayers has been studied extensively both in experiment and in theory. Vist and Davis [12] presented a careful study of the DPPC/cholesterol multi-bilayer system using both ^{2}H NMR and calorimetry. Analysis of the data from both of these experiments plus results from EPR measurements led to the phase diagram of Fig. 2.2a [43]. The phase diagram shows three distinct phases, a solid-ordered phase **so**, a liquid-disordered phase **ld**, and a liquid-ordered phase **lo** at high cholesterol concentrations. The **so** phase and the **ld** phase are equivalent to the gel phase and the liquid crystalline phase of pure lipid bilayers respectively. The interesting features of the phase diagram include three separate two-phase coexistence regions, a three-phase line where the **ld**, **so** and **lo** phases are all in coexistence at a single temperature, and the occurrence of a new phase **lo**, which was called the β-phase by Vist and Davis, at high cholesterol concentrations. Cholesterol dissolves easily in a phase with no crystalline structure but—due to its rigid steroid ring structure—prefers the neighbouring acyl chains to be in a state of high conformational order. Therefore, at low cholesterol concentrations it associates with the **so** and **ld** phases equally; but at high cholesterol concentrations, it induces conformational order in the fluid state and inhibits crystallization in the low temperature phase. As a result, the new phase **lo** is introduced at high cholesterol concentrations. The characteristics of the **lo** phase can be summarized as follows [12]:

i. The bilayer has a lateral diffusion rate which is comparable to that of the **ld** phase

ii. Axial molecular re-orientation is rapid, having rotational diffusion rates comparable to those of the **ld** phase

iii. The phospholipid chains are highly ordered

iv. The bilayer is thicker than found for the **ld** phase but thinner than in that of the **so** phase

v. A greater tension is required to stretch the bilayer in the **lo** phase than in the **ld** phase.

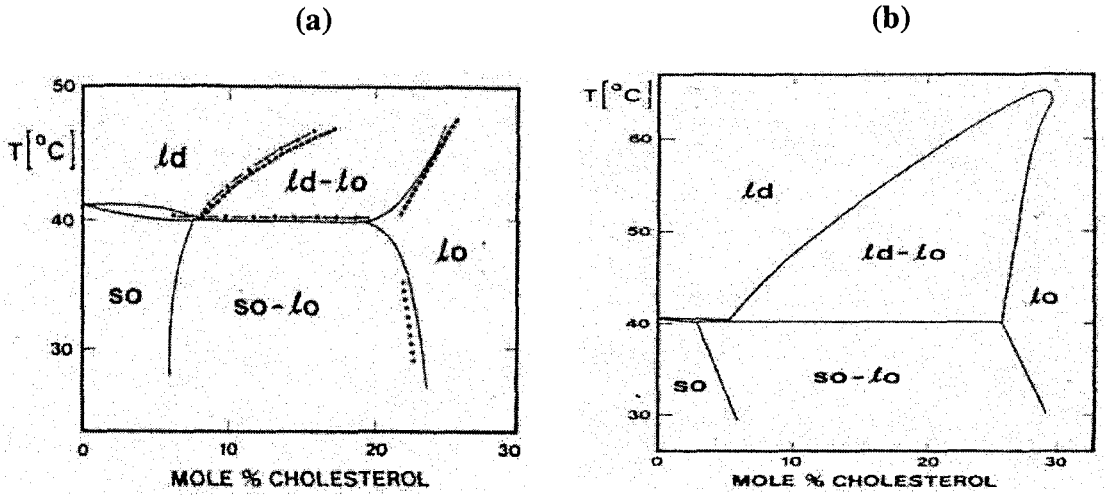

Figure 2.2 **a) Experimental phase diagram for the DPPC/cholesterol system as determined by NMR spectroscopy and differential scanning calorimetry (——) and other experimental techniques. b) Theoretical phase diagram.**
Reproduced from reference [43] with permission of the author.

A general consensus of different experimental studies is that cholesterol results in thicker and mechanically stronger bilayers that, nevertheless, retain the characteristics of a fluid, i.e., relatively low viscosity and rapid lateral diffusion and, at the macroscopic-continuum level, no shear restoring force [67].

Ipsen *et al.* [43] have developed a theoretical model for lipid/cholesterol bilayers which successfully reproduced the essential features of the above experimental phase diagram (Fig. 2.2a). In order to account for the dual effects of cholesterol in inhibiting the

formation of a crystalline structure and making the acyl chain rigid, Ipsen's model was designed to give a description of lipid monolayers and bilayers in terms of two degrees of freedom, one for the chain conformations and the other for the positional order. It is based on the Pink model combined with a modified multi-state Potts model which is used to treat the positional degrees of freedom in an approximate manner. The parameters for the lipid-cholesterol interactions were chosen to give a qualitative phase diagram as close as possible to the experimental phase diagram. The corresponding theoretical phase diagram is shown in Fig. 2.2b. However, the problem with the Pink-Potts model is that it is difficult to interpret the Potts variables microscopically. Cruzeiro-Hansson *et al.* [28], therefore, proposed a reduced model which is correct for low cholesterol concentrations. We present the details of this model in the following section with the modifications which we made in order to apply the model to systems with high cholesterol concentrations.

2.2.1 Model for Lipid/Cholesterol Bilayers

Cruzeiro-Hansson *et al.* [28] modified the Pink model to include interactions between lipid chains and smooth hydrophobic molecules such as cholesterol, which can be regarded as substitutional impurities. This model was originally constructed to describe the phase behaviour of lipid/cholesterol bilayers at low cholesterol concentrations, up to about 10 mol%. Therefore, it does not describe their physical properties at higher cholesterol concentrations.

The complete Hamiltonian of the lipid/cholesterol bilayer is given by:

$$\mathcal{H} = \mathcal{H}_o^L + \mathcal{H}_o^C + \mathcal{H}_{LL} + \mathcal{H}_{CC} + \mathcal{H}_{LC} \tag{2.13}$$

where $\mathcal{H}_o^L$ and $\mathcal{H}_{LL}$ are the lipid non-interacting energy and the lipid-lipid interaction energy given by Eq.(2.9) and (2.10) respectively. The Cruzeiro-Hansson model assumes that cholesterol is a stiff, hydrophobically smooth molecule with no internal degrees of freedom. $\mathcal{H}_o^C$ then represents the effect of the internal pressure on the cholesterol molecules, with cross-sectional area of cholesterol assigned as $A_C = 32\text{Å}^2$:

$$\mathcal{H}_o^C = \Pi \sum_i A_c \mathcal{L}_{i,c} \,. \tag{2.14}$$

The interactions between lipid-cholesterol and cholesterol-cholesterol assume the same form as for the lipid-lipid interaction described in Section 2.1, and they are given by:

$$\mathcal{H}_{LC} = -J_o \sum_{<i,j>} \sum_{\alpha=1}^{10} I_\alpha I_c(\alpha) \left(\mathcal{L}_{i,\alpha} \mathcal{L}_{j,c} + \mathcal{L}_{j,\alpha} \mathcal{L}_{i,c} \right) \tag{2.15}$$

and

$$\mathcal{H}_{CC} = -J_o \sum_{<i,j>} I_c^{\,2} \mathcal{L}_{i,c} \mathcal{L}_{j,c} \,, \tag{2.16}$$

where the occupation variable $\mathcal{L}_{i,c}$ for cholesterol is defined as:

$$\mathcal{L}_{i,c} = \begin{cases} 1 \text{ if there is a cholesterol molecule at site i} \\ 0 \text{ otherwise} \end{cases} \tag{2.17}$$

Therefore,

$$\mathcal{L}_{i,c} + \sum_{\alpha=1}^{10} \mathcal{L}_{i,\alpha} = 1. \tag{2.18}$$

Note that, in Eqs. (2.15) and (2.16), the same J_o as in the model for single-component lipid bilayers is used. This is because the van der Waals interaction

corresponding to the contribution of cholesterol is being accounted for in $I_C(\alpha)$. In other words, $I_\alpha I_C(\alpha)$ denotes the van der Waals interaction between acyl chains and cholesterol in units of J_o. Similarly, I_C^2 denotes the van der Waals interaction between cholesterol and cholesterol in units of J_o.

Note that, in the original Cruzeiro-Hansson model, a constant I_C instead of $I_C(\alpha)$ was used in all lipid-cholesterol interactions, giving the following Hamiltonian, instead of Eq. (2.15):

$$\mathcal{H}_{LC} = -J_o \sum_{<i,j>} \sum_{\alpha=1}^{10} I_\alpha I_c \left(\mathcal{L}_{i,\alpha} \mathcal{L}_{j,c} + \mathcal{L}_{j,\alpha} \mathcal{L}_{i,c} \right). \tag{2.19}$$

In this thesis, we extend the Cruzeiro-Hansson model by replacing I_C by $I_C(\alpha)$ which depends on the conformational state α of the lipid chain interacting with cholesterol. This is an attempt to describe the physical properties of the system at high cholesterol concentrations, which the original model did not do. A mean-field calculation by Cruzeiro-Hansson *et al.* and Ipsen [28] shows that $I_C = 0.45$ is a good choice which produces a phase diagram that resembles DPPC/cholesterol mixtures for *Xc* up to about 10%. In this thesis we adopt this value for all $I_C(\alpha)$ except for $I_C(5)$ of DPPC/cholesterol bilayers, the value of which we increase progressively from 0.45 to 2 in our investigation (see Ch. 5). In the Pink model, state 5 of a lipid chain is the kink state (see Fig.2.1). In our modification of the model, the kink state was chosen to represent the many possible lipid chain conformations that are predominant in the **lo** phase/complexion. This is because of the hypothesis that the respective structures of cholesterol and a lipid chain in the kink state are sterically compatible with each other

(Fig. 2.3) and, therefore, it is energetically favourable for them to be nearest neighbours. Furthermore, the conformational order parameter for a lipid chain in the kink state in our model is in the range of that for the **lo** phase in experiments with high sterol concentrations. Mendelsohn *et al.* [112] have also shown using infrared studies that there is a marked decrease of the number of *gauche* bonds in bilayers with high cholesterol concentrations (i.e., the **lo** phase) as compared to that in a single-component system.

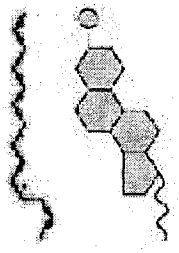

Figure 2.3 Cartoon representation of the conformation of a lipid chain in the kink state and a cholesterol molecule.

2.3 Binary Lipid Bilayers

Natural membranes are multi-component systems that contain a large number of different lipid species in addition to molecules that are intrinsically incorporated in the bilayers such as sterols and proteins. Such systems have complex phase diagrams with regions of thermodynamic phase coexistence. In an attempt to understand the phase equilibria in the multi-component systems, a first step is to investigate binary lipid bilayers. It has been demonstrated both experimentally and theoretically that gel-fluid, gel-gel or even fluid-fluid [50] coexisting domains are present in binary lipid bilayers. The hypothesis is that membrane heterogeneity and differentiated lateral membrane organization are relevant for function in some types of biological membranes.

Using mean-field theory, Risbo *et al.* [68] obtained the phase diagrams for DMPC/DPPC, DMPC/DSPC and DLPC/DSPC bilayers shown in Fig. 2.4. A 'universal' mismatch parameter Γ—to be discussed in Section 2.3.1—was used for the calculations of these phase diagrams. Fig. 2.4 shows that there are different phase coexistence regions in each binary system. It can be seen that the coexistence region becomes broadened and that there is a progressive enhancement of the non-ideal mixing behaviour as the difference in acyl-chain length is increased. For instant, in the DLPC/DSPC system (Fig. 2.4c), which possesses the largest hydrophobic mismatch among the three, the two lipids exhibit only limited solubility in the gel phase, resulting in a dramatic peritectic behaviour and a gel-gel coexistence. Phase diagrams derived from computer simulation results [50] show features similar to those of Fig. 2.4. Moreover, experimentally determined phase diagrams are mostly in good agreement with numerical calculations, with the exception of the DMPC/DSPC bilayer, which is somewhat controversial. Results from small-angle neutron scattering have predicted that this mixture also exhibits peritectic behaviour [69].

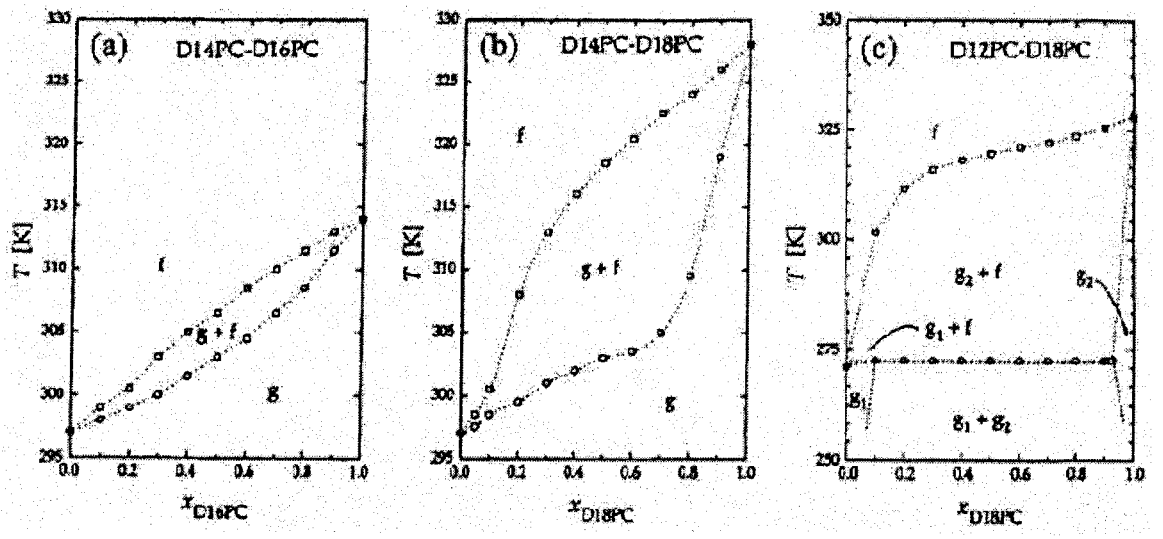

Figure 2.4 **Phase diagrams for three lipid mixtures determined from mean-field calculations. (a) DMPC/DPPC, (b) DMPC/DSPC and (c) DLPC/DSPC. The labels denote gel (g, g_1, g_2) and fluid (f) single-phase regions. Fluid-gel and gel-gel phase coexistence regions are denoted by g+f, g_1+f, g_2+f, and g_1+g_2 respectively. Reproduced from reference [68] with permission of the publisher and consent of the authors.**

2.3.1 Model for Binary Lipid Bilayers

Jørgensen *et al.* [50] developed a model for binary lipid bilayers based on the original Pink model. Two different saturated lipid species with the same polar head group but different chain lengths (e.g., DMPC and DPPC) are considered. A coupling term which accounts for the incompatibility of acyl chains of different hydrophobic lengths has been added to the original Pink Hamiltonian. This kind of mismatch interaction has also been used in systems of lipids with transmembrane proteins [70-72]. The complete Hamiltonian for the binary lipid bilayer composed of lipid species A and B is:

$$\mathcal{H} = \mathcal{H}_o^A + \mathcal{H}_o^B + \mathcal{H}_{LL}^{AA} + \mathcal{H}_{LL}^{BB} + \mathcal{H}_{LL}^{AB}. \qquad (2.20)$$

$\mathcal{H}_o^A$ and $\mathcal{H}_o^B$ are the non-interacting energies of lipids A and B which assume the same form as Eq.(2.9), and are written as:

$$\mathcal{H}_o^A = \sum_i \sum_{\alpha=1}^{10} \left(E_\alpha + \Pi A_\alpha^A \right) \mathcal{L}_{i,\alpha}^A \tag{2.21}$$

and

$$\mathcal{H}_o^B = \sum_i \sum_{\alpha=1}^{10} \left(E_\alpha + \Pi A_\alpha^B \right) \mathcal{L}_{i,\alpha}^B . \tag{2.22}$$

Note that for a particular intermediate configurational state $\alpha \in [2,9]$, A_α^A and A_α^B and, hence, $\mathcal{H}_o^A$ and $\mathcal{H}_o^B$ are different. This is because A_α is defined as $A_\alpha = A_1 \frac{L_1}{L_\alpha}$ (see section 2.1), where L_1, the length in the all-*trans* state, is different for lipid A and lipid B.

$\mathcal{H}_{LL}^{AA}$ and $\mathcal{H}_{LL}^{BB}$ represent the interactions between like species as described in Eq. (2.10), and are now written as:

$$\mathcal{H}_{LL}^{AA} = -J_A \sum_{<i,j>} \sum_{\alpha,\beta=1}^{10} I_\alpha^A I_\beta^A \mathcal{L}_{i,\alpha}^A \mathcal{L}_{j,\beta}^A \tag{2.23}$$

and

$$\mathcal{H}_{LL}^{BB} = -J_B \sum_{<i,j>} \sum_{\alpha,\beta=1}^{10} I_\alpha^B I_\beta^B \mathcal{L}_{i,\alpha}^B \mathcal{L}_{j,\beta}^B . \tag{2.24}$$

Note that the strengths of interactions are different for the two species, due to the different values of J_A and J_B, as well as I_α^A and I_α^B.

Finally, $\mathcal{H}_{LL}^{AB}$ gives the following interaction between lipid species A and B:

$$\begin{aligned} \mathcal{H}_{LL}^{AB} = & -J_{AB} \sum_{<i,j>} \sum_{\alpha,\beta=1}^{10} \left(I_\alpha^A I_\beta^B \mathcal{L}_{i,\alpha}^A \mathcal{L}_{j,\beta}^B + I_\alpha^B I_\beta^A \mathcal{L}_{i,\alpha}^B \mathcal{L}_{j,\beta}^A \right) \\ & + \Gamma \sum_{<i,j>} \sum_{\alpha,\beta=1}^{10} \left(\left| L_{i,\alpha}^A - L_{j,\beta}^B \right| \mathcal{L}_{i,\alpha}^A \mathcal{L}_{j,\beta}^B + \left| L_{i,\alpha}^B - L_{j,\beta}^A \right| \mathcal{L}_{i,\alpha}^B \mathcal{L}_{j,\beta}^A \right) . \end{aligned} \tag{2.25}$$

The first term on the right hand side of Eq. (2.25) represents the regular van der Waals interaction between lipid species A and B. The interaction strength is taken to be the geometric average $J_{AB} = \sqrt{J_A J_B}$, an ansatz used in the original paper by Pink *et al.* [50, 68] which gave reasonable results in comparison with experiments. There exist other possible choices of J_{AB}, such as $J_{AB} = J_A$ for which J_A is the interaction strength of the lipid species with shorter chain length. $\mathcal{L}^A_{i,\alpha}$ and $\mathcal{L}^B_{j,\beta}$ are the occupational variables for lipid species A and B respectively. The second term on the right hand side of Eq. (2.25) was included to account for the mismatch of hydrophobic lengths between species A and B. There Γ is a mismatch interaction constant which is assumed to be 'universal' in the sense that its value does not depend on lipid chain length. It has been shown both by computer simulation [50] and two-component regular solution theory using a phenomenological mean-field approach [68] that a wide range of binary lipid phase diagrams can be described in terms of Γ. The value of Γ used in this thesis is 0.038×10^{-13} erg/Å [68], and the chain length L_α denotes the number of C-C chain segments in a lipid chain as discussed in section 2.1.

2.4 Model for Ternary Lipid Bilayers

In order to study ternary systems containing two lipid species and cholesterol, we combine the Cruzeiro-Hansson model of Section 2.2 for lipid/cholesterol bilayers and the model by Jørgensen of Section 2.3 for binary lipid mixtures. The complete Hamiltonian of a system composed of lipid A, lipid B and cholesterol (C) can now be written as:

$$\mathcal{H} = \mathcal{H}_o^A + \mathcal{H}_o^B + \mathcal{H}_o^C + \mathcal{H}_{LL}^{AA} + \mathcal{H}_{LL}^{BB} + \mathcal{H}_{LL}^{AB} + \mathcal{H}_{CC} + \mathcal{H}_{LC}^{\gamma}, \tag{2.26}$$

where $\mathcal{H}_o^A$, $\mathcal{H}_o^B$ and $\mathcal{H}_o^C$, given in Eq. (2.9), (2.10) and (2.14), are the respective non-interacting Hamiltonians for lipid chain species *A* and *B*, and cholesterol. $\mathcal{H}_{LL}^{AA}$ and $\mathcal{H}_{LL}^{BB}$ represent the lipid-lipid interactions between like lipid species and are given by Eq. (2.23) and (2.24). $\mathcal{H}_{LL}^{AB}$ is the interaction between different lipid species, as given in Eq. (2.25). $\mathcal{H}_{CC}$ is described by Eq. (2.16) for the cholesterol-cholesterol interactions. $\mathcal{H}_{LC}^{\gamma}$, the lipid-cholesterol interaction, is written as follows:

$$\mathcal{H}_{LC}^{\gamma} = -J_{LC} \sum_{\gamma=A,B} \sum_{<i,j>} \sum_{\alpha=1}^{10} I_{\alpha}^{\gamma} I_{\alpha,c} \left(\mathcal{L}_{i,\alpha}^{\gamma} \mathcal{L}_{j,c} + \mathcal{L}_{i,c} \mathcal{L}_{j,\alpha}^{\gamma} \right). \tag{2.27}$$

In this thesis, we use $J_{AB} = \sqrt{J_A J_B}$ as the interaction constant not only for the interactions between lipid *A* and lipid *B*, but also for the cholesterol-cholesterol interactions in the ternary system. Moreover, we use the same coupling constant J_{LC} in Eq.(2.27) for the interaction of lipid *A*-cholesterol and lipid *B*-cholesterol. This is based on the assumption that the coupling between cholesterol and acyl chains with the same head group do not depend on the length of an acyl chain if it is as long as, or longer than cholesterol. In particular, for the system DLPC/DPPC/cholesterol (Ch. 7) which we studied extensively, we adopted the value of J_{DPPC} not only for the interaction between DPPC and cholesterol, but also for the interaction between DLPC and cholesterol, based on the assumption mentioned above. Finally, we changed $I_{\alpha,C}$ from a fixed value of 0.45, which was used in the original Cruzeiro-Hansson model, to a value which depends on the

respective conformational state (as discussed in Section 2.2.1 for lipid/cholesterol bilayers) in order to produce results that agree with experiment.

3 Monte Carlo Simulation Method

Statistical Mechanics may be thought of as a set of rules which gives the precise mathematical relationship between the microscopic and macroscopic (thermodynamic) descriptions of a physical system. If the fundamental physical laws governing the interactions between the microscopic constituents of the physical system are known, the related statistical mechanics can be formulated mathematically in terms of equations involving multi-dimensional integrals. In other words, statistical mechanics provides a powerful technique for calculating thermodynamic functions of a system from its Hamiltonian. However, difficulties in calculation arise when dealing with complicated Hamiltonians of many-particle systems. For instance, the number of lipid molecules in a typical prokaryotic cell membrane is typically of the order of 10^{11}. The large number of molecules involved poses major difficulties for a theoretical description of the system based on molecular microscopic interaction models. Only for very simplified models—made possible at the expense of physical reality and detail of description—is it possible to perform any analytically exact calculations. It is at this point where computer simulation techniques become indispensable in making progress in the statistical mechanical description of many-particle systems. By using a fast computer, the integrals of statistical mechanics may be evaluated with an accuracy which is only limited by the computer power available.

Computer simulation techniques—as opposed to analytical techniques—are purely numerical in nature. The computer is used to 'simulate' directly the behaviour of a physical system, taking as its starting point the fundamental equations of statistical mechanics. In other words, simulations are basically like experiments which are carried out on a well-defined system, with full control over every experimental parameter. There exist two major types of computer simulation techniques which have proved successful in the study of phase transitions, namely molecular dynamics methods and Monte Carlo methods. In a molecular dynamics simulation, the deterministic time-evolution of the system is calculated by a numerical integration of the Newtonian equations of motion. By contrast, in a Monte Carlo simulation, certain stochastic elements are introduced which facilitate the evaluation of the statistical mechanical equations. This method directly simulates a given distribution, such as the canonical distribution. There are no dynamics in the sense that the computer generates states of the finite system with a weight proportional to, for example, the probability density of the canonical distribution.

Monte Carlo simulations are employed to study different lipid and lipid/cholesterol systems throughout this thesis. The details of the method will be described in the following subsections. We first begin by introducing the idea and rationale of random sampling techniques in Monte Carlo simulations in Section 3.1. Then we present the ways of evaluating thermodynamic functions via these sampling techniques in Section 3.2. In Section 3.3 and 3.4, details of the Metropolis Monte Carlo algorithm and its implementation on the lipid and lipid/cholesterol systems are discussed.

3.1 Sampling Methods

When evaluating definite integrals with "classical" numerical integration methods, we divide each coordinate over which we want to integrate into n equal intervals. Then we apply approximations such as the rectangular approximations, e.g., Simpson's rule, when summing over the regular array of points. The essence of the Monte Carlo method, i.e., the way that it differs from the "classical" method of evaluating integrals, is that it integrates over a random sample of points instead of over a regular array of points. Different Monte Carlo procedures exist based on their different sampling techniques, and the sampling techniques are in turn characterized by the bias imposed on the sampling scheme.

For instance, a simple sampling technique is the *Sample Mean Method*, based on the mean value theorem of calculus. The mean value theorem states that, if f is continuous on the interval $[a,b]$, then the integral,

$$F = \int_a^b dx\, f(x), \tag{3.1}$$

is determined by the average value of the integrand $f(x)$ in the range $a \le x \le b$, multiplied by the interval size $(b-a)$. Random numbers x_i are chosen from a uniform distribution in the interval $[a,b]$ in order to sample the value of $f(x)$. The estimated value of the integral after n trials is

$$F_n = (b-a)\frac{1}{n}\sum_{i=1}^{n} f(x_i). \tag{3.2}$$

It has been shown [73] that, in evaluating higher dimensional integrals with equation (3.2), random sampling yields a more accurate result than sampling from a regular array of points, while the opposite applies to lower dimensional integrals.

To estimate the integral,

$$F = \int_{a_1}^{b_1} \cdots \int_{a_n}^{b_n} dx_1 \cdots dx_n f(x_1, \cdots, x_n), \tag{3.3}$$

with the *Sample Mean Method* for m trials, we have

$$F_m = (b_1 - a_1) \cdots (b_n - a_n) \frac{1}{m} \sum_{i=1}^{m} f(x_{1i}, \cdots, x_{ni}), \tag{3.4}$$

where $x_{1i}, \cdots, x_{ni}$ are independent random numbers from uniform distributions in the interval $[a_1, b_1], \cdots, [a_n, b_n]$.

The *Sample Mean Method* employs uniformly distributed random numbers in the estimation of the integrals. However, this is not the most efficient sampling method. Instead, it is in general desirable to sample the integrand $f(x)$ more often in regions of x where $|f(x)|$ is large or rapidly varying. Therefore we introduce an improved Monte Carlo procedure called *Importance Sampling*, which is a scheme to collect statistical information according to its importance for a particular problem. *Importance Sampling* is the sampling method used throughout this thesis. We rewrite F as

$$F = \int_a^b dx \left[\frac{f(x)}{p(x)} \right] p(x), \tag{3.5}$$

where $p(x)$ is a positive function such that $\int_a^b dx\, p(x) = 1$. Therefore, it enables us to evaluate F by sampling the value of $\frac{f(x)}{p(x)}$ according to the probability distribution $p(x)$ and constructing the sum

$$F_n = \frac{1}{n}\sum_{i=1}^{n}\frac{f(x_i)}{p(x_i)}. \tag{3.6}$$

Note that in the case of a uniform distribution, $p(x) = \frac{1}{(b-a)}$, and (3.6) reduces to the *Sample Mean Method* (3.2).

For an integral $F = \int_a^b dx\, f(x)$, the error estimate associated with a Monte Carlo calculation is proportional to the standard deviation $\sigma = \sqrt{< f^2 > - < f >^2}$ of the integrand [73]. The advantage of the *Importance Sampling Method* is that it allows us to choose a form of $p(x)$ which minimizes the variance of the integrand $f(x)/p(x)$. In other words, an appropriate choice of $p(x)$ which mimics $f(x)$ especially when $f(x)$ is large makes the integrand $f(x)/p(x)$ slowly varying, and hence reduces the variance.

The above can be generalized to n-dimensions by rewriting F as

$$F = \int_{a_1}^{b_1}\cdots\int_{a_n}^{b_n} dx_1\cdots dx_n \frac{f(x_1,\cdots,x_n)}{p(x_1,\cdots,x_n)}\, p(x_1,\cdots,x_n), \tag{3.7}$$

where $p(x_1,\cdots,x_n)$ is a positive function such that $\int_{a_1}^{b_1}\cdots\int_{a_n}^{b_n} p(x_1,\cdots,x_n) = 1$. The integral is then evaluated by sampling according to the probability distribution $p(x_1,\cdots,x_n)$ and constructing the following sum with m trials:

$$F_m = \frac{1}{m}\sum_{i=1}^{m}\frac{f(x_{1i},\cdots,x_{ni})}{p(x_{1i},\cdots,x_{ni})}. \tag{3.8}$$

3.2 Computation of Thermodynamic Functions using Importance Sampling Method

In statistical physics, the thermodynamic average of an observable $A(\vec{x})$ in canonical ensemble can be computed from the model Hamiltonian $\mathcal{H}$ as

$$< A(\vec{x}) >_T = \frac{1}{Z}\int_V d\vec{x}\, A(\vec{x}) \exp\left[\frac{-\mathcal{H}(\vec{x})}{k_B T}\right], \tag{3.9}$$

where

$$Z = \int_V d\vec{x} \exp\left[\frac{-\mathcal{H}(\vec{x})}{k_B T}\right]. \tag{3.10}$$

The vector $\vec{x}$ represents the set of variables describing the considered degrees of freedom of the system in phase space, Z is the partition function, and V is the volume of the phase space over which the integration is preformed. The specific heat $C_p(T)$ per lipid molecule and the isothermal compressibility $\kappa_T(T)$ can be determined from the enthalpy and volume fluctuations in the individual Monte Carlo steps using the fluctuation-dissipation theorem [106]:

$$C_p(T) = \frac{1}{N' k_B T^2}(<\mathcal{H}^2> - <\mathcal{H}>^2) \tag{3.11}$$

$$\kappa_T(T) = \frac{1}{k_B T <V>}(<V^2> - <V>^2), \tag{3.12}$$

where N' is the total number of molecules in the system.

In two-dimensional systems such as the lipid system considered in this thesis, the volume V is replaced by the total lateral surface area A of the system. Therefore, we wrote the expression for the lateral area isothermal compressibility of Eq. (3.12) as:

$$\kappa_T(T) = \frac{1}{k_B T < A >}(< A^2 > - < A >^2). \tag{3.13}$$

In order to implement the Monte Carlo method to compute the observable $A(\vec{x})$, we replace (3.9) by a summation using a characteristic subset of phase space points $\vec{x}_1, \vec{x}_2, \cdots, \vec{x}_m$, to get the following, which gives (3.9) in the limit $m \to \infty$:

$$< A(\vec{x}) > = \frac{\sum_{i=1}^{m} A(\vec{x}_i) \exp\left[\frac{-\mathcal{H}(\vec{x}_i)}{k_B T}\right]}{\sum_{i=1}^{m} \exp\left[\frac{-\mathcal{H}(\vec{x}_i)}{k_B T}\right]} . \tag{3.14}$$

In the *Importance Sampling Method*, the phase space points $\vec{x}_i$ are chosen according to the probability distribution,

$$\mathcal{P}(\vec{x}_i) \propto \exp\left[\frac{-\mathcal{H}(\vec{x}_i)}{k_B T}\right]. \tag{3.15}$$

Then, the expression for $< A(\vec{x}) >$ becomes:

$$< A(\vec{x}) > = \frac{\sum_{i=1}^{m} A(\vec{x}_i) \exp\left[\frac{-\mathcal{H}(\vec{x}_i)}{k_B T}\right] / \mathcal{P}(\vec{x}_i)}{\sum_{i=1}^{m} \exp\left[\frac{-\mathcal{H}(\vec{x}_i)}{k_B T}\right] / \mathcal{P}(\vec{x}_i)} , \tag{3.16}$$

which simplifies to

$$< A(\vec{x}_i) > = \frac{1}{m} \sum_{i=1}^{m} A(\vec{x}_i) . \tag{3.17}$$

Algorithms for implementing the *Importance Sampling Method* are described in the next section.

3.3 Metropolis Algorithm

Metropolis *et al.* [74] proposed an algorithm for evaluating thermodynamic averages via the sum (3.17) by defining a Markov process and choosing a probability distribution $\mathcal{P}(\vec{x}_i)$ which satisfies (3.15). A Markov process is a stochastic process with a transition probability $W(\vec{x}_i \rightarrow \vec{x}_{i+1})$ which does not depend on the previous history of the system. Here $\vec{x}_i$ and $\vec{x}_{i+1}$ are values of the same variable in sequential states in phase space. In other words, a Markov process can be described as a 'random walk' in phase space. To ensure the process converges toward equilibrium, it is sufficient (but not necessary) to satisfy the detailed balance condition, which is basically that of microscopic reversibility:

$$\mathcal{P}(\vec{x}_i)W(\vec{x}_i \rightarrow \vec{x}_{i+1}) = \mathcal{P}(\vec{x}_{i+1})W(\vec{x}_{i+1} \rightarrow \vec{x}_i). \tag{3.18}$$

We can rewrite the above equation as

$$\frac{W(\vec{x}_i \rightarrow \vec{x}_{i+1})}{W(\vec{x}_{i+1} \rightarrow \vec{x}_i)} = \frac{\mathcal{P}(\vec{x}_{i+1})}{\mathcal{P}(\vec{x}_i)} = \exp\left[-\frac{\delta\mathcal{H}(\vec{x}_{i+1}, \vec{x}_i)}{k_B T}\right], \tag{3.19}$$

where $\delta\mathcal{H}(\vec{x}_{i+1}, \vec{x}_i) = \mathcal{H}(\vec{x}_{i+1}) - \mathcal{H}(\vec{x}_i)$.

It can be seen that we have some flexibility in the choice of $W(\vec{x}_i \rightarrow \vec{x}_{i+1})$. In the Metropolis Monte Carlo algorithm, $W(\vec{x}_i \rightarrow \vec{x}_{i+1})$ is specifically chosen as follows:

$$W(\vec{x}_i \to \vec{x}_{i+1}) = \begin{cases} \frac{1}{\alpha}\exp(-\frac{\delta\mathcal{H}}{k_B T}) & \text{if } \delta\mathcal{H} > 0 \\ \frac{1}{\alpha} & \text{otherwise} \end{cases}, \tag{3.20}$$

where α is a factor which is usually chosen as unity.

Now, let us suppose that we have a system of N particles. A microstate or configuration of the system is determined by a set of fixed values of the variables which describes the configurational state of the system. Let m_i denote the values of the variables associated with the i^{th} particle of the system. The configuration of the system is then completely specified by $\Omega = (m_1, m_2, \cdots, m_N)$. Based on Eq. (3.20), the Metropolis Monte Carlo algorithm for a canonical ensemble can be implemented as follows:

1. Choose an arbitrary (e.g., random) initial configuration Ω^1.
2. Choose a trial state Ω^* (e.g., randomly select one phase point i and change its state randomly).
3. Calculate the energy change $\delta\mathcal{H} = \mathcal{H}(\Omega^*) - \mathcal{H}(\Omega^1)$.
4. If $\delta\mathcal{H} \leq 0$, the trial state is accepted as the new configuration, i.e., $\Omega^2 = \Omega^*$.
5. If $\delta\mathcal{H} > 0$, the transition is allowed with the transition probability $\exp(-\frac{\delta\mathcal{H}}{k_B T})$ as follows:
   - i. Choose a random number ξ from a uniform distribution in the interval [0,1].
   - ii. If $\xi \leq \exp(-\frac{\delta\mathcal{H}}{k_B T})$ the move to the trial state is accepted and $\Omega^2 = \Omega^*$.
   - iii. If $\xi > \exp(-\frac{\delta\mathcal{H}}{k_B T})$ the move to the trial state is rejected and the old configuration is counted as a new one $\Omega^2 = \Omega^1$.

6. Choose a new trial state Ω^* and repeat the procedure.

Although we have only presented the Metropolis algorithm for the canonical ensemble in this section, generalizations to other ensembles such as the isothermal-isobaric ensemble and the grand-canonical ensemble are straightforward. For instance, the algorithm for an isothermal-isobaric ensemble is exactly the same as for the canonical ensemble except with the substitution for E of $E+pV$ ($E+pA$ for 2-dimensional systems).

3.4 Implementation of the Metropolis Monte Carlo Algorithm for Lipid Systems

In choosing a trial state Ω^* for the system, different dynamics can be employed depending on the model under study. In this thesis, we have considered two different kinds of dynamics, namely, Glauber dynamics [75] and Kawasaki dynamics [76]. Glauber dynamics involves a change of state (a change of conformational state in our case) and, therefore, the conformational order parameter is not conserved. Kawasaki dynamics involves the interchange of two sites i and j (neighbouring sites in our case), thereby conserving the conformational order parameter of the system. While Glauber dynamics is the only dynamics required for the Pink model for single-component lipid systems, both Glauber and Kawasaki dynamics have been applied to the related models for lipid/cholesterol systems, binary lipid systems, and ternary systems with two lipid species and cholesterol.

Detailed models of lipid and lipid/cholesterol systems usually consider thousands of possible microscopic conformations for a given lipid chain. However, the models that are used in this thesis have all of these configurations regrouped into a small number of states, each having the same energy and an associated degeneracy.

In the Pink model—as described in Chapter 2—all lipid chain conformations with the same energy and the same length are considered to be in the same conformational state. A total of 10 conformational states, each with an associated degeneracy D_α, are considered. In applying the Metropolis Monte Carlo algorithm, we replace the energy E_α of state α by $E_\alpha - kT\log D_\alpha$ and sample from the 10 conformational states. This will give us the same result as if we had sampled from each individual configuration. Therefore, in calculating the energy change δH from the original configuration Ω^1 to a trial configuration Ω^*, using Glauber dynamics in which only one lipid chain has changed conformation, we arrive at the following expression for the energy difference (δH) between two chain in states α and β:

$$\delta H = E_\alpha - E_\beta - kT\log\frac{D_\alpha}{D_\beta}, \tag{3.21}$$

where $E_\alpha - E_\beta$ can be calculated from the corresponding Hamiltonian and $\frac{D_\alpha}{D_\beta}$ is the ratio of the respective degeneracy of the old and new conformational states of the lipid chain. In the case of Kawasaki dynamics, the energy change δH would be:

$$\delta H = E_\alpha - E_\beta - kT\log\frac{D_\alpha}{D_\beta} = E_\alpha - E_\beta, \tag{3.22}$$

because there is no change in the population of each conformational state and, therefore, no change in the total degeneracy of the system.

The procedures of the Metropolis algorithm for single-component lipid system, lipid/cholesterol system, binary lipid system, and ternary lipid/cholesterol system are listed below. Note that, whenever an energy change is mentioned, it always refers to the quantity $E - kT \log D$.

3.4.1 Implementation for Single-Component Lipid System in Pink Model

Consider a two dimensional triangular lattice with $N = L \times L$ sites, where each site is occupied by a lipid chain in one of the 10 different conformational states. Periodic boundary conditions (Fig. 3.1) are imposed on the system in order to minimize the finite size effects. The Metropolis algorithm for single-component lipid bilayers based on the Pink Model is as follows:

1. Choose a lattice site i randomly.
2. Choose a random trial state from 1 to 10 for the lipid chain at site i.
3. Calculate the change in energy δH involved in the change of state according to the Pink Hamiltonian in Section 2.1.2.
4. Follow steps 4, 5, and 6 of the Metropolis algorithm in Section 3.3.

When this algorithm is applied the same number of times as the number of sites ($N = L \times L$) in the system, the system is said to have evolved one Monte Carlo step. A single Monte Carlo step is our unit of time, although it may not be related to the real time in a physical system, because the dynamics of a physical system is very different than that used in Monte Carlo simulations.

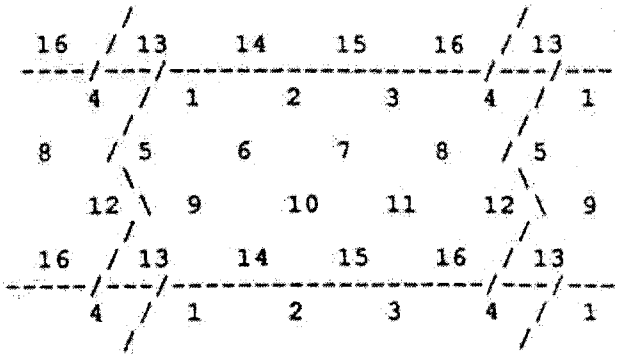

Figure 3.1 Periodic boundary conditions of a 4 x 4 system in our MC simulations. Reproduced from reference [62] with permission of the author.

3.4.2 Implementation for Lipid/Cholesterol System in Cruzeiro-Hansson Model

For lipid bilayers containing cholesterol molecules, the sites of the triangular lattice are either occupied by a lipid chain in one of ten conformational states or by a cholesterol molecule. The respective numbers of lipid sites and cholesterol sites depend on the cholesterol concentration we assigned to the system initially. The following is the implementation of the Metropolis Monte Carlo algorithm for the lipid/cholesterol system using the Cruzeiro-Hansson Model:

1. Choose a lattice site i randomly.
2. If the site i contains a lipid chain, follow steps 2. and 3. of the procedure for the single-component lipid membrane, using the Hamiltonian in Section 2.2.1.
3. If the site i contains a cholesterol molecule, select one of its nearest neighbour sites j randomly. If the site j is occupied by a cholesterol molecule, return to step 1. of the procedure. If the site j contains a lipid chain, then consider the exchange of cholesterol i and lipid chain j as a trial configuration Ω^* and compute the change in energy δH for the system according to the Hamiltonian in Section 2.2.1.
4. Follow steps 4, 5, and 6 of the Metropolis algorithm in Section 3.3.

Note that the above procedure for lipid/cholesterol system involves both Glauber dynamics (step 2) for lipid chains and Kawasaki dynamics (step 3) between lipid chains and cholesterol molecules.

As mentioned before, the system is said to have evolved one Monte Carlo step after this algorithm has been applied N times.

3.4.3 Implementation for Binary Lipid System in Jørgensen Model

We now consider a system containing two different lipid species, A and B, each with ten different conformational states available to them. Therefore, each site in our triangular lattice can take on one of the twenty different conformational states. The number of sites available to each of the lipid species depends on the mole percentage of the two lipids that we assigned initially. Let us allocate conformational states 1 to 10 (i.e., $\alpha \in [1,10]$) for lipid A and states 11 to 20 (i.e., $\alpha \in [11,20]$) for lipid B. In this thesis, we have used two different algorithms for the binary system. The first one is used by Jørgensen *et al.* in their original work [50], where trial states are chosen either with Glauber dynamics or Kawasaki dynamics, each with ½ of the chance. The second algorithm was proposed by Boal [77] and is first used in this thesis, in which both Glauber and Kawasaki dynamics are applied to trial states at every move. The two algorithms for binary lipid systems are as follows:

Algorithm 1

1. Choose a lattice site i randomly.
2. Pick a random number $r \in [0,1]$.

3. If $r \leq 0.5$, apply Glauber dynamics. Choose a random trial state from 1 to 10 for the lipid chain at site i if it is lipid species 1, or from 11 to 20 if it is lipid species 2. Consider that as the trial configuration Ω^*.

4. If $r > 0.5$, apply Kawasaki dynamics by select one of its nearest neighbour sites j randomly, and consider the exchange of cholesterol i and lipid chain j as a trial configuration Ω^*.

5. Calculate the change in energy δH involved in the change of state according to the Pink Hamiltonian in Section 2.3.1.

6. Follow steps 4, 5, and 6 of the Metropolis algorithm in Section 3.3.

Algorithm 2

1. Choose a lattice site i randomly.

2. Select one of its nearest neighbour sites j randomly.

3. Choose random trial states (1 to 10 for lipid A, 11 to 20 for lipid B) for both sites i and j respectively, while conserving the lipid species in that site.

4. Consider the exchange of lipid chain i and lipid chain j with new states chosen in step 3 as a trial configuration Ω^*.

5. Calculate the change in energy δH involved in the change of state according to the Pink Hamiltonian in Section 2.3.1.

6. Follow steps 4, 5, and 6 of the Metropolis algorithm in Section 3.3.

Note that, in algorithm 2, both Glauber and Kawasaki dynamics are applied in step 4 of the procedure. In our simulations, both algorithms yield the same result, although algorithm 2 reaches equilibrium with fewer Monte Carlo steps than algorithm 1.

3.4.4 Implementation for Ternary Lipid Cholesterol System

The ternary system that we study consists of two lipid species A and B as well as cholesterol. Therefore, we have a total of 21 different conformational states in the system, with state 1 to 10 representing lipid A, state 11 to 20 representing lipid B, and state 21 corresponding to cholesterol. As before, the number of sites available to different species

depends on their respective concentration in the mixture. Both Glauber and Kawasaki dynamics are being used in the way proposed by Boal [77] as in Algorithm 2 of the binary lipid system in Section 3.4.3. The detailed algorithm is as follow:

1. Choose a lattice site i randomly.
2. Select one of its nearest neighbour sites j randomly.
3. If site i is not occupied by a cholesterol, then choose a random trial state (1 to 10 for lipid A, 11 to 20 for lipid B) for site i, while conserving the lipid species in that site. Repeat this procedure for site j.
4. If site i is occupied by a cholesterol, then set the trail state of site i as cholesterol. Same for site j.
5. Consider the exchange of site i and site j with new states chosen in step 3. as a trial configuration Ω^*.
6. Calculate the change in energy δH involved in the change of state according to the Pink Hamiltonian in Section 2.4.
7. Follow steps 4, 5, and 6 of the Metropolis algorithm in Section 3.3.

The Monte Carlo simulation results presented in this thesis are for a system on a triangular lattice with periodic boundary conditions (Fig. 3.1). The lattice sizes used in the simulation were $N = 100 \times 100$ for the single-component system and $N = 60 \times 60$ for the binary and the ternary systems. 100 Monte Carlo (MC) steps were used for the warm up before the first configuration was taken. For the calculation of the thermodynamic averages and the response functions of the systems (e.g., lateral area, energy, specific heat, etc.), at least 50 equilibrium configurations are averaged over. Snapshots of microconfigurations were obtained after 20000 MC steps. To ensure all configurations that are averaged over are independent of each other, they are separated by at least 20 MC steps from each other.

4 Results for Single-Component Lipid Bilayers

In this section we present the results from the numerical Monte Carlo simulations on the ten-state Pink model of the main transition in single-component saturated diacyl phosphatidylcholine (PC) bilayers. Systems of diacyl PC bilayers with different chain lengths were investigated, including DLPC (m=12), DMPC (m=14), DPPC (m=16), DSPC (m=18), DAPC (m=20) and DBPC (m=22) bilayers. Simulations were preformed on a 100×100 lattice. The systems were warmed up with 100 MC steps before the first configuration was taken. Thermodynamic quantities and response functions were averaged over at least 50 equilibrium configurations, each separated by 20 MC steps. Snapshots of microconfigurations were obtained after 20000 MC steps.

The results for DLPC, DMPC, DPPC and DSPC bilayers (i.e., m=12 to 18) are used to compare with previous simulation results. We also extended the simulations to DAPC (m=20) and DBPC (m=22) bilayers to further the investigation of the dependence of the bilayer properties on chain length.

Fig. 4.1 shows the temperature dependence of the average internal energy per molecule $E(T)$, average cross-sectional area per molecule $A(T)$, and average nematic order parameter per molecule $S(T)$. These three quantities exhibit a dramatic increase at a temperature T_m corresponding to the particular PC species. Fig. 4.2 shows the temperature dependence of the specific heat $C_p(T)$ and the isothermal compressibility

$\kappa_T(T)$, calculated from the energy fluctuations and area fluctuations using Eq. (3.11) and (3.13), respectively. A large peak is observed respectively in $C_p(T)$ and $\kappa_T(T)$ at the corresponding T_m for the different lipid species. The peak at the transition temperature decreases in height as the acyl-chain length is reduced. However, at temperatures away from T_m a pronounced enhancement of the response functions is still obtained for shorter acyl-chain lengths.

Note that, in experimental studies, T_m is commonly used to denote the main phase transition temperature at which the system makes a transition from the gel phase to the liquid crystalline phase. As discussed in Ch.1, the nature of the main phase transition for the experimental DPPC bilayers is proposed by several groups to be weakly first-order but close to a critical point. On the other hand, in theoretical studies of the Pink model, one way to determine the nature of the 'main phase transition' in the model is by using the Ferrenberg-Swendsen re-weighting techniques [108] and the Lee and Kosterlitz finite-size scaling [109, 110]. Using these methods, Corvera, Laradji and Zuckermann [27] and Mouritsen [107] showed that the Pink model for PC bilayers with the parameters used in this thesis does not exhibit a first order phase transition for $m<20$ in the thermodynamic limit (the free-energy barrier vanishes with increasing system size), whereas for $m\geq 20$, the free-energy barrier increases with system size signalling the occurrence of a first-order phase transition. They also found that the case of $m=18$ is close to being at the borderline.

From this discussion, we can now determine the phase terminology that can be used to describe PC lipid bilayers studied within the framework of the Pink model. First

of all, T_m denotes the midpoint of the region at which thermodynamic quantities exhibit a dramatic increase as T increases, which would also coincide with the midpoint of the peak that occurs in the response functions. In this context, T_m does not necessarily denote a transition temperature in the ordinary sense, as such a transition does not exist for $m<20$. For DAPC and DBPC where $m\geq 20$, a first-order phase transition is present and, hence, regular phase terminology can be used. The phases below and above T_m are denoted as the **so** (solid-ordered) phase and the **ld** (liquid-disordered) phase, which were already introduced in Ch. 1. On the other hand, for DLPC, DMPC, DPPC and DSPC where $m<20$, no real phase transition is present. Therefore, we describe the system below T_m as the '**so** microscopic complexion' ('**so** mc') and the system above T_m as the '**ld** microscopic complexion' ('**ld** mc'). The same terminology will be used throughout the thesis, that is, the term 'phase' will only be used if a first-order phase transition is present. Otherwise the system will be described as having a 'microscopic complexion' ('mc').

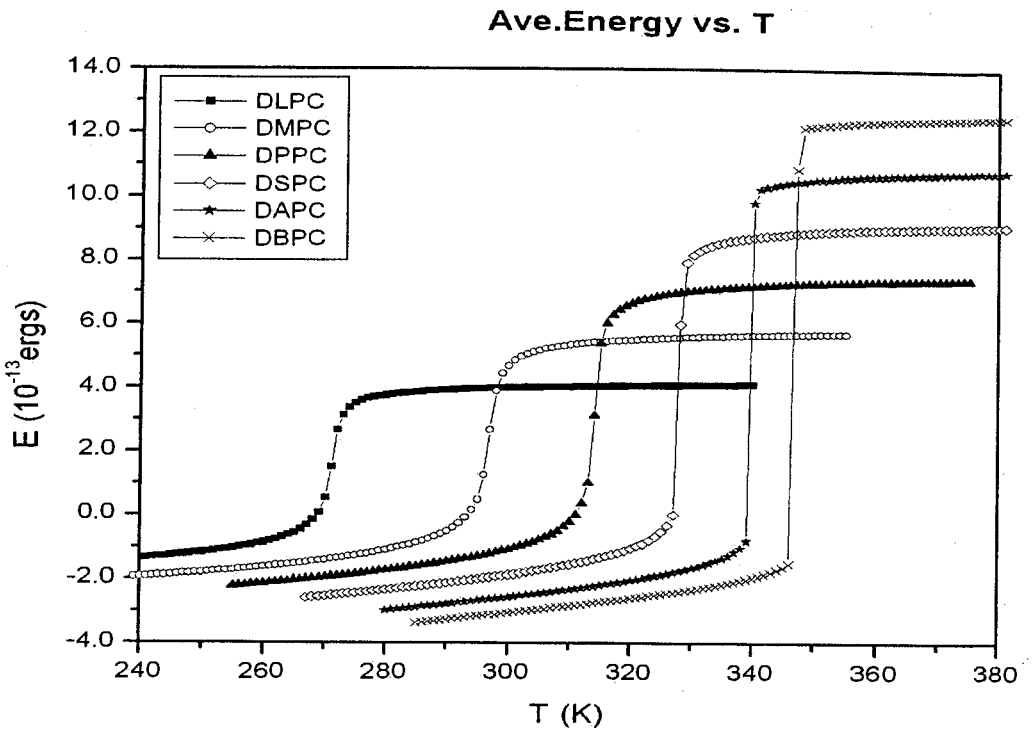
Ave.Energy vs. T
DLPC
DMPC
DPPC
DSPC
DAPC
DBPC
E (10^{-13} ergs)
T (K)
14.0
12.0
10.0
8.0
6.0
4.0
2.0
0.0
-2.0
-4.0
240
260
280
300
320
340
360
380

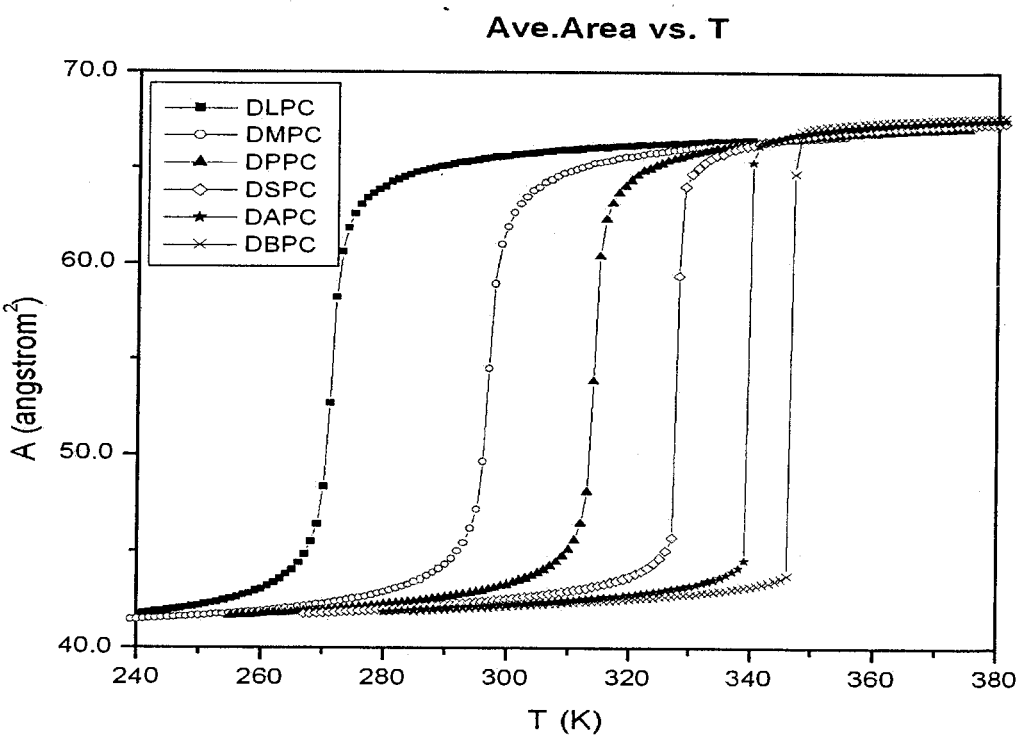
Ave.Area vs. T
DLPC
DMPC
DPPC
DSPC
DAPC
DBPC
A (angstrom^2)
T (K)
70.0
60.0
50.0
40.0
240
260
280
300
320
340
360
380

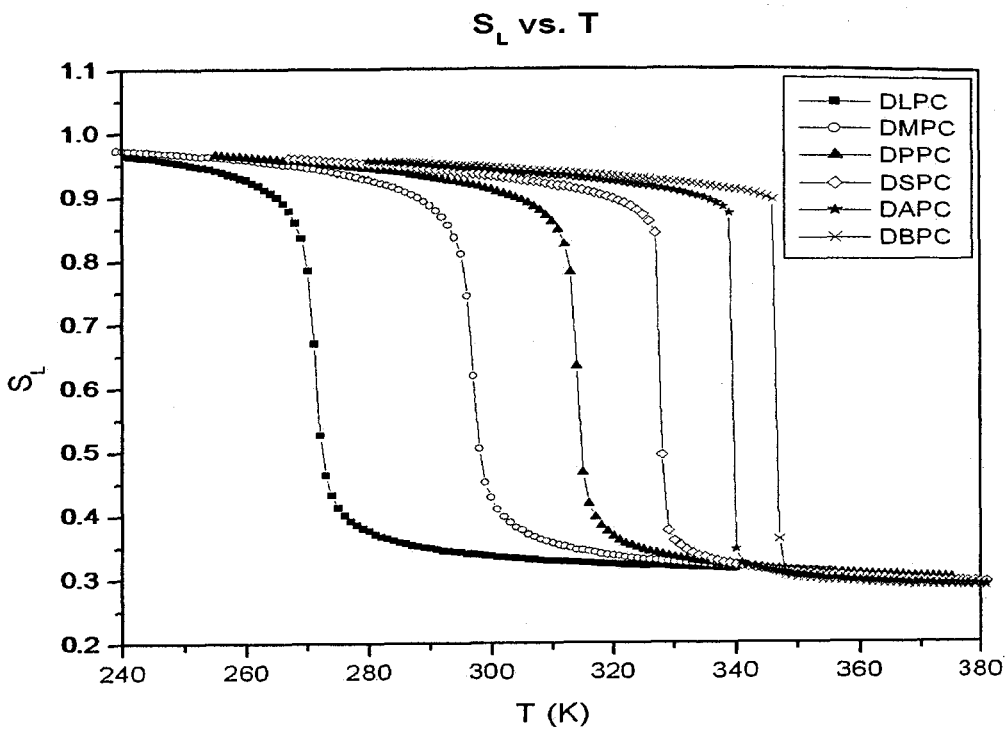

Figure 4.1 **Average internal energy per molecule E, average cross-sectional area per molecule A and nematic order parameter per molecule S versus T of DLPC, DMPC, DPPC, DSPC, DAPC and DBPC bilayers.**

Note that $E = \frac{1}{N'} < \mathcal{H} >$ where N' is the total number of molecules in the system and $\mathcal{H}$ is given by Eq. (2.8-10), $A =< A_\alpha >$ and $S =< S_\alpha >$ where S_α is given by Eq. (2.6).

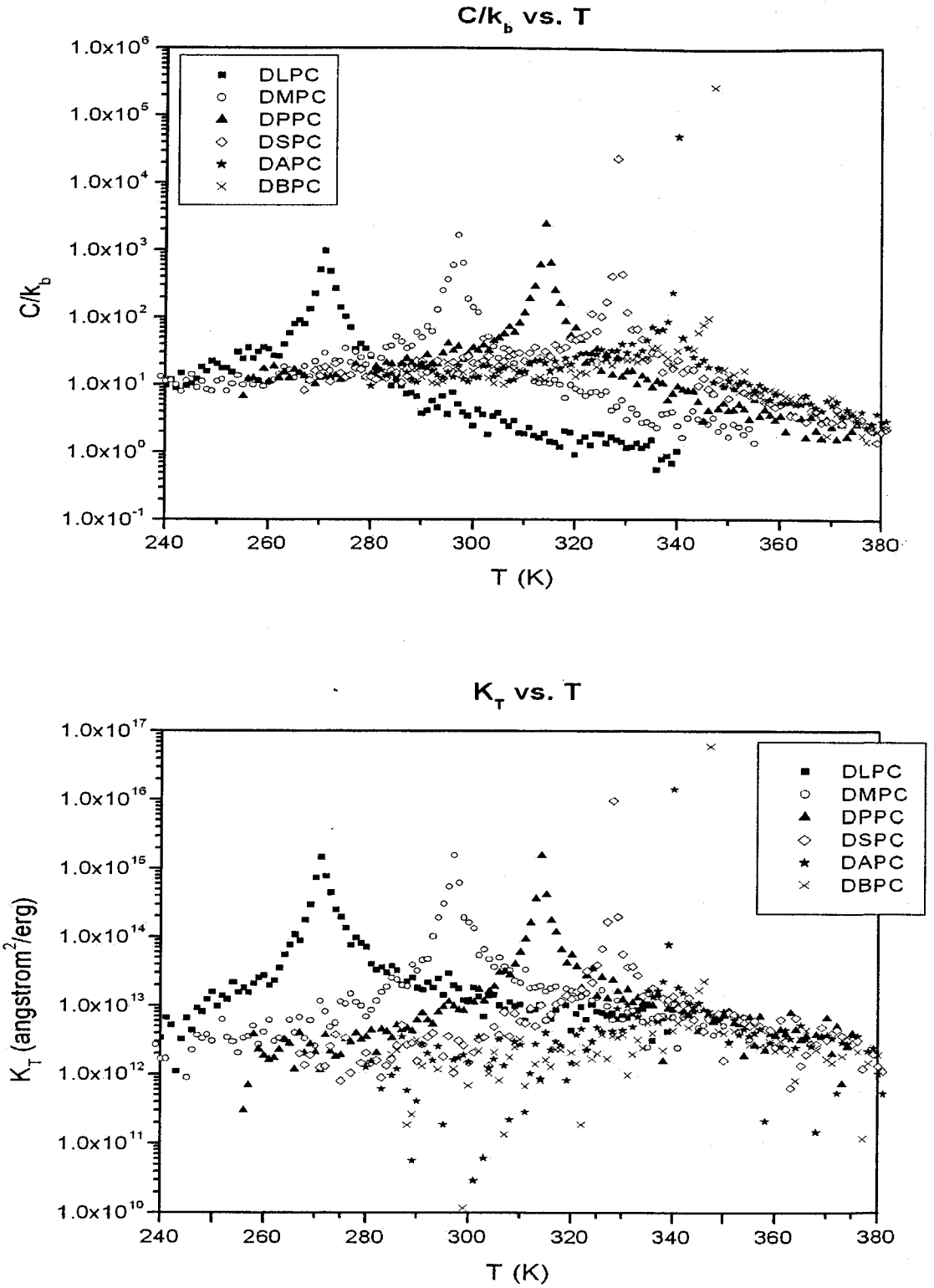

Figure 4.2 **Specific heat per lipid molecule C_p and isothermal compressibility K_T versus T of DLPC, DMPC, DPPC, DSPC, DAPC and DBPC bilayers.**
C_p is calculated using Eq. (3.11) and κ_T is calculated using Eq. (3.13).

Snapshots of microconfigurations for DPPC in thermodynamic equilibrium are shown in Fig. 4.3 at temperatures below, at, and above T_m. As discussed previously, no first-order transition occurs in the case of DPPC (m=16). It has been pointed out by Mouritsen [111] that, for DPPC as well as PC species with m<20, the Pink model exhibits quasi-critical behaviour in the neighbourhood of T_m and is consequently dominated by thermal fluctuations. Previous Monte Carlo simulation studies have identified the microscopic phenomena underlying the fluctuations near T_m [27, 28, 54, 78] as the occurrence of a dynamic lipid-domain formation phenomenon. As seen in Fig. 4.3, the strong lateral density fluctuations are manifested in the formation of domains of the '**ld** mc' in the '**so** mc' below T_m, and domains of the '**so** mc' in the '**ld** mc' above T_m. It has also been shown [78] that this domain formation is a dynamic one: clusters are continuously created and annihilated and they persistently fluctuate in size.

The results of DLPC, DMPC, DPPC and DSPC bilayers presented in this section are in agreement with previous simulations [57, 62, 78]. The results for DAPC and DBPC are also shown to be consistent with the expected trend.

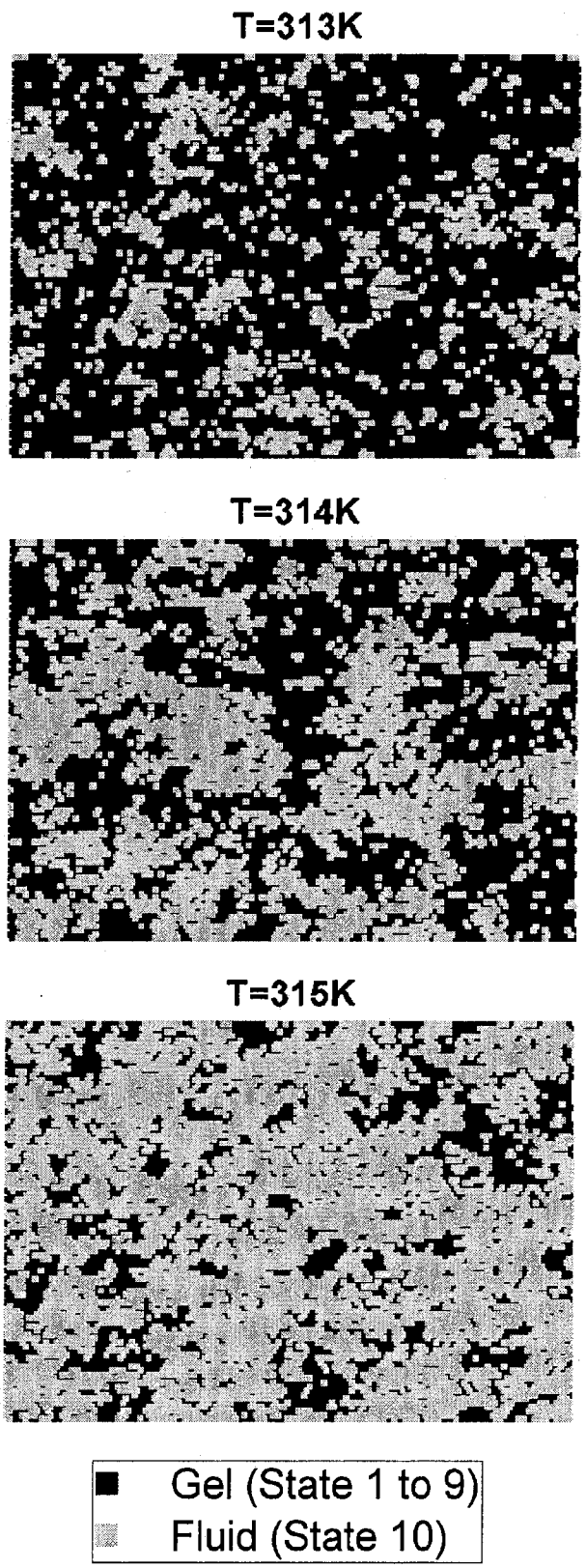

Figure 4.3 **Snapshots of simulated microconfigurations of DPPC lipid bilayers at temperatures below (313K), at (314K), and above (315K) the main transition temperature T_m.**

5 Results for Lipid/Cholesterol Bilayers

Monte Carlo simulations of the Cruzeiro-Hansson Model of lipid/cholesterol bilayers were performed using the algorithm presented in Section 3.4.2. The effects of cholesterol in diacyl phosphatidylcholine (PC) bilayers as a function of acyl chain length from m=12 to m=22 were investigated. Here we only present the results of DLPC (m=12)/cholesterol and DPPC (m=16)/cholesterol in detail, in order to serve as a point of reference for the study of DLPC/DPPC/cholesterol bilayers in Chapter 7. MC simulations of DMPC (m=14), DPPC (m=16) and DSPC (m=18) with the original parameters [28] have been performed by Cruzeiro-Hansson et al. [28] as well as Corvera [62], with which our results will be compared.

In our simulations, cholesterol concentrations (Xc) from 5 mol% (i.e., Xc=0.05) to 50 mol% (i.e., Xc=0.5) were added to the system. As mentioned in Section 2.2.1, the original Cruzeiro-Hansson model was intended only for lipid/cholesterol systems with low cholesterol concentrations, i.e., $x_C \leq 0.1$ [28]. Therefore, the results of this model with higher cholesterol concentrations are not expected to be reliable. We have modified the model by increasing the original $I_C(5)$=0.45 of DPPC/cholesterol bilayers in an attempt to accommodate systems with higher cholesterol concentrations. Values of $I_C(5)$ ranging from 1 to 2 are used in our study. Results from both the original Cruzeiro-Hansson Model and the modified model are presented and compared in this section.

Monte Carlo simulations in this chapter is performed on a 100×100 lattice, with a warm-up of 500 MC steps, thermodynamic properties and response functions are

averaged over 500 equilibrium configurations, snapshots of microconfigurations are obtained after 400,000 MC steps.

5.1 Simulation Results for DLPC/Cholesterol and DPPC/Cholesterol Bilayers using the Cruzeiro-Hansson Model (i.e., $I_C(1\text{-}10)$=0.45)

Shown in Fig. 5.1 are the thermodynamic properties of DLPC/cholesterol and DPPC/cholesterol bilayers as a function of temperature for several cholesterol concentrations. In Fig. 5.1a and 5.1e, A_{AVE} is the area averaged over all lipids and cholesterol molecules calculated using $A_{AVE} =< A_\alpha >$, whereas in Fig. 5.1b and 5.1f, A_L represents the average phospholipid area excluding cholesterol and is calculated with $A_L = \frac{A - x_C A_C}{1 - x_C}$. Similarly, E_{AVE} is the energy averaged over all molecules in the bilayer calculated with $E_{AVE} = \frac{1}{N'} < \mathcal{H} >$, where N' is the total number of molecules in the system and $\mathcal{H}$ is given by Eq. (2.13). S_L is the average conformational order per lipid chain excluding cholesterol, which is assumed to have no conformational freedom, and is calculated by using $S_L =< S_\alpha >$, where S_α is given by Eq. (2.6).

As discussed in Ch.4, no phase transition exists for single-component DLPC (m=12) and DPPC (m=16) bilayers in the Pink model with the parameters used in this thesis. Similarly, DLPC/Cholesterol and DPPC/Cholesterol bilayers do not exhibit phase transitions in the experimental region. and phase coexistence in this model (evidence will be presented below). Therefore, the same definition of T_m as in Ch. 4 will be used in this

chapter, and the term 'microscopic complexion' will be used instead of 'phase'. In the single-component DLPC and DPPC bilayers, the thermodynamic properties exhibit a large change when passing through T_m despite the absence of a sharp phase transition. Fig. 5.1 shows that this change in the thermodynamic properties across T_m is reduced by the addition of cholesterol. For instance, Fig.5.1a and 5.1e show that, as Xc increases, the difference of A_{AVE} on the two sides of T_m is smaller, and A_{AVE} decreases at temperatures away from T_m. However, for a region of temperature just below T_m, the relationship between A_{AVE} and Xc is more complicated. Therefore, the phospholipid area A_L is shown in Fig. 5.1b and 5.1f, in which the dilution effect of cholesterol has been suppressed. The graphs show that cholesterol has an expansion effect in the '**so** microscopic complexion' ('**so** mc') and a contraction effect in the '**ld** microscopic complexion' ('**ld** mc'). A similar trend can be found in the E_{AVE} in Fig.5.1c and 5.1g, where the addition of cholesterol increases the average energy below T_m and decreases the average energy above T_m. This implies that cholesterol tends to induce the formation of *gauche* bonds or excitations below T_m, and suppress the formation of *gauche* bonds or excitations above T_m. The above observations are confirmed by the graphs of the conformational order parameter S_L shown in Fig. 5.1d and 5.1h. Cholesterol induces conformational disorder below T_m but induces conformational order above T_m.

DLPC **DPPC**

(a)

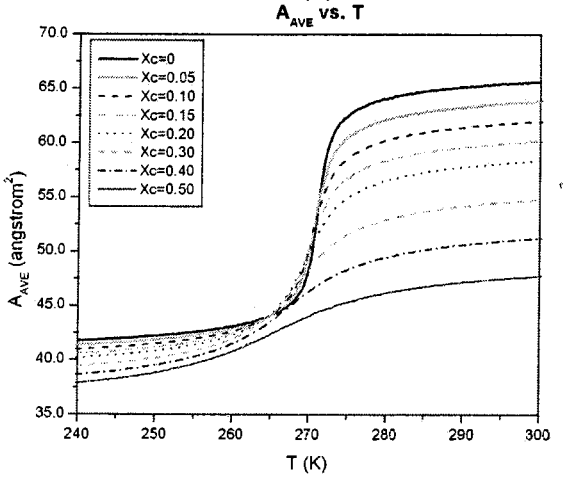

(e)

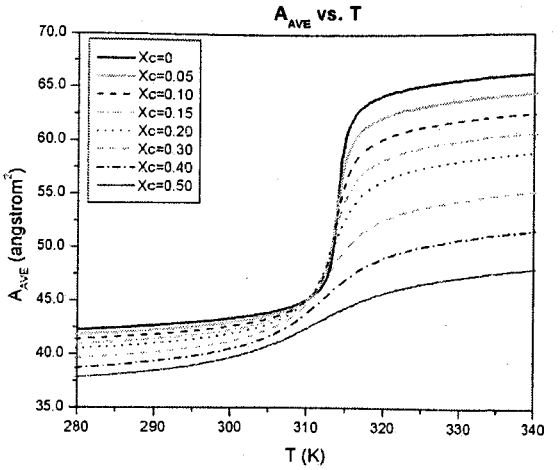

(b)

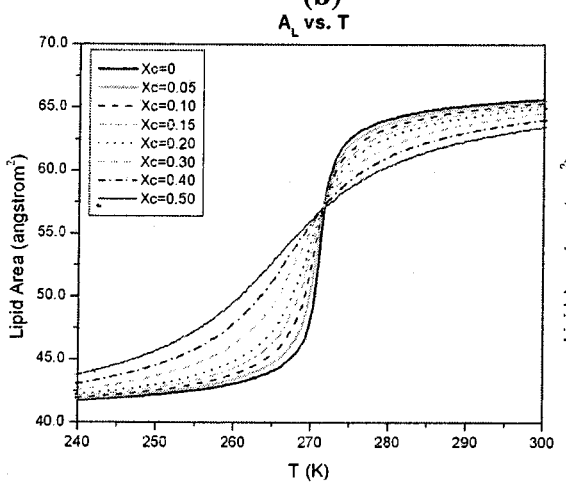

(f)

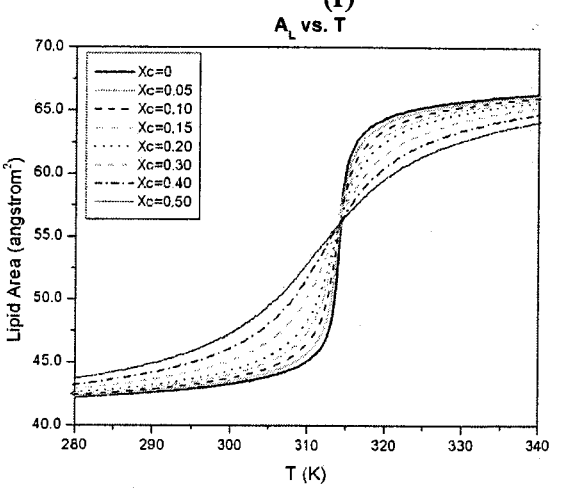

(c)

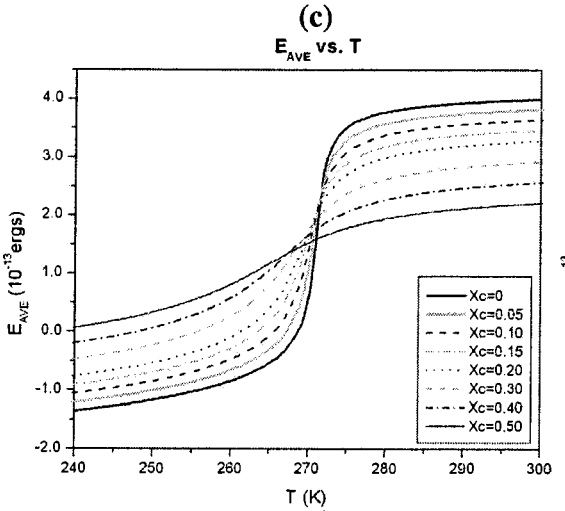

(g)

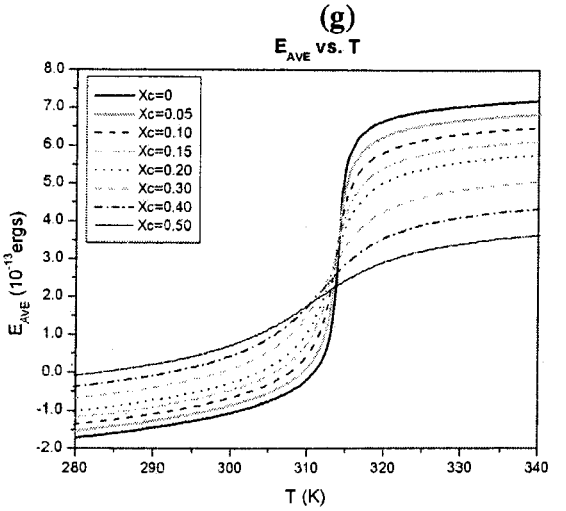

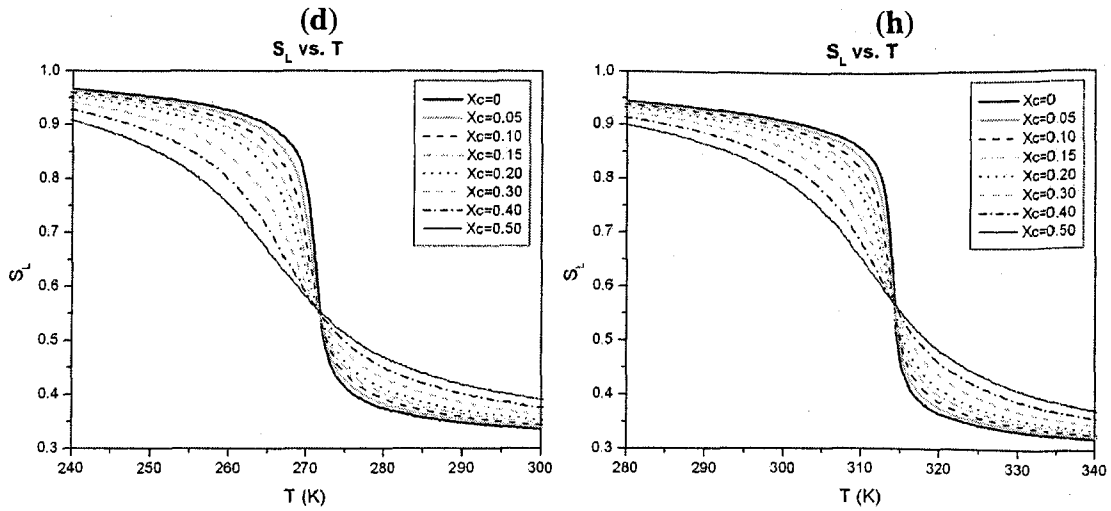

Figure 5.1 **(a) & (e) Average area per molecule A_{AVE}, (b) & (f) average area per lipid molecule (A_L), (c) & (g) average energy per molecule (E_{AVE}) and (d) & (h) average conformational order parameter per lipid chain (S_L) versus temperature for DLPC/cholesterol and DPPC/cholesterol bilayers.**

The specific heat C_p (Eq. 3.11) and the isothermal lateral compressibility K_T (Eq. 3.13) versus temperature for DLPC/cholesterol and DPPC/cholesterol bilayers are shown in Figs. 5.2, 5.3, 5.4 and 5.5. It is seen that, as cholesterol concentration increases, the peak height in the response functions decreases. The broadening of the peak caused by the addition of cholesterol is observed here, which agrees with the observations of the reduction of the changes of thermodynamic properties across T_m. Finally, a careful look at the position of T_m of DPPC/Chol bilayers shows that it decreases from 314K to 312K when Xc is increased from 0 to 0.5, which agrees with the mean-field calculations (discussed below). Similarly, the T_m of DLPC/Chol bilayers is observed to decrease from 271K to 265K over the same range of cholesterol concentrations.

In conclusion, the addition of cholesterol smoothes out the changes of the bilayers as temperature increases, and the system passes continuously from the '**so** mc' to the '**ld**

mc'. The above observations agree with the original work by Cruzeiro-Hansson *et al.* [28].

Fig. 5.6 shows the phase diagram of DPPC/Chol bilayers deduced from the specific heat peaks (Fig.5.4) as an illustration. As discussed above, the results calculated with this model for high cholesterol concentrations (Xc>0.1) are not expected to be reliable, but we include them here for the sake of completeness and for comparison with our modified model in the next section. Moreover, DPPC/Chol bilayers do not have a real phase transition in our model and, therefore, the position of the (rounded) peaks in the specific heat graphs do not represent the temperature of a phase transition but, rather, a smeared region where the system pass continuously from the '**so** mc' to the '**ld** mc'. In the phase diagram, this smeared region is represented by hollow squares and it decreases from 314K to 312K when Xc is increased from 0 to 0.5.

For the sake of completeness, a phase diagram derived from mean-field calculations by Cruzeiro-Hansson *et al.* [28] with the same parameters as the present simulations is shown in Fig. 5.7. Since mean-field calculations exclude fluctuations, a well-defined first order phase transition is present for the single-component DPPC bilayers, and a narrow coexistence region with a modest freezing-point depression is present in the mixture. However, in their work of Monte Carlo simulations on the same system with the same parameters, no signs of this phase separation are observed within the resolution limit [28].

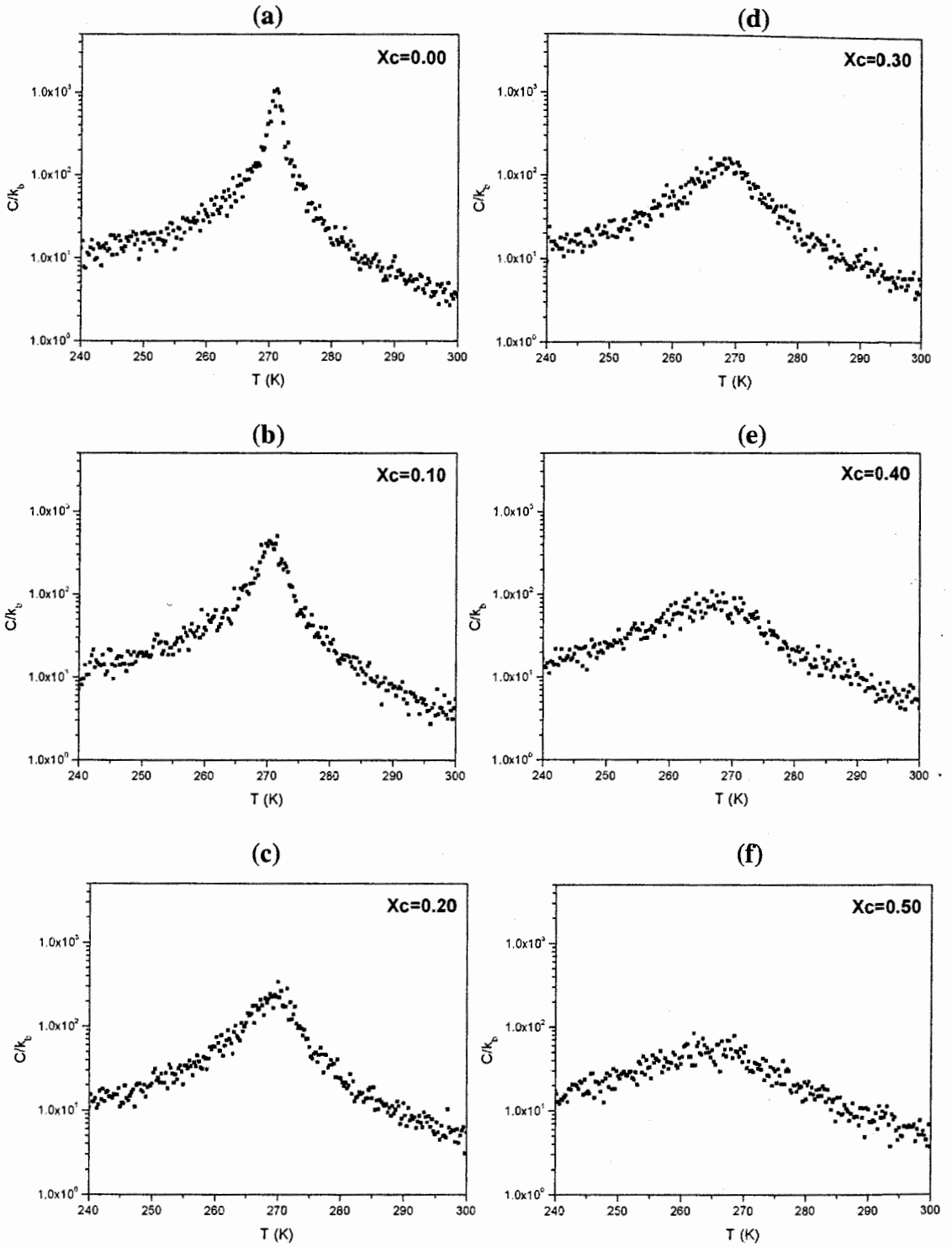

Figure 5.2 **Specific heat per molecule (C_p) versus temperature of DLPC/cholesterol bilayers.**

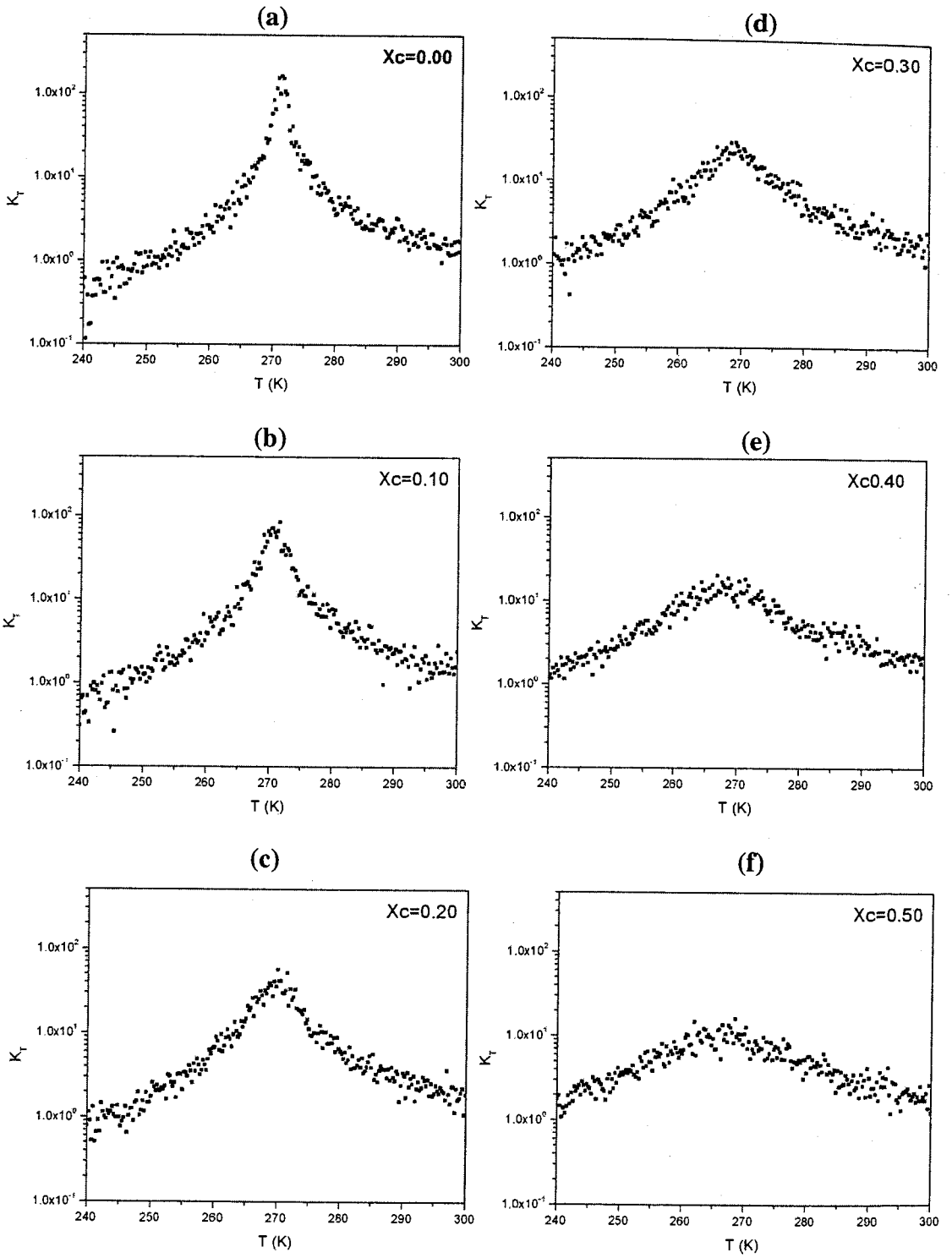

Figure 5.3 **Isothermal lateral compressibility (K_T) versus temperature of DLPC/cholesterol bilayers.**

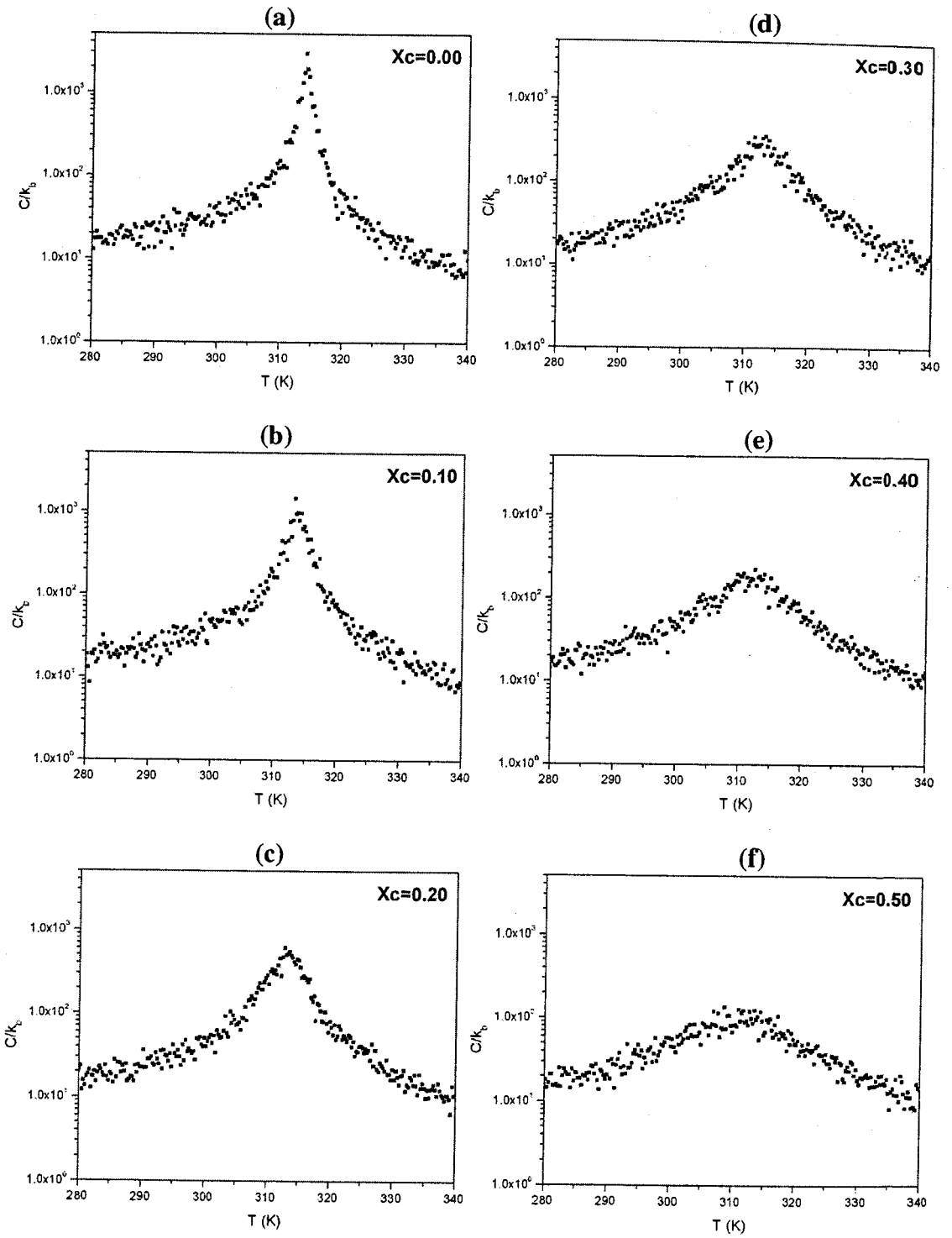

Figure 5.4 **Specific heat per molecule (C_p) versus temperature of DPPC/cholesterol bilayers.**

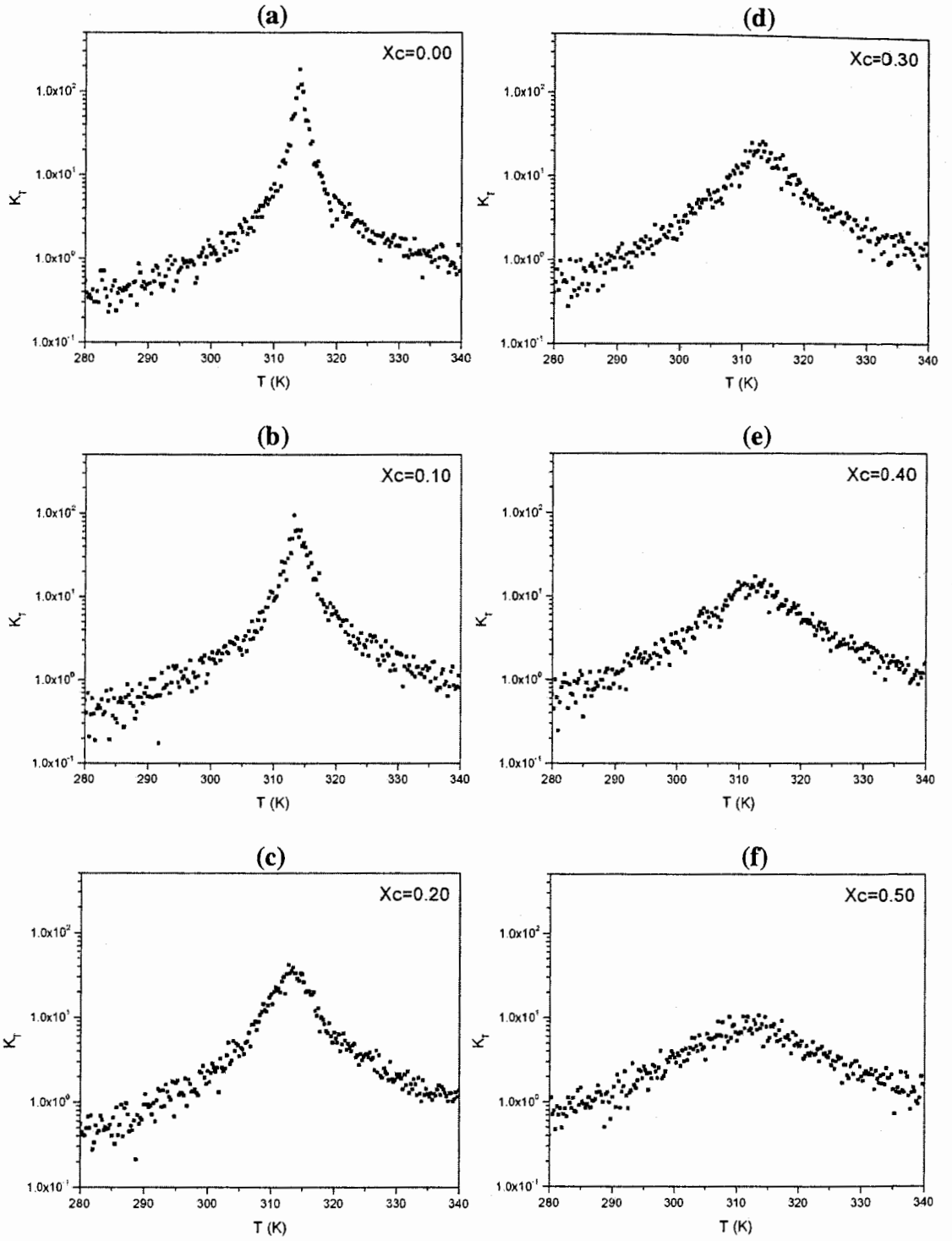

Figure 5.5 **Isothermal lateral compressibility (K_T) versus temperature of DPPC/cholesterol bilayers.**

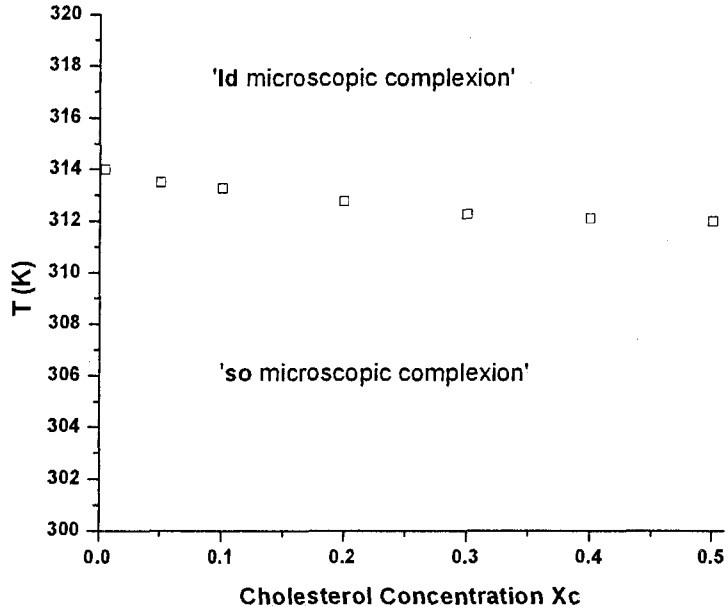

Figure 5.6 **Phase diagram of DPPC/Chol bilayers for the original Cruzeiro-Hansson model (i.e., *Ic(1-10)*=0.45). Hollow squares are the peak positions of the specific heat graphs (Fig. 5.3), which denote a smeared region where the system passes continuously from the 'so mc' to the 'ld mc' without a sharp phase transition.**

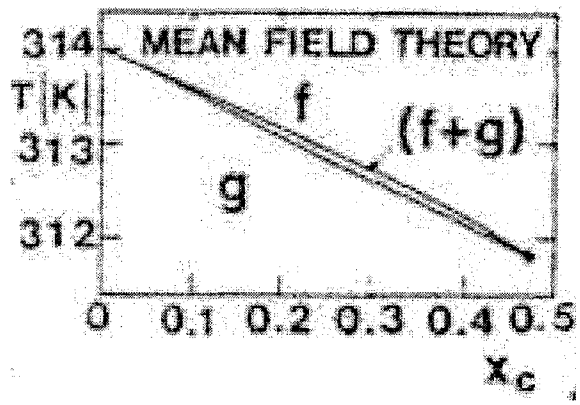

Figure 5.7 **Phase diagram of DPPC/Chol bilayers calculated by mean-field theory.**
The gel (so) and fluid (ld) phases are denoted by g and f and the coexistence region by (g+f). The heavy dot denotes a critical end-point in the phase diagram.

Although we only present the results of DLPC/cholesterol and DPPC/cholesterol here, the trends across a series of lipid/cholesterol bilayers having different acyl chain lengths ranging from m=12 (DLPC) to m=22 (DBPC) were also examined. We observed that the dependence of T_m on the acyl chain length (as in the single-component lipid bilayers in Ch. 4) is also present here. Namely, bilayers containing lipids with longer acyl chain lengths have higher T_m and vice versa. Overall, cholesterol was found to have the same systematic effects on lipids with different acyl chain lengths for all of the thermodynamic properties investigated.

Fig. 5.8 shows snapshots of microconfigurations of DPPC/cholesterol bilayers with different cholesterol concentrations at different temperatures. The results of DLPC/cholesterol bilayers are not shown here because the effects of cholesterol on that system are very similar to that of DPPC/cholesterol bilayers. The snapshots give us an indication of the manner in which the system changes microscopically as a function of cholesterol concentration. First, going across the snapshots as temperature increases (i.e., from left to right) for any one concentration of cholesterol (Xc), we observe the system changes continuously from the '**so** mc' to '**ld** mc'. However, highly disordered chains (state 10) are always present in the '**so** mc' and more ordered chains (states 1 to 9) are always present in the '**ld** mc'. This heterogeneous membrane structure has also been observed in the snapshots for single-component bilayers (Ch. 4), and is a result of the lateral density fluctuations as discussed previously. Since the fluctuations are particularly strong near T_m, membrane heterogeneity should also be most prominent there, as shown by the snapshots at 313K. For a detailed discussion of the membrane heterogeneity for the same model please see [28].

Now let us look at the snapshots taken at 313K, as it is close to T_m=314K for single-component DPPC bilayers. At Xc=0, we observe an '**ld** mc' in the background of the '**so** mc', which indicates that the system is below T_m. However, as Xc increases, the area covered by the '**so** mc' decreases and the area covered by the '**ld** mc' increases. This is due to the shift of T_m caused by the addition of cholesterol described earlier, namely, T_m is above 313K at Xc=0 and below 313K at Xc=0.50. In other words, when we increase cholesterol concentration from 0 mol% to 50 mol% at 313K, the system is gradually changing from one of '**so** mc' to a '**ld** mc'.

All simulation results of this section agree with the original work of Cruzeiro-Hansson *et al.* [28] and the thesis of Corvera [62].

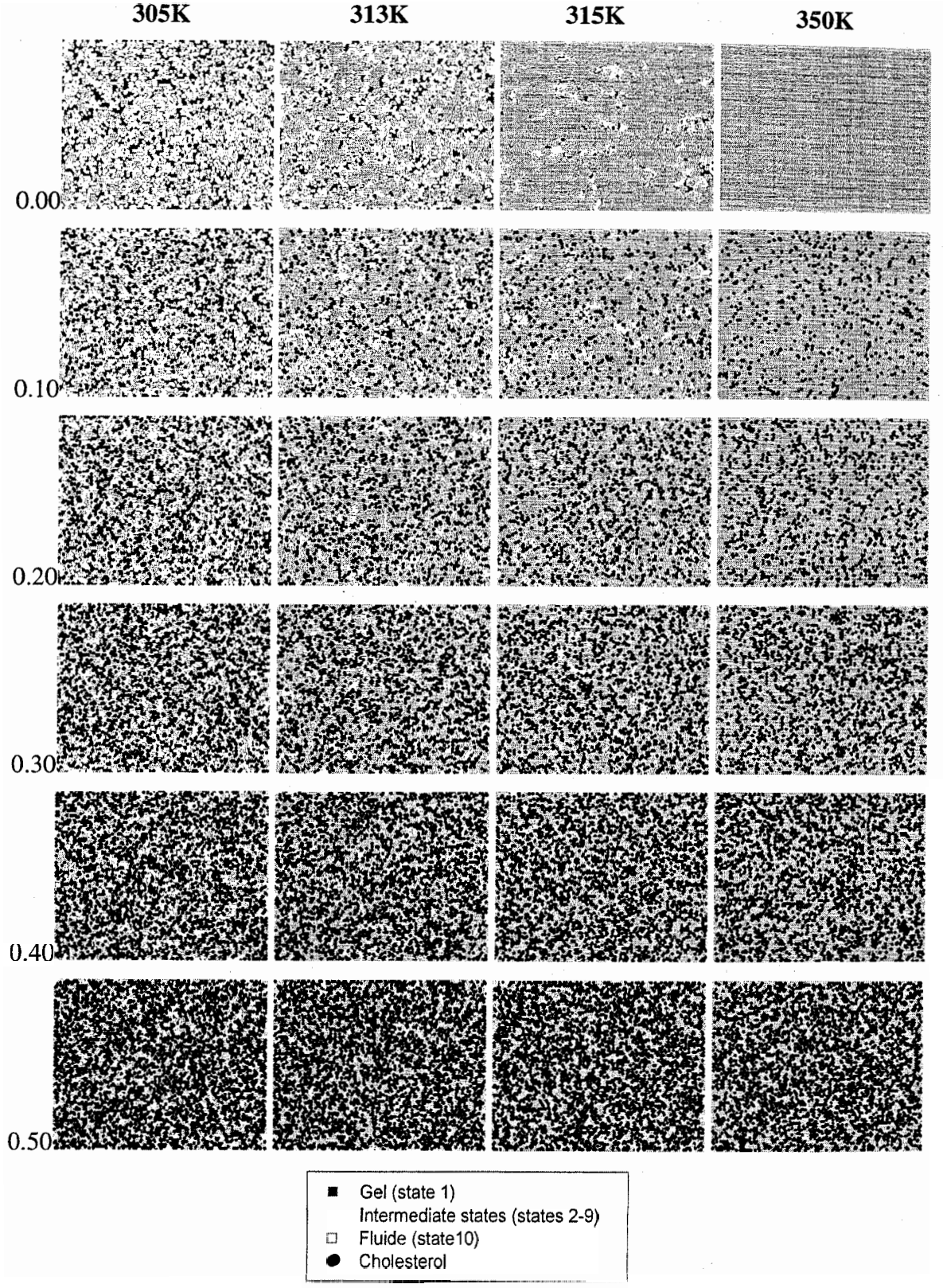

Figure 5.8 **Snapshots of simulated microconfigurations for T=295K, 313K and 315K with various cholesterol concentrations Xc (vertical axis) for DPPC/cholesterol bilayers.**

5.2 Simulation Results for DPPC/cholesterol Bilayers with the Modified Cruzeiro-Hansson Model (i.e., $I_C(5)$=1.5, 2)

In our modified model, the interaction constant $I_C(5)$ between lipid chains in state 5 and cholesterol is changed from the original value of 0.45 to a higher value. This results in a stronger interaction between cholesterol molecules and DPPC lipid chains in the kink state. As mentioned in Section 2.2.1, this modification is based on the hypothesis that a DPPC lipid chain in the kink state (i.e., state 5) is sterically compatible with a cholesterol molecule and, also, that the kink state has a molecular order parameter similar to that found from experiments in the **lo** phase. Furthermore, Mendelsohn *et al.* [112] have shown in infrared studies that there is a marked decrease in the number of *gauche* bonds in bilayers with high cholesterol concentrations (i.e., the **lo** phase) as compared to that in a single-component system. In this thesis, lipid/cholesterol systems with the parameter $I_C(5)$ ranging from 0.45 to 2 were investigated. Note that different values of $I_C(5)$ can be used to represent different sterol molecules having different affinities for a lipid chain in the kink state. Therefore, the 'cholesterol' in our simulation could represent a generic sterol molecule. We found that systems with the parameter $I_C(5)$= 1.5 and 2 are particularly interesting. $I_C(5)$=1.5 is relevant to the parameter set which gives the best comparison to experiment in the ternary lipid system in Ch. 7, and $I_C(5)$=2 shows interesting phase behaviour which does not exist in the cases with lower $I_C(5)$ values. Results of these two cases are presented in this section.

5.2.1 $I_C(5)$=1.5

Figs. 5.9, 5.10 and 5.11 show the thermodynamic properties, specific heat and snapshots of microconfigurations of DPPC/cholesterol bilayers with $I_C(5)$=1.5. Comparison of these graphs to Figs. 5.1, 5.4 and 5.5, where $I_C(5)$=0.45, shows that the increase of $I_C(5)$ magnifies the effects of cholesterol on the bilayer. The peak of the specific heat (Fig. 5.10) at T_m is further broadened, and the changes of the values of A_{AVE}, A_L, E_{AVE} and S_L (Fig. 5.9) across T_m are smaller compared to the case of $I_C(5)$=0.45. In particular, Fig. 5.9 clearly shows that the thermodynamic properties at $T>T_m$ approach those at $T<T_m$ as cholesterol concentration increases. For instance, when $I_C(5)$ is increased from 0.45 to 1.5, the value of the order parameter S_L at 50°C with Xc=0.30 changes from 0.40 to 0.67 and that of Xc=0.20 changes from 0.38 to 0.55. In other words, there is a significant increase in the average lipid chain conformational order at $T>T_m$ as $I_C(5)$ is increased. Table 5.1 shows the values of S_L calculated from ^{2}H-NMR data by Hsueh *et al.* [14] for ergosterol and by Endress *et al.* [81] for ergosterol, cholesterol and lanosterol. They are compared to the values of S_L from our simulation results with $I_C(5)$=0.45, 1.5 and 2, respectively. The values of S_L from experimental studies for different sterols are calculated from the relation, $M_1 = \frac{\pi}{\sqrt{3}}(\frac{e^2 q\theta}{h})\langle|S_{CD}|\rangle$ and $\langle S_L\rangle = 2\times\langle|S_{CD}|\rangle$, where M_1 is the first moment directly obtained from the ^{2}H-NMR experiment. Values of M_1 are directly read off from the graph of M_1 versus temperature from reference [14], and the values of $\langle|S_{CD}|\rangle$ are calculated from the average of the S_{CD} values of each carbon atom position along the acyl chain in reference [81].

Comparison of the theoretical and experimental values of S_L in Table 5.1 shows that our modification of the Cruzeiro-Hansson model with increased $I_C(5)$ values is a great improvement in modelling lipid/sterol bilayers with high sterol contents. For instance, considering the simulation results for $I_C(5)$=1.5, the conformational order parameter calculated from the modified model for 30 mol% cholesterol at T=50°C and T=60°C are much closer to that of the data by Thewalt *et al.* [14] than the original model .

However, in addition to the effects described above, we also observed that using $I_C(5)$=1.5 affects the T_m of the lipid/cholesterol bilayer. For instance, when Xc is increased from 0 to 0.5, T_m increases from 314K to 337K, instead of decreasing to 312K as in the case of $I_C(5)$=0.45. We hypothesize that this increase of T_m is due to the strong affinity of cholesterol to the kink state, such that higher temperatures are required for the system to pass completely to the '**ld** mc'. This effect can also be seen in the snapshots of microconfigurations in the following.

Fig. 5.11 shows the snapshots of microconfigurations with $I_C(5)$=1.5. Snapshots at 318K and 350K are shown instead of those at 315K (as was presented in Section 5.1) because 315K is no longer above T_m for higher Xc due to the increase in T_m with Xc, as discussed earlier. Comparing these snapshots to those of $I_C(5)$=0.45 (Fig. 5.8), we see a significant increase in the number of the intermediate states (states 2 to 9) as cholesterol concentration increases. Therefore, the system can no longer be classified as in the '**ld** mc' above T_m at higher concentrations of cholesterol. The strong interaction between cholesterol and the kink state leads to the sequestering of the kink state by cholesterol, and, hence, to the formation of the '**lo** microscopic complexion' ('**lo** mc'). As the use of the term 'microscopic complexion' indicates, this is not a distinct phase, but it has the

same symmetry as the '**so** mc' and the '**ld** mc', except that each of them is dominated by different lipid chain conformations. The lateral surface area, conformational energy and molecular order parameter of a lipid chain in the intermediate states are between those of a lipid chain in state 1 and state 10. Therefore, the '**lo** mc' is more compactly packed than the '**ld** mc' but less so than the '**so** mc'. Similarly, it has an average energy and conformational order in between those of the '**so** mc' and the '**ld** mc'.

Fig. 5.12 shows a partial schematic phase diagram of the DPPC/Cholesterol system with $I_C(5)$=1.5, as determined from an inspection of the snapshots of microconfigurations and the specific heat graphs. The most likely scenario is that the phase diagram is separated into three parts as follows. Above T~320K, the snapshots indicate that there is a closed region of phase coexistence between an '**ld** mc' and an '**lo** mc'. The horizontal lines indicate the approximate position of the phase boundary as deduced from the snapshots. The midpoints of the vertical lines close to 320K gives the position of a peak in the specific heat. The dotted lines above T~360K schematically indicate the closure of the phase coexistence region with the dot representing a critical point. However, this line has not been calculated numerically. It is also likely that there is a region of phase coexistence between an '**so** mc' and an **lo** phase with a critical point below 290K, but this region has not been investigated. The snapshots between 290K and 320K give little indication of phase separation. However we have included in the phase diagram the weaker possibility of such a phase separation as indicated by the dotted lines.

Table 5.1 **Experimental and theoretical molecular order parameter of binary DPPC bilayers containing different concentrations of sterol at (a) T=50°C and (b) T=60°C.**

(a) T=50°C

$\langle S_L \rangle$ \ Sterol Concentration	10 mol%	20 mol%	30 mol%	40±1 mol%*
MC simulation with $I_C(5)$=0.45	0.37	0.38	0.40	0.43
MC simulation with $I_C(5)$=1	0.39	0.46	0.54	0.63
MC simulation with $I_C(5)$=1.5	0.44	0.55	0.67	0.80
MC simulation with $I_C(5)$=2	0.43	0.52	0.62	0.75
DPPC/ergosterol bilayer [14]	0.38	0.48	0.61	0.68
DPPC/ergosterol bilayer [81]	--	--	--	0.54
DPPC/cholesterol bilayer [81]	--	--	--	0.64
DPPC/lanosterol bilayer [81]	--	--	--	0.60

(b) T=60°C

$\langle S_L \rangle$ \ Sterol Concentration	10 mol%	20 mol%	30 mol%	40±1 mol%*
MC simulation with $I_C(5)$=0.45	0.34	0.35	0.36	0.38
MC simulation with $I_C(5)$=1	0.35	0.38	0.43	0.50
MC simulation with $I_C(5)$=1.5	0.38	0.45	0.54	0.66
MC simulation with $I_C(5)$=2	0.39	0.47	0.58	0.71
DPPC/ergosterol bilayer [14]	0.34	0.42	0.51	0.63

* The data from [14] are for 42 mol% while those from MC simulations and [81] are for 40 mol%.

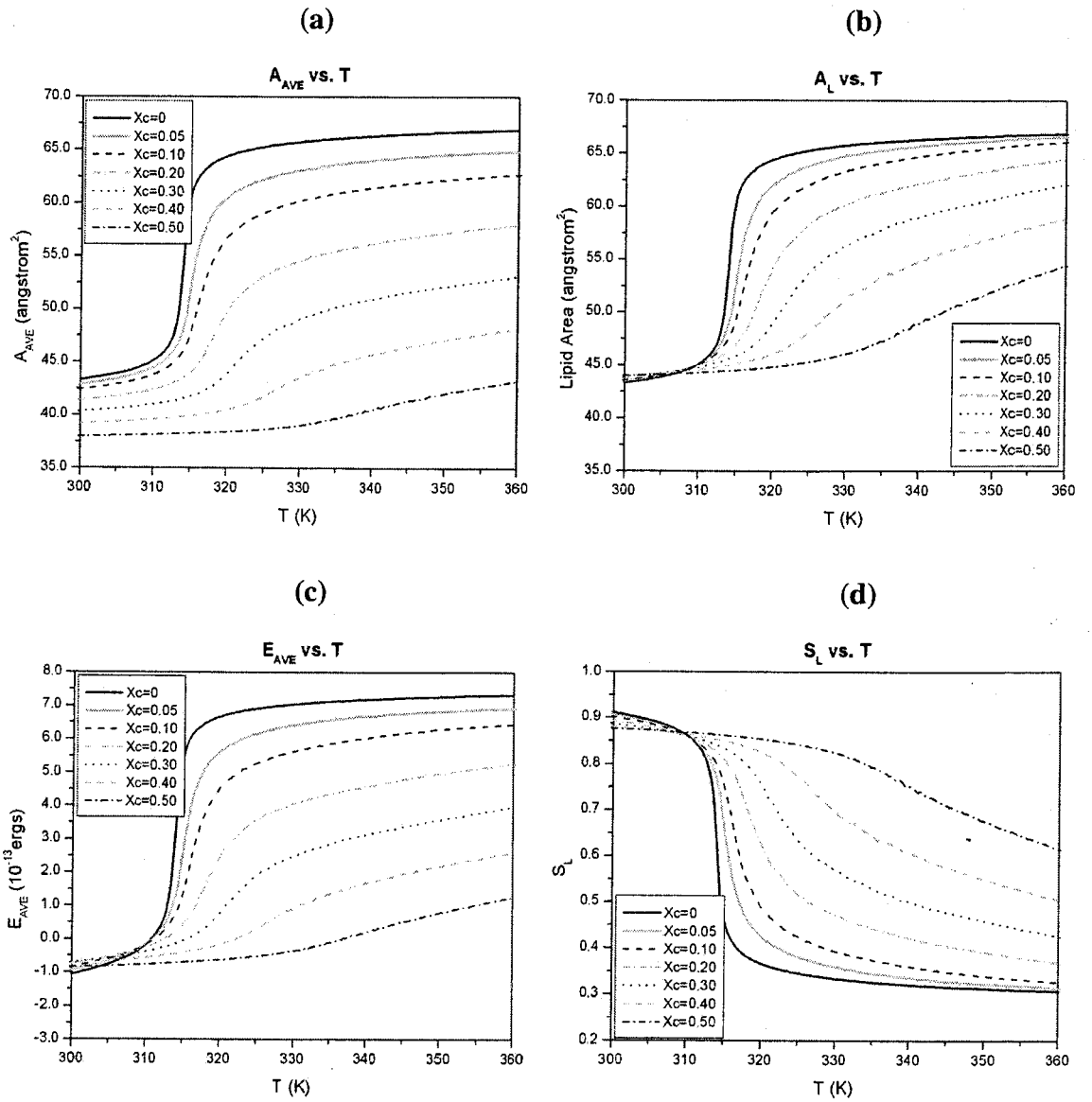

Figure 5.9 a) Average area per molecule (A_{AVE}), b) average area per phospholipid molecule (A_L), c) average energy per molecule (E_{AVE}) and d) average conformational order parameter per lipid chain (S_L) versus temperature for DPPC/cholesterol bilayers with $I_C(5)$=1.5.

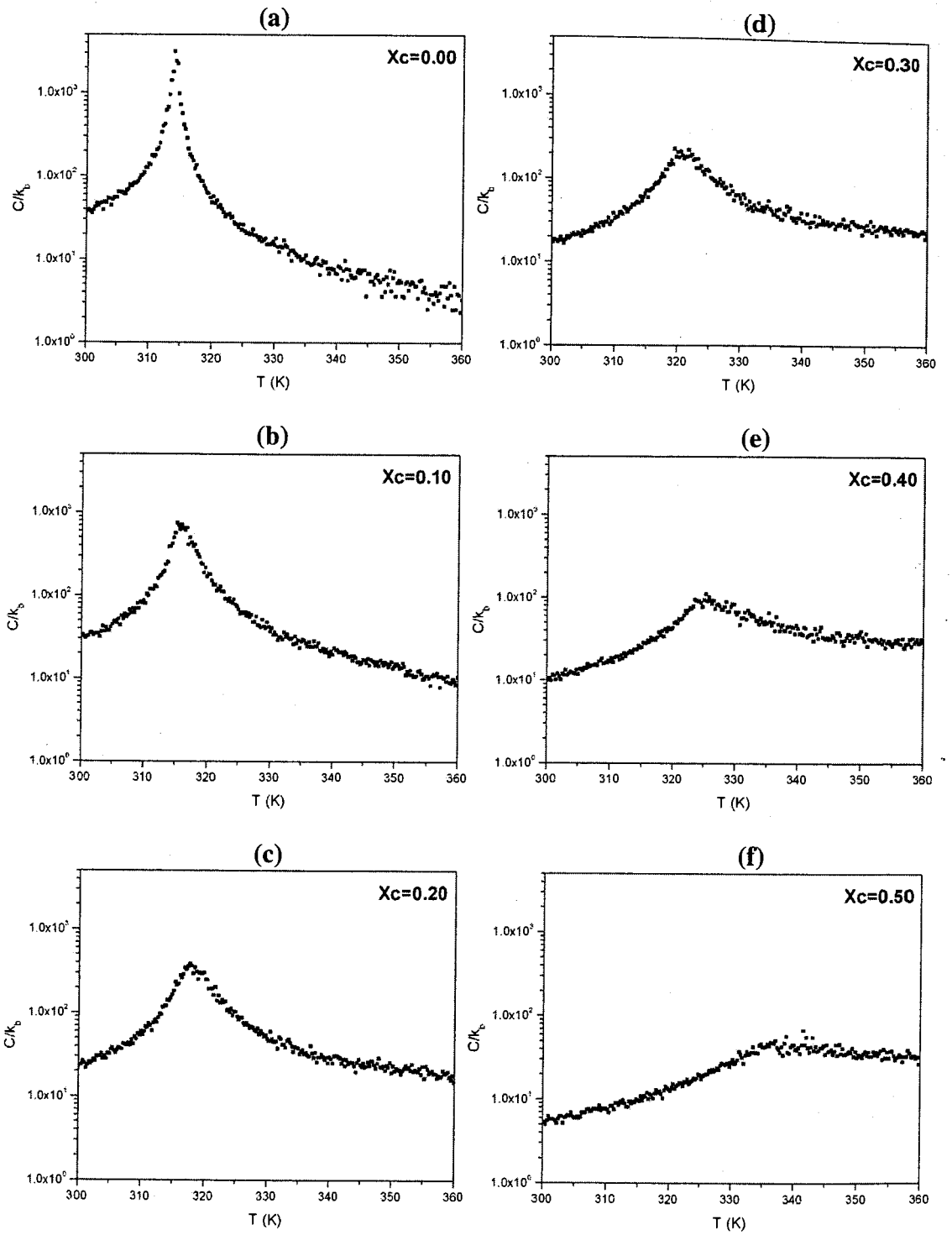

Figure 5.10 Specific heat per molecule (C_p) of DPPC/cholesterol bilayers with $I_C(5)$=1.5.

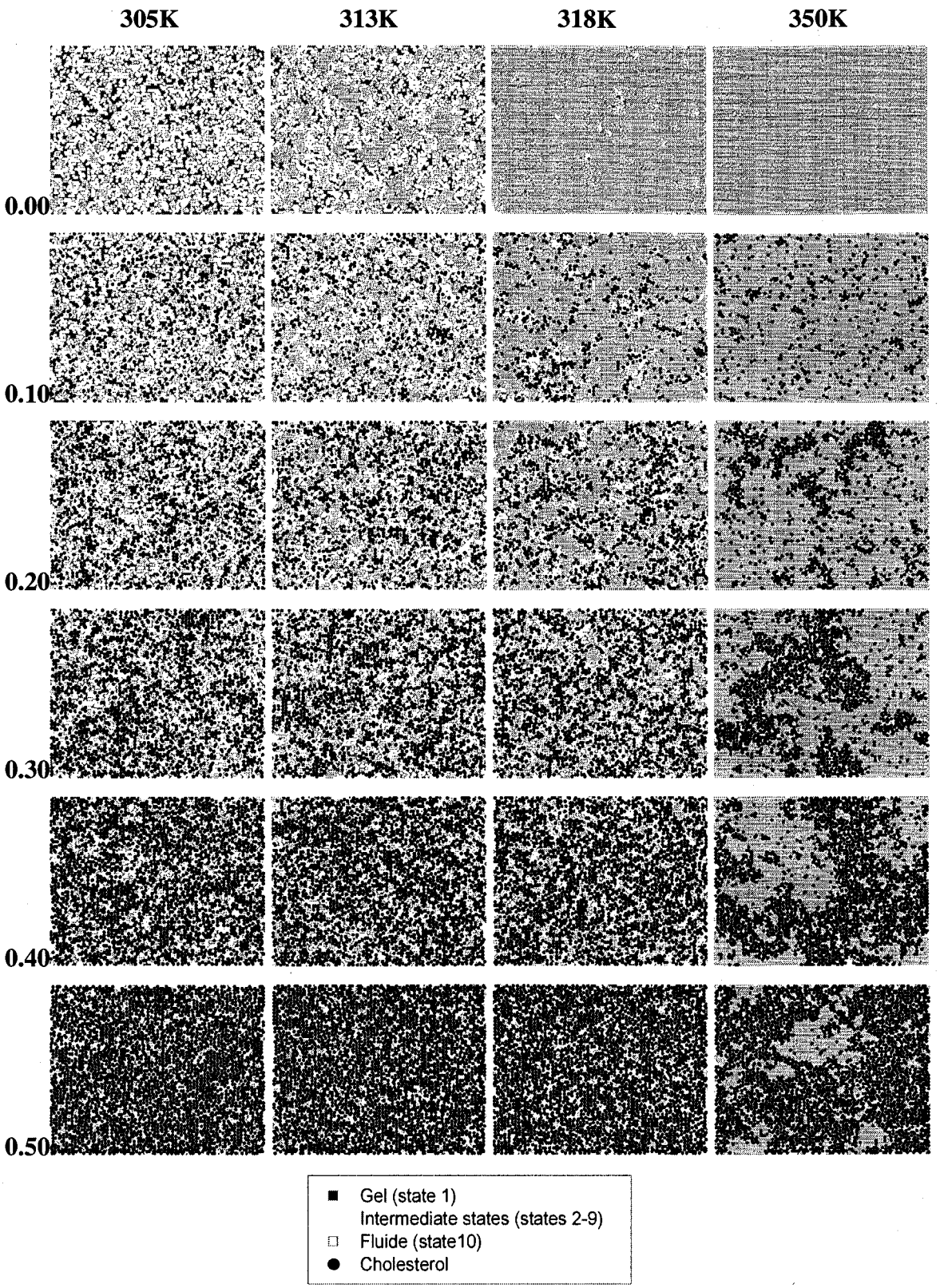

Figure 5.11 **Snapshots of simulated microconfigurations at T=305K, 313K, 318K and 350K with various cholesterol concentrations Xc (vertical axis) for DPPC/cholesterol bilayers, with $I_C(5)$=1.5.**

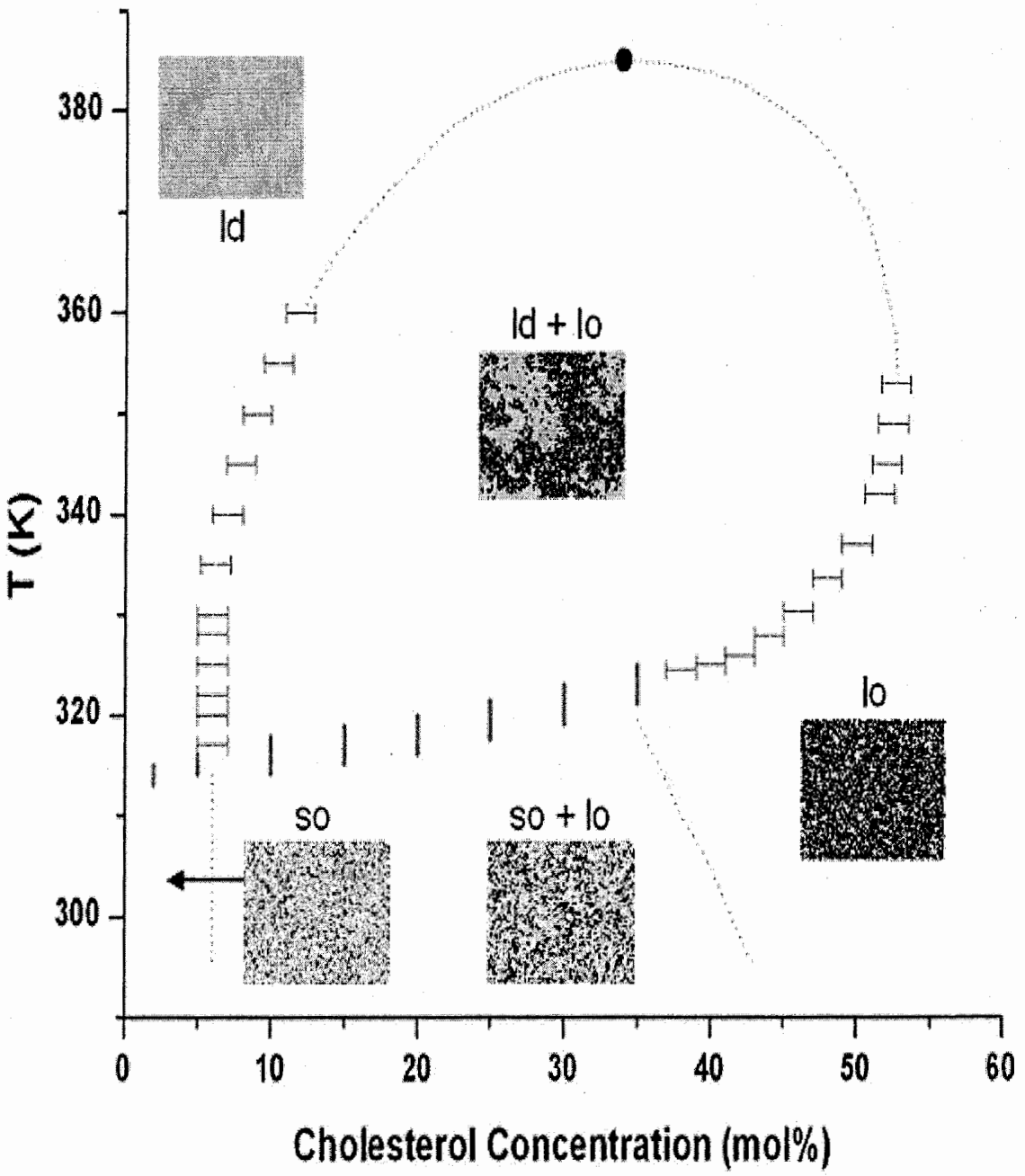

Figure 5.12 **Phase diagram of the DPPC/cholesterol bilayers with $I_C(5)$=1.5. Horizontal error bars are phase boundaries obtained from the inspection of the snapshots. The midpoints of the vertical line indicate the positions of peaks of the specific heat graphs. Dotted lines are hypothetical as explained in the text.**

5.2.2 $I_C(5)=2$

Figures 5.13, 5.14 show the thermodynamic properties and the specific heat versus temperature of the DPPC/Cholesterol bilayers with the parameter $I_C(5)=2$. The two most notable differences from the case with $I_C(5)=1.5$ are (i) the specific heat peak (Fig. 5.14) at T_m becomes sharper in the cases of $Xc<0.5$ and it disappears altogether at $Xc=0.5$ and (ii) the appearance of another peak near 353K which can be seen clearly for the cases with $Xc\geq 0.2$. This behaviour is also reflected, in a different way, in the thermodynamic properties shown in Fig. 5.13. Firstly, the change of the values of the thermodynamic properties across T_m is sharper than for the case of $I_C(5)=1.5$. Secondly, a 'bump' appears near 353K for high concentrations of cholesterol. These two features of the system will be interpreted in light of the snapshots of microconfigurations presented in the following.

Figure 5.15 shows snapshots of the microconfigurations at different temperatures and Xc values for the case with $I_C(5)=2$. One major difference from the previous cases with lower $I_C(5)$ values is the appearance of a new phase similar to the '**lo** mc' but nevertheless with a distinct symmetry (this phase covers the bilayers entirely at T=305K, 313K, 318K with $Xc=0.5$). This phase consists of one cholesterol molecule surrounded by lipid chains in the intermediate states at its six nearest neighbour sites. In its ideal composition (i.e., without defects), this phase consists of two lipid chains per one cholesterol molecule, or 50:50 in mole percent ratio of lipid molecules (two lipid chains make up one lipid molecule) to cholesterol molecules. This phase is known in another context as the $\sqrt{3}\times\sqrt{3}$ phase, because the length of the sides of the unit cell is increased by the factor $\sqrt{3}$ relative to the original triangular lattice [114]. Both the '**lo** mc' and the

$\sqrt{3}\times\sqrt{3}$ phase are liquid-ordered in nature. This $\sqrt{3}\times\sqrt{3}$ sublattice is an artifact of our lattice model, since in reality the **lo** phase is a liquid phase and does not have a lattice structure.

The snapshots in Fig. 5.15 clearly show that the system exhibits phase coexistence phenomena. For example, we can see the coexistence of the $\sqrt{3}\times\sqrt{3}$ phase and the '**so** mc' at 305K with Xc=0.3 and the coexistence of the $\sqrt{3}\times\sqrt{3}$ phase and the '**ld** mc' at 350K with Xc=0.3. The specific heat peak at T_m lies between these two regions, which indicates a rapid but continuous change of the '**so** mc' into the '**ld** mc'. However, as discussed before, the '**so** mc' and the '**ld** mc' are not distinct phases and, therefore, the specific heat peaks at T_m do not correspond to a three-phase line. At temperatures around 353K (not shown here), the coexistence of the $\sqrt{3}\times\sqrt{3}$ phase and the '**ld** mc' becomes the coexistence of the ordinary '**lo** mc' (i.e., same as the '**lo** mc' of the case with $I_C(5)$=1.5) and the '**ld** mc'. This change is indicated by the second peak in the specific heat graphs. Finally, at very high temperatures with 0.5>Xc>0.65, the specific heat graphs (not shown here) show another peak which corresponds to that of the system going from the $\sqrt{3}\times\sqrt{3}$ phase into the '**lo** mc' + '**ld** mc' phase coexistence region. A partial schematic phase diagram of the DPPC/Cholesterol bilayers with $I_C(5)$=2 is shown in Fig. 5.16. Again, this phase diagram is obtained by using the information from the snapshots of microconfigurations and the specific heat graphs. Near Xc=0, the system behaves similarly to the single-component DPPC bilayers, where the '**so** mc' continuously changes into the '**ld** mc' as temperature increases. As cholesterol concentration increases, the behaviour of the system begins to diverge from that of the single-component bilayer. As before, horizontal error bars indicate the approximate boundaries of the phase

coexistence region obtained by inspection of the snapshots. Vertical lines around 315K and 353K indicate the peak positions from the specific heat graphs. Although we do not have data at very high temperatures, the dotted lines along with the critical point represent the closure of the phase coexistence region which we hypothesized to exist in consideration of the topology of the phase diagram. Moreover, it needs to be pointed out that, at cholesterol concentrations beyond 50 mol%, we observe the disordering of the $\sqrt{3}\times\sqrt{3}$ into an '**lo** mc', which is represented by the dotted line in the phase diagram. This is due to the fact that the $\sqrt{3}\times\sqrt{3}$ phase can only exist in the stoichiometry of one lipid molecule (i.e., two lipid chains) to one cholesterol molecule. Thus, it is impossible for the $\sqrt{3}\times\sqrt{3}$ phase to exist when cholesterol concentration is much higher than 50 mol%.

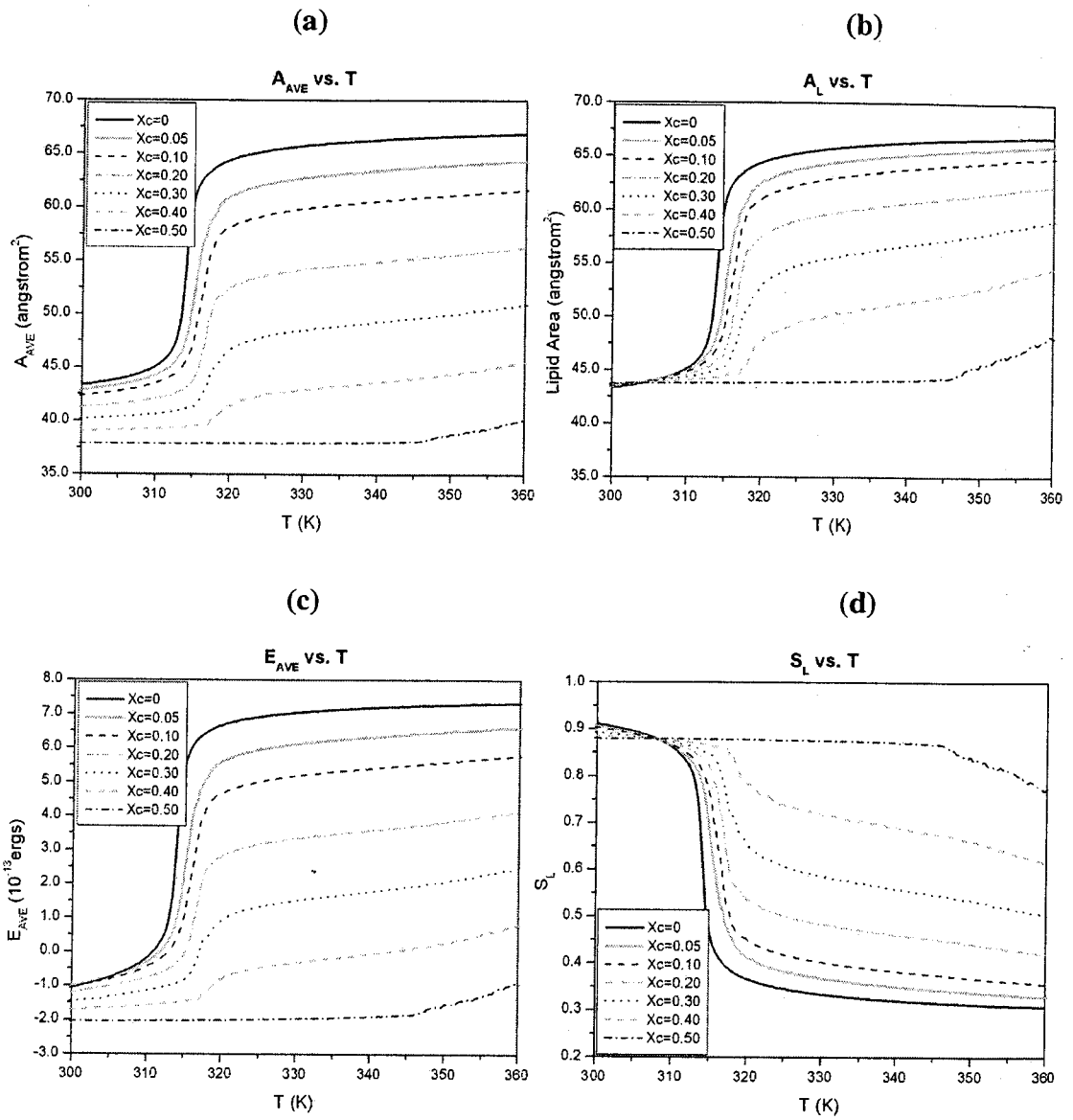

Figure 5.13 a) Average area per molecule (A_{AVE}), b) average area per phospholipid molecule (A_L), c) average energy per molecule (E_{AVE}) and d) average conformational order parameter per lipid chain (S_L) versus temperature for DPPC/cholesterol bilayers with $I_C(5)$=2.

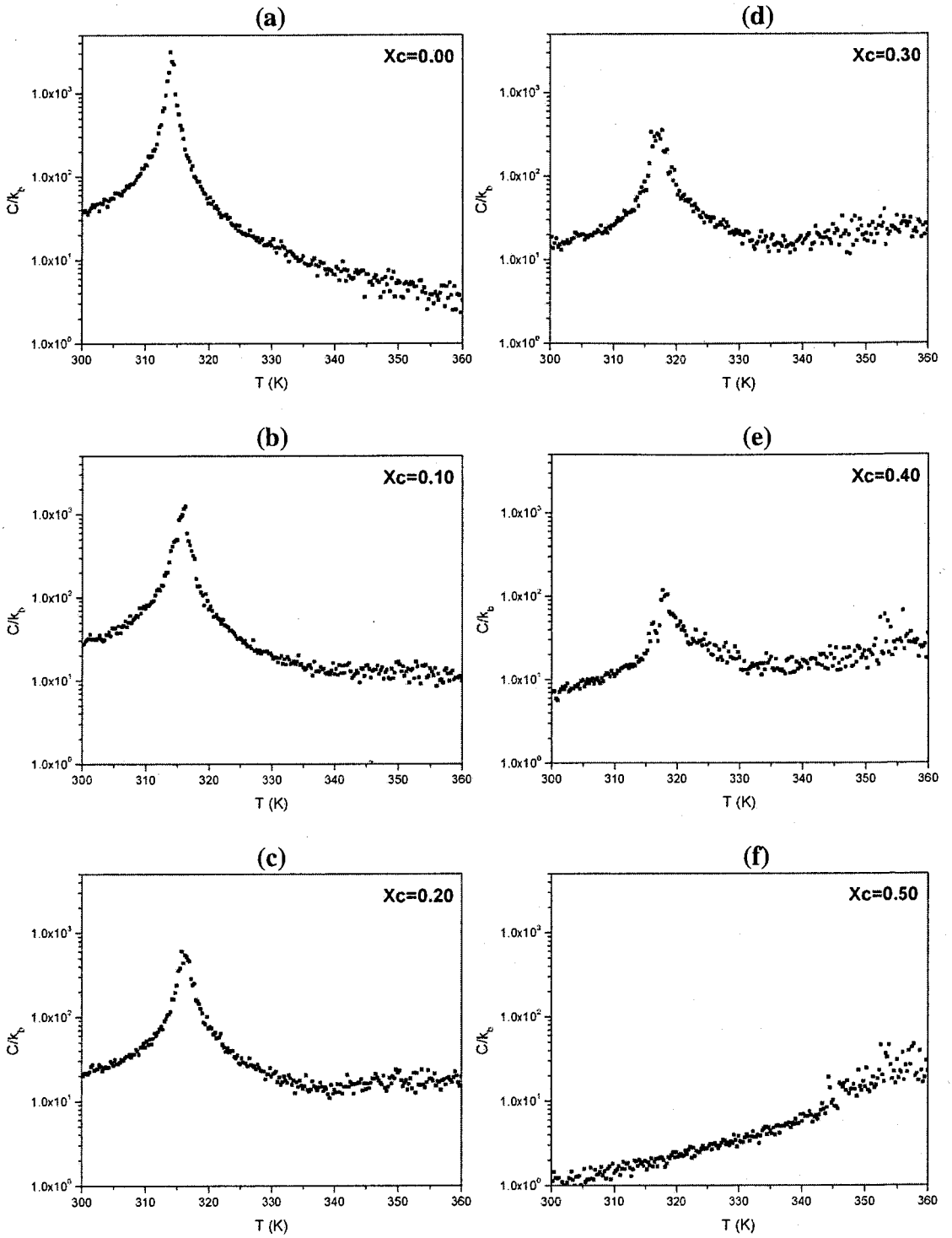

Figure 5.14 Specific heat per molecule (C_p) of DPPC/cholesterol bilayers with $I_C(5)$=2.

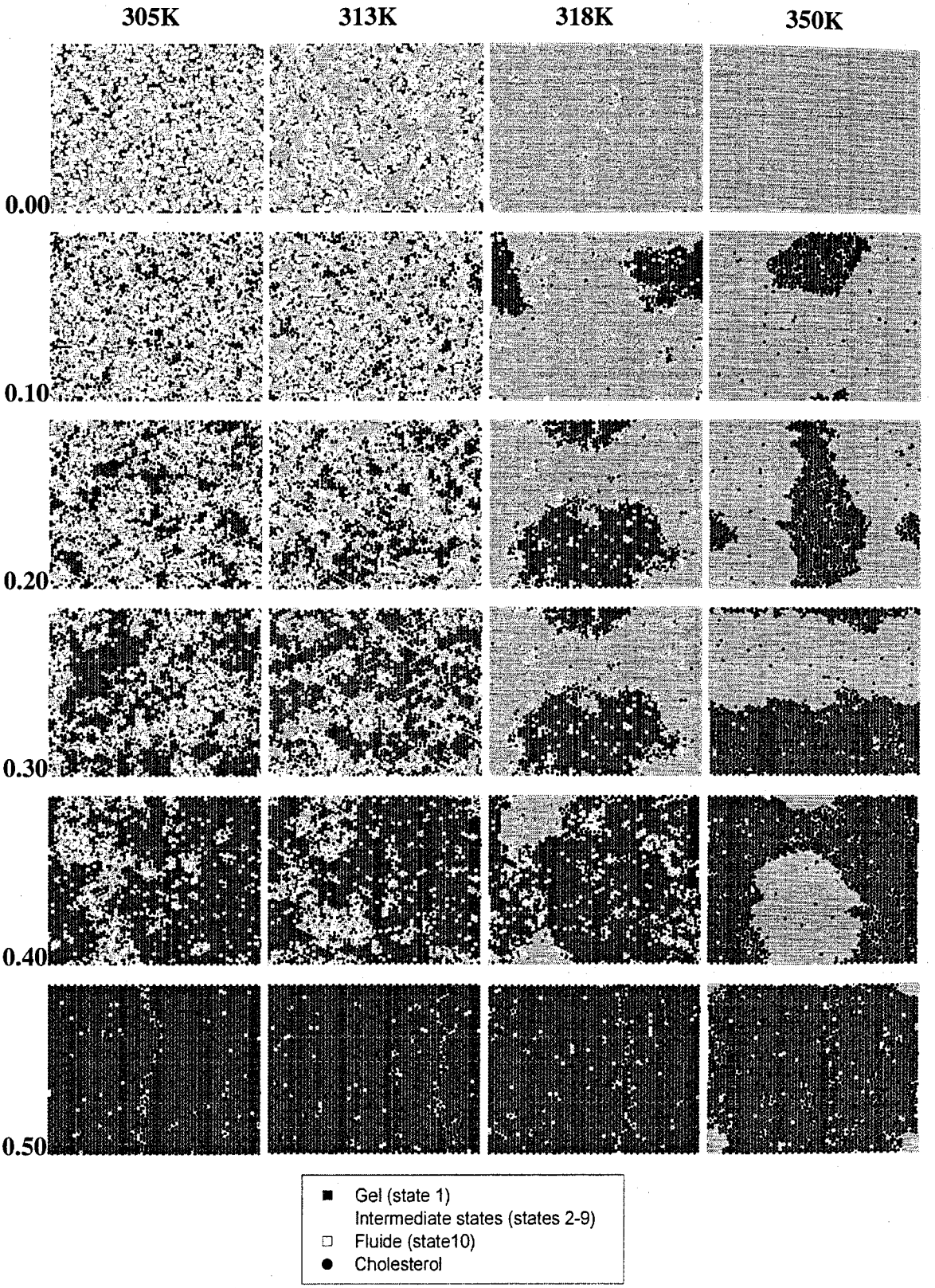

Figure 5.15 **Snapshots of simulated microconfigurations at T=305K, 313K, 318K and 350K with various cholesterol concentrations Xc for DPPC/cholesterol bilayers, with $I_C(5)$=2.**

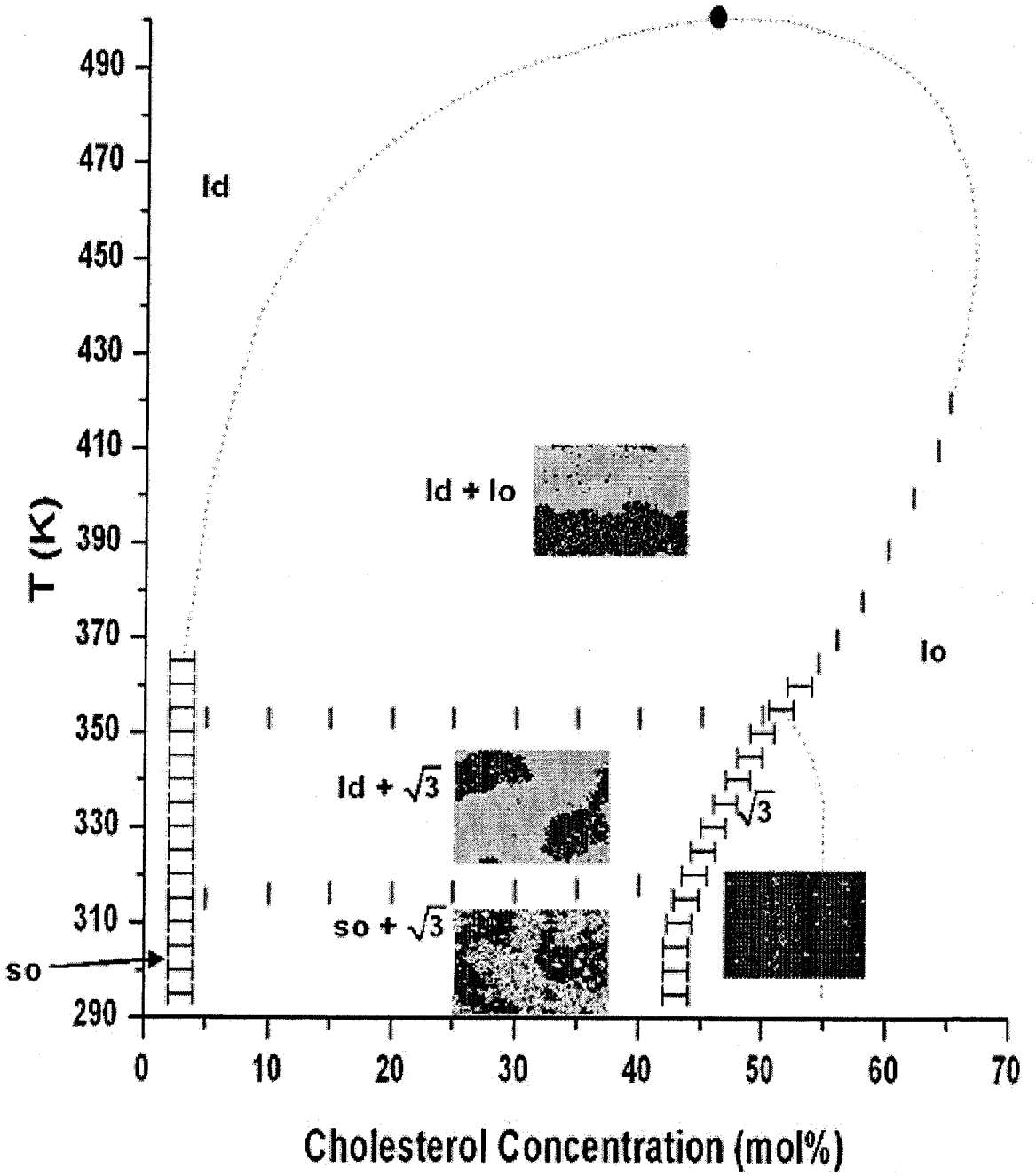

Figure 5.16 **Phase diagram of the DPPC/Cholesterol bilayers with $I_C(5)$=2.**
Horizontal error bars are phase boundaries obtained from the inspection of the snapshots. The midpoints of the vertical lines indicate the positions of the peaks of the specific heat graphs. The dotted line which closes the phase separation region must exist for topological reasons; as well as the one which separates the $\sqrt{3}x\sqrt{3}$ phase and the 'lo mc'. However, we have not determined their position numerically. '$\sqrt{3}$' refers to the $\sqrt{3}x\sqrt{3}$ phase.

6 Results for Binary Lipid Bilayers

In this section we present our results for the DLPC/DPPC binary lipid bilayers based on the binary lipid model of Eq. (2.20) used by Jørgensen *et al.* [50], who did not examine this particular binary mixture. This model is a modification of the 10-state Pink Model. Mixtures of DLPC (m=12) and DPPC (m=16) in various proportions were studied in order to provide a basis for the investigation of the effects of cholesterol on binary lipid mixtures in the next chapter. Metropolis Monte Carlo simulations were performed using both algorithms 1 and 2 listed in Section 3.4.3, for which identical results were obtained. However, since algorithm 2 is more efficient than algorithm 1 in reaching equilibrium, only results from using algorithm 2 are presented in this section.

All simulations in this section are performed on a 60×60 lattice. Warm-ups of at least 500 MC steps are used, all thermodynamic properties and response functions are averaged over 500 equilibrium configurations, and snapshots of microconfigurations are taken after 400,000 MC steps.

6.1 Simulation Results for DLPC/DPPC Bilayers

Fig. 6.1 shows all the thermodynamic properties of the DLPC/DPPC bilayers in various proportions. In Fig. 6.1 (a), the average area per molecule is shown as a function of temperature. The curve on the far left is for the single-component DLPC bilayers while the one on the far right is for single-component DPPC bilayers. All the curves in between

represent DLPC/DPPC mixtures of different proportions. Let us look at the DLPC/DPPC (40/60) mixture (i.e., the fourth curve from the left). The average area A_{AVE} of this mixture increases rapidly between approximately 279K and 304K, and two points of inflection are present at approximately 281K and 303K. Similar changes in A_{AVE}, at different temperatures, are observed for mixtures of other proportions. Starting with the DLPC/DPPC (80/20) mixture (the second curve from the left), the rapid rise in A_{AVE} as well as the inflection points move towards higher temperatures as DPPC is added to the system. This resembles a typical two-phase behaviour, where the beginning and the end of the rapid rise in A_{AVE} signals that the system is entering and leaving a two-phase region. The boundary of this two-phase region and the phase behaviour of the system will be discussed in details when we present the response functions and the microconfigurations in the later part of this section.

Fig. 6.1 (b) shows the average energy per molecule E_{AVE} versus temperature. This agrees with the graphs of A_{AVE} vs. T in the sense that there is a region, whose location depends on the composition of the mixture, where a rapid increase in E_{AVE} is observed. Figs. 6.1(c) and (d) show the average conformational order parameter per lipid chain versus temperature for DLPC (S_{DLPC}) and DPPC (S_{DPPC}), respectively. Note that the irregularities of the 20:80 curve (far right) of the S_{DLPC} and the 80:20 curve (far left) of the S_{DPPC} are caused by insufficient statistics of DLPC or DPPC chains in the mixtures when their respective concentrations are low. Both the conformational order parameters S_{DLPC} and S_{DPPC} show that the system enters and then leaves a two-phase region as temperature increases. Note that this can only be observed if there is some degree of

mixing of the two lipid species. The mixing of the binary system will be illustrated again with the snapshots of microconfigurations.

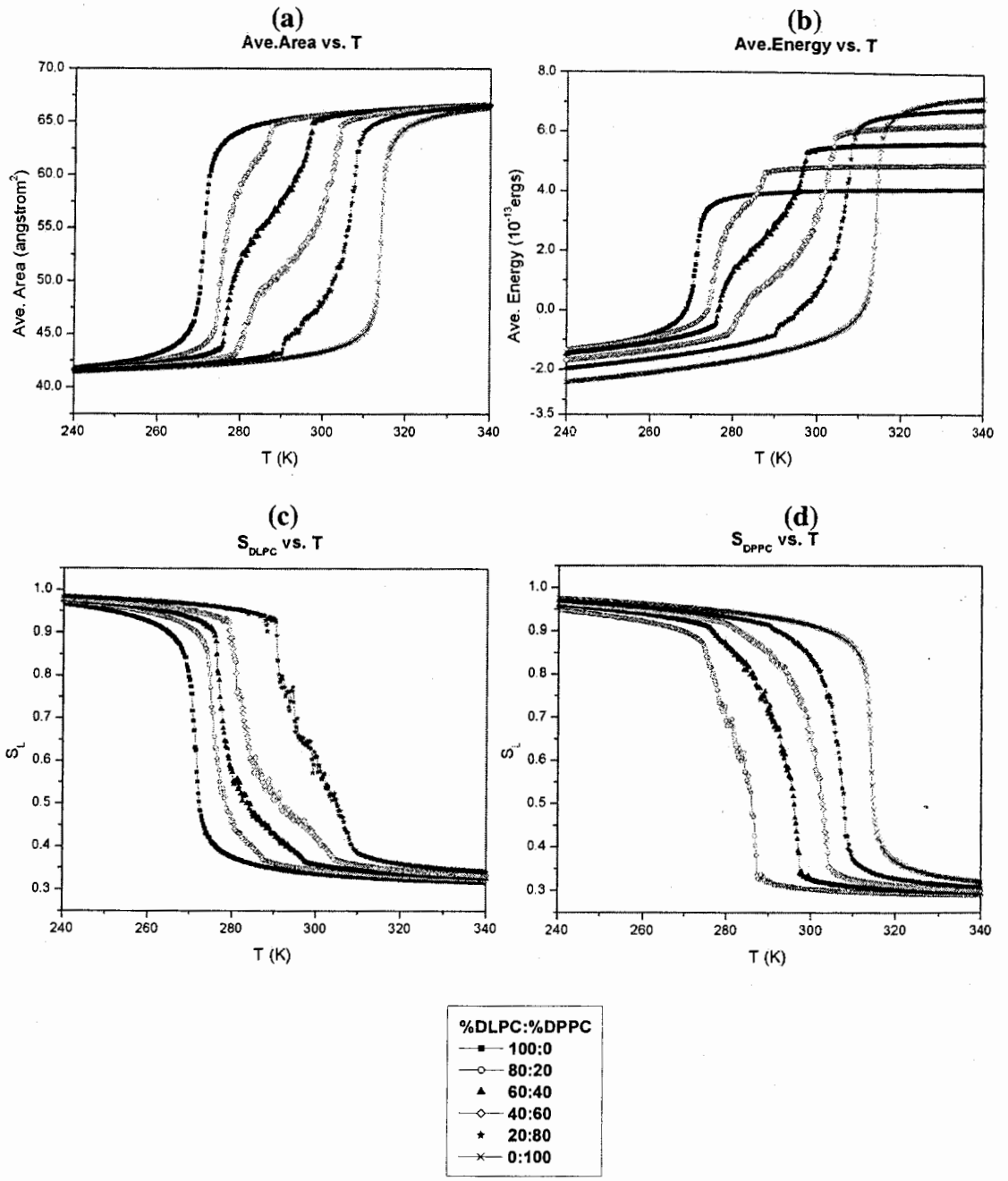

Figure 6.1 **(a) Average area per molecule (A_{AVE}), (b) average energy per molecule (E_{AVE}), (c) average conformational order parameter per DLPC lipid chain (S_{DLPC}) and (d) average conformational order parameter per DPPC lipid chain (S_{DPPC}) versus temperature for DLPC/DPPC bilayers.**

Graphs of specific heat per molecule (C_p) versus temperature and of isothermal compressibility κ_T versus temperature are shown in Figs. 6.2 and 6.3. Note that all the graphs for the DLPC/DPPC mixtures display two peaks, which occur at temperatures that

depend on the composition of the mixtures. The positions of these peaks are the same as the positions of the inflection points of the thermodynamic properties presented above. These points give the boundaries of the two-phase region.

We now discuss the phase behaviour of the DLPC/DPPC system by making use of the specific heat graphs (Fig. 6.2) as well as the snapshots of microconfigurations (Fig.6.4). First, we focus on the DLPC/DPPC (40/60) mixture. The specific heat plot exhibits two peaks at 281K and 303K, respectively, which indicate the boundaries of the two-phase region, as discussed above. The snapshot of microconfigurations at 258K, i.e., below the first peak of C_p, shows that the system contains mainly lipid chains of DLPC and DPPC in states 1 to 9. The system is in the '**so** mc' and the snapshot shows that a certain degree of mixing occurs. At temperatures between the two peaks in the C_p plot, i.e., 282K, 290K and 300K, the system is in the two-phase region and the snapshots clearly show the phase separation of the '**ld** mc' from the '**so** mc'. Both the '**ld** mc' and the '**so** mc' contain various proportions of DLPC and DPPC chains which depend on the temperature of the system. At 310K, i.e., above the second peak of C_p, the system has left the two-phase region and is now in the **ld** phase. Again, this snapshot shows that DLPC and DPPC exhibit some degree of mixing in the **ld** phase.

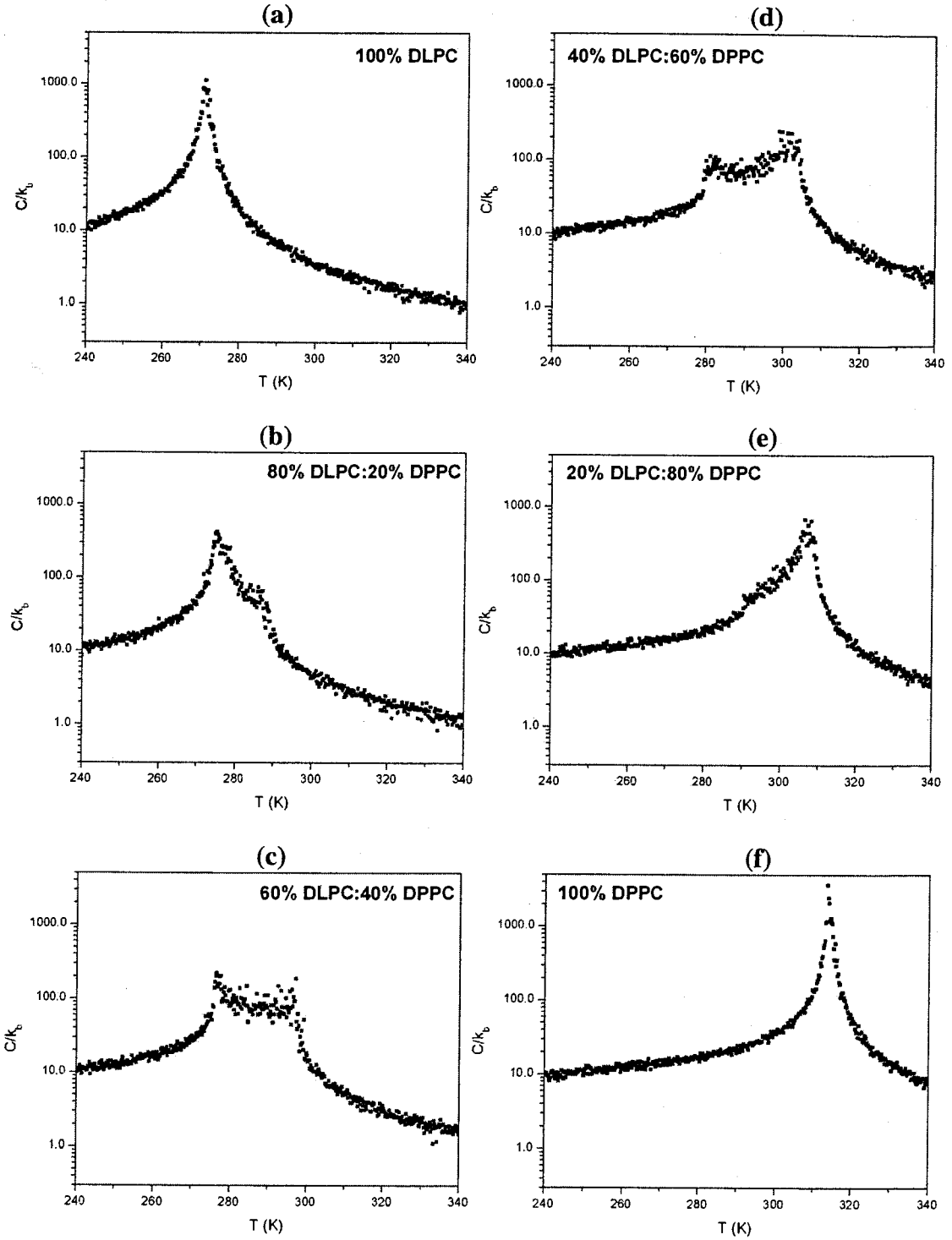

Figure 6.2 **Specific heat per molecule (C_p) versus T of DLPC/DPPC bilayers.**

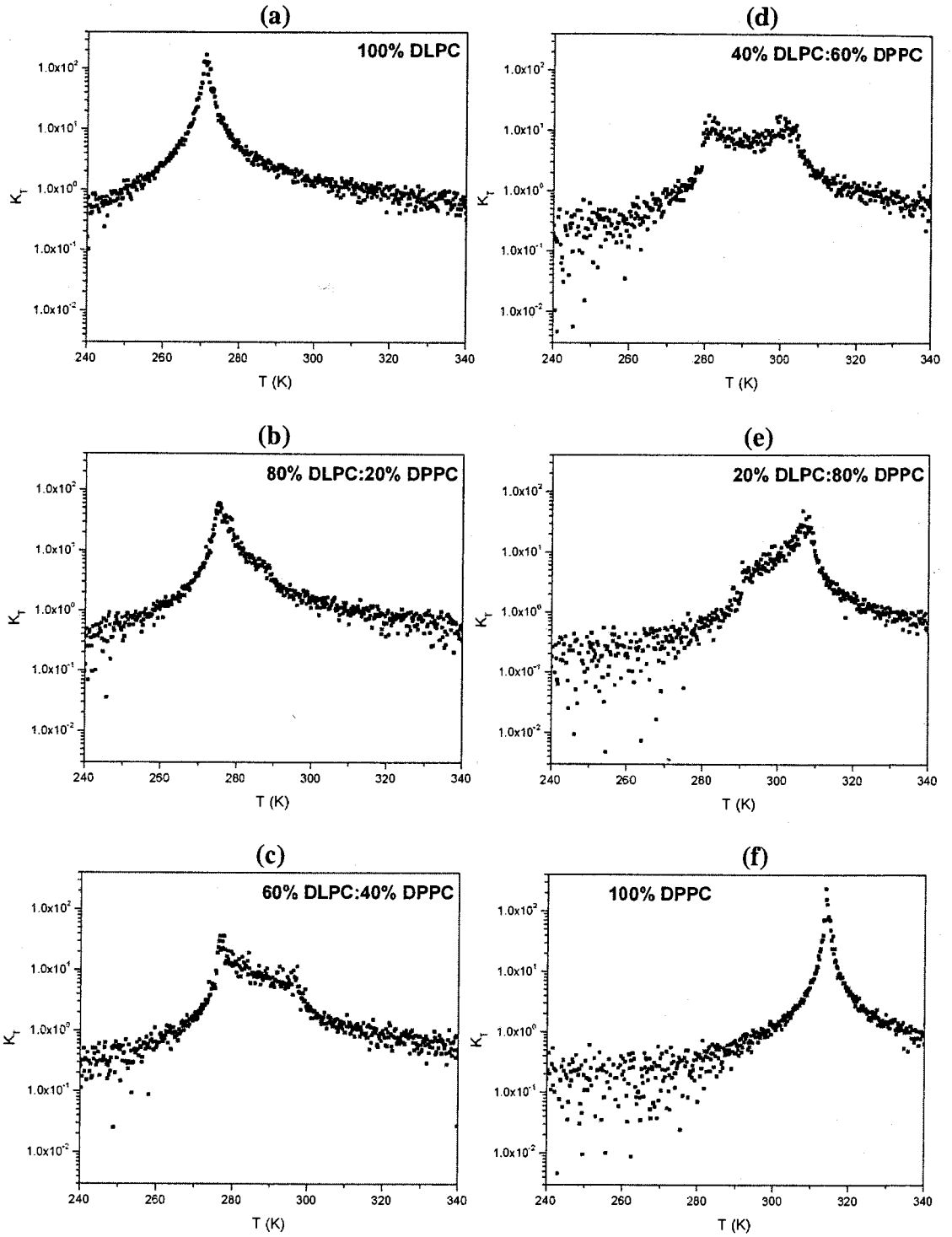

Figure 6.3 **Isothermal lateral compressibility (K_T) versus T of DLPC/DPPC bilayers.**

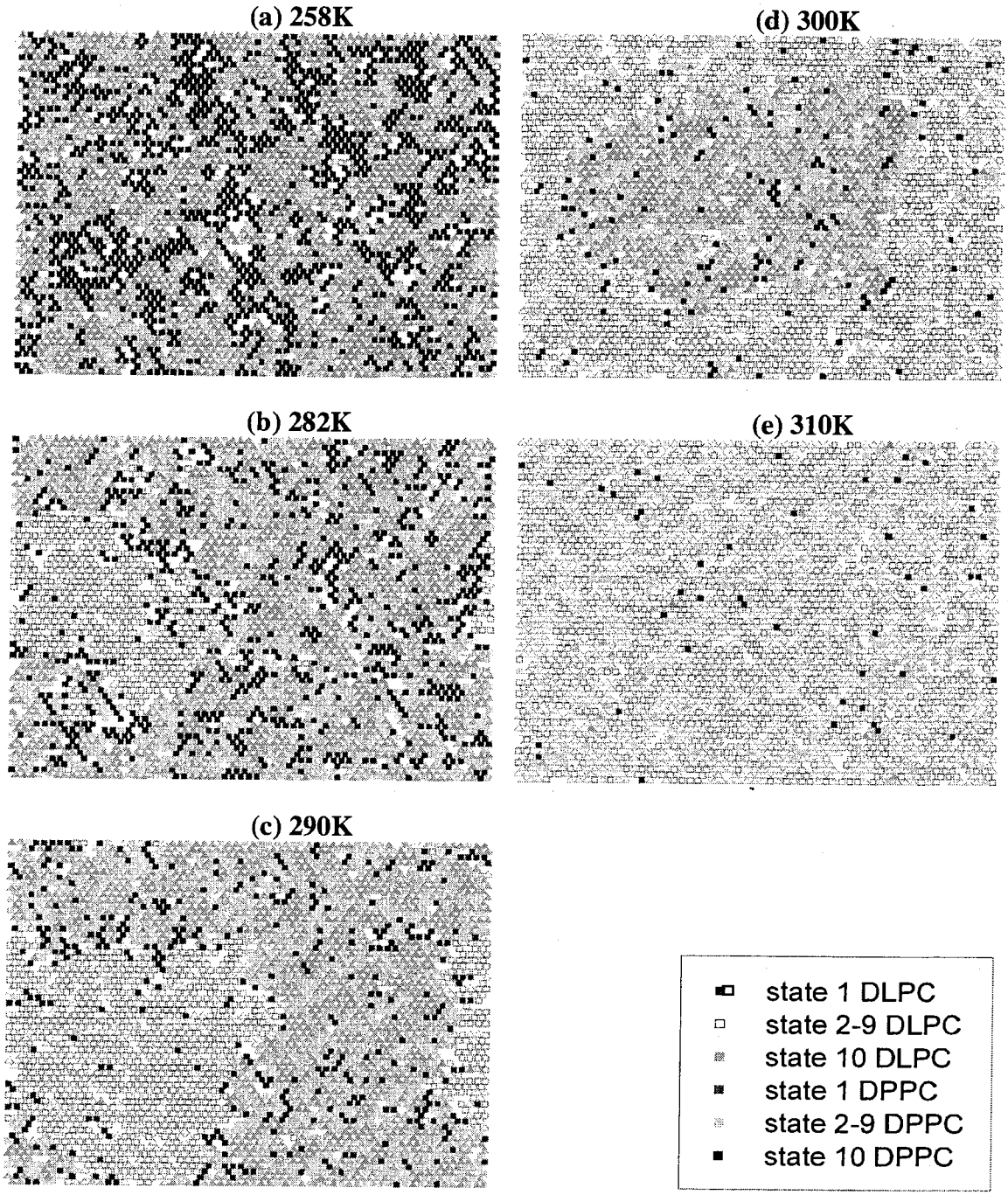

Figure 6.4 **Simulated microconfigurations of 40:60 mixture of DLPC/DPPC bilayers at various temperatures.**
State 1, state 2-9 and state 10 correspond to gel, intermediate states and fluid respectively.

Fig. 6.5 is the phase diagram obtained from the peak positions of the specific heat verses temperature (Fig. 6.2). As shown in the snapshots of microconfigurations and as discussed above, the region under the lower curve (solidus) is the **so** phase, the region above the upper curve (fluidus) is the **ld** phase, and the region in between the two curves is the two-phase region where the **so** and the **ld** phases coexist. Due to the fact that there are no phase transitions in the single-component DLPC and DPPC systems in the Pink model, the two curves in Fig. 6.5 do not extend to the vertical axis of the graph. Instead, the lens-shaped area that represents the two-phase region is expected to end at an upper and lower critical point. We do not concern ourselves with the precise determination of the location of these critical points in the present study. Nevertheless, the snapshots of microconfigurations for different compositions of DLPC and DPPC (not shown here) show that two-phase separation is present for the 20/80, 40/60, 60/40 and the 80/20 mixtures. Therefore, the upper and lower critical points should be located approximately between 0 and 20 mol% DPPC, and between 80 and 100 mol% DPPC respectively.

Fig. 6.6 is a comparison of our simulation results to the FTIR by Silvius *et al.* [16]. The C-H and the C-D stretching frequencies measured with FTIR are sensitive to *gauche* bond formations and, hence, to the conformational order of the lipid chains [113]. Therefore, it is possible to compare the conformational order parameters calculated from our model to the FTIR data. The experimental points were obtained by Silvius *et al.* [16] from the onset and completion of the peaks of the first derivatives of the sum of the frequencies ($\nu_{CH}+\nu_{CD}$) of the respective C-H and C-D stretching bands of DLPC and DPPC-d_{62} [16]. In a similar way, the theoretical points are determined from the onset and completion of the peaks of the first derivatives of the sum of the conformational order

parameters (S_{DLPC} +S_{DPPC}) of DLPC and DPPC respectively. Note that these points, obtained from the above experimental and theoretical methods, are not a perfect guide to the correct phase diagram in the strictest sense. For instance, a phase diagram should not contain more than one point at the vertical axes (0% DPPC and 100% DPPC). Moreover, DLPC and DPPC does not exhibit first order phase transition in the Pink model, and therefore a correct theoretical phase diagram should not contain any points in the vertical axes (see Fig. 6.5). However, the above method is useful in that it provides a way of comparing theoretical and experimental results. Fig. 6.6 shows that a reasonable agreement is obtained between our theoretical conformational order parameters and the frequencies of the FTIR stretching bands.

Fig. 6.7 shows our Monte Carlo simulations results (labelled as theoretical results) and the data from Differential Scanning Calorimetry (DSC) by Van Dijck *et al.* [82]. With the DSC results, the low temperature points were obtained by the author from the intersection of the slope of the descending arm of the heat capacity curve with the baseline. The high temperature points were obtained from the intersections of the slope of the ascending arm of the heat capacity curve with the baseline [82]. The theoretical results were obtained in the same manner from the theoretical specific heat curves in Fig. 6.2. Same as Fig. 6.6, Fig. 6.7 is not a plot of the phase diagram in the strictest theoretical sense. However, the DSC data is a useful comparison to our theoretical results. Fig. 6.7 shows that reasonable agreement of our theoretical specific heat with the DSC scans is obtained.

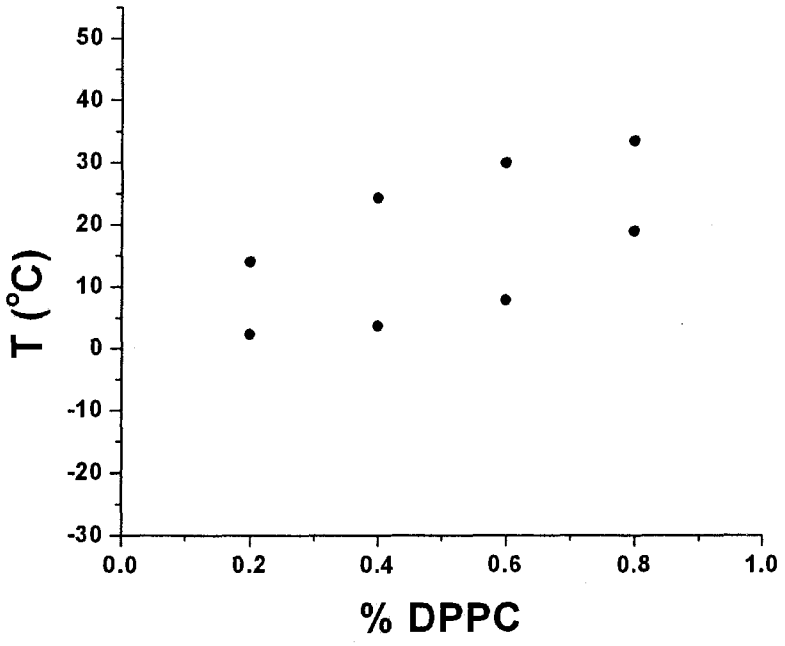

Figure 6.5 Phase diagram of the DLPC/DPPC bilayers from our simulation results. Points in the phase diagram are the peak positions of the specific heat versus temperature graphs (Fig. 6.2).

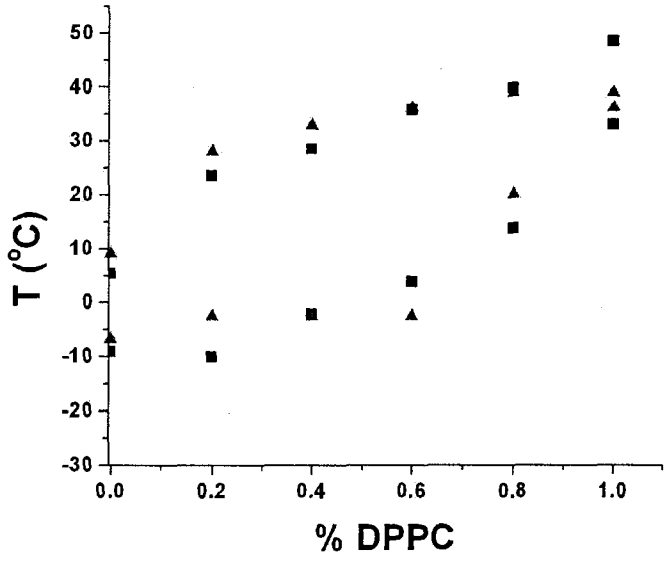

Figure 6.6 Comparison of MC simulations results with FTIR data by Silvius *et al.* [16]. The triangles are data from FTIR experiments, whereas the squares are from simulation results.

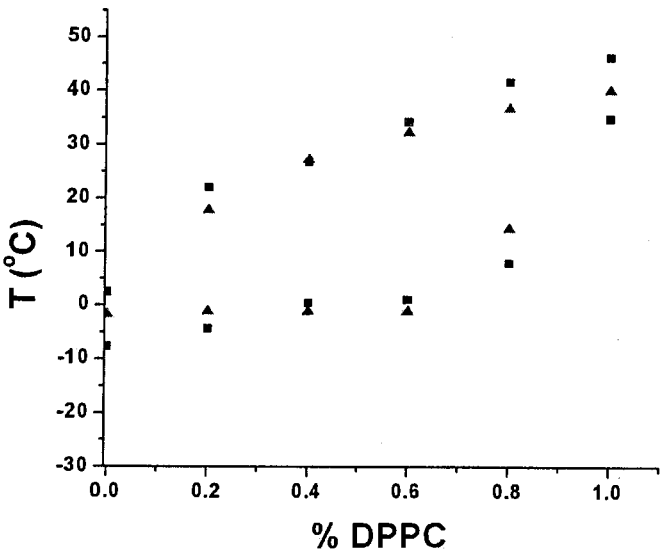

Figure 6.7 **Comparison of MC simulation results to Differential Scanning Calorimetry (DSC) data by Van Dijck *et al.* [82].**
Triangles are data from DSC experiments; the squares are from simulation results.

7 Results for Ternary Lipid/Cholesterol Bilayers

In this chapter we study ternary systems containing two lipid species and cholesterol. The particular ternary system to be studied is a lipid bilayer composed of DLPC, DPPC and cholesterol molecules. The ratio of DLPC to DPPC is maintained at 2:3 (40 mol% to 60 mol% in total PCs) and the cholesterol concentration is varied from 0 mol% to 40 mol%. This particular ternary system was investigated experimentally by Silvius *et al.* [16], motivated by the idea that domain formation might provide a possible understanding of the nature of membrane "rafts".

In previous chapters, we studied the properties of lipid/cholesterol bilayers (Chapter 5) and binary mixtures of DLPC and DPPC (Chapter 6). It had already been shown that the original parameters of Cruzeiro-Hansson *et al.* [28] did not lead to an understanding of lipid/cholesterol bilayer properties at higher cholesterol concentrations. Our results in Chapter 5 indicated that it is necessary to replace the original parameter I_C=0.45 in the lipid-cholesterol interaction (Eq. (2.19)) by the parameters $I_C(\alpha)$, which depends on the conformational state, α, of the respective lipid chains (Eq. (2.15)). For DPPC/cholesterol bilayers, we assumed that the cholesterol molecule interacts most strongly with lipid chains in the kink conformation (α=5). In order to obtain reasonable values of the ^{2}H-NMR order parameter, a considerable increase in $I_C(5)$ was required ($I_C(5)$=1.5 and 2), while $I_C(\alpha)$ for $\alpha \neq 5$ retained the original value of 0.45. We examined the properties of DLPC/cholesterol bilayers in a similar manner; but, unfortunately, there is no consistent ^{2}H-NMR data for DLPC/cholesterol bilayers of the type found for DPPC.

In the case of DLPC/DPPC binary lipid bilayers, we were able to fit the experimental phase diagrams available (Fig. 6.4 and 6.5) using the method of Jørgensen *et al.* [50]. This gave reliable parameters for the interactions between these two lipid molecules which can be used for the study of the ternary mixture.

In this chapter we apply the information and parameters from Chapter 4 to 6 to the numerical simulation of the properties of ternary DLPC/DPPC/cholesterol bilayers. The simulations use the Hamiltonian of Eq. (2.26). Our purpose is to compare with the experimental results of Silvius *et al.* [16] for the ternary mixture. To this purpose we adopted the following strategy. The values of the parameters for the pure lipids and the binary lipid mixture used in Chapter 4 and 6 were generally not changed. We then examined in detail how changes in the lipid-cholesterol interaction parameters $I_C(\alpha)$ for both DLPC and DPPC affect the simulation results for the ternary mixture.

This chapter is organized as follows. The strategy for exploration of the parameter space of $I_C(\alpha)$ is discussed in Section 7.1. Section 7.2 presents the simulation results for the thermodynamic properties of the ternary mixtures. In Section 7.3, we correlate the results obtained from the response functions with the microscopic nature of the system shown in the snapshots generated by the simulations. Then, in Section 7.4, the calculated values of the molecular order parameters and their relation to the experimental results of Silvius *et al.* [16] are presented.

Monte Carlo simulations in this chapter is performed on a 100×100 lattice, with a warm-up of 500 MC steps, thermodynamic properties and response functions are averaged over 500 equilibrium configurations, snapshots of microconfigurations are obtained after 400,000 MC steps.

7.1 Monte Carlo Simulation Strategy

The strategy adopted in this chapter is to explore the parameter space of $I_C(\alpha)$ while initially keeping all other parameters from Chapter 4 to 6 unchanged. This includes using the original values of the lipid-lipid interaction parameters I_α^γ (where γ is either DLPC or DPPC) as in Eq. (2.15). Moreover, we adopted the value of the coupling constant J_{DPPC} used in the Pink model as the J_{LC} of both DLPC-cholesterol and DPPC-cholesterol interactions in Eq. (2.27). This is because the experimental results of Silvius *et al.* [16] show that DLPC and DPPC behave very similarly in the ternary mixture at high cholesterol concentrations. Furthermore, we assumed that the coupling between cholesterol and the acyl chain with the same head group remains the same if the acyl chain is longer than cholesterol, which is applicable for both DLPC and DPPC chains. Note that, as in Chapter 2, the subscript α refers to the lipid chain states as follows: α=1, 2, ..., 10 for the ten states of DLPC and α=11, 12, ..., 20 for the ten states of DPPC respectively. Moreover, we also use notations such as $DPPC_{\alpha=15}$ to refer to, for example, a DPPC chain in state 15.

The primary purpose in our study of the ternary lipid bilayers is to understand the behaviour of the system with high cholesterol concentrations and at physiological temperatures, i.e., around 310K or 37°C. Therefore, different points in the $I_C(\alpha)$ parameter space are chosen for investigation due to their relevant properties in this case. In this section we concentrate on a qualitative description of the results for the ternary system at 310K and at high cholesterol (~30 mol%-40 mol%) concentrations. In addition,

properties of the ternary system with different cholesterol concentrations and different temperatures will be included in the discussion in the later part of this chapter.

The exploration of parameter space requires a systematic manipulation of the parameters $I_C(\alpha)$ (α=1, ..., 20) which control the lipid-cholesterol interaction. Table 7.1 shows all the points in the $I_C(\alpha)$ parameter space which we have investigated. The original parameters used by Cruzeiro-Hansson *et al.* for the lipid/cholesterol bilayers and by Jørgensen *et al.* [50] for the binary lipid bilayers (i.e., $I_C(1\text{-}20)$=0.45) is labelled as case (m) at the lower left corner of the table. We began our investigation by looking at case (e), where $I_C(15)$=1 (i.e., the kink state of DPPC) with all other $I_C(\alpha)$ values remaining at 0.45. In this case, we focus on the interaction of the kink state of DPPC chains with cholesterol in the ternary system while not changing for the moment the interaction of DLPC with cholesterol. Next, we tried out different sets of $I_C(\alpha)$ values systematically. In this process, we found that the parameter set $I_C(2\text{-}9,15)$ =2 (case (h)) induces a strong coupling between DLPC and DPPC and causes both lipids to behave very similarly at high cholesterol concentrations. This set of parameters also leads to the formation of a new phase (discussed in the sections that follows) and causes the system to acquire new phase behaviour not seen in case (e). We consider case (h) as the limiting case in our exploration of the $I_C(\alpha)$ parameter space because we found that further increments of $I_C(\alpha)$ cause little change in the ternary system.

In order to understand how the ternary system acquires totally different behaviour with the above two sets of parameters, we set out to investigate the parameter space of $I_C(\alpha)$ step by step. We began with $I_C(15)$=1 (case (e)) and gradually increased $I_C(2\text{-}9)$—the interaction between intermediate states of DLPC and cholesterol—until we arrived at

$I_C(2\text{-}9,15)$=1 (case (l)). In going along this path in the $I_C(\alpha)$ parameter space, we found that the interaction of DLPC with cholesterol gradually became more effective, as is shown by the increasing number of intermediate state DLPC chains along this path. After reaching $I_C(2\text{-}9,15)$=1, we then gradually increased the interaction between both lipids and cholesterol simultaneously by changing $I_C(2\text{-}9,15)$ from 1 to 2. In this manner, we arrived at the limiting case of $I_C(2\text{-}9,15)$=2 (case (h)). Along this path in the parameter space, we observed an increasing affinity for the intermediate states of both lipids to cholesterol that ultimately leads to phase separation phenomena (Fig. 7.10 to 7.12).

In addition to going from point (e) to point (h) in the $I_C(\alpha)$ parameter space through point (l), we also investigated an alternate path in the parameter space going through point (a) of Table 7.1. From point (e) to point (a) in Table 7.1, we gradually increased the value of $I_C(15)$ from 1 to 2. As we approached point (a) ($I_C(15)$=2) in the parameter space, we see an increasingly strong interaction between intermediate DPPC chains and cholesterol, which ultimately leads to phase separation (Fig. 7.10 to 7.12). However, the lipid species in the phase-separated regions in the system seen in this series ((e) to (a)) is different from the one seen in the series (l) to (h). Finally, we looked at the point in the parameter space of $I_C(\alpha)$ between (a) and (h) labelled as case (f). Phase separation is seen along this path but with a change in the content of the phases. The phase behaviour of the system based on the response functions, snapshots of microconfigurations and molecular order parameters will be discussed in detail in the following sections.

Table 7.1 **All points in the $I_C(\alpha)$ parameter space that we investigated. Note that the axes are not to scale. All the $I_C(\alpha)$ values not specified in the table are given the original value of 0.45.**

$I_C(15)$								
	2	(a)	(f)					(h)
	1.75	(b)					(i)	
	1.5	(c)				(j)		
	1.25	(d)			(k)			
	1	(e)	(g)	(l)				
	0.7							
	0.45	(m)						
		0.45	0.7	1	1.25	1.5	1.75	2

$I_C(2\text{-}9)$

7.2 Thermodynamic Properties

Figures 7.1, 7.2 and 7.3 show the average area per molecule (A_{AVE}), average area per lipid molecule (A_L) and average energy per molecule (E_{AVE}) versus temperature for the DLPC/DPPC(40/60)/cholesterol bilayers. The letter label of each graph refers to the particular parameter set being used in that graph as listed in Table 7.1. Graph (m) gives the simulation results with the unmodified parameter set $I_C(1\text{-}20)$ =0.45, which serves as a comparison for the other graphs with modified parameters.

Fig. 7.1 shows the average area (A_{AVE}) versus temperature for the ternary lipid bilayers. As mentioned in the previous chapter, the average area is the lateral surface area averaged over all molecules—DLPC, DPPC and cholesterol—in the bilayer. Therefore, it

shows the overall effect of cholesterol on the bilayer as a whole. In the absence of cholesterol (Xc=0), all the graphs in Fig. 7.1 display two inflection points at 281K and 303K, respectively. These points give the boundaries of the two-phase coexistence region of the DLPC/DPPC (40/60) bilayers, which are in complete agreement with our results in Chapter 6. The two-phase coexistence boundaries can also be seen in the graphs of the average area per lipid molecule versus temperature in Fig. 7.2 and of average energy versus temperature in Fig. 7.3.

As the cholesterol concentration is increased from Xc=0 to Xc=0.4, the two inflection points mentioned above are gradually merged into a single inflection point, located between 270K and 303K depending on the values of I_C. The single inflection point appears at Xc>0.2 for cases (h) to (l) in the right hand column of graphs, and at Xc>0.3 for all the other cases. This phenomenon as Xc is increased, signals a change in the phase behaviour of the system. The system is gradually moving away from the coexistence of the '**ld** mc' and the '**so** mc' of the binary DLPC/DPPC bilayers as discussed in Ch. 6. We will discuss the phase behaviour in detail when we present the snapshots of microconfigurations in the later part of this chapter. Nevertheless, the observation that the single inflection point appears at lower Xc values for the series (h) to (l) than for the series (a) to (e) indicates that the stronger interaction between DLPC and cholesterol ($I_C(2\text{-}9) \geq 1$) for cases (h) to (l) allows cholesterol to act more efficiently in changing the behaviour of the system. Another observation for all cases when Xc is increased is a slight area contraction below 270K and a much stronger area contraction above 303K as seen in Fig. 7.1. This area contraction above 303K implies the system is more '**lo**' like, i.e., more compact, than in the '**ld** microscopic complexion' in the system.

The result is a progressively smaller difference of the average area between the low T end and the high T end as Xc is increased, as can be seen even more clearly in Fig. 7.2.

The graphs of average area per lipid molecule (A_L) versus temperature are shown in Fig. 7.2. In these plots, cholesterol molecules have been excluded, showing the average lateral area of the lipid molecules only. These graphs reveal that the net effect of adding cholesterol to the lipid bilayers at temperatures below 270K is, in fact, an area expansion. This again implies that the addition of cholesterol renders the system more **lo**-like. Now we can see that the area contraction that was observed in Fig. 7.1 is an apparent effect caused by the averaging of the areas of lipid molecules and cholesterol molecules—which have a smaller area than the lipid molecules—in the bilayers. A similar masking effect is also present in the average energy versus temperature graphs, Fig. 7.3.

Fig. 7.3 shows that the addition of cholesterol causes a considerable decrease in the average energy of the system at temperatures above 303K, which implies the presence of an increasing number of lipid chains in the conformational states lower than state 10. Similarly, the increase in energy below 270K implies the presence of an increasing number of lipid chains in the intermediate states—which have higher energies than lipid chains in state 1—and can be seen in cases with $I_C(\alpha) \leq 1.5$ (i.e., (c) to (e), (j) to (l), (g) and (m)). This effect is not obvious in the other graphs.

Next, we describe the effects of changing the values of $I_C(\alpha)$ of the ternary bilayers, based on Fig. 7.2 and 7.3. We observed that increasing the values of $I_C(\alpha)$ of bilayers with low concentrations of cholesterol has only a small effects on the bilayers. However, when we increase the values of $I_C(\alpha)$ of bilayers with high concentrations of

cholesterol, we observe a considerable change in the area and the energy of the bilayers at temperatures above 303K, as well as a modification of the shape of graph between 270K and 303K. For instance, the value of A_L at temperatures above 303K decreases progressively as the values of $I_C(\alpha)$ increases (i.e.,(e)→(a) and (l)→(h)). The effect can be observed clearly by contrasting the Xc=0.40 curves in cases (a) and (h), which have the highest $I_C(\alpha)$ values, with case (m), which has the lowest $I_C(\alpha)$ values. The value of A_L with Xc=0.40 at 310K is 62Å^2 in case (m), 53Å^2 in case (a) and 50Å^2 in case (h), respectively, which corresponds to almost a 20% decrease as $I_C(\alpha)$ changes from 0.45 to 2 (α=15 in (a) and α={2-9,15} in (h)). This shows that the effects of cholesterol on the bilayers are magnified by increasing the values of $I_C(\alpha)$.

Furthermore, the modification of the shape of the graphs at high Xc in Figs. 7.2 and 7.3 between 270K and 303 K also signals a change in the phase behaviour of the system. In Fig. 7.2, the graphs with Xc=0.40 and $I_C(15)$=1 (case (e)) show an initially smooth and gradual area expansion (which begins at about 280K). However, when the value of $I_C(15)$ reaches 2 (case (a)), a much shaper area expansion is present at 272K. This phenomenon can be explained as follows. The larger the value of $I_C(15)$, the stronger the attraction between cholesterol and DPPC, which in turns results in the exclusion of DLPC chains from the DPPC-cholesterol regions. In other words, when sufficiently strong interactions between DPPC and cholesterol are introduced, cholesterol sequesters DPPC such that the remaining DLPC molecules, which are phase-separated from the DPPC-cholesterol region, undergo a separate melting. The sharp area expansion observed at 272K with $I_C(15)$ =2 and 40% cholesterol signals this melting of DLPC. This

phenomenon will also be analysed in Section 7.4, which deals with the actual microconfigurations of the system.

A similar sharpening of the area expansion is observed when $I_C(2\text{-}9,15)$ is increased from 0.45 to 2 in the right hand column of Fig. 7.2 (i.e., (l)→(h)). With $I_C(2\text{-}9,15)$ =2 and Xc=0.40 (case (h)) the abrupt area expansion occurs at 291K instead of at 272K as for case (a). In this series (cases (h) to (l)), we give cholesterol the same affinity with states 2 to 9 of DLPC as with state 5 of DPPC. Most of the lipid chains in these states are, therefore, sequestered by cholesterol, leaving the remaining lipid chains to go through a separate melting as T increases without the influence of cholesterol. The cholesterol-rich regions, as well as the cholesterol-poor regions, now contain both DLPC and DPPC chains. The content of the phase-separated regions are, therefore, one of the major differences between case (a) and case (h). Furthermore, the fact that cholesterol-rich and cholesterol-poor phases contain both DLPC and DPPC chains in case (a) indicates that coupling occurs between DLPC and DPPC lipid chains and, with the parameters $I_C(2\text{-}9,\ 15)$=2, cholesterol is able to mix the two lipid species relatively well. The phase behaviour of this case will be examined further in Section 7.4.

The graphs of E_{AVE} versus T in Fig. 7.3 show that, at T>303K, the average energy of the system decreases as the value of $I_C(\alpha)$ is increased (i.e., (e)→(a) and (l) →(h)). For example, the value of E_{AVE} at 310K and 40 mol% cholesterol decreases from 3.3×10^{-13} ergs in case (m) to -0.2×10^{-13} ergs in case (a) and -0.5×10^{-13} ergs in case (h). A lower value of the energy at high temperatures implies that more lipid chains are in conformationally more ordered states, such as the intermediate states, as opposed to state 10. In fact, this renders the system more **lo**-like as described earlier. On the other hand,

the change in the value of E_{AVE} as a function of $I_C(\alpha)$ cannot be seen clearly in Fig. 7.3. As with the graphs of A_{AVE} versus T, this is due to the masking effect of cholesterol in the calculation of the average energy per molecule of the system. When the parameter $I_C(15)$ and $I_C(2\text{-}9,15)$ approaches 2 (Figs. 7.3a and h), a sharp change of energy is observed at about 272K and 291K respectively. This agrees exactly with the observations from the graphs of A_{AVE} versus T and A_L versus T.

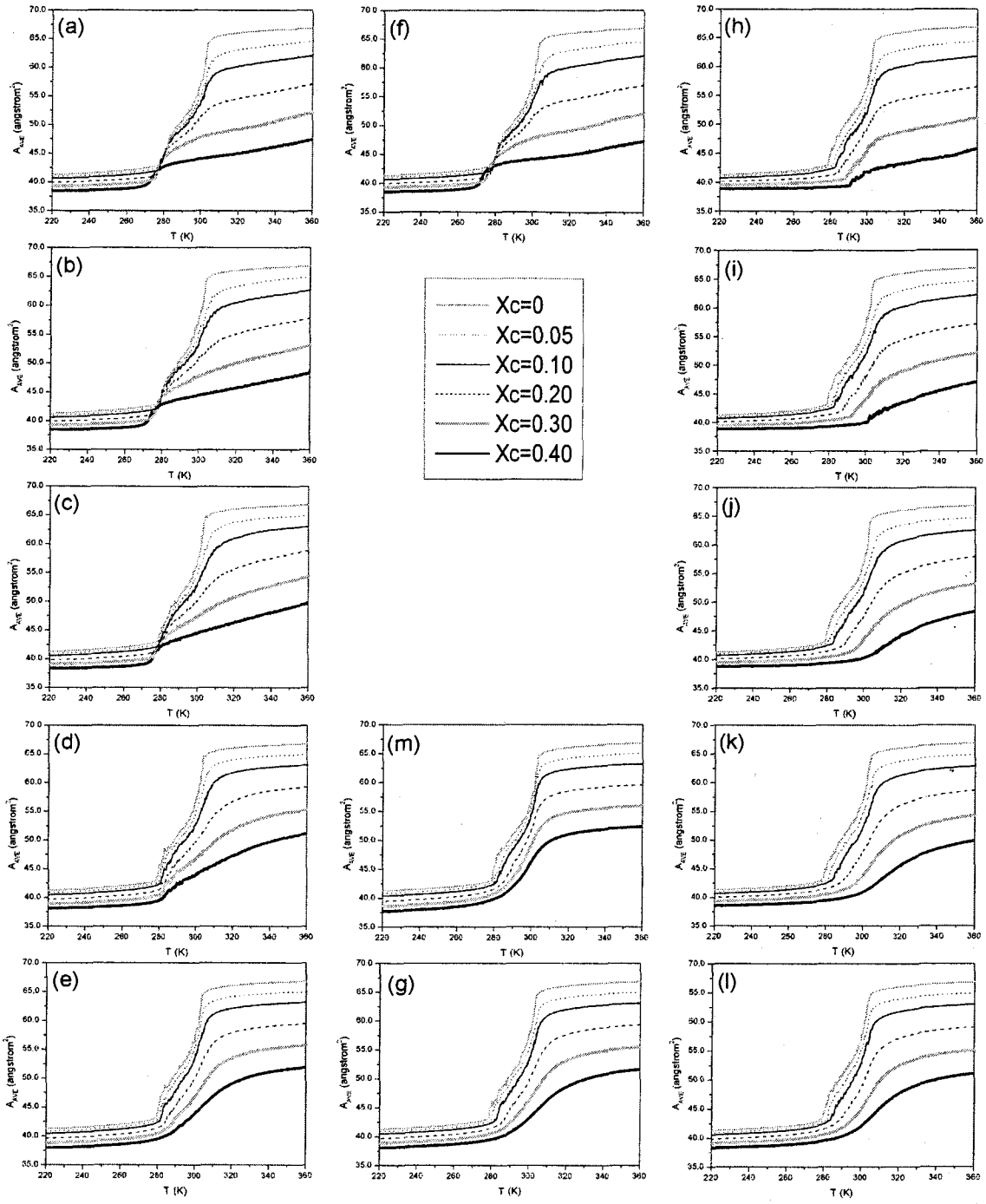

Figure 7.1 **Average area per molecule (A_{AVE}) versus temperature for DLPC/DPPC(4:6)/cholesterol bilayers**

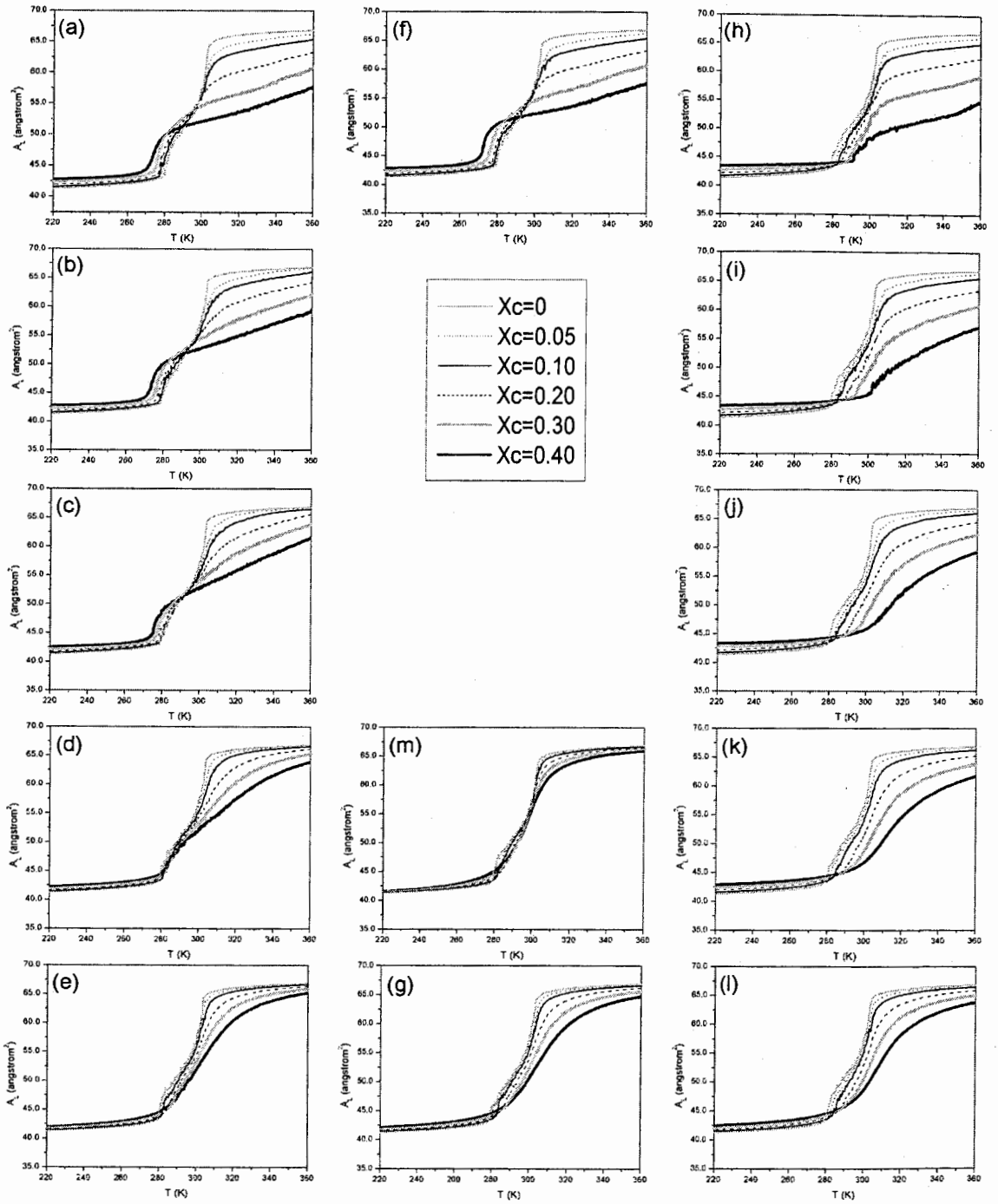

Figure 7.2 Average area per lipid molecule (A_L) versus temperature for DLPC/DPPC(4:6)/cholesterol bilayers.

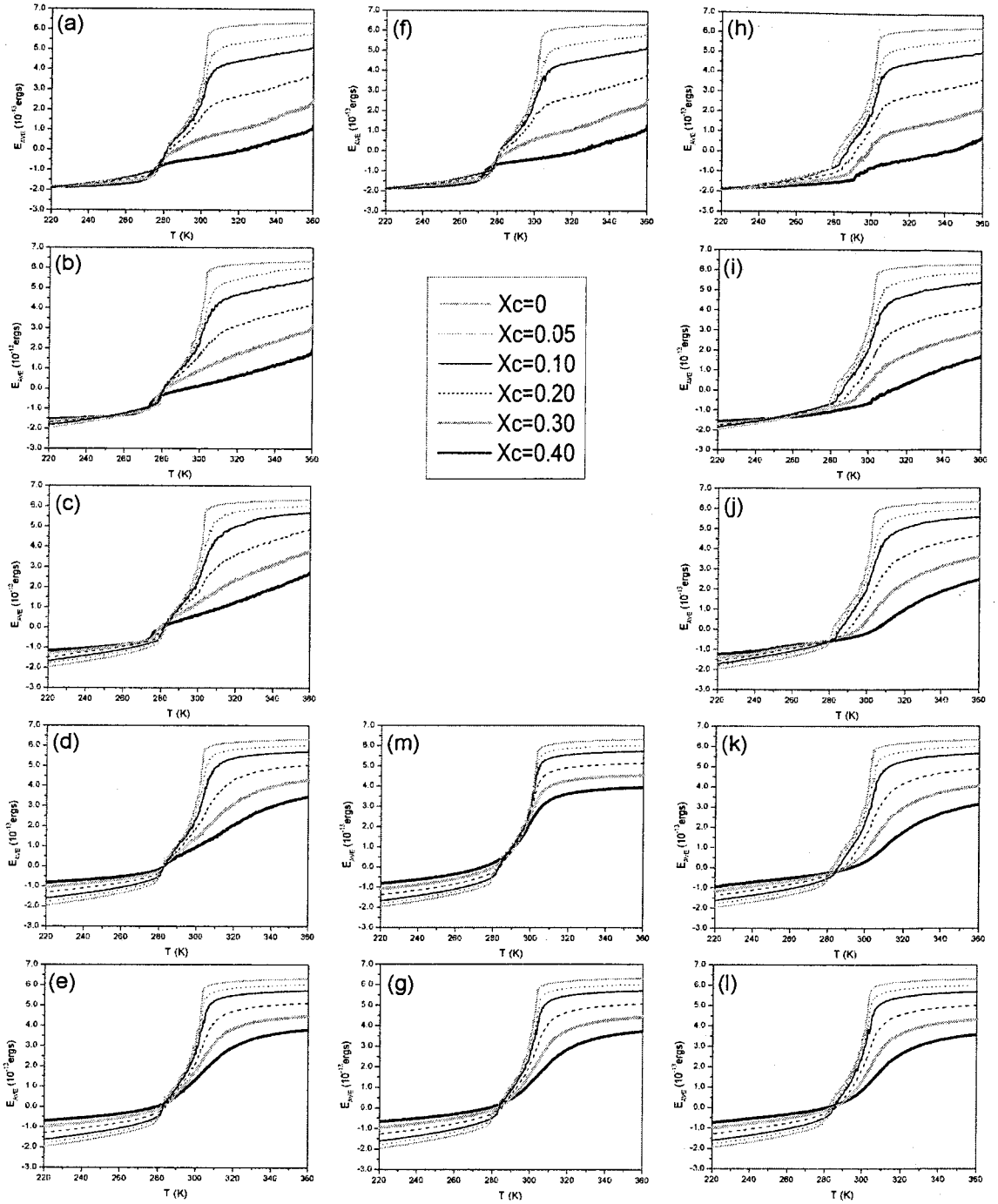

Figure 7.3 Average energy per molecule (E_{AVE}) versus temperature for DLPC/DPPC(4:6)/cholesterol bilayers

7.3 Response Functions and Microconfigurations

In this section we present graphs for the response functions and the corresponding snapshots of microconfigurations as obtained from our Monte Carlo simulation results for the ternary lipid bilayers. An analysis of the response functions together with the snapshots allows us to correlate the thermodynamic behaviour of the system with its real space nature.

Figs. 7.4 to 7.6 show the graphs of specific heat versus temperature for different values of $I_C(\alpha)$ with cholesterol concentrations Xc=0.1, 0.2 and 0.4. The labelling of each graph corresponds to the parameter set $I_C(\alpha)$ as laid out in Table 7.1. Figs. 7.10, 7.11 and 7.12 show the corresponding microconfigurations at the physiological temperature of 310K for Xc=0.1, Xc=0.2 and Xc=0.4, respectively, also calculated using the parameter sets listed in Table 7.1. Figs. 7.13, 7.14 and 7.15 show specifically the microconfigurations for Xc=0.1, 0.2 and 0.4, respectively, with the parameter sets $I_C(5)$=1 to 2 (i.e., (e) to (a)) at 260K, 288K, 310K and 330K. Figs. 7.16, 7.17 and 7.18 give microconfigurations for Xc=0.1, 0.2 and 0.4, respectively, with the parameter sets $I_C(2\text{-}9, 5)$=1 to 2 (i.e., (l) to (h)) with the same temperature sequence.

The graphs of specific heat in Figs. 7.4 and 7.5 show that, at cholesterol concentrations below Xc=0.2, there exist two separate peaks at 281K and 303K. These two peaks correspond to the two inflection points observed in the thermodynamic properties, as discussed in the previous section. On the other hand, there exists only one peak in the specific heat for systems with higher Xc, which also agrees with the observation of only one inflection point in the thermodynamic properties. In particular, at

Xc=0.4 (Fig. 7.6), the peak position is found to be at 272K for case (a) (i.e., $I_C(15)$=2) and at 291K for case (h) (i.e., $I_C(2\text{-}9,15)$=2). As expected, the above general observations agree with the results for the thermodynamic properties in Section 7.2. In the following subsections, we discuss the details of the phase behaviour of the ternary lipid bilayers with regard to the qualitative observations from the specific heat and the corresponding microconfigurations shown in the snapshots. Section 7.3.1 deals with cases (a) to (e), which correspond to bilayers with different values of $I_C(15)$. Section 7.3.2 presents the data of cases (h) to (l) in which different values of $I_C(2\text{-}9,15)$ were used.

7.3.1 $I_C(15)$ ={1, 1.25, 1.5, 1.75, 2}

Fig. 7.13 (a) to (e) shows the snapshots of microconfigurations with 10 mol% cholesterol and at four different temperatures with $I_C(15)$ values ranging from 1 to 2. Snapshots are selected at particular temperatures according to the graph of specific heat of the binary DLPC/DPPC(4:6) bilayers in Fig. 6.2 (d). At T=288K, the binary bilayer is in the **so-ld** phase coexistence region, while at T=260K and T>310K, the system is below and above the coexistence region, respectively. In Fig. 7.13, the sequence of configurations from (e) to (a) corresponds to a change of the values of $I_C(15)$ from 1 to 2 in increments of 0.25 from one graph to the next.

We first examine the behaviour of the system with $I_C(15)\leq 1.5$ across the temperature spectrum. In Figs. 7.13 (e) to (c), where $I_C(15)$ varies from 1 to 1.5, the phase behaviour of the system at 260K can be classified as the '**so** microscopic complexion' ('**so** mc') using the same terminology as in Chapter 5. At 288K, the snapshot shows a

two-phase coexistence phenomenon, which we classified as the coexistence of the DPPC-rich '**lo** mc' and the DLPC-rich '**ld** mc'. As temperatures continue to increase to 310K and beyond, cases (d) and (e) are observed to leave the two-phase coexistence region gradually and enter the '**ld** mc' region. On the other hand, in case (c), where $I_C(15)$=1.5, the phase coexistence of the '**lo** mc' and the '**ld** mc' persists to 310K and then gradually passes into the '**ld** mc' at higher temperatures.

As the value of $I_C(15)$ increases, the ternary system begins to behave very differently from the binary system. In particular, the number of DPPC chains in the kink state ($DPPC_{\alpha=15}$) increases, as seen in Table 7.2. The increasingly strong tendency of cholesterol to associate with $DPPC_{\alpha=15}$ makes the presence of $DPPC_{\alpha=15}$ favourable in the immediate neighbourhood of cholesterol, as opposed to lipid chains in other states. When the value of $I_C(15)$ is increased beyond 1.5 (cases (a) and (b)), the interaction between cholesterol and $DPPC_{\alpha=15}$ becomes so strong that it eventually leads to the emergence of a new phase—the $\sqrt{3}\times\sqrt{3}$ phase, which was first introduced in Ch. 5. As discussed before, this phase is rich in cholesterol and lipid chains in the intermediate states. In cases (a) and (b), this phase consists of cholesterol molecules on a sublattice surrounded by six intermediate state DPPC chains on its neighbouring sites. Almost all cholesterol molecules are located in the $\sqrt{3}\times\sqrt{3}$ phase, while the rest of the system is depleted of cholesterol. All snapshots for cases (a) and (b) show a phase separation of this $\sqrt{3}\times\sqrt{3}$ phase from the rest of the system. At 260K, we observe the phase coexistence of the $\sqrt{3}\times\sqrt{3}$ phase with an '**so** mc' that contains both DLPC and DPPC chains. At 288K, the system is now in a three-phase coexistence region, where we have the coexistence of the

$\sqrt{3}\times\sqrt{3}$ phase, a '**so** mc' rich in DPPC chains, and a '**ld** mc' rich in DLPC chains. This three-phase coexistence disappears as temperature continues to increase. At 310K and 330K, we observe the phase coexistence of the $\sqrt{3}\times\sqrt{3}$ phase and a '**ld** mc' which contains both lipid species. Again, note that the $\sqrt{3}\times\sqrt{3}$ phase is seen to persist at all temperatures in cases (a) and (b). In particular, as temperature increases from 310K to 330K, the total area covered by the $\sqrt{3}\times\sqrt{3}$ phase in the bilayers appears to undergo relatively little change. In fact, this is also reflected in the relatively 'flat' tail on the high temperature side of the specific heat peak in Fig. 7.4 (a) and (b), in contrast to the more rapidly declining tail for cases (d) and (e), where the system is rapidly entering the mixed '**ld** mc' region. Summarizing the observations in cases (a) and (b), we see that, when the value of $I_C(15)$ is greater than 1.5, the $\sqrt{3}\times\sqrt{3}$ phase emerges, and the system now contains a three-phase coexistence region. This $\sqrt{3}\times\sqrt{3}$ phase is relatively stable with increasing temperatures, while the cholesterol-depleted region is observed to melt as temperature increases.

Table 7.2 Percentage of DPPC chains in state 15 out of all DPPC chains in the system at 310K for cases (a), (b), (c), (d), (e) with *Xc*=0.1, 0.2 and 0.4.

Xc	(a)	(b)	(c)	(d)	(e)
0.1	23%	20%	18%	10%	5%
0.2	45%	42%	37%	23%	12%
0.4	93%	83%	73%	53%	31%

The influences of cholesterol on the bilayers become stronger when we increase cholesterol concentration to 20 mol%. Table 7.2 shows that an increased *Xc* leads to an

increased number of DPPC chains in the kink state ($DPPC_{\alpha=15}$) at the expense of the other states (α=[11-14,16-20]), which can also be seen by comparing the snapshots in Figs. 7.13 and 7.14. In other words, an increased number of cholesterol molecules in the system favours the presence of $DPPC_{\alpha=15}$ and as a consequence decreases the number of DPPC chains in the other states. In cases (a) and (b), we observe the presence of the $\sqrt{3}\times\sqrt{3}$ phase. The phase behaviour of these cases is qualitatively similar to that at Xc=0.1 (Fig. 7.13), only with more cholesterol in the system the $\sqrt{3}\times\sqrt{3}$ phase has now grown to cover a larger area in the system. Cases (c) to (e) also have behaviour which is qualitatively similar to that of Xc=0.1, but all with a larger area covered by the '**lo** mc'.

One point to note is that, since the 'lo mc' in case (c) now persists to higher temperatures than in the case of Xc=0.1, we expect that the specific heat 'tail' on the high temperature side of the peak will have a less negative slope. Comparing the specific heat graphs in Figs. 7.4(c) and 7.5(c) confirms this observation from the snapshots.

Fig. 7.15 shows the snapshots of microconfigurations of the same series ((a) to (e)) with 40 mol% cholesterol. Comparing these graphs with those for Xc=0.10 (Fig. 7.13) and Xc=0.20 (Fig. 7.14), we again observe increased numbers of $DPPC_{\alpha=15}$ due to an increased concentration of cholesterol in the system (also see Table 7.2). One major difference between the bilayers with Xc=0.4 and the ones with lower Xc values is that the **lo**-like regions now dominate the bilayer. It is seen most clearly in cases (a) and (b), where the $\sqrt{3}\times\sqrt{3}$ phase occupies more than 50% of the total surface area of the bilayers. Instead of observing the $\sqrt{3}\times\sqrt{3}$ phase in a background of cholesterol-poor

regions as in the Figs. 7.13 and 7.14, we are now seeing clusters of the cholesterol-poor regions in a background of the $\sqrt{3}\times\sqrt{3}$ phase.

Inspecting the snapshots of case (e) (i.e., $I_C(15)$=1) with increasing cholesterol concentrations (i.e., Figs. 7.13(e) to 7.15(e)), we observed that the phase separation phenomenon has gradually disappeared (note especially the snapshots at 288K). At the same time, the two relatively sharp peaks in the specific heat graphs in Figs. 7.4(e) and 7.5(e), which give the two-phase boundaries, have disappeared in Fig. 7.6(e), when *Xc* reaches 0.4. In fact, the specific heat graph in Fig. 7.6(e) shows that the system passes continuously from the '**so** mc' to the '**ld** mc' as temperature increases. This shows the effect of cholesterol is to remove the phase separation.

Let us now look at the other extreme, i.e., when $I_C(15)$ approaches 2. Inspection of the snapshots of case (a) with increasing cholesterol concentrations reveals a large increase of the number of $DPPC_{\alpha=15}$ chains at the expense of the other conformational states. At *Xc*=0.4, DPPC exists almost entirely in the form of $DPPC_{\alpha=15}$ at all temperatures, whereas the number of DPPC chains in state 1 or state 10 is insignificant (e.g., Table 7.2 shows that at 310K, 93% of the DPPC chains are in state 15). Furthermore, the $DPPC_{\alpha=15}$ chains are seen to have an almost exclusive association with cholesterol and are, therefore, almost exclusively found in the $\sqrt{3}\times\sqrt{3}$ phase. This leads to a type of phase behaviour different from the case with lower *Xc* values. At 260K, we observe a coexistence of the DLPC '**so** mc' with the $\sqrt{3}\times\sqrt{3}$ phase. As temperature increases, the '**so** mc' gradually melts to the '**ld** mc', independent of the $\sqrt{3}\times\sqrt{3}$ phase, which remains relatively unaffected by temperature increase. In other words, the three-

phase coexistence that is observed with lower values of *Xc* at 288K is no longer present here. This is confirmed by the corresponding graph of specific heat in Fig. 7.6(a). Here, a single sharp peak is observed at about 271K instead of the two peaks observed in Figs. 7.4(a) and 7.5(a).

7.3.2 I_C(2-9,15) ={1, 1.25, 1.5, 1.75, 2}

In this section we present the graphs of specific heat and the corresponding snapshots of microconfigurations for cases (l) to (h), in which the parameters $I_C(2\text{-}9,15)$ vary from 1 to 2. The graphs of specific heat for *Xc*=0.1, 0.2 and 0.4 are located in the right hand column of Fig. 7.4 to 7.6 and the corresponding microconfigurations, in Fig. 7.16 to 7.18.

For *Xc*=0.1, the graphs of specific heat for cases (h) to (l) in the right hand column in Fig. 7.4 look very similar to those of cases (a) to (e) in the left hand column. Two peaks are observed in all graphs, which represent the boundaries of the phase coexistence region, except that the low temperature peak is located at a slightly higher temperature (around 285K) than that for cases (a) to (e) (around 282K). Fig. 7.16 shows the corresponding snapshots of microconfigurations at *Xc*=0.1. In cases (j) to (l), where the value of $I_C(2\text{-}9,15)$ is at or below 1.5, the bilayers at 260K can be classified as being in the '**so** mc'. At 288K, we observe the coexistence of the DPPC-rich '**lo** mc' with the DLPC-rich '**ld** mc', as in the case of (c) to (e) discussed above. As temperature continues to increase, the system gradually leaves the two-phase region and it eventually becomes a mixture of both lipid species in the '**ld** mc'. In Figs. 7.16 (i) and (h), where the value of $I_C(2\text{-}9,15)$ equals 1.75 and 2, we again see the presence of the $\sqrt{3}\times\sqrt{3}$ phase. However,

the content of this phase is now different from that of cases (a) and (b). The intermediate state lipid chains that surround each cholesterol molecule now include both lipid species, instead of DPPC chains alone as in cases (a) and (b). At 288K, we observe a three-phase coexistence, which includes the $\sqrt{3}\times\sqrt{3}$ phase, the DPPC-rich '**so** mc', and the DLPC-rich '**ld** mc'.

We now examine the snapshots of microconfigurations with Xc=0.2 in Fig. 7.17. One major difference between the system with Xc=0.2 and the one with Xc=0.1 is that the **lo**-like region now covers a larger area. This again proves that an increase of Xc results in an increase of the number of lipid chains in states α={2-9,15}, which eventually leads to the growth of the **lo**-like regions in the system. Moreover, the phase separation of the '**lo** mc' and the '**ld** mc' in cases (j) to (l) has gradually disappeared (see snapshots at 288K). This is also reflected in the specific heat graphs, in Fig. 7.5(j) to (l), where the two peaks gradually merge.

Figs. 7.6 and 7.18 show the heat capacities and the corresponding snapshots of microconfigurations of the system with 40 mol% cholesterol. Here, again, we see an increase in the number of lipid chains in states {2-9,15} and an increase in the area of the **lo**-like regions. In cases (j) and (l), we observe that the system changes continuously from the '**so** mc' to the '**ld** mc' as temperature increases, which is also reflected in the rounded broad peak in the corresponding graphs of specific heat, Fig. 7.6. However, when we increase the values of $I_C(2\text{-}9,15)$ beyond 1.5 (cases (i) to (h)), the system begins to exhibit phase separation. At 260K and 288K, phase separation of the $\sqrt{3}\times\sqrt{3}$ phase and a DPPC-rich '**so** mc' is observed. On the other hand, at 310K and 330K, phase separation of the $\sqrt{3}\times\sqrt{3}$ phase and an '**ld** mc' which contains both lipid species is observed. These

results are different from cases (a) to (e). Firstly, at temperatures below 288K, almost all DLPC chains are sequestered by cholesterol into the $\sqrt{3}\times\sqrt{3}$ phase and, therefore, the cholesterol-poor regions are depleted of DLPC. However, the '**ld** mc' that is present at 310K and 330K consists of both DLPC and DPPC chains, which implies that some of the DLPC chains from the $\sqrt{3}\times\sqrt{3}$ phase have melted into the '**ld** mc' as temperature increases, even though it only occurs to a small extent. Furthermore, we also observe that the rounded broad peak in case (l) with $I_C(2\text{-}9,15)=1$ gradually becomes sharpened as the values of $I_C(2\text{-}9,15)$ approach 2. This signals the occurrence of phase separation, and the details of this case will be discussed below.

The partial schematic phase diagram of case (h) where $I_C(2\text{-}9,15)=2$ is shown in Fig. 7.19. This phase diagram is obtained from the specific heat graphs and the snapshots of microconfigurations. As before, horizontal error bars indicate the approximate boundaries of phase separation regions obtained from the snapshots. The midpoint of the vertical lines indicates the position of the specific heat peaks at different *Xc* and *T*. We conjecture that there should be closure of the phase-separation region at higher temperatures because of the overall topology of the phase diagram. This closure is indicated by the dotted line that ends at a critical point. Near *Xc*=0, the system behaves like the binary DLPC/DPPC (40/60) bilayers (see Ch. 6), with the '**so** mc' below approximately 281K, the '**ld** mc' above 303K, and the two-phase region in between. At slightly higher cholesterol concentrations and temperatures below 353K, the $\sqrt{3}\times\sqrt{3}$ phase emerges. Two two-phase regions ('**so** mc'+ $\sqrt{3}\times\sqrt{3}$ and '**ld** mc'+ $\sqrt{3}\times\sqrt{3}$) are observed and one three-phase region ('**so** mc'+ '**ld** mc'+ $\sqrt{3}\times\sqrt{3}$) is found between them. If we increase cholesterol concentration to 50 mol%, the entire system will be in

the $\sqrt{3}\times\sqrt{3}$ phase. However, if one fixes an intermediate cholesterol concentration and then increases the temperature to above 350K, we would observe a disordering of the $\sqrt{3}\times\sqrt{3}$ phase to a regular '**lo** mc', resulting in the coexistence of the '**ld** mc'+ '**lo** mc'. On the other hand, in the region of the phase diagram where cholesterol concentration is much higher than 50 mol%, we observe the disordering of the $\sqrt{3}\times\sqrt{3}$ phase into an '**lo** mc'. This disordering, similar to the case of $I_C(5)$=2 for DPPC/Cholesterol bilayers, is due to the incorrect stoichiometry of the components, since the $\sqrt{3}\times\sqrt{3}$ phase can only exist near lipid/Chol (1:1). This boundary is indicated by the dotted line in the phase diagram. Note that some of the data at high temperatures and high cholesterol concentrations that were used in drawing the phase diagram are not presented in this section.

In conclusion, by increasing the interactions between both DLPC-cholesterol and DPPC-cholesterol, both lipid species became involved in both the cholesterol-rich (i.e., the $\sqrt{3}\times\sqrt{3}$ phase and the '**lo** mc') and the cholesterol-poor regions. In other words, with a high enough value of $I_C(2\text{-}9,15)$ and under the influence of cholesterol, a coupling between the two lipid species can be achieved which makes DLPC and DPPC chains behave in a very similar way.

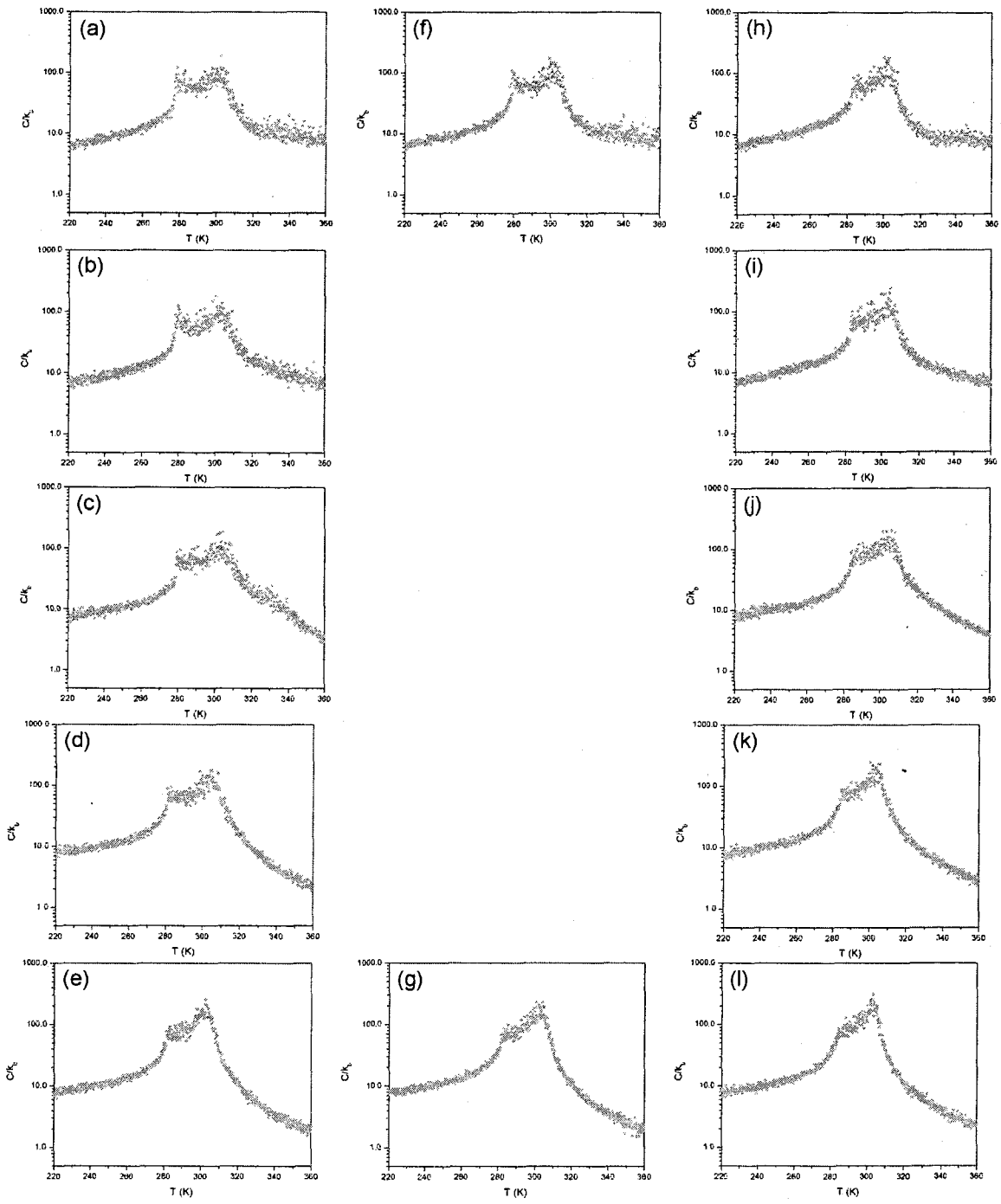

Figure 7.4 **Specific Heat (C_p) versus temperature with 10% cholesterol (Xc=0.10) for DLPC/DPPC(4:6)/cholesterol bilayers**

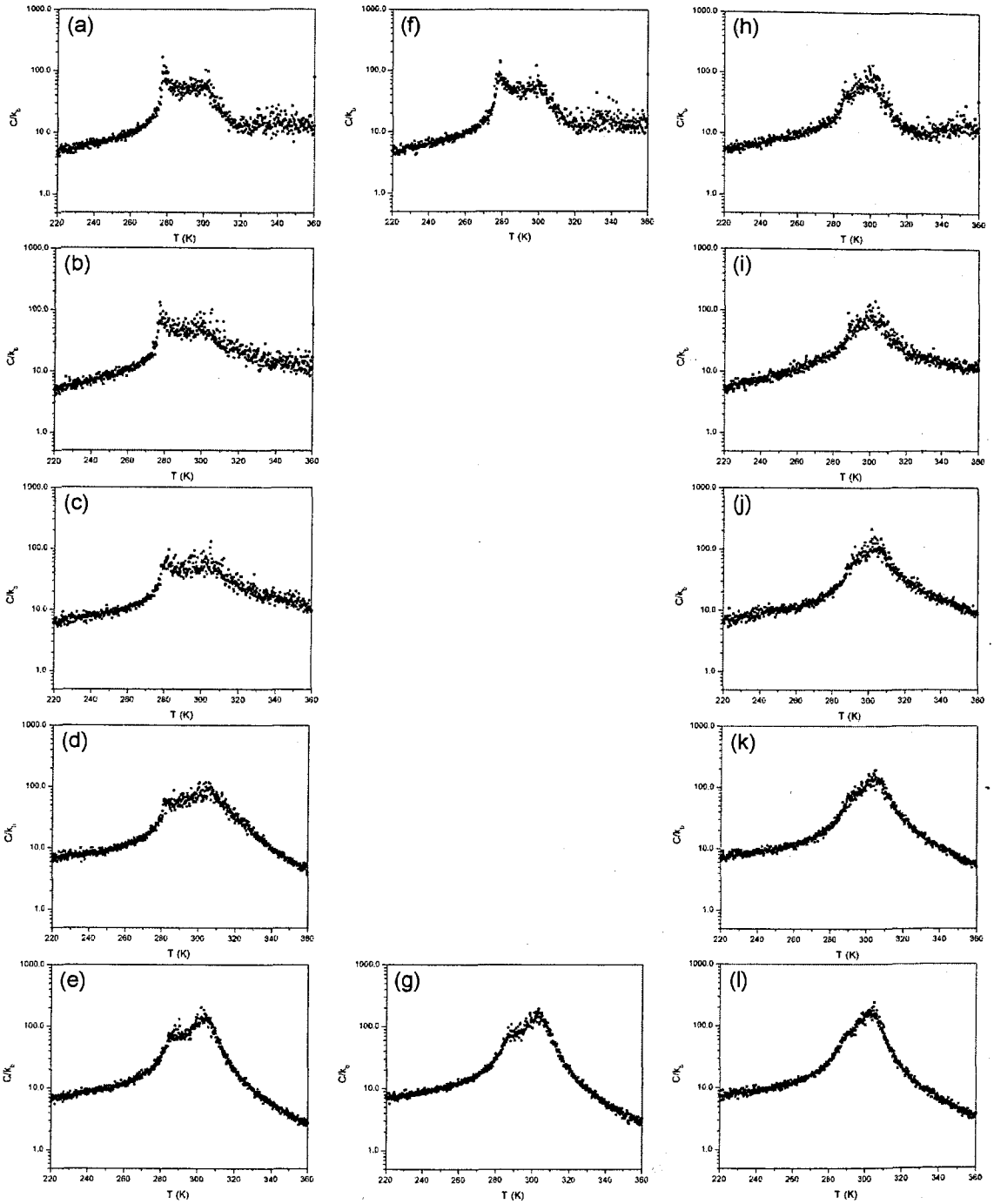

Figure 7.5 Specific Heat (C_p) versus temperature with 20% cholesterol (Xc=0.2) for DLPC/DPPC(4:6)/cholesterol bilayers

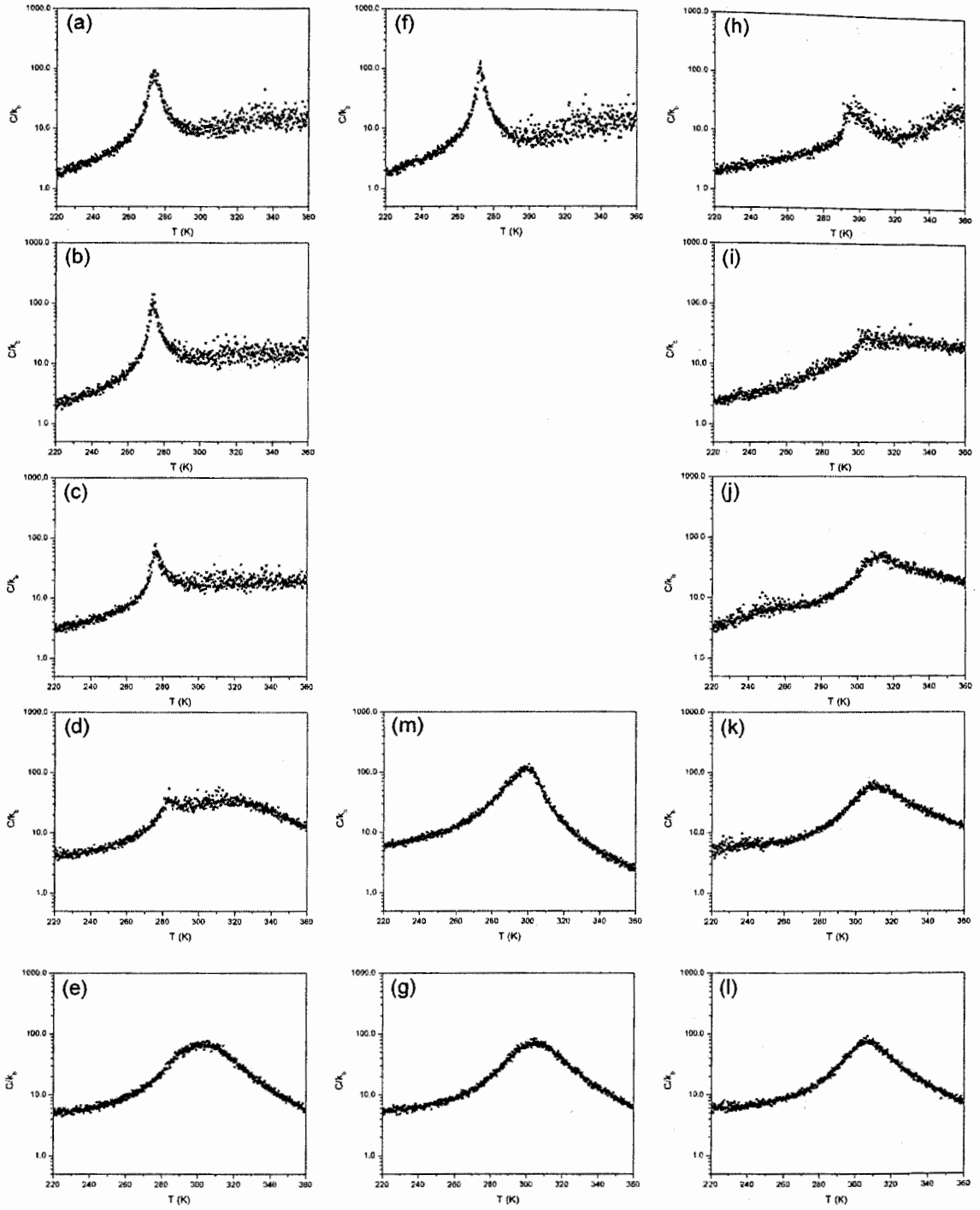

Figure 7.6 **Specific Heat (C_p) versus temperature with 40% cholesterol (Xc=0.4) for DLPC/DPPC(4:6)/cholesterol bilayers**

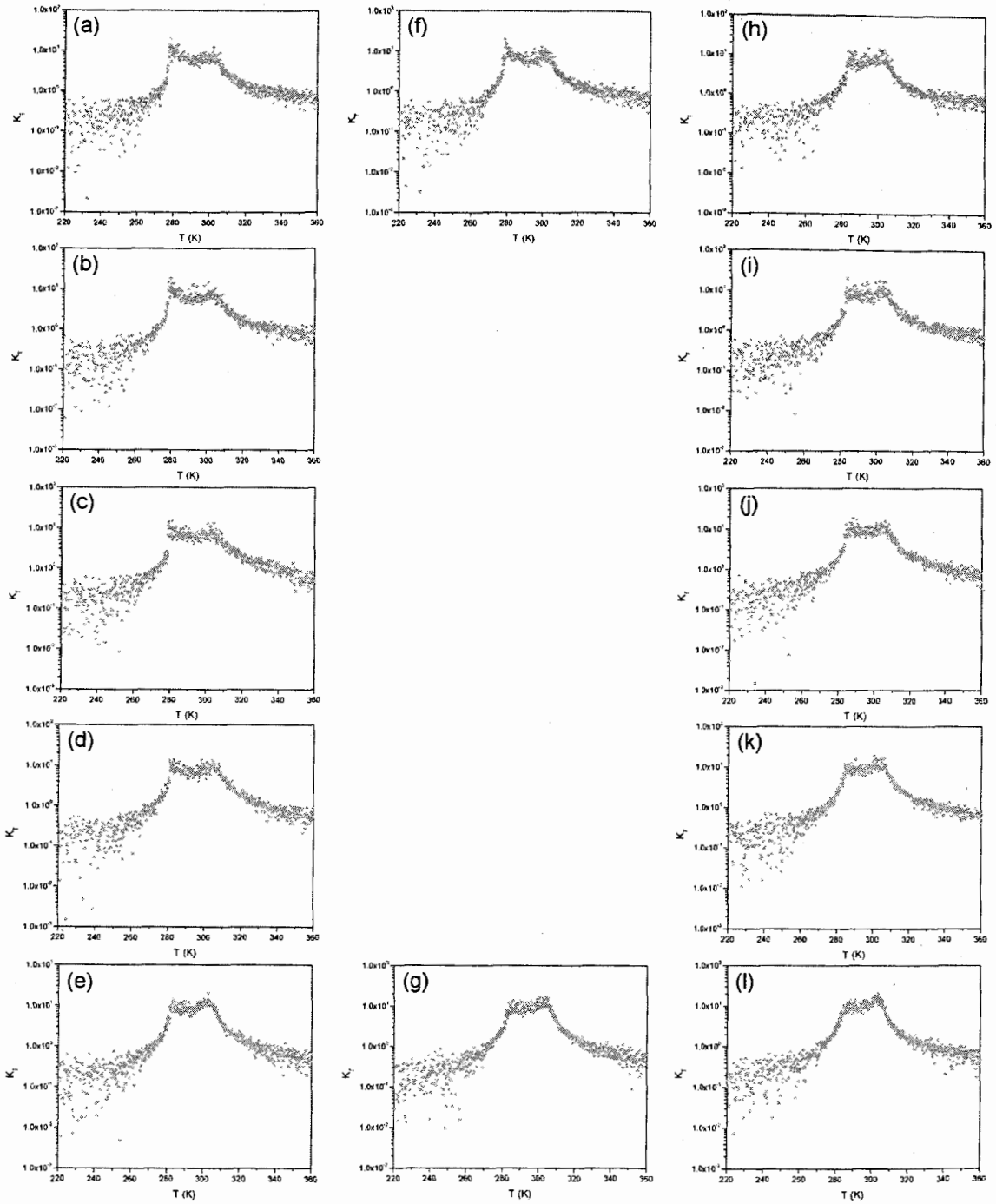

Figure 7.7 **Isothermal lateral compressibility (K_T) versus temperature with 10% cholesterol (Xc=0.1) for DLPC/DPPC(4:6)/cholesterol bilayers**

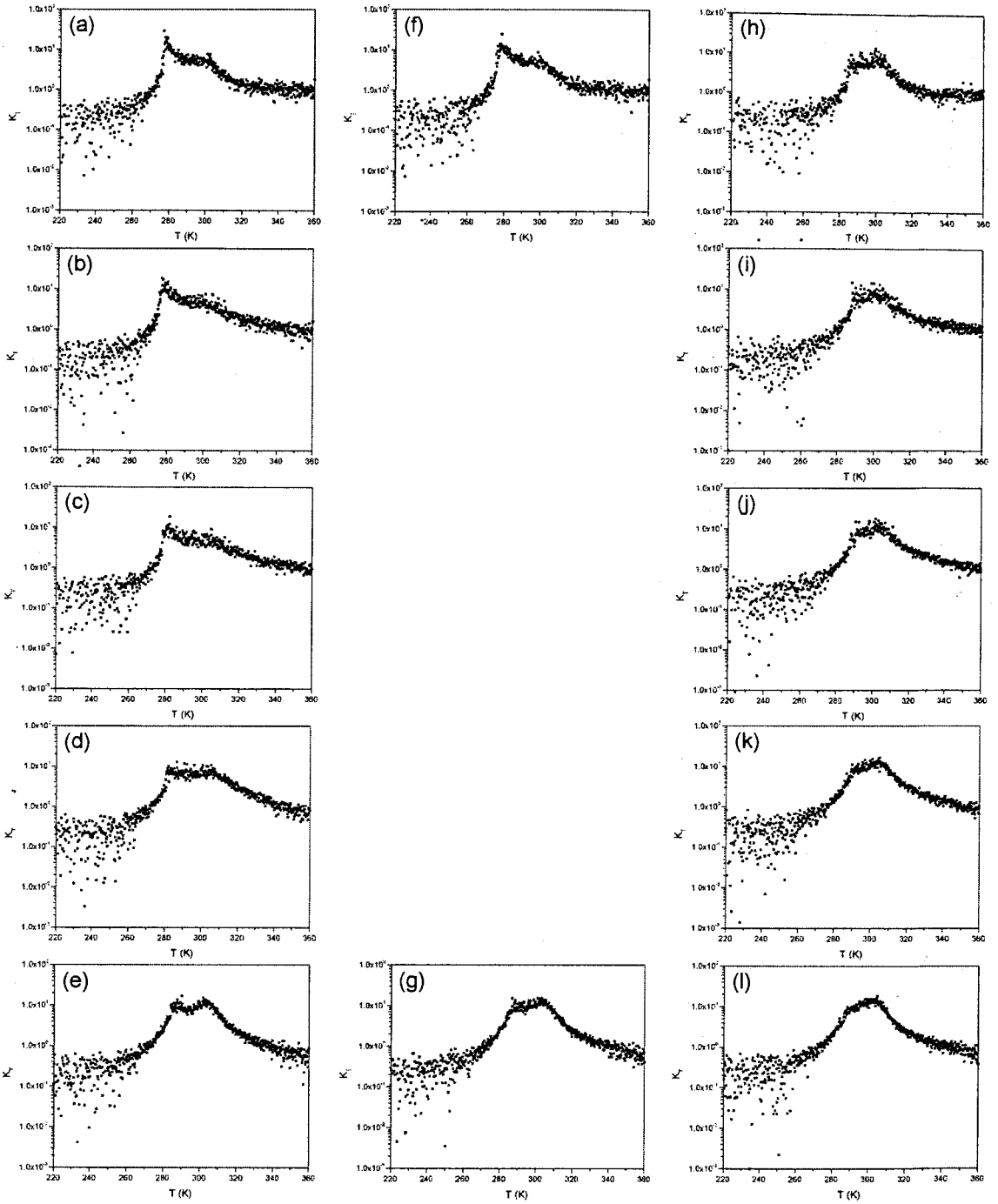

Figure 7.8 **Isothermal lateral compressibility (K_T) versus temperature with 20% cholesterol (Xc=0.2) for DLPC/DPPC(4:6)/cholesterol bilayers**

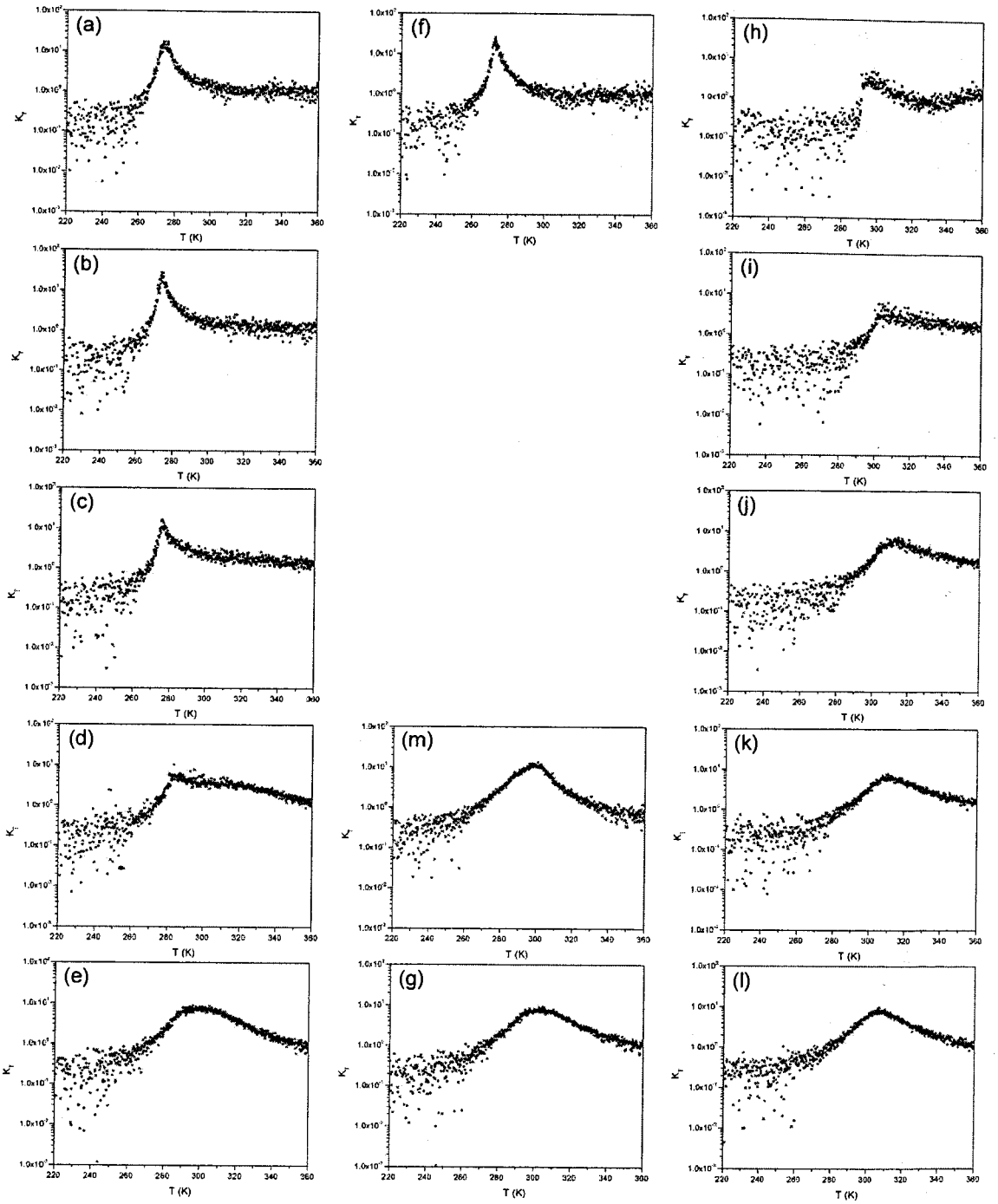

Figure 7.9 **Isothermal lateral compressibility (K_T) versus temperature with 40% cholesterol (Xc=0.4) for DLPC/DPPC(4:6)/cholesterol bilayers**

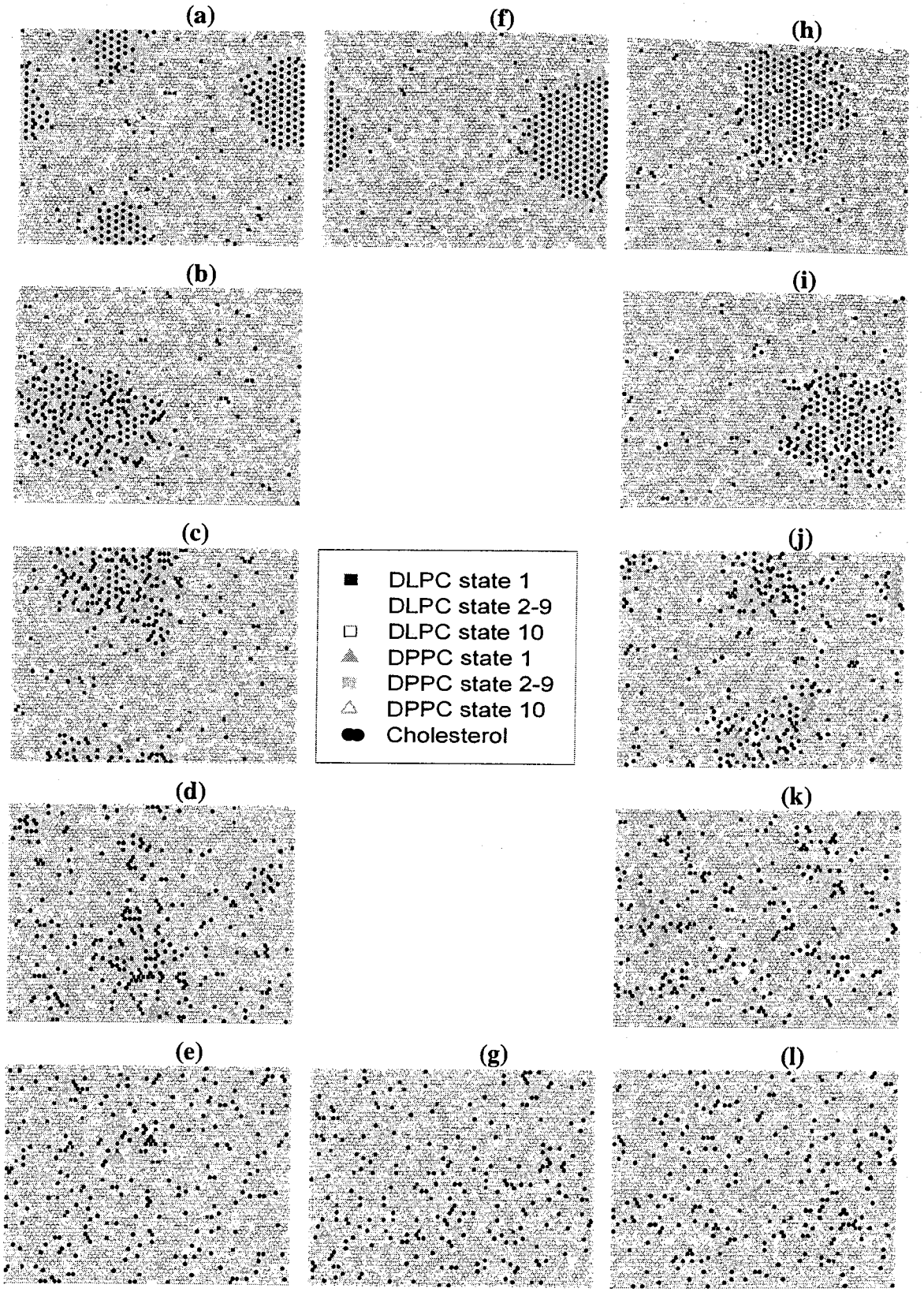

Figure 7.10 Simulated microconfigurations for DLPC/DPPC(4:6)/cholesterol bilayer with 10% Cholesterol (Xc=0.1) at 310K.

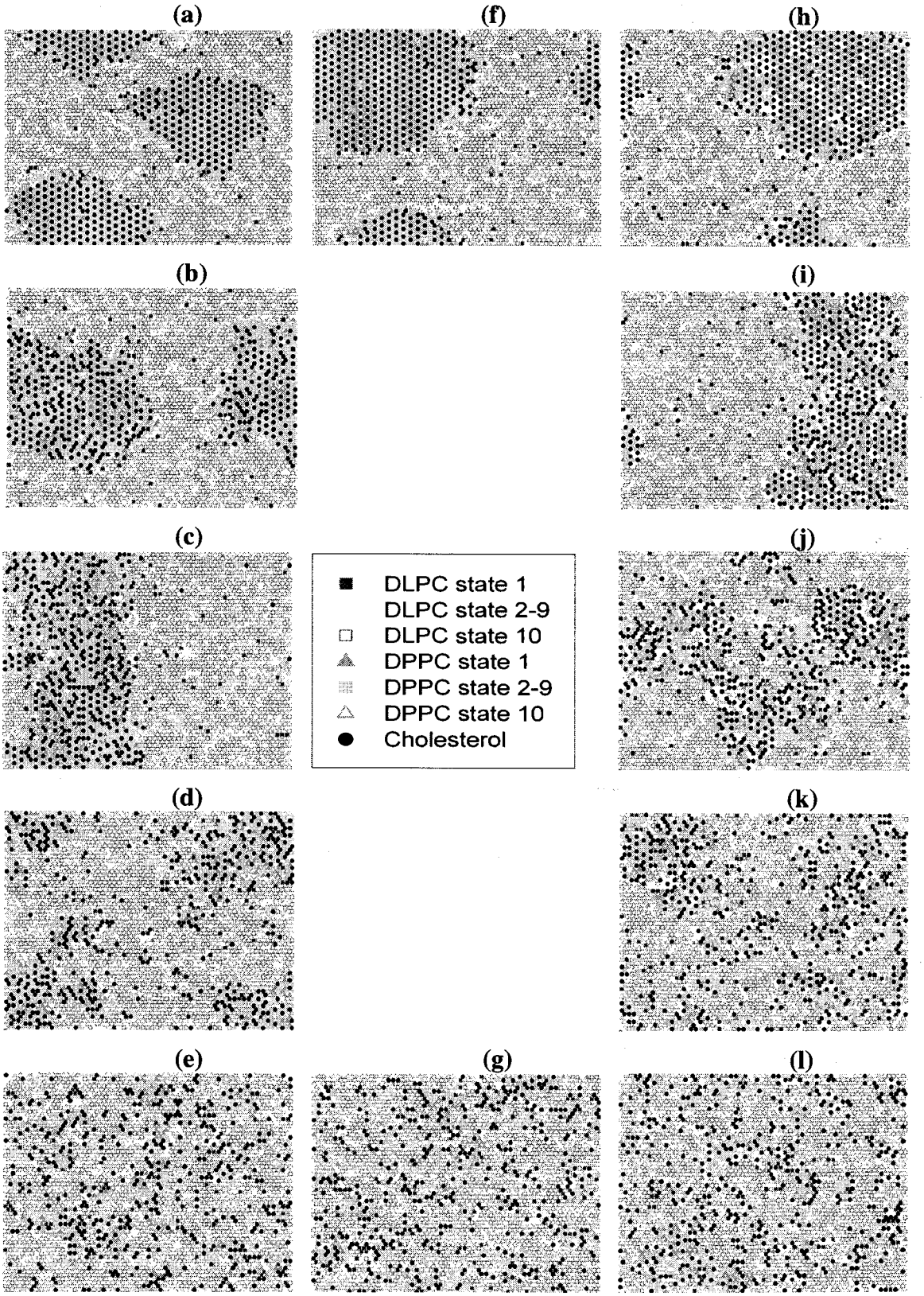

Figure 7.11 Simulated microconfigurations for DLPC/DPPC(4:6)/cholesterol bilayer with 20% Cholesterol (Xc=0.2) at 310K.

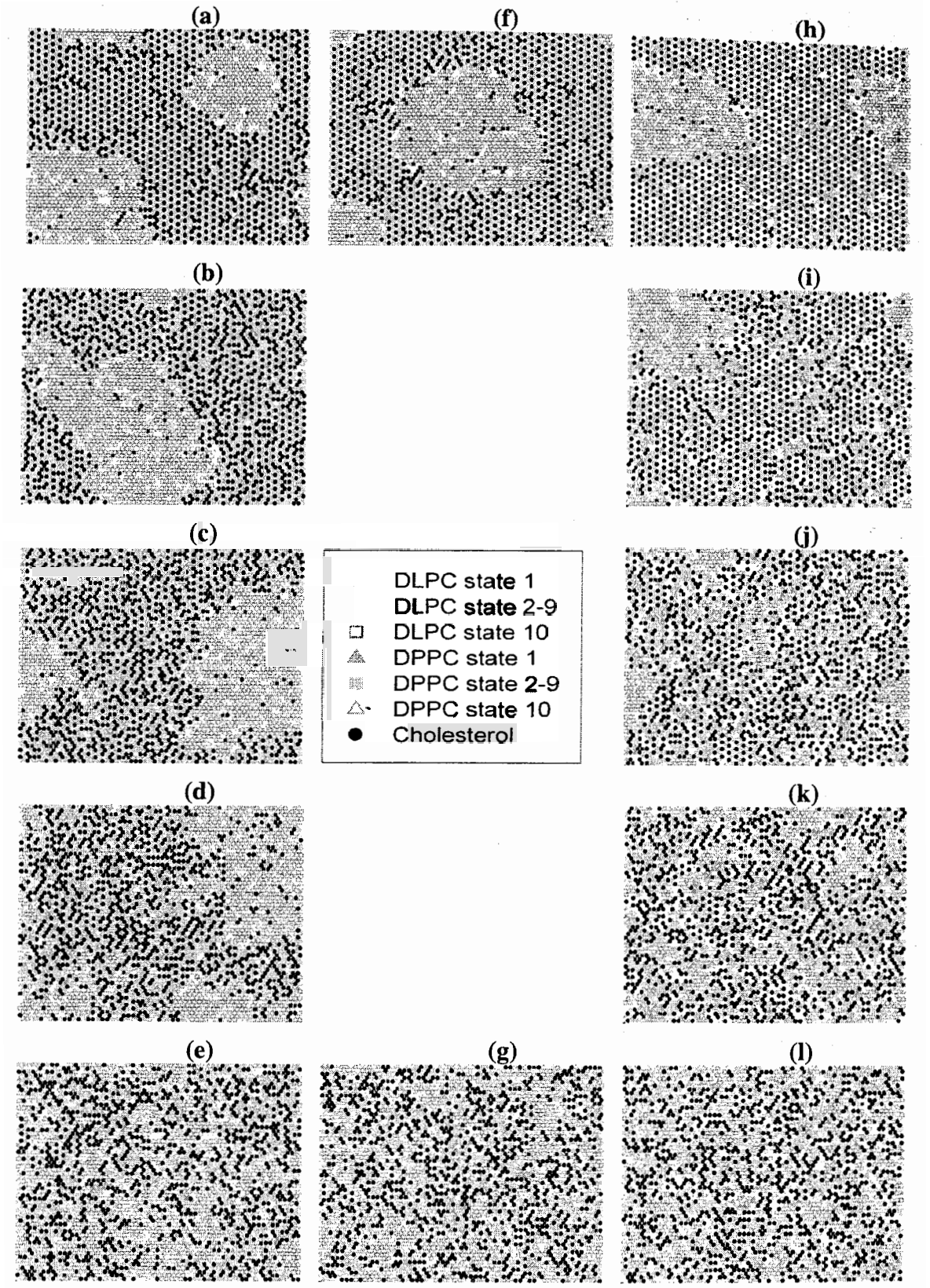

Figure 7.12 Simulated microconfigurations for DLPC/DPPC(4:6)/cholesterol bilayer with 40% Cholesterol (Xc=0.4) at 310K.

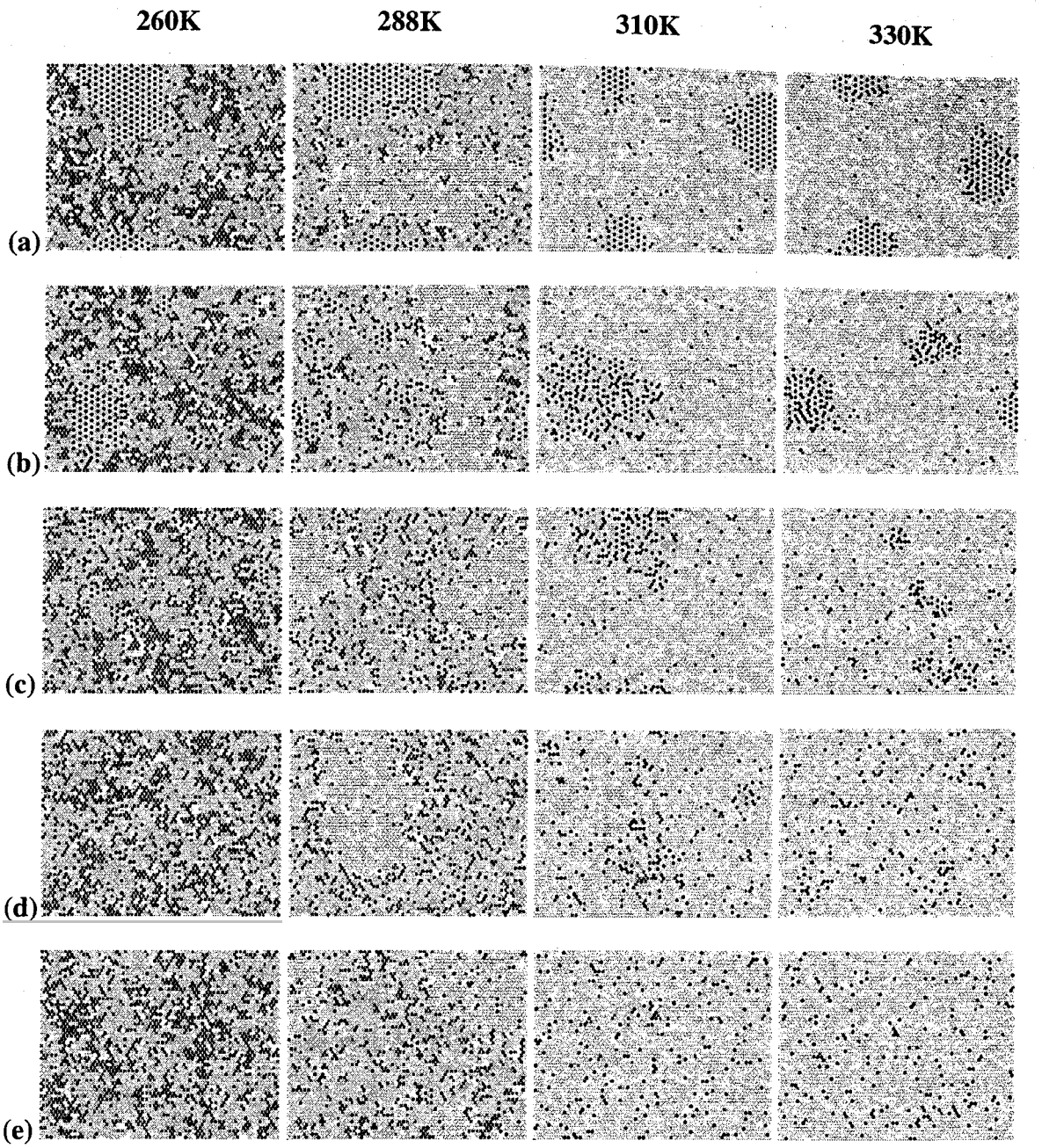

Figure 7.13 imulated microconfigurations for DLPC/DPPC(4:6)/cholesterol bilayers with (a) $I_C(15)$=2, (b) $I_C(15)$=1.75, (c) $I_C(15)$=1.5, (d) $I_C(15)$=1.25, (e) $I_C(15)$=1 with Xc=0.10 at different temperatures.

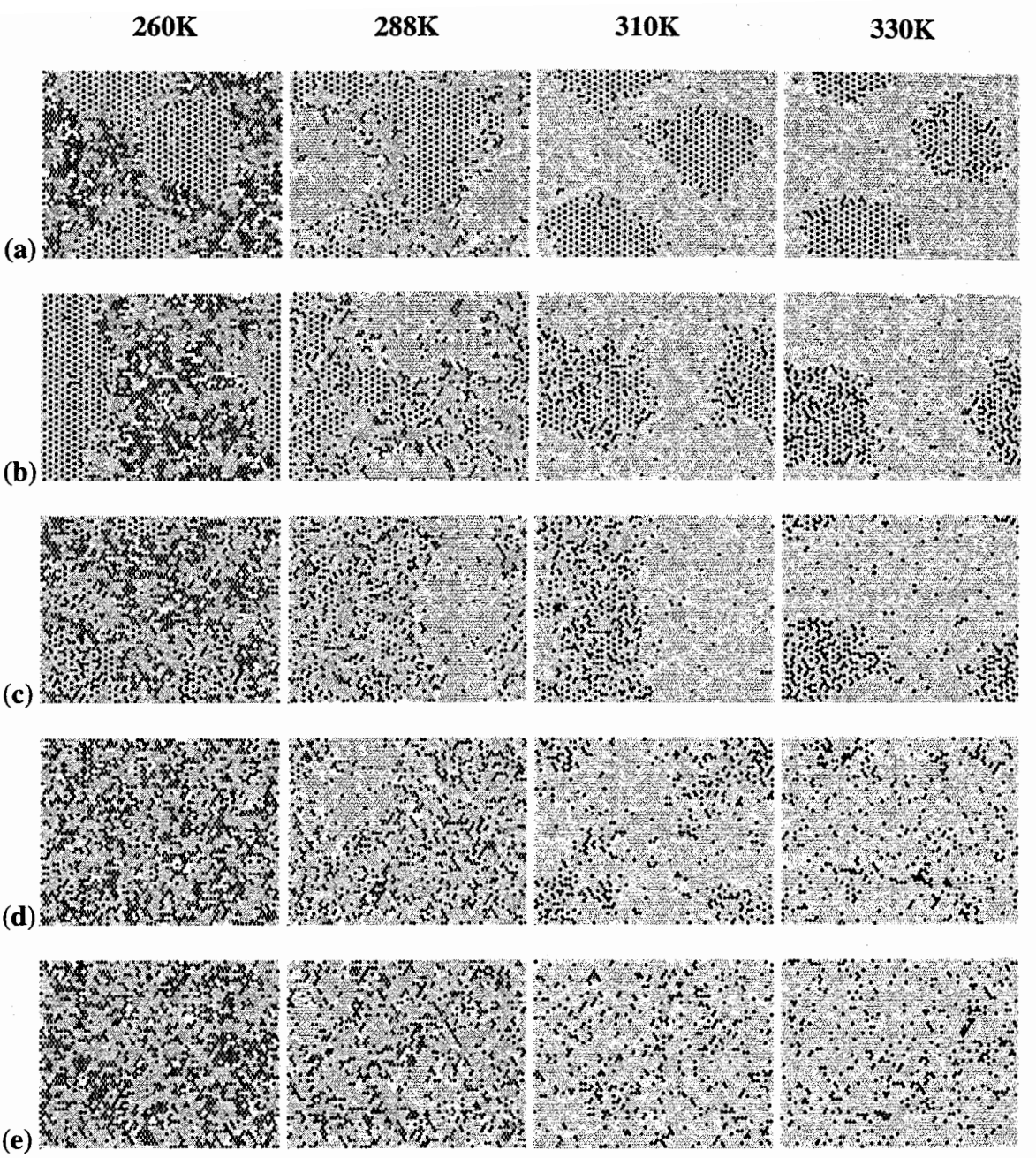

Figure 7.14 Simulated microconfigurations for DLPC/DPPC(4:6)/cholesterol bilayers with (a) $I_C(15)$=2, (b) $I_C(15)$=1.75, (c) $I_C(15)$=1.5, (d) $I_C(15)$=1.25, (e) $I_C(15)$=1 with Xc=0.20 at different temperatures.

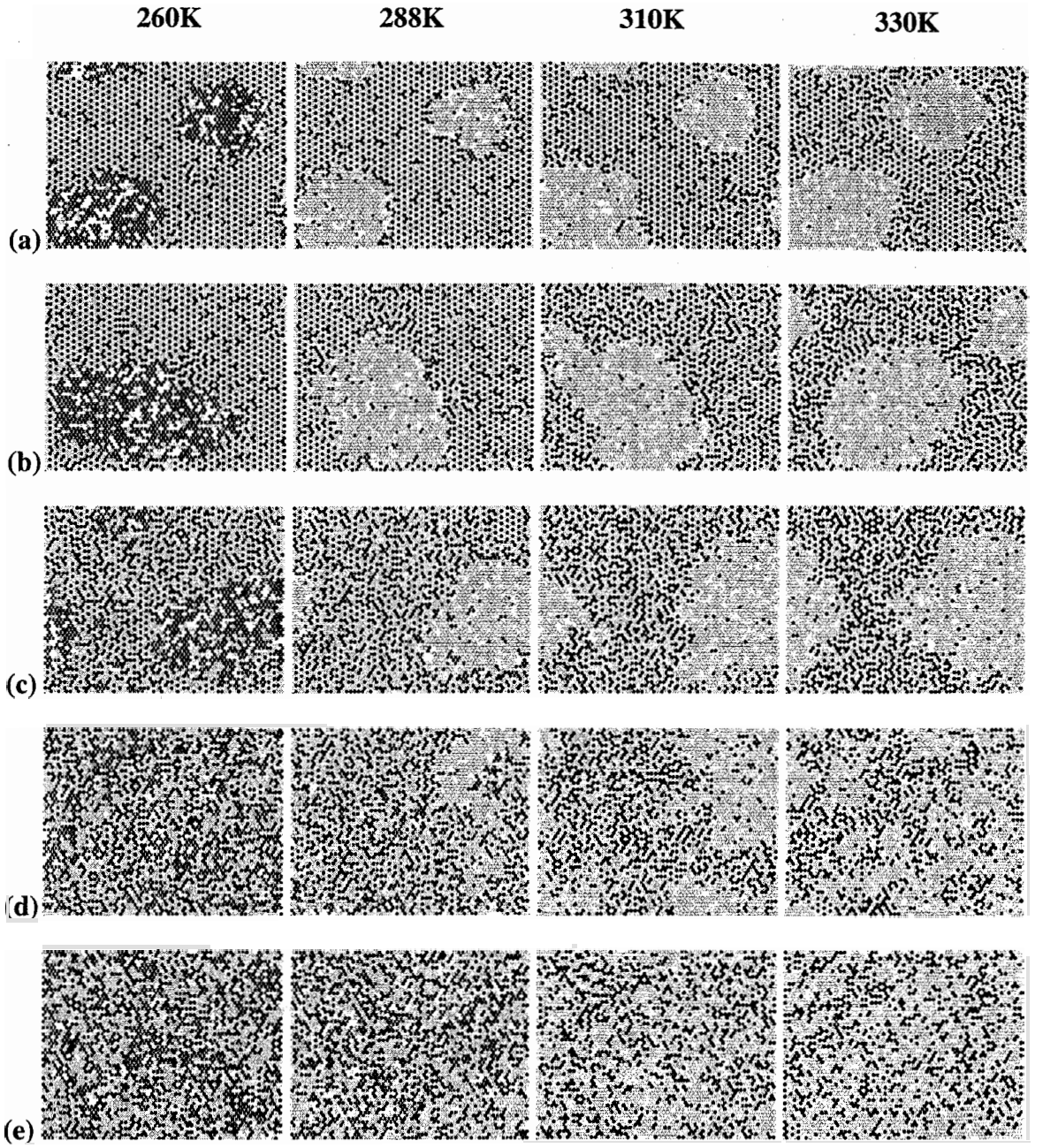

Figure 7.15 **Simulated microconfigurations for DLPC/DPPC(4:6)/cholesterol bilayers with (a) $I_C(15)$=2, (b) $I_C(15)$=1.75, (c) $I_C(15)$=1.5, (d) $I_C(15)$=1.25, (e) $I_C(15)$=1 with Xc=0.40 at different temperatures.**

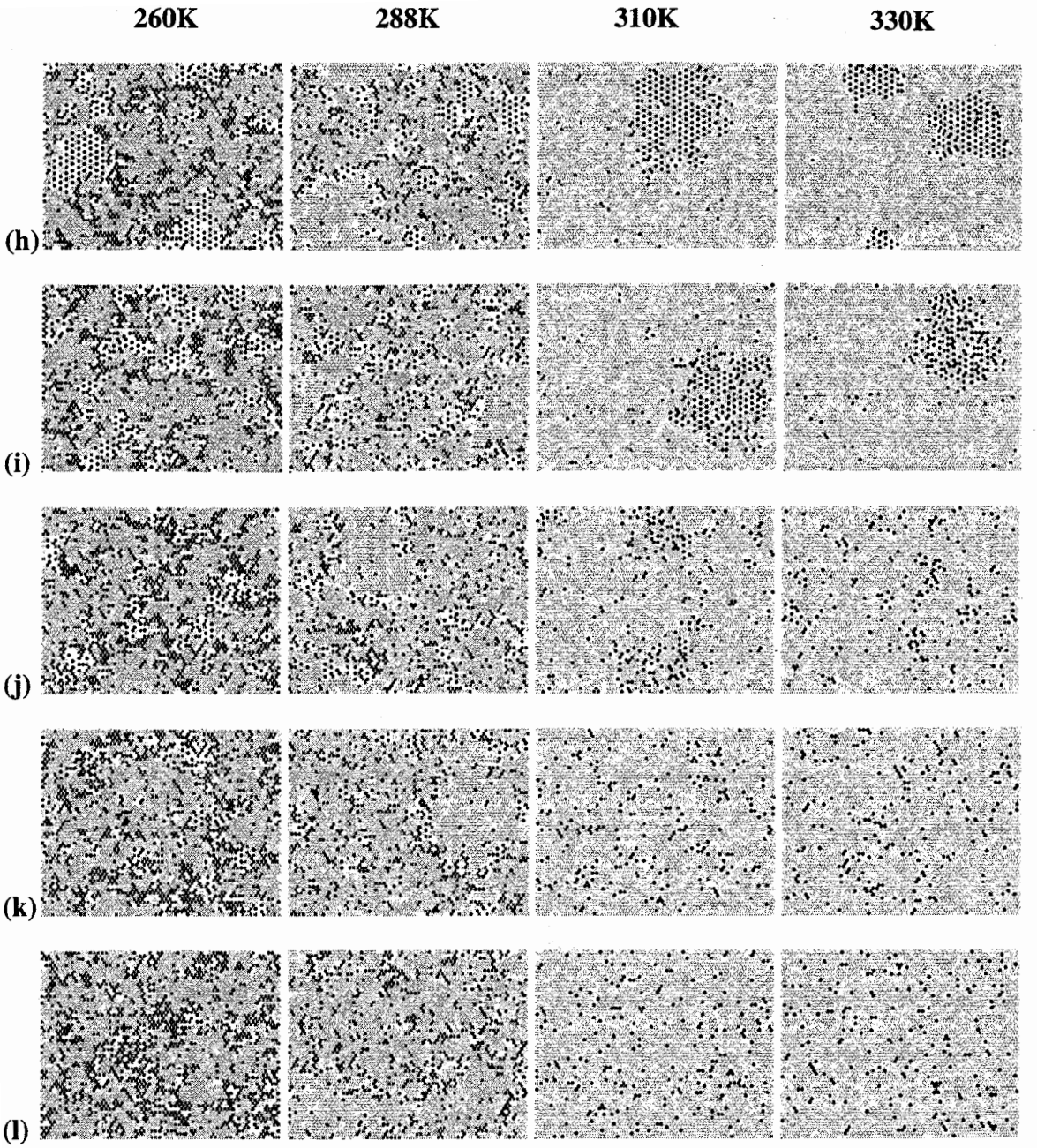

Figure 7.16 **Simulated microconfigurations for DLPC/DPPC(4:6)/cholesterol bilayers with (h) $I_C(2\text{-}9,15)$=2, (i) $I_C(2\text{-}9,15)$=1.75, (j) $I_C(2\text{-}9,15)$=1.5, (k) $I_C(2\text{-}9,15)$=1.25, (l) $I_C(2\text{-}9,15)$=1 with Xc=0.10 at different temperatures.**

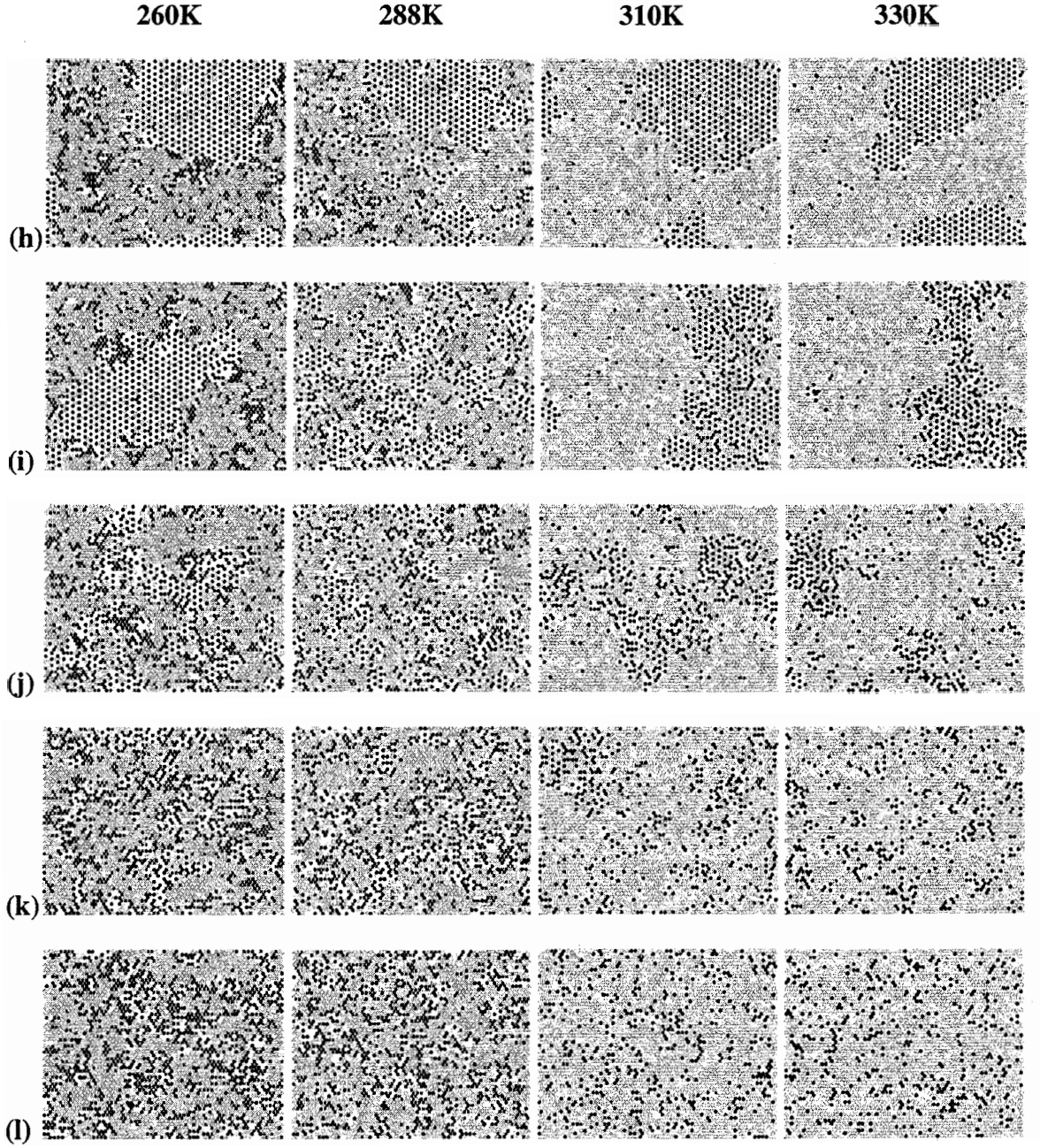

Figure 7.17 **Simulated microconfigurations for DLPC/DPPC(4:6)/cholesterol bilayers with (h) $I_C(2\text{-}9,15)$=2, (i) $I_C(2\text{-}9,15)$=1.75, (j) $I_C(2\text{-}9,15)$=1.5, (k) $I_C(2\text{-}9,15)$=1.25, (l) $I_C(2\text{-}9,15)$=1 with Xc=0.20 at different temperatures.**

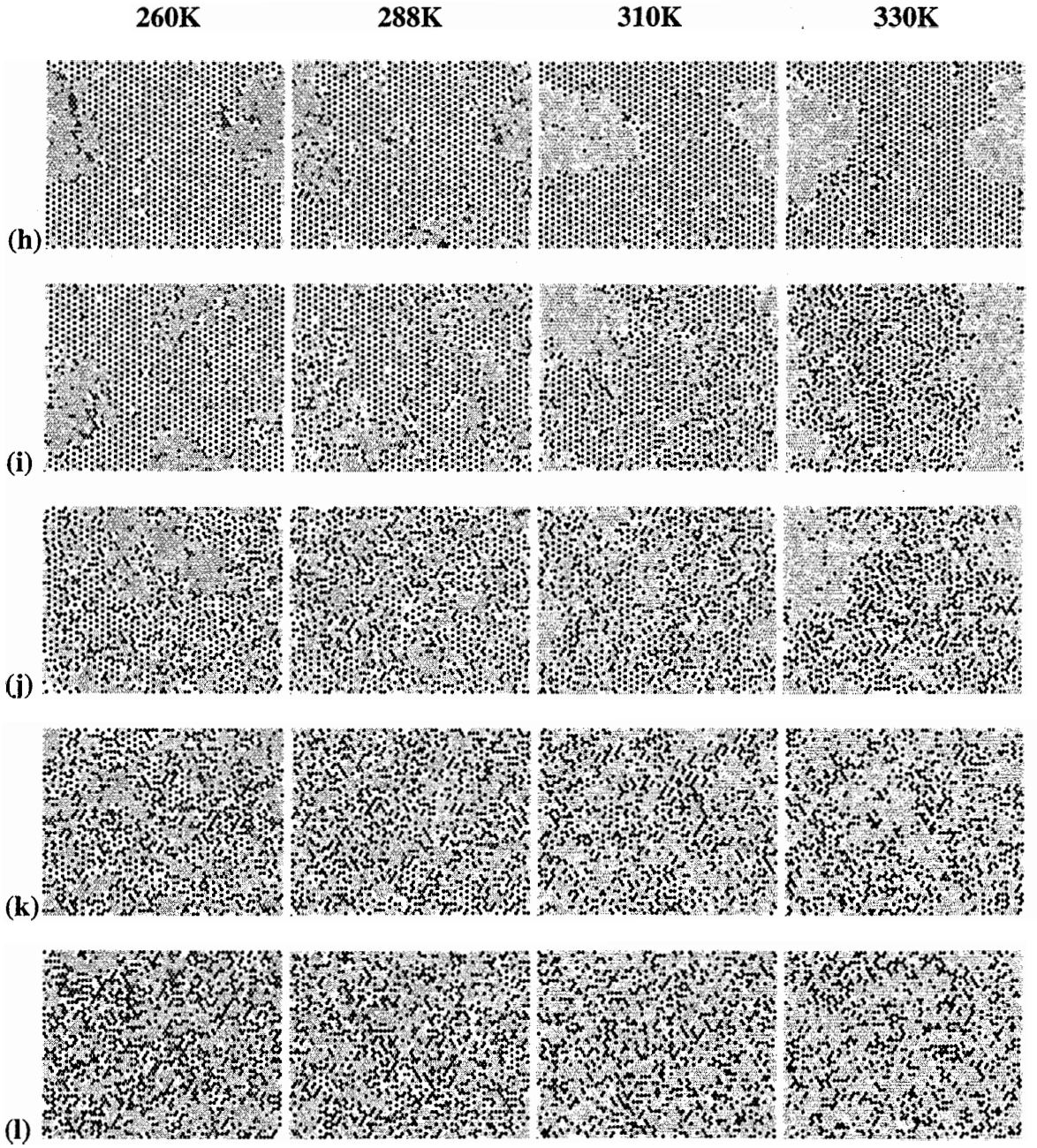

Figure 7.18 Simulated microconfigurations for DLPC/DPPC(4:6)/cholesterol bilayers with (h) $I_C(2\text{-}9,15)$=2, (i) $I_C(2\text{-}9,15)$=1.75, (j) $I_C(2\text{-}9,15)$=1.5, (k) $I_C(2\text{-}9,15)$=1.25, (l) $I_C(2\text{-}9,15)$=1 with Xc=0.40 at different temperatures.

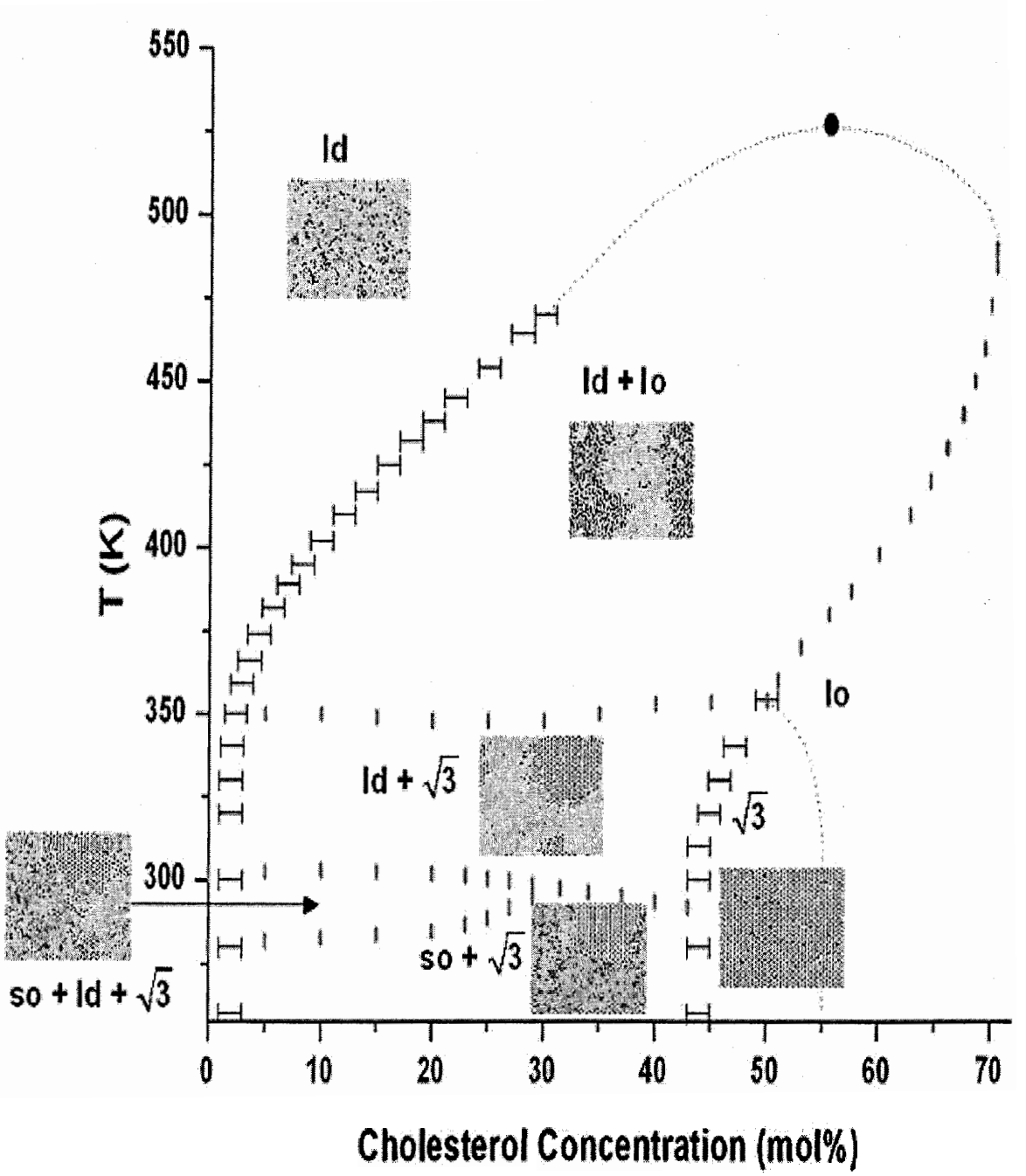

Figure 7.19 **Phase Diagram of DLPC/DPPC (40/60)/Cholesterol with $I_C(2\text{-}9, 15)$=2. Horizontal error bars are phase boundaries obtained from the inspection of the snapshots. The midpoints of the vertical lines indicate the positions of the peaks of the specific heat graphs. The positions of the dotted lines have not been calculated numerically, but must exist for topological reasons. '$\sqrt{3}$' refers to the $\sqrt{3}x\sqrt{3}$ phase. The solid circle refers to a critical point.**

7.4 Molecular Order Parameters

Figs. 7.20 and 7.21 show the respective molecular order parameters of DLPC and DPPC in the ternary lipid bilayers. The graphs in the left hand column of Fig. 7.20 show that, as the value of $I_C(15)$ increases, the inflection point for DLPC gradually shifts towards lower temperatures. For instance, the inflection point at Xc=0.40 has shifted from approximately 280K to 271K as $I_C(15)$ is increased from 1 to 2. This agrees with the graph of the specific heat, Fig. 7.6(a), which shows a sharp peak at 271K. The fact that this temperature is the same as the T_m of a single-component DLPC bilayer implies that this peak is mainly due to the DLPC melting in the ternary system. This is also confirmed by the snapshots in Fig. 7.15, which show that the DLPC chains in the cholesterol-poor region pass from the '**so** mc' to the '**ld** mc' without the influence of cholesterol or DPPC as temperature increases. On the other hand, if we look at the same series of molecular order parameters for DPPC with Xc=0.40, Fig. 7.21, we observe that, as $I_C(15)$ increases (i.e., from (e) to (a)), the difference of S_{L2} across the inflection point becomes smaller and smaller. This results in a relatively high order among DPPC chains even at very high temperatures. When this observation is correlated with the microconfiguration plots in Fig. 7.15, it shows that most DPPC chains are, in fact, highly ordered, since they exist as $DPPC_{\alpha=15}$ in the $\sqrt{3}\times\sqrt{3}$ phase which remains stable as temperature increases.

The graphs in the right hand column of Figs. 7.20 and 7.21 show quite a different scenario. Let us look at the case with Xc=0.40. As $I_C(2\text{-}9,15)$ increases from 1 to 2, we see that the molecular order parameters of both DLPC and DPPC at high temperatures increase in magnitude, similarly to the behaviour of DPPC in the left hand series of

graphs. However, neither the change in S_{L1} nor that in S_{L2} across the inflection points is completely removed in case (h), when $I_C(2\text{-}9,15)$=2. Instead, this change is observed to become more abrupt when the value of $I_C(2\text{-}9,15)$ approaches 1.75. Both S_{L1} and S_{L2} now contain an inflection point at the same temperature, which is approximately 291K. This agrees with the graphs of specific heat (Fig. 7.6(h)), which show a single peak at 291K, and the snapshots (Fig. 7.18) which shows that both DLPC and DPPC chains are involved in the cholesterol-poor regions, which melt at high temperature and thus reflecting the lowering the conformational order of the system.

The molecular order parameters in cases (h) and (j) are presented separately in Fig. 7.22 as a comparison to the FTIR results by Silvius *et al.* [16]. The FTIR data shows the frequency shift of the methylene symmetric stretching mode versus temperature for DLPC/DPPC-d_{62} mixtures (4:6 molar ratio) containing increasing molar percentages of cholesterol. As discussed in Ch. 5, the frequencies of the methylene symmetric stretching mode are related to the conformational order of the lipid chains in the bilayer [113]. The molecular order parameters from the MC simulations are plotted with an inverted vertical scale for the convenience of comparison to the FTIR data. The FTIR data show that, as *Xc* increases, the inflection points of both the DLPC and DPPC curves first begin to converge, then gradually decrease in magnitude, and are eventually eliminated. At *Xc*=0.40, both lipid species are observed to behave in a very similar way, exhibiting no large or abrupt change in the stretching frequencies. We now compare our simulation results to the FTIR data. One extreme case in our simulations is case (h) with $I_C(2\text{-}9,15)$=2. We find that this set of parameters gives us a system which has the highest conformational order at high temperatures and, also, that the DLPC and DPPC chains are

most strongly coupled. Fig. 7.22 shows that, in case (h), both the DLPC and DPPC curves begin to converge at Xc=0.05, and the changes in the conformational order across the inflection point decrease with the increase of Xc. At Xc=0.4, the conformational order of both lipid species is much larger than those at Xc=0.0. These observations are in good agreement with the FTIR data. However, the same graph also shows that both curves exhibit sharp changes at the same temperature T=18°C. Despite the fact that this indicates a coupling between the two lipid species which is favourable, the abrupt nature of this change does not agree with the experimental results. Inspection of Fig. 7.20 and 7.21 shows that this abrupt change begins to appear when $I_C(2\text{-}9,15)$ is greater than 1.5. Therefore, case (j), which has the parameter set $I_C(2\text{-}9,15)$=1.5, is the system which will possess the highest conformational order at high temperatures while not exhibiting an abrupt change. As we can see in Fig. 7.22, the shape of the molecular order parameters in case (j) has a better resemblance to the experimental result than that of case (h) up to Xc=0.30. However, at Xc=0.40, the conformational order parameter of both lipids, especially DPPC, is not as high as that of case (h).

In conclusion, we are able to mimic different aspects of a real system using difference values of the parameter $I_C(2\text{-}9,15)$. Case (h) with $I_C(2\text{-}9,15)$=2 possesses the highest conformational order at high temperatures, while case (j) with $I_C(2\text{-}9,15)$=1.5 does not have an abrupt change in the conformational order parameters. Both cases resemble the shape of the FTIR data to a considerable extent, and each has its own favourable characteristics towards modelling a real bilayer.

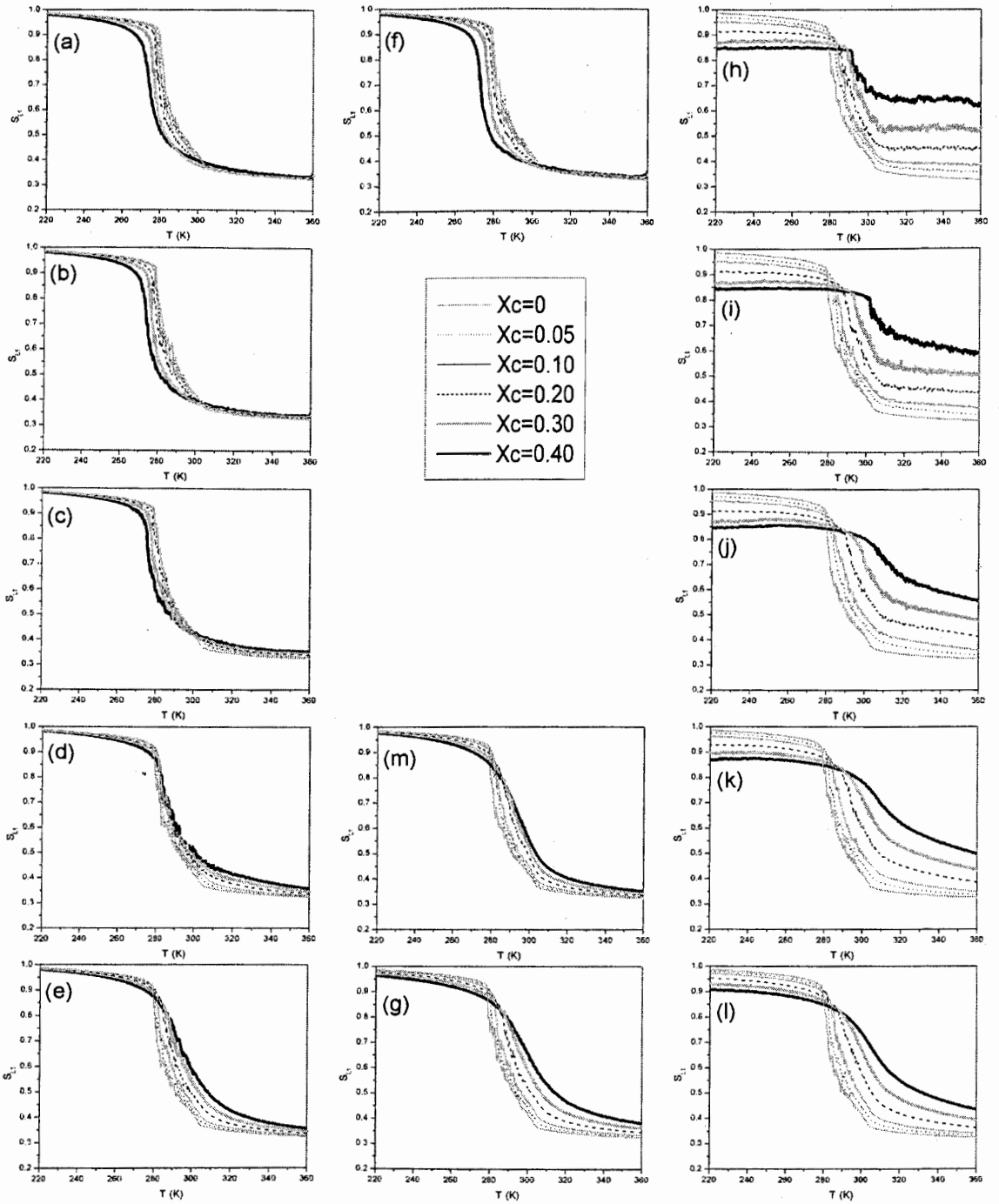

Figure 7.20 Molecular order parameter of DLPC (S_{LI}) versus temperature for DLPC/DPPC(4:6)/cholesterol bilayers

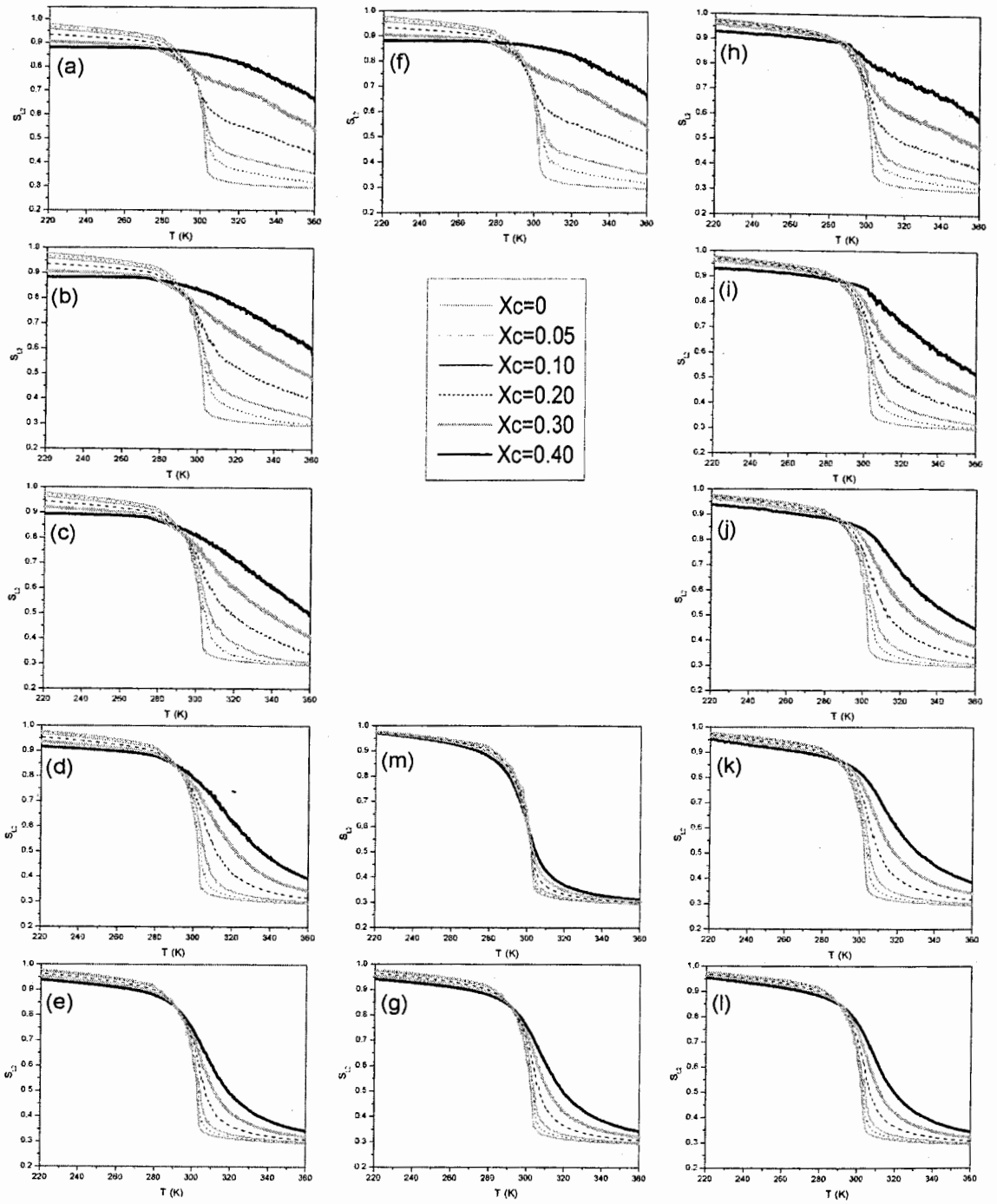

Figure 7.21 Molecular order parameter of DPPC (S_{L2}) versus temperature for DLPC/DPPC(4:6)/cholesterol bilayers

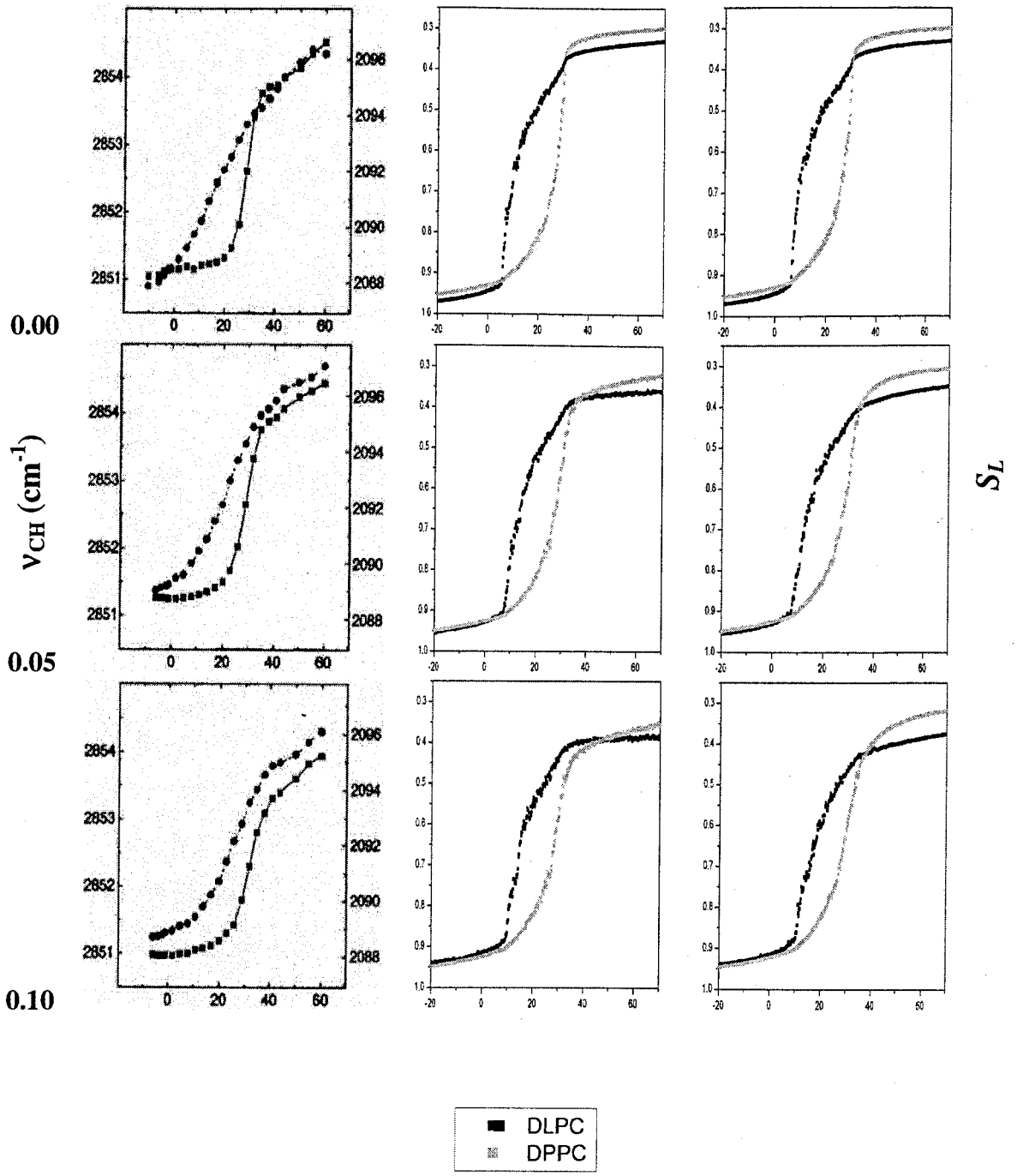
Xc
FTIR [16]
I_C(2-9,15)=2
I_C(2-9,15)=1.5
0.00
0.05
0.10
ν_{CH} (cm^{-1})
S_L
DLPC
DPPC

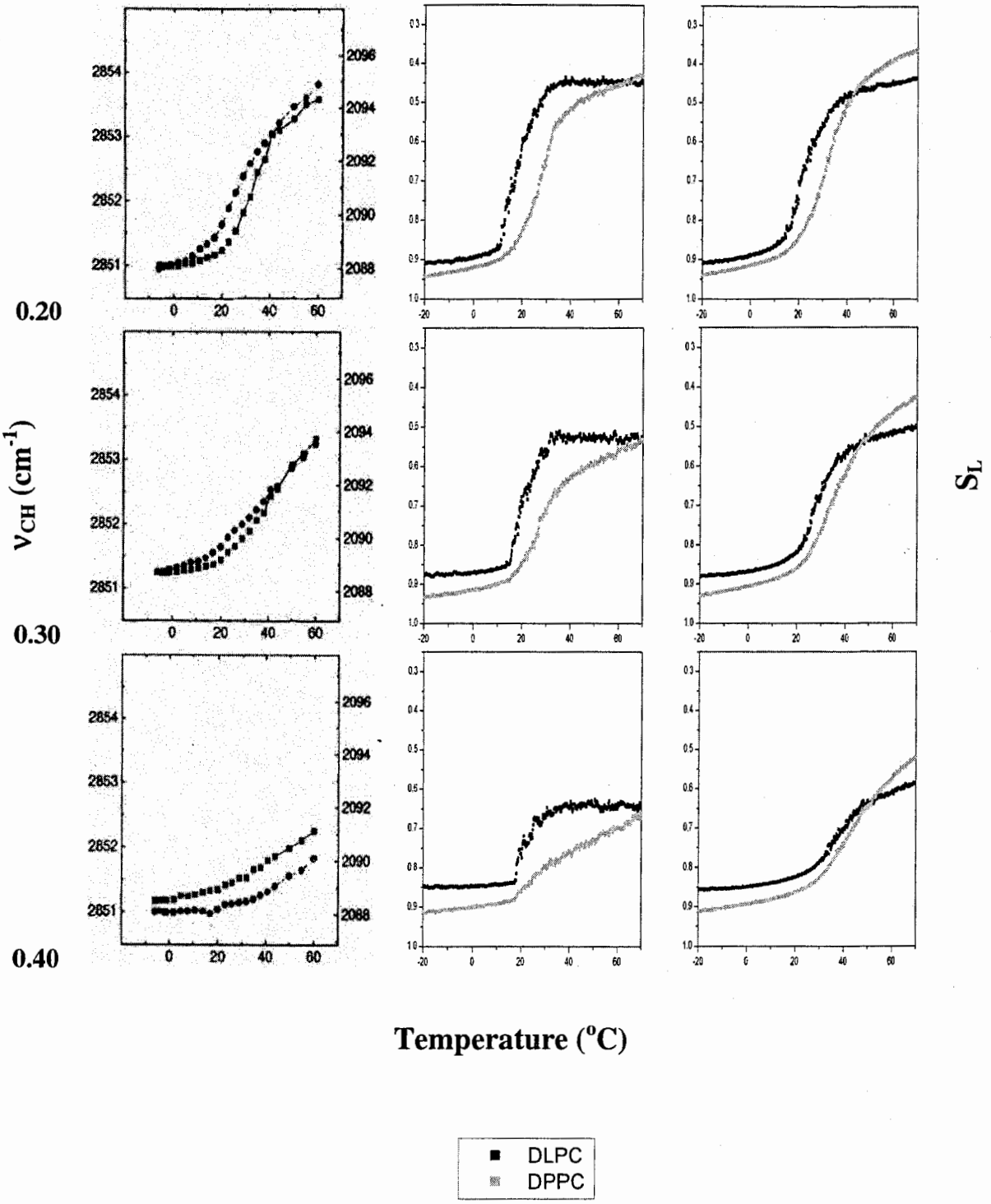

Figure 7.22 **Molecular order parameters (S_L) versus temperature of DLPC/DPPC(4:6)/cholesterol bilayers with $I_C(2\text{-}9,15)$=2 (middle column) and $I_C(2\text{-}9,15)$=1.5 (right column) in comparison with the FTIR data (left column) adapted from Silvius *et al.* [16].**
The FTIR data is obtained from DLPC/DPPC-d_{62} mixtures (4:6 molar ratio) where the data points represent (●) C-H stretch and (■) C-D stretch respectively. The molecular order parameters from MC simulations are plotted with an inverted vertical scale to aid visual comparison with FTIR data.

8 Conclusion

A summary of the results presented in Ch. 4 to Ch. 7 is first given here. As stated previously, the main purpose of this thesis is the investigation of binary and ternary lipid/sterol bilayers. We began by confirming that our MC simulations were in agreement with previous simulations for single-component PC bilayers with acyl chain lengths ranging from m=12 to m=18. Our results, presented in Ch. 4, were found to be in excellent agreement with those of Corvera *et al.* [62] using the same algorithm and parameters. This ensured the correctness of our code and demonstrated the reproducibility of the simulation results. Ch. 4 also serves to demonstrate how the Pink model describes the main phase transition of a single-component lipid bilayer. Thermodynamic properties, response functions and snapshots of microconfigurations were presented for the cases of m=12 to m=22. In summary, the simulation result shows an abrupt transition at T_m for $m \geq 20$, and a rapid but continuous change in the thermodynamic properties and response functions across T_m for cases with shorter chain lengths*. Moreover, we observed the accompaniment of significant thermal fluctuations away from T_m which is a consequence of a system being close to a critical point. These thermal fluctuations also manifest themselves through microdomain formation as can be observed in the snapshots.

* It has already been shown [27, 107] that the Pink model for PC bilayers with the parameters used in this thesis exhibits first order phase transitions for PC species with chain length $m \geq 20$, and does not have phase transitions for $m<20$ even though the system is close to a critical point and hence exhibit critical phenomena.

In the next step, MC simulations were used to investigate the effect of the addition of sterol to PC lipid bilayers, the results of which are presented in Ch. 5. First, simulations for the original Cruzeiro-Hansson model, which was intended for lipid systems with low cholesterol concentrations ($x_C \leq 0.1$), were repeated. In this case, cholesterol was found to reduce the changes in the thermodynamic properties and response functions across T_m. Moreover, below T_m (i.e., in the '**so** mc'), cholesterol was found to expand the area, increase the average energy, and induce conformational disorder in the bilayer, while the opposite effects were observed above T_m (i.e., in the '**ld**. All the above observations are in excellent agreement with the original simulations of Cruzeiro-Hansson *et al.* [28].

We then extended the Cruzeiro-Hansson model of lipid-cholesterol bilayers to accommodate systems with high sterol concentrations. Since there are not as yet any ^{2}H-NMR experiments on DLPC/sterol bilayers available, the greater part of our work was carried out for the DPPC/sterol bilayers. The parameter $I_C(5)$, which gives the strength of interaction between a sterol molecule a lipid chain in the kink state, was increased from the original value of 0.45 to 2.0 progressively. This sequence of $I_C(5)$ values can also be used to represent various types of sterol molecules that have different strengths of interaction with a lipid chain. The molecular order parameters calculated from the modified model at T=50°C and T=60°C with $I_C(5)$=1.5 are in good agreement with the experimental data by Thewalt *et al.* [14].as compared with the original model The snapshots of microconfigurations show that for $1 \leq I_C(5) \leq 1.5$, the bilayers transform continuously from the '**so** mc' to the '**ld** mc' by passing through the '**lo** mc' as temperature increases. The '**lo** mc' was found to coexist with the '**so** mc' or the '**ld** mc'

under some conditions, and the phase behaviour of the bilayers is summarized in the phase diagram in Fig. 5.12. When we increased the value of $I_C(5)$ to 2, the system exhibited phase separation phenomena. A new phase, the $\sqrt{3}\times\sqrt{3}$ phase emerged, and it was observed to coexist with the '**so** mc' and the '**ld** mc' at different temperatures and cholesterol concentrations. In particular, the $\sqrt{3}\times\sqrt{3}$ phase was observed to grow in area with increasing concentrations of sterol until it became the only phase in the system at Xc=0.50.

The next step in our analysis was to investigate binary lipid bilayers containing DLPC and DPPC using the method by Jørgensen *et al.* [50]. This model is an extension of the original Pink model for single-component lipid bilayers. Our results for this case are presented in Ch. 6. Two inflection points were observed in the graphs of thermodynamic properties which gives the boundaries of the coexistence region of the **so** phase and the **ld** phase. The phase boundary does not extend to the 100% DLPC or 100% DPPC, since neither lipid species exhibits phase transitions on their own. The phase behaviour of the binary DLPC/DPPC bilayers is summarized in the phase diagram in Fig. 6.5. The topology of the phase diagram indicates a certain degree of mixing of the two lipid species, even though it is far from ideal mixing. Our simulation results of this system were compared to experimental FTIR [16] and calorimetry [82] data and good agreement of our results with experiments was obtained Snapshots of microconfigurations of DLPC/DPPC (40:60) mixture show that local structures and membrane heterogeneities exist at all temperatures, and that phase coexistence was observed between 282K and 300K.

Simulation results for the ternary lipid bilayers containing sterol are presented in Ch. 7. The parameters used in Ch. 4 to 6 were combined in order to simulate ternary lipid bilayers containing DLPC, DPPC and sterol. The model used is a combination of Jørgensen's model for binary lipid bilayers and the Cruzeiro-Hansson model for lipid/cholesterol bilayers. A systematic exploration of the parameter space $I_C(\alpha)$ was performed in order to understand the effect of different interaction strengths between sterol molecules and lipid chains in different states. In the process, we found that the use of the values $I_C(15)=\{1, \ldots, 2\}$ and $I_C(2\text{-}9,15)=\{1, \ldots, 2\}$ gave quite interesting effects for the bilayers. An increase in the parameter set $I_C(15)$ or $I_C(2\text{-}9,15)$ favours the existence of lipid chains in intermediate conformations, and hence induces the formation of the **lo**-like regions. A value of $I_C(15)$ or $I_C(2\text{-}9,15)$ at or below 1.5 results in the formation of the '**lo** mc'. On the other hand, values of $I_C(15)$ or $I_C(2\text{-}9,15)$ beyond 1.5 induce the formation of the $\sqrt{3}\times\sqrt{3}$ phase. This phase is observed to phase-separate from either the '**so** mc' or the '**ld** mc' depending on the temperature of the system. $I_C(15)$ favours the formation of intermediate DPPC chains, while $I_C(2\text{-}9,15)$ favours the formation of both intermediate DLPC and DPPC chains. Therefore, the content of the **lo**-like region is different for systems with $I_C(15)=\{1, \ldots, 2\}$ and $I_C(2\text{-}9,15)=\{1, \ldots, 2\}$. For instance, at high values of $I_C(15)$, the $\sqrt{3}\times\sqrt{3}$ phase is composed predominately of intermediate DPPC chains and sterol. On the other hand, large values of $I_C(2\text{-}9,15)$ result in a $\sqrt{3}\times\sqrt{3}$ phase with both intermediate DLPC and DPPC chains as well as sterol. At extremely high values of $I_C(\alpha)$ (e.g., $I_C(15)=2$ or $I_C(2\text{-}9,15)=2$) and high concentrations of sterol (e.g., $Xc=0.4$), the $\sqrt{3}\times\sqrt{3}$ phase is found to persist to very high temperatures. In other words, the $\sqrt{3}\times\sqrt{3}$ phase appears to be relatively unaffected as temperature

increases while the rest of the system passes from the '**so** mc' to the '**ld** mc'. In these cases, a rapid change in the thermodynamic properties and the response functions was observed, which signifies the occurrence of this melting.

Our simulation results were also compared to the experimental FTIR data by Silvius *et al.* [16] on DLPC/DPPC/cholesterol bilayers. We were able to model different aspects of the experimental data by using different sets of parameters in the parameter space under examination. The case with $I_C(2\text{-}9,15)=2$ creates a system with the highest conformational order found in our simulations at high temperatures. Moreover, the DLPC and DPPC chains in this system were also found to behave very similarly, as shown in the snapshots and the graphs of order parameters in Ch. 7. These two characteristics of the simulated system are highly desirable in light of the experimental findings by the above group. However, the drawback of using such a high value of I_C is that it leads to a rapid change in the physical properties as described above, which was not observed experimentally. Among the different parameter sets we tested, the case with $I_C(2\text{-}9,15)=1.5$ gave the best overall comparison with experimental data. The order parameters of this system display a gradual and continuous decrease with increasing temperature, and the similar behaviours of the two lipid species indicate a considerable degree of coupling. This is therefore the parameter set which results in a system with the highest average conformational order at high temperatures found in our simulations, displaying coupling between the two lipid species, while remaining free from any rapid changes in the physical properties of the system.

In conclusion, we have achieved significant improvement over the original Cruzeiro-Hansson model in modelling binary lipid/sterol bilayers with high sterol content

(>10 mol%), and our initial investigation of the ternary lipid/sterol bilayers has produced promising results.

In addition to the results presented in this thesis, further investigations are in progress. We have recently found from our simulations that T_{mix}, the temperature where inhomogeneity disappears, lies between 306K to 310K [102]. This is consistent with the data by London *et al.* [97] who found that T_{mix}=308K for 12SLPC/DPPC bilayers.

Recently, Berkowitz *et al.* [98] used MD simulations to study the strength of all the different hydrogen bonds that could possibly exist between the hydroxyl group of cholesterol and the headgroup of DPPC or DLPC, whether directly or indirectly, via a water bridge. They found that, in binary lipid/cholesterol mixtures with 40 mol% cholesterol, both DLPC and DPPC exhibit 1:1 and 2:1 complex formations with cholesterol at 279K and 323K, respectively, due to hydrogen bonding. In particular, they found that DLPC prefers the 1:1 complex with cholesterol, while DPPC carries a slightly larger population of 2:1 complexes than 1:1 complexes. In our simulations of the same DPPC/sterol mixture with the parameter $I_C(5)$> 1 (Fig.5.11 and 5.15) at 318K, the ratio of DPPC molecules to sterol in the **lo**-like region is at least 1:1. On the other hand, the interaction energy in our model (e.g., -1.2 kcal/mol between the kink state of DPPC and sterol in the case of $I_C(5)$=1.5), is found to be much smaller than the minimum cut-off energies for the hydrogen bonding (-2.8 kcal/mol) in their calculations. This difference is as expected, since, firstly, the populations of hydrogen-bonded pairs in their system are very small (of the order of a thousandth or smaller) and, hence, the average interaction energy between a pair of molecules should be much weaker than that of a hydrogen bond. Secondly, the hydrogen bonds that Berkowitz *et al.* considered only exist between the

headgroups of phospholipid and cholesterol, which does not take into account the interactions between the lipid chains. In fact, the conformation of the lipid chain plays a crucial role in determining the overall interactions between a lipid and a sterol molecule, and in many cases steric hindrance results in weaker interaction energies and unfavourable interactions. With this rationale, it is reasonable to suppose that the interaction energies in our model, which is intended to describe the overall average interaction between a sterol molecule and a lipid chain in a specific state, should take on a much smaller magnitude than that of a hydrogen bond.

Another recent model, proposed by Huang and Feigenson [101], is the Umbrella Model. It emphasizes that cholesterol, with a small hydroxyl group, must rely on the phospholipid headgroup to shield its large hydrophobic body completely from water. This hydrophobic interaction provides a favourable attraction between cholesterol and phospholipid, or an unfavourable energy penalty for cholesterol cluster formation. The MC simulations of the Umbrella Model on a lattice with strong cholesterol-phospholipid multibody interaction led to a regular distribution of cholesterol, which produced patterns such as the "hexagonal pattern" and the "maze pattern". Despite the fact that we only consider pairwise nearest-neighbour interactions in our model instead of the multibody interactions used by the above group, our results with high values of I_C led to **lo** domains with a regular distribution of sterol, some of which resemble these regular patterns. However, it needs to be mentioned that, these patterns are artifacts of the lattice which, however, does not represent the fluid nature of the **lo** phase and is therefore not entirely realistic.

Further calculations and investigations of the ternary lipid/sterol bilayers that can be preformed include cluster analysis and the extraction of structural factors from our data. Furthermore, lattice models such as the one used here have their limitations in that they do not allow proper description of the fluid phase of the lipid bilayers. In addition to the conformational degrees of freedom that we have considered, translational degrees of freedom can also be included by the use of off-lattice models [44]. This is particularly beneficial for the system we studied, since both **lo** and **ld** phase are fluid phases. However, despite the possible shortcomings of the lattice model, its use has allowed us to study large numbers of molecules, thus permitting a detailed theoretical study of the phase transition properties with reasonable computer time. Therefore, our simulations serve as a good indication of the behaviour of ternary lipid bilayers containing sterols and give an order of magnitude estimate for the parameter sets to be used to continue this investigation with off-lattice models.

Appendix A

Selection Rules for the Intermediate Conformational States in the Pink Model

In the Pink model, 10 different acyl chain conformational states are permitted. Between the ground state (all-*trans*) and state 10 (the highly excited state), there are eight intermediate energy states, which are low energy excitations of the all-*trans* conformations. The eight intermediate energy states in the Pink model are selected according to the following rules:

- The first two chain segments are kept fixed in a *trans* configuration.
- The chains have at most three *gauche* bonds.
- The length of the chains is at most three units shorter than that of the all-*trans* conformations.
- The chains do not fold back upon themselves.
- The first two *trans* segments define a plane. The first *gauche* bond takes the molecule out of the plane in two possible directions (a two-fold degeneracy). If a second *gauche* bond occurs (as in states 5 to 9) it is only allowed to return the molecule to the plane (i.e., a second *gauche* bond is non-degenerate).
- If a third *gauche* bond occurs (as in states 8 and 9) the molecule again comes out of the plane in two possible directions and the *gauche* bond has a two-fold degeneracy

except if the second and third *gauche* bonds are next to each other. In this case only one of the direction is allowed and this *gauche* bond is non-degenerate.

Bibliography

[1] Bloch, K., *Blonds in Venetian Paintings, the Nine-banded Armadillo, and Other Essays in Biochemistry* (Yale University Press, New Havan) 1994, Ch. 2.

[2] Bloch, K., CRC Crit. Rev. Biochem. **14**, 47 (1983).

[3] Yeagle, P., *Cholesterol in Membrane Models* (Finegold, L. ed.), Ch. 1, CRC Press, Boca Raton (1993).

[4] Miao, L., Nielsen, M., Thewalt, J., Ipsen, J.H., Bloom, M., Zuckermann, M.J. and Mouritsen, O.G., Biophys. J. **82**, 1429 (2002).

[5] Mauch, D.H., Nägler, K., Schumacher, S., Göritz, C., Müller, E., Otto, A., Pfrieger, F. W., Science **294**, 1354 (2001).

[6] Ohvo-Rekilä, H., Ramstedt, B., Leppimäki, P. and Slotte, J. P., Prog. Lip. Res. **41**, 66 (2002).

[7] Pike, L., J. Lip. Res. **44**, 655 (2003).

[8] Edidin, M., Annu. Rev. Biophys. Struct. **32**, 257 (2003).

[9] van Meer, G., Stelzer E.H., Wijnaendts-van-Resandt, R.W. and Simons, K., J. Cell Biol. **105**, 1623 (1987).

[10] Sprong, H., van der Sluijs, P. and van Meer, G., Nat. Rev. Mol. Cell Biol. **2**, 504 (2001).

[11] Biltonen, R.C., J. Chem. Thermodynamics, **22**, 1 (1990).

[12] Vist, M.R., Davis, J.H., Biochemistry **29**, 451 (1990).

[13] Ladbrooke, B.D., Williams, R.M. and Chapman, D., Biochim. Biophy. Acta **150**, 333 (1968).

[14] Hsueh, Y-W, Gilbert, K., Trandum, C., Zuckermann, M. and Thewalt, J., "The effect of ergosterol on dipalmitoylphosphatidylcholine bilayers: a deuterium NMR and calorimetric study", submitted to Biophy. J. (2003).

[15] Zuckermann, M.J., Ipsen and J.H., Mouritsen, O.G., *Cholesterol in Membrane Models* (Finegold, L. ed.), Ch. 9, CRC Press, Boca Raton (1993).

[16] Silvius, J.R., del Giudice, D. and Lafleur, M., Biochemistry **35**, 15198 (1996).

[17] Veatch, S.L. and Keller, S. L., Biophys. J. **85**, 3074 (2003).

[18] Silvius, J.R., Biophys. J. **85**, 1034 (2003).

[19] Marčelja, S., Biochim. Biophys. Acta **367**, 165 (1974).

[20] Nagle, J.F., J. Chem. Phys. **58**, 252 (1973).

[21] Nagle, J.F., J. Chem. Phys. **63**, No. 3, 1255 (1975).

[22] Caillé, A., Rapini, A., Zuckermann M.J., Cros, A., and Doniach, S., Can. J. Phys. **56**, 348 (1978).

[23] Doniach, S., J. Chem. Phys. **68** (11), 4912 (1978).

[24] Phillips, M.C. and Chapman, D., Biochim. Biophys. Acta **163**, 301 (1968).

[25] Mouritsen, O.G., Boothroyd, A., Harris, R., Jan, N., Lookman, T., MacDonald, L., Pink, D.A., and Zuckermann, M.J., J. Chem. Phys. **79**, 2027 (1983).

[26] Pink, D.A., Green, T.J., and Chapman, D., Biochemistry **19**, 345 (1980).

[27] Corvera Poiré, E., Laradji, M., Zuckermann, M.J., Phys. Rev. E, **47**, 696 (1993).

[28] Cruzeiro-Hansson, L., Ipsen, J.H. and Mouritsen, O.G., Biochim. Biophys. Acta **979**, 166 (1989).

[29] Sugár, I.P., Thompson, T.E. and Biltonen, R.L., Biophys. J. **76**, 2099 (1999).

[30] Michonoca-Alexova, E.I. and Sugár, I.P., Biophys. J. **83**, 1820 (2002).

[31] Heimburg, T. and Ivanova, V.P., Phy. Rew. E **63**, 041914 (2001).

[32] Whitmore, M.D., Whitehead, J.P. and Roberge, A., Can. J. Phys. **76**, 831 (1998).

[33] Cantor, R.S. and McIlroy, P.M., J. Chem. Phys. **91** (1), 416 (1989).

[34] Scheutjens, J.M.H.M. and Fleer, G.J., J. Phys. Chem. **83**, 1619 (1979).

[35] Feller, S.E., Venable, R.M. and Pastor, R.W., Langmuir **13**, 6555 (1997).

[36] Nagle, J.F., Biophys. J. **64**, 1476 (1993).

[37] Tieleman, D.P. and Berendsen, H.J.C., J. Chem. Phys. **105**, 4871 (1996).

[38] Saiz, L. and Klein, M., Acc. Chem. Res. **35**, 482 (2002).

[39] Lopez, C.F., Moore, P.B., Shelley, J.C., Shelley, M.Y. and Klein, M., Comp. Phy. Comm. **147**, 1 (2002).

[40] Chiu, S.W., Clark, M., Balaji, V., Subramaniam, S., Scott, H.L. and Jakobsson, E., Biophy. J. **69**, 1230 (1995).

[41] Essmann, U. and Berkowitz, M.L., Biophys. J. **76**, 2081 (1999).

[42] Ipsen, J.H., Karlström, G., Mouritsen, O.G., Wennerström, H. and Zuckermann, M.J., Biochim. Biophy. Acta **905**, 162 (1987).

[43] Ipsen, J.H., PhD Thesis, The Technical University of Denmark (1989).

[44] Nielsen, M., Miao, L., Ipsen. J.H., Zuckermann, M.J. and Mouritsen, O.G., Phy. Rew. E, **59**, 5790 (1999).

[45] Scott, H.L., Biophys. J. **59**, 445 (1991).

[46] Chiu, S.W., Jakobsson, E., Mashi, R.J. and Scott, H.L., Biophys. J. **83**, 1842 (2002).

[47] Chiu, S. W., Jakobsson, E. and Scott, H.L., Biophys. J. **80**, 1104 (2001).

[48] Tu, Kechuan, Klein, M.L. and Tobias, D.J., Biophys. J. **75**, 2147 (1998).

[49] Smondyrev, A. and Berkowitz, M.L., Biophys. J. **77**, 2075 (1999).

[50] Jørgensen, K., Sperotto, M.M., Mouritsen, O.G., Ipsen, J.H., and Zuckermann, M.J., Biochim. Biophys. Acta **1152**, 135 (1993).

[51] Mouritsen, O.G., *Molecular Description of Biological Membranes by Computer Aided Conformational Analysis*, Vol.1 (Brasseur, R., ed.), pp. 3-83, CRC Press., Boca Raton (1990).

[52] Davis, J.H., Biophy. J., **27**, 339-358 (1979).

[53] Hatta, I., Imaizumi, S. and Akutsu, Y., J. Phys. Soc. Japan, **53**, 882 (1984).

[54] Mouritsen, O.G. and Zuckermann, M., Eur. Biophys. J., **12**, 75 (1985).

[55] Mitaku, S., Jippo, T. and Kataoka, R., Biophys. J., **42**, 137 (1983).

[56] Zhang, Z. and Zuckermann, M., Phys. Rev. A, **46**, 6707 (1992).

[57] Wu, Y., Master Thesis, McGill University (1998).

[58] Marčelja, S., J. Chem. Phys. **60**, No.9, 3599 (1974).

[59] Caillé, A., Pink, D., de Verteuil, F., and Zuckermann, M.J., Can. J. Phys. **58**, 581 (1980).

[60] Tardieu, A., Luzzati, V. and Reman, F.C., J. Mol. Bio. **75**, 711 (1972).

[61] Trauble, H., Sackmann, E., J. Am. Chem. Soc. **94**, 4499 (1972).

[62] Corvera Poiré, E., Master Thesis, McGill University (1990).

[63] Nagle, J.F., Proc. Natl. Acad. Sci. U.S.A. **70**, 3443 (1973a).

[64] Salem, L., J. Chem. Phys. **37**, 2100 (1962).

[65] Seelig, A. and Seelig, J., Biochemistry **13**, 4839 (1974).

[66] Schindler, H. and Seelig, J., Biochemistry **14**, 2283 (1975).

[67] Thewalt, J., Hanert, C. E., Linseisen, F.M., Farrall, A.J. and Bloom, M., Acta Pharm. **42**, 9 (1992).

[68] Risbo, J., Sperotto, M.M. and Mouritsen, O.G., J. Chem. Phys. **103**, 3643 (1995).

[69] Knoll, W., Ibel, K. and Sackmann, E., Biochemistry **20**, 6379 (1981).

[70] Mouritsen, O.G. and Sperotto, M.M., *Thermodynamics of Surface Cell Receptors* (Jackson., M., ed.), pp. 127-181, CRC Press., Boca Raton (1993).

[71] Mouritsen, O.G. and Bloom, M., Annu. Rev. Biophys. Biomol. Struct. **22**, 147 (1993).

[72] Zhang, Z., Sperotto, M.M., Zuckermann, M.J., and Mouritsen, O.G., Biochim. Biophys. Acta **1147**, 154 (1993).

[73] Gould, H. and Tobochnik, J., *An Introduction to Computer Simulation Methods Part 2*, pp.333-337, Addison-Wesley Publishing Company (1987).

[74] Metropolis, N., Rosenbluth, A.W., Rosenbluth, M.N., Teller, A.H., and Teller, E., J. Chem. Phys. **21**, 1087 (1953).

[75] Glauber, R.J., J. Math. Phys. **4**, 294 (1963).

[76] Kawasaki, K., *Phase Transitions and Critical Phenomena*, Vol. 5b, Academic, New York (1976).

[77] Boal, D., private communication.

[78] Ipsen, J.H., Jørgensen, K. and Mouritsen, O.G., Biophys. J. **58**, 1099 (1990).

[79] Mouritsen O.G., Biochim. Biophys. Acta **731**, 217 (1983).

[80] Laradji, M., Guo, H., Grant, M. and Zuckermann, M.J., *Advances in Chemical Physics Vol. LXXXIX*, pp159-238, John Wiley and Sons, Inc., New York (1995).

[81] Endress, E. *et.al.*, Langmuir **18**, 3293 (2002).

[82] Van Dijck, P.W.M., Kaper, A.J. Oonk, H.A.J. and De Gier, J., Biochim. Biophy. Acta **470**, 58 (1977).

[83] Jähnig, F., J. Chem. Phys. **70**, 3279 (1979).

[84] Mouritsen, O.G., *Computer Studies of Phase Transitions and Critical Phenomena*, Springer-Verlag, Berlin (1984).

[85] Bloom, M., Evans, E. and Mouritsen, O.G., Q. Rev. Biophys., **24(3)**, 293 (1991).

[86] Bloom, M., Evans, E. and Mouritsen, O.G., Q. Rev. Biophys. **24**, 293 (1991).

[87] Lai, E., J. Cell Biol., **162(3)**, 365 (2003).

[88] Sackmann, E., *Physical Foundations of the Molecular Organization and Dynamics of membranes. Biophysics* (Hope, W., Lohmann, W., Markl, H., Ziegler, H. eds.), pp.425-457, Springer-Verlag, New York (1983).

[89] Recktenwald, D.J. and McConnell, H.M., Biochemistry **20**, 4505 (1981).

[90] Copeland, B.R. and McConnell, H.M., Biochim. Biophy. Acta **599**, 95 (1980).

[91] Cruzeiro-Hansson, L., *Solutions and a Physical Model of Active Transport.* PhD thesis, The Technical University of Denmark, 1988.

[92] Alberts, B., Bray, D., Lewis, J., Raff, M., Roberts, K. and Watson, J.D., *Molecular Biology of the Cell*, 3rd edition, Garland Publishing, New York (1994).

[93] Wu, W-G and Chi, L-M., J. Am. Chem. Soc. **113**, 4683 (1991).

[94] Needham, D. and Nunn, R.S., Biophys. J. **58**, 997 (1990).

[95] Robertson, R. N., *The Lively Membranes*, Cambridge University Press, 1983.

[96] Pierce, S. K., Nature Rev. Immunol., **2**, 96 (2002).

[97] London, E., Brown, D.A. and Xu, X., Meth. Enzy. **312**, 272 (2000).

[98] Pandit, S.A., Bostick, D. and Berkowitz, M.L., Biophys. J. **86**, 1345 (2004).

[99] Anderson, T.G. and McConnell, H.M., Biophys. J. **81**, 2774 (2001).

[100] McConnell, H.M. and Vrljic, M., Annu. Rev. Biophys. Biomol. Struct. **32**, 469 (2003).

[101] Huang, J. and Feigenson, G.W., Biophys. J. **76**, 2142 (1999).

[102] Preliminary results. Investigation are still in progress.

[103] Chiras, D., *Human Biology: Health, homoeostasis, and the environment*, Jones and Bartlett Publishers, 1991.

[104] Karp, G., *Cell and Molecular Biology: Concepts and Experiments*, 3rd edition, John Wiley and Sons Inc., 2001.

[105] Lee, A.G., Biochim. Biophys. Acta **472**, 237 (1977).

[106] Hill, T. L., *An Introduction to Statistical Thermodynamics*, Dover Publications, New York, 1960.

[107] Mouritsen, O.G., *Advances in Computer Simulations of Liquid Crystals* (Pasini, P. and Zannoni, C., eds.), Ch.7, Kluwer Academic Publ., BV, The Nederland (1998).

[108] Ferrenberg, A. M. and Swendsen, R. H., Phys. Rev. Lett. **61**, 2635 (1998).

[109] Lee, J. and Kosterlitz, J. M., Phys. Rev. Lett. **65**, 137 (1990).

[110] Lee, J. and Kosterlitz, J. M., Phys. Rev. B **43**, 3265 (1991).

[111] Mouritsen, O.G., Chem. & Phys. Lipids **57**, 179 (1991).

[112] Mendelsohn, R., Davies, M.A., Schuster, H.F., Xu, Zhenchun and Bittman, R., Biochemistry **30**, 8558 (1991).

[113] Nabet, A., Auger, M., Pézolet, M., Appl., Spectrosc. **54**, 948 (2000).

[114] Dash, J.G., *Films on Solid Surfaces*, Academic Press, New York (1975).

[115] Mondat, M., M.Sc. Thesis, McGill University, 1982.

[116] O. G. Mouritsen, private communication.

[117] Thewalt, J., private communication.